Politecnico di Milano

SCHOOL OF CIVIL, ENVIRONMENTAL AND LAND MANAGEMENT ENGINEERING

MASTER OF SCIENCE IN CIVIL ENGINEERING

Analytical evaluation of the reaction forces at the connections between primary structure and cladding panels

---

Advisor:
Prof. Luca Martinelli

Co-Advisor:
Prof. Bruno Alberto Dal Lago

Co-Advisor:
Prof. Francesco Foti

Candidate:
Giacomo Zucchiatti

Milano - May 19, 2022

Abstract

Industrial structures are generally composed by a pre-cast structural frame, closed at the four sides by cladding panels, constrained to the frame by means of specific connections. In the case of a seismic event, the forces generated by the ground motion are transmitted from the frame to the panels through these anchoring devices. The main objective of this work is to analyze and simplify the procedure involved in the combination rule adopted to obtain the maximum value of these forces. In particular, in the most advanced seismic codes, earthquake loads are often defined by means of pseudo-acceleration RS and the use of modal superposition analysis is strongly recommended. Several rules for the peak value combination of modal responses have been derived on the basis of random vibration theory. The simplest one is the Square Root of Sum of Squares (SRSS) combination rule, ignoring the correlation between modes. However it provides excellent nodal response estimates only with particular characteristics (structure with well separated natural frequencies and not too lightly damped and earthquake excitations containing a wide band of frequencies). When these conditions are not respected, the correlation between modal responses cannot be neglected. In such cases, the modal combination should be performed using the Complete Quadratic Combination (CQC) rule, defining coherent correlation coefficients. In particular, by assuming the ground motion as a stationary, gaussian and zero mean process, then the input process is simply defined by its Autocorrelation function, or alternatively, by the corresponding Power Spectral Density Function (PSDF). In such a case, random vibration theory provides useful tools allowing for a simple evaluation of correlation coefficients consistent with any input Power Density. Unfortunately, the majority of the codes characterize the ground excitation anticipated at the site by means of elastic response spectra. Therefore the evaluation of consistent correlation coefficients requires a preliminary evaluation of the PSD of the seismic excitation compatible with the assigned response spectrum. In literature various methods have been proposed to this purpose.

Summing up, the goal of the work is centered on the evaluation of the reaction forces which generate at the connection between frame and claddings. To do so, a modal superposition analysis is used. The center of the formulation is related to the fact that the ground motion will be here seen as the contribution of a fictitous mode of the structure with infinite frequency. On one hand this allows to reduce the complexity of the formulation, but on the other it makes it necessary to rely on a modal combination rule to compute the maximum values of the solution. In order to account for the interaction between the modes, the Complete Quadratic Combination rule is used. This procedure requires however the knowledge of the correlation coefficients between the modes involved. This is why the first part of the thesis will be devoted to exploit the main conceopt behind the theory of the Spectral analysis, in order to obtain a closed form solution for such coefficients. The proposed formulations should be validated by considering the different class of soils and damping ratios. The reliability of the method will

be finally assessed also in the non linear field, when the structural model enters its post-elastic behaviour.

Sommario

Le più generali strutture industriali fanno riferimento ad una struttura composta da un telaio primario pre-fabbricato delimitato ai lati da pannelli di tamponamento. Tali elementi di chiusura sono connessi alla struttura principale per mezzo di specifici ancoraggi. Ed è proprio tramite questi meccanismi di ritenzione che durante un evento sismico, le forze generate dall'accelerazione del suolo vengono trasmesse dal telaio ai pannelli. Scopo di questo lavoro è quello di sviluppare una procedura semplificata finalizzata al calcolo dei valori massimi di queste forze. In particolare, nei codici più recenti, il carico sismico viene modellato tramite il concetto di Spettro di Risposta, e l'utilizzo dell'analisi modale è fortemente consigliato. A tal proposito, facendo riferimento ai principi della teoria stocastica, varie tecniche di combinazione modale sono state sviluppate al fine di arrivare al valore di picco della risposta. Il metodo più semplice e immediato (Square Root of the Sum of the Squares - SRSS) prevede il calcolo del valore massimo trascurando la correlazione tra i modi. I risultati forniti sono tuttavia affidabili solamente nel caso in cui i modi di vibrare siano caratterizzati da frequenze ben distinte, e un contributo viscoso sufficientemente elevato. In caso contrario, la SRSS non è adottabile, e l'analisi modale va effettuata utilizzando un diverso metodo di combinazione modale, la Complete Quadratic Combination Rule (CQC). In particolare, guardando all'azione sismica come ad un processo stazionario e Gaussiano, è possibile caratterizzare l'input del problema semplicemente in termini della Densità Spettrale associata all'evento. Il problema è legato al fatto che, come detto, la maggior parte delle Normative rappresenta il terremoto in termini dello Spettro di Risposta Elastico. Per questo motivo la valutazione dei coefficienti di correlazione richiede prima di tutto la valutazione della relativa Densità Spettrale, modellata in modo tale da risultare compatibile con lo Spettro di risposta in oggetto. In letteratura vari metodi sono disponibili a riguardo. Una volta dunque individuato il modello di Funzione di densità Spettro compatibile, l'obiettivo del lavoro è quello di definire una procedura di calcolo semplificata che consenta di ottenere in forma chiusa il valore dei coefficienti di correlazione da adottare in seguito nell'analisi modale. La validità della formulazione proposta verrà poi valutata non sono utilizzando un modello lineare, ma anche investigando quello che succede in campo plastico, tenendo in considerazione i processi di plasticizzazione della struttura.

Contents

List of Figures

List of Tables

Chapter 1

Introduction

1.1 General aspects

Precast concrete is an alternative to cast-in-situ concrete. While cast-in-situ concrete is cast in its actual location, precast concrete is cast at another location and is then lifted to its final resting place and fixed securely. This means that unlike cast-in-situ construction, which is monolithic or continuous, precast concrete buildings are made of separate pieces that are bolted or connected together. This kind of structures gained a wide popularity since the second half of the 19-th century, where they were used as industrial, commercial, and in some cases also residential buildings, with the main frame system enclosed at each side by pre-cast concrete panels (Figure *1.1*). The large diffusion of such structures puts in evidence the aspect related to the safety which must be assured to the people working or living inside.

Figure 1.1: Pre-cast structure with cladding panels

During an earthquake, the effect of the seismic actions produce consequences not only on the structural frame, but affects also the lateral infils elements, cladding panels, which enclose the internal spaces. The panels are connected to the primary system by means of anchoring system placed both at the ground level and on top of the frame. In such cases, the consequence of a seismic event is the generation of internal stresses in these anchoring

devices. The inadequate seismic behaviour of the cladding panel connections and their consequent failure occured under recent earthquakes, this gave rise to the necessity for a revision of the design philosophy adopted for this kind of structures.

(a) (b)

(c) (d)

Figure 1.2: Behaviour of the cladding panels: (a) and (b) collpase of the panels, (c) and (d) damages at the connections

In the current work, the presented problem is analyzed in detail, modelling the structure as a linear 1 DOF oscillator, where the presence of the cladding panels is accounted through a correction coefficient which modifies the natural period of the model. The key point however is related to the fact that the effects of the ground motion is here seen as the contribution of an additional fictitous mode characterized by infinite frequency. In this way the forces at the connections will depend on the contribution of two modes: (1) the principal mode of the structure, (2) the second one modelled as if the structure had infinite stiffness. By representing the specified earthquake as a random process, the goal is to compute the maximum values of the above mentioned actions for any seismic event. To do so, a linear Response Spectrum method based on the modal combination using the CQC rule is here adopted, avoiding the high computational costs required by a time history analysis.
Another way could have been to rely on a probabilistic handling of the assigned seismic action, which would allow for the full statistical character-

ization of the response of linear systems in the modal space, including the response peak distribution, avoiding the combination of modal responses. However, if on one hand the random vibrtion approach is appealing from the statistical point of view, on the other hand it is not yet accepted as a method of analysis by practitioner engineers and design codes. Together with the fact that, by following this path, the analytical evaluation of the peak factors would have been much more complex and time consuming. This is why a Response Spectrum method is here adopted, which exploits the basics of the superposition principles of modal analysis, making use of the random vibration theory only when it comes to compute the correlation coefficients entering the CQC rule.
To do so, two important points must be tackled:

1. the definition of a Response Spectrum compatible Power Spectral Density (PSD)

2. the correct evaluation of the correlation between modes, needed to properly compute the peak value of the response

Reagrding point 1, number of methods have been proposed for the generation of a RS compatible PSD. Here an analytical model is exploited, which provides a parametric formulation for the compatible PSD, where the coefficients are evaluated as closed form functions of the seismic codes RS parameters.
For what concerns the second point, early rational approaches tried to take this correlation into account by introducing cross modal terms depending on the duration of the earthquake, as well as modal frequency and damping ratio values. With time, additional procedures relying on more refined models were defined. In particular, the motion produced by earthquake accelerations is random in nature, and so in order to capture this aspect, more advanced approaches taking full advantage of stochastic analysis have been proposed. Therefore, by looking at the ground motion as a stationary, gaussian and zero mean event, then the input process is simply defined by its Autocorrelation function, or alternatively, by the corresponding PSD. In addition, if the system is linear and with constant coefficients, the response process after the transient phase, that can be very short if the system is stiff and damped enough, preserves the same properties of the input and so it is stationary, gaussian and zero mean process. In this way the response of the structure can be characterized from the stochastic point of view by its PSD. Several works took advantage from these considerations, adopting the concepts typical of random vibration analysis. At the end, in order to obtain the required correlation coefficients, one must first of all compute the related spectral moments, and this requires the resolution of the convolution integral involving the expression of the Response Spectrum compatible PSD previously obtained. The problem can be easily solved by means of numerical integration. However, in order to obtain an analytical solution of the problem, a manipulation of the expressions providing a RS compatible

PSD is needed, thus simplifying the complexity of the computations. Different analytical formulations will be proposed, and the results obtained by means of the Response Spectrum method will be compared.
However, the structural behavior of pre-cast structures is highly non-linear, even for small displacements. The problem is that no reliable information are available to determine in a rigorous way the most proper value of the behaviour factor to be used. Therefore, relevant inaccuracies in the determination of the seismic response are introduced.
This is why, the second part of the thesis will be devoted to the validation of the above mentioned RS method also in the non linear field.
A non linear time history analysis (NLTHA) is for sure the method able to provide the most reliable results, due to the fact that seismic response of a structure is always dynamically non linear. This procedure however is not so widespread, first of all due to the difficulties in the choices of the structural variable to adopt in the post-elastic field, and second for its high computational costs.
This justtifies the choice to limit the NLTHA as a final verification step, rather than a design method. The right compromise between the simplifications offered by a linear analysis, and the complexity of a non linear analysis in time, is represented by a non linear static analysis. The method is much more handy and immediate, providing the response of a highly nonlinear structure in terms of maximum displacement and maximum shear force. Such informations will be then exploited to implement the RS method after plasticization occurs. On the other hand the numerical outputs coming from the NLTHA are used as reference results.

1.2 Literature review

The problem regarding the evaluation of the maximum values of the reaction forces at the connections between the frame and the cladding panels of pre-cast industrial buildings is a topic not already well treated by the engineering community. This is why, in order to get a first hint on how to characterize these actions, the work of other authors on analogous problems have been analyzed. Of great importance to this purpose has been the work of Der Kiureghian and Pozzi [1]. Here the authors presented a method for evaluating the peak floor acceleration for a shear walls structure, in which the forces generated at the floor levels share a certain similarity with the cladding forces under investigation. The method accounts for the rigid contribution of the truncated higher modes, where the ground acceleration is seen as the contribution assured by an hypothetical infinite frequency mode of the structure. Cacciola et al [18], like other authors, proposed a formulation to be adopted for the combination of modes in the evaluation of the peak response. They stated how it was possible to approximate the correlation coefficients by referring to a white noise excitation when the duration of the earthquake is much longer than the period of the modal oscillators. However when a structure has significant modes outside the range of input frequencies, the above assumption fails. A possible solution is to characterize the seismic event by means of its Power Spectral Density, allowing for a simple evaluation of the correlation coefficients by using the tools provided by the random vibration theory. The advantages of this approach are pointed out by Der Kiureghian and Pozzi [2] in which the authors present the benefits of exploiting the principle of a stochastic analysis for the seismic design of nuclear power plants to circumvent the costs of the time history analysis based on artificially generated accelerograms. Unfortunately, most seismic codes characterize the ground motion by means of the elastic spectra. Therefore, a spectral representation of a seismic event coherent with the assigned Response Spectrum is needed. In their seismic analysis of submerged floating tunnels, Martinelli et al [3], proposed a procedure which is centered around the fact that the parameters defining the PSD are the output of a numerical procedure aiming at minimizing the difference between the resultant median Pseudo acceleration Spectrum of the generated time histories and the EN1998 Spectra. An alternative method was proposed by Falsone and Neri [4], in which the authors used an iterative procedure, introducing at the end the concept of filter equations in order to correct the approximated shape obtained for the PSD. Another very handy and accurate model was instead proposed by Cacciola et al [18], in which the authors highlighted the fact that, if the input is wide-banded and the oscillator frequency is not far beyond the significant range of input frequencies, the parameters entering the equation of the input variance are not too sensitive to the PSD shape. This allows to approximate the actual ground acceleration PSD with a constant piecewise function, allowing for a direct formulation of the PSD expression itself. For the aims of this work however, great benefits were assured by taking advantage from the formulation

proposed by Barone et al [5]. The authors, in order to define an analytic PSD function, performed an extensive numerical campaign by varying the intensity and shape of the assigned RS. It was observed that the method always returns numeric PSD functions having the same qualitatively shape. Hence, it is straightforward to describe the PSD function as a four-branches piecewise function. For what concerns the analytical evaluation for the correlation coefficient ρ_{ij}, of great importance has been the work by Vincent Denoel [6] on the timescale separation technique to be used for the computation of spectral quantities, which is related to the fact that the existence of multiple time scales in the response translates into the existence of several well-distinct peaks in the spectra.
A comparison with the formulations proposed by Moschen et al [7] and Der Kiureghian et al [8] in hypothesis of white noise input is proposed. On the other hand, the second part of the work will be instead focused on the analysis of the structure in the non linear field. The goal is to verify the validity of the RS method also when the elastic behaviour assumption is not valid anymore. Of great importance to understand the main features of the problem has been the work by Dal Lago et al [9]. The authors dealt with seismic retrofitting of industrial buildings, with precise indications on how to properly model the non linearities of the structure.

1.3 Objective of the work

Summing up, the work here presented is centered around the computation of the forces which arise at the connections between the frame and the cladding panels in industrial structures. In particular the main goal is to define a simplified analytical formulation of the problem, avoiding the necessity to make use of heavy numerical analysis.
To do so, the thesis is organized in three main parts:

1. Definition of an analytical method providing a Response Spectrum compatible Power Spectral Density

2. Implementation of the Response Spectrum method in the elastic field

3. Implementation of the Response Spectrum method after plasticization occurs

This is why, the theory background, the proposed formulations and the presentation of the results will be organized in the following chapters:

- Chapter 2 will be devoted to revise the basic principles and the main aspects associated to the concept of Spectral analysis

- Chapter 3 deals with the concept of RS compatible Power Density. After revising the works of some authors, the adopted analytical PSD formulation is presented

- Chapter 4 introduces the theory behaind the Response Spectrum method proposed by der Kiureghian et al [8], presenting the main aspects and assumptions adopted by the author

- Chapter 5 faces for the first time the analytical formulation for evaluating the forces at the connections. Starting from the equation of motion for the SDOF oscillator, and exploiting the principles proposed by Der Kiureghian et al [1] it provides at the end the complete formulation of the CQC rule, accounting for the influence of the cladding panel.

- Chapter 6, Chapter 7 and Chapter 8 are devoted to present the different analytical formulation adopted in this work to obtain the coefficient of correlation. In particular

  - Chapter 6 treats the theories proposed by Der Kiuregian [8] and Moschen [7] in hypothesis of white noise
  - Chapter 7 provides the results obtained via Denoel's Multiple Timescale spectral theory
  - Chapter 8 explains the analytical results obtained by exploiting the computational capacity of the *CAS* (Computer Algebra System) *wxMaxima*

- Chapter 9 contains the final results obtained by means of the different formulations

As mentioned, the second part of the work is devoted to the analysis of the model in the non linear field. To do so, thanks to the software *Straus7*, a finite element model is defined. However, before entering the non linear analysis, a validation of the results obtained in Chapter 9 is proposed. This was needed due to the fact that the results proposed in Chapter 9 are based on the assumption of infinite rigid panels. In reality however, these elements are not completely rigid, with intrinsic vibration modes. Summing up, Chapter 10 has two goals: (1) to validate the proposed analytical formulations based on the hypothesis of rigid panel behavior, and (2) to build the FE models which will be used later for the non linear analysis.
Finally, Chapter 11 and Chapter 12 will deal with the analysis the post elastic behaviour of the models. In particular:

- Chapter 11 will be devoted to present the results obtained through the implmentation of the NLTHA implemented with Straus7 for the differrnt models implemented. These results will be used as reference solutions.

- Chapter 12 will be focused on the valdation of the RS method when the structure enters the non linear behaviour.

Final considerations and conclusions are reported in Chapter 13

Chapter 2

Basic principles of the spectral analysis

In the majority of the building codes the seismic actions are defined in terms of the expected maximum response of a single-degree-of freedom (SDOF) system in terms of pseudo-acceleration Response Spectrum (RS). The RS represents the absolute maximum value of a selected response parameter experienced, during the so called design earthqueke, by a SDOF system varying its natural period, and for a selected value of the damping ratio. A building code RS curve is determined by the expected SDOF system response at a particular site. The RS analysis however is strictly valid only for linear SDOF systems, and its use for the evaluation of MDOF systems implies some approximations. [5]
Conversely, a proper probabilistic handling of the assigned seismic action would allow for the full statistical characterization of the response of linear systems in the nodal space, including the response peak distribution, avoiding the combination of modal responses and allowing for an effective assessment of the structural reliability. [10]
It is recognized that the most rigorous way of modelling the seismic excitation is to consider zero-mean Gaussian processes that, under some assumptions, can also be assumed as stationary. The complete probabilistic characterization of the input can be then achieved by the knowledge of its Power Spectral Density (PSD) function. [11] However, if on one hand the random vibration approach is appealing for its statistical nature, it is not yet accepted as a method of analysis by practitioners engineers. Furthermore, most seismic design codes specify the earthqueke motion in terms of the response spectrum, and not the PSD. It is therefore desirable to develope a method of analysis based on the response spectrum specification of the input motions, and which is able to incorporate the fundamental notions of the random vibration theory.

This is exactly how the Response Spectrum method adopted for the aim of this thesis works. In particular, the Complete Quadratic Rule is organized in such a way that: (1) the seismic input are provided in terms of the ordinates of a EC8 prescribed Response Spectrum, while (2) the correlation

are computed by exploiting the results of the spectral analysis. In the next paragraph, the concept of Power Spectral Density and Frequency response Function are introduced.

2.1 Input-Output response

Many engineering applications are based on the input/output representation of a system, which is well suited to study the stochastic response of deterministic systems to random input. There is a wide variety of such applications in the various fields of engineering, and the response of a civil structure under seismic actions is one of them [11]. In many of these applications the timescales T associated with the system are significantly different from those t of the loading, so that the response turns out to be a composition of components with different timescales [12].
Traditional simulation techniques turnes out to be not efficient for the resolution for these kind of problems, due to the fact that they would have to simultaneously resolve the different scales, relying on a very short time steps, causing very long simulations. On the other hand, stochastic spectral analysis appears as a valuable tool to solve these issues. Indeed, the loading is usually given with a spectral representation, i.e. a set of spectra defined on multidimensional frequency spaces. [13]
Among them, the above mentioned PSD, represents the distribution of the variance of th process over the frequency domain. More generally, the *j-th* order spectrum represents the distribution of the *j-th* stationary cumulant over a frequency domain of dimension $R^{(j-1)}$.
The objective of a spectral analysis is to determine the spectra of the response in terms of those of the input and eventually integrate them in the corresponding frequency spaces in order to determine the cumulants of the response. A canonical version of the spectral analysis, is the one in which the *j-th* order spectrum of the response is defined as:

$$\mathbf{S_x}(\mathbf{w^{(j)}}) = H(w^{(j)})H^{(*)}(w^{(j)})S_p(w^{(j)}) \tag{2.1}$$

where $w^{(j)} = w1, .., w_{j-1}$ with $j > 1$, gathers the independent variables of the frequency space, $H(w^{(j)})$ is the frequency kernel function, $H(w^{(j)})^{(*)}$ represents its conjucated, and $S_p(w^{(j)})$ and $S_x(w^{(j)})$ respectively stand for the *j-th* order spectra of the loading and of the response.
A brief explaination of the theory behind the above mentioned variables is reported in the next paragraphs.

2.2 Fourier Transform

Before dealing with the concept of Frequency Response Function and Power Spectrum, another point must be tackled first: the notion of Fourier analysis.
The theory behind the Fourier analysis has a wide range of applications

in various scientific and mathematical fields. By considering the case of a SDOF system under the effect of a loading repeating in time for equal time intervals T, Fourier proved how such periodic function can be expressed as a summation of a number of infinite sinusoidal terms (sine and cosine). Such summation is known as *Fourier series*. In particular, a periodic function $F(t)$ can be rewritten as:

$$\begin{aligned} F(t) &= a_0 + a_1 \cos wt + a_2 \cos 2wt + a_3 \cos 3wt + ... + a_n \cos nwt + \\ &= b_1 \sin wt + b_2 \sin 2wt + b_3 \sin 3wt + ... + b_n \sin nwt \end{aligned} \tag{2.2}$$

where $w = \frac{2\pi}{T}$ is the frequency, while T is the period of the function. For what concerns the coefficients a_0 a_n and b_n, they can be evaluated as:

$$\begin{aligned} a_0 &= \frac{1}{T} \int_{t_1}^{t_1+T} F(t)dt \\ a_n &= \frac{2}{T} \int_{t_1}^{t_1+T} F(t) \cos nwtdt \\ b_n &= \frac{2}{T} \int_{t_1}^{t_1+T} F(t) \sin nwtdt \end{aligned} \tag{2.3}$$

where t_1 is usually assumed equal to $\frac{T}{2}$ or zero. The expressions of (2.3) can be rewritten in exponential form, by substituting the trigonometric functions with their Euler formulation:

$$\begin{aligned} \sin nw &= \frac{e^{inw} - e^{-inw}}{2i} \\ \cos nw &= \frac{e^{inw} + e^{-inw}}{2} \end{aligned} \tag{2.4}$$

obtaining:

$$F(t) = \sum_{n=-\infty}^{\infty} c_n e^{inwt} \tag{2.5}$$

where:

$$c_n = \frac{1}{T} \int_0^T F(t) e^{-inwt} dt \tag{2.6}$$

In general however, random vibrations are not periodic in time, therefore the frequency analysis requires an extensions of the Fourier series to the case of non periodic functions, the *Fourier transform.*, which allow for a wider treatment of the problem of random vibrations.
The Fourier transform can be seen as the integral of the Fourier series as the period of the function goes to infinite. In particular, by replacing (2.6) in (2.5), and by using a fictitous time variable τ instead of t:

$$F(t) = \sum_{n=-\infty}^{\infty} \frac{1}{T} \int_{-T/2}^{T/2} F(\tau) e^{-inw\tau} e^{inw\tau} d\tau \tag{2.7}$$

Now, by considering the limit of $T \to \infty$:

$$F(t) = \frac{1}{2\pi} \int_{-\infty}^{\infty} \Big[\int_{-\infty}^{\infty} F(\tau) e^{-iw\tau} d\tau \Big] e^{iwt} dw \tag{2.8}$$

which is the Fourier integral for $F(t)$.
Now, since the function inside the square brackets is dependent on w only, (2.8) can be split into two parts:

$$C(w) = \frac{1}{2\pi} \int_{-\infty}^{\infty} F(\tau) e^{-iw\tau} d\tau \tag{2.9}$$

and

$$F(t) = \int_{-\infty}^{\infty} C(w) e^{iwt} dw \tag{2.10}$$

The validity of these two relation is based on the condition:

$$\int_{-\infty}^{\infty} |F(t)| dt < \infty \tag{2.11}$$

The function $C(w)$ is the so called *Fourier transform* of $F(t)$, and the two forms the so called *Fourier transform couple*.

2.3 Power Density Spectrum

Before dealing with the definition of Power Spectrum, a brief introduction to the concept of *correlation* is needed. The correlation is a measure of the dependency between two random realzizations.
By considering the two signals represented in Figure (*2.1*), the correlation between them is computed by multiplying the ordinates of the two for each time instant t, computing at the end the average of all the values.
Now, by considering as before two realizations $x_1(t)$ and $x_2(t)$, where in this case $x_1(t)$ has the same behaviour of $x_2(t)$, but it is simply tranlated in time by a quantity τ, $x_1(t) = x_2(t+\tau)$. Then the correlation between $x_2(t)$ and $x_1(t)$ is known as *autocorrelation function* $R(\tau)$, and it is defined as:

$$R(\tau) = \lim_{T\to\infty} \frac{1}{T} \int_0^T x(t)x(t+\tau)dt \tag{2.12}$$

When $\tau = 0$, the autocorrelation reduces to the average of the squares:

$$R(0) = \lim_{T\to\infty} \frac{1}{T} \int_0^T |x(t)|^2 dt = \bar{x^2} \tag{2.13}$$

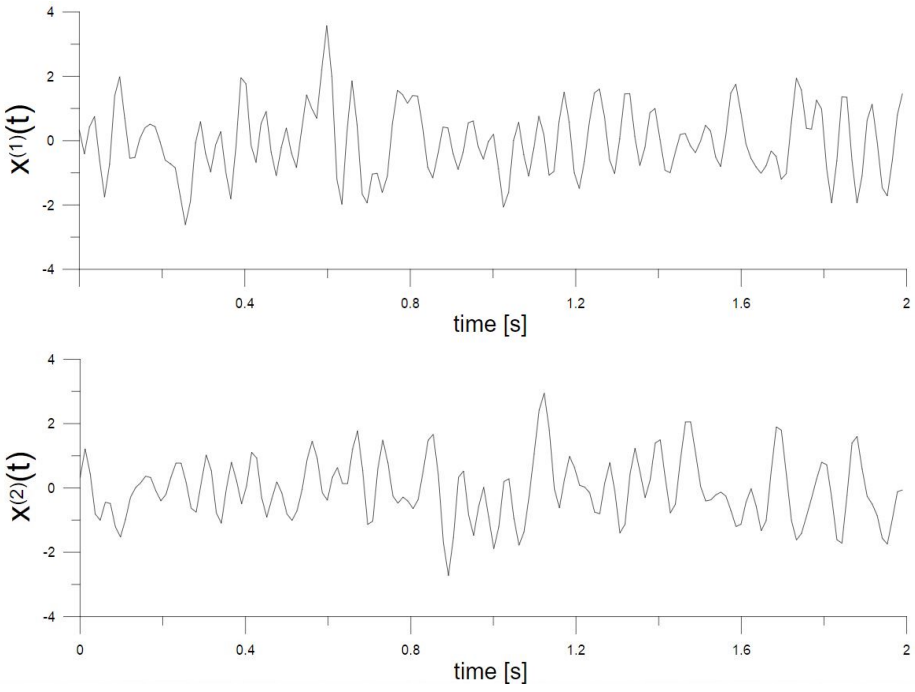

Figure 2.1: Random realizations in time

Given the fact that the second realization $x_2(t)$ is delayed wrt the first one, it happens that $R(\tau) = R(-\tau)$ is symmetric wrt the origin, and $R(\tau)$ is always lower than $R(0)$. Finally, if a random realization $x(t)$ is normalized in such a way that the average value of the process is zero, then, by assuming that $x(t)$ has no periodic components, its autocorrelation function $R_x(\tau)$ tends to zero as τ increases:

$$\lim_{\tau \to \infty} R_x(\tau) = 0 \tag{2.14}$$

This to say that, if $R_x(\tau)$ satisfies condition (*2.14*), it is possible to apply (*2.9*) and (*2.11*) in order to obtain the Fourier transform of $R_x(\tau)$ and its inverse:

$$S_x(w) = \frac{1}{2\pi} \int_{-\infty}^{\infty} R_x(\tau) e^{-iw\tau} d\tau \tag{2.15}$$

and

$$R_x(\tau) = \int_{-\infty}^{\infty} S_x(w) e^{iwt} dw \tag{2.16}$$

where $S_x(w)$ is the so called Power Spectral Density Function (PSDF) for the realization $x(t)$
The most important property of $S_x(w)$ is expolited when considering $\tau = 0$ in (*2.16*):

$$R_x(0) = \int_{-\infty}^{\infty} S_x(w) 0 dw \tag{2.17}$$

and by recalling relation (*2.13*):

$$\bar{x^2} = \int_{-\infty}^{\infty} S_x(w) dw \tag{2.18}$$

This means that that the the average value of the square of a realization, i.e. its energy content, is represented by the area envelope by the diagram of the PSDF.

2.4 Frequency Response Function

The kernel operator $H(w^{(j)})$ which enters (*2.1*) is the so called Frequency Response Function (FRF), which provides in the frequency domain the response of a MDOF system starting from the input loading.
Now, by focusing on the domain of interest R^1, to arrive to its formulation, it is needed to start by considering the time response $x(t)$ of a MDOF linear system:

$$x(t) = \int_{-\infty}^{\infty} h(t-\tau) p(\tau) d(\tau) \tag{2.19}$$

with $h(t)$ being the impulse response function of the system and $p(t)$ the multiple-point excitation input.
In the frequency domain, the frequency response $X(w)$ emerges by the application of the *Fourier transform operator* :

$$F[y(t);w] = \int_{-\inf}^{\inf} y(t)e^{-i\varepsilon}dt \tag{2.20}$$

to each member of (*2.19*), where i is the complex unit. The final result is:

$$X(w) = H(w)P(w) \tag{2.21}$$

as a consequence of the duality theorem.
By making the functional dependencies explicit, (*2.21*) can be re-written in a more detailed form, which will be adopted throughout the work:

$$X(\hat{w}, w_i, \xi_i) = H(\hat{w}, w_i, \xi_i)P(\hat{w}) \tag{2.22}$$

being $\hat{w}$ the forcing frequency, w_i the structural frequency associated to the $i-th$ mode, and ξ the structural damping coefficient.

2.5 Spectral analysis

In the last years it has been recognized that the most accurate way of modelling the seismic actions which affect the structural systems is by making use of the concept of Gaussian stochastic processes; moreover, if the strong motion phase dominates the earthquake, and the structural system is linear, stiff and damped enough, then the seismic exitation can be approximated as a stationary event [4]. As a consequence, the seismic motion can be stocastically characterized by the only knowledge of its time independent PSD. Under these assumptions on the input process, the transient phase of the system can be very short wrt to the earthquake duration time, therefore the structural response can be considered a stationary process as well. Thus it can be stochastically characterized by the knowledge of its PSD.
This to say that, the frequency domain approach (*2.21*) is well suited to study the response of deterministic structures subjected to stacastic loading, since both the response $X(w)$ and the loading $P(w)$ are viewed as stochastic processes.
Therefore, under the general assumptions presented before:

$$S_X(\hat{w}, w_i, \xi_i) = H(\hat{w}, w_i, \xi_i)S_P(\hat{w})H^*(\hat{w}, w_i, \xi_i) \tag{2.23}$$

The aim of the spectral analysis is associated to the computations of the response spectral moments:

$$\lambda_{ij} = Re\Big[\int_0^{\inf} H_i(\hat{w}, w_i, \xi_i)H_j^*(\hat{w}, w_i, \xi_i)S_P(\hat{w})d\hat{w}\Big] \tag{2.24}$$

Finally, the correlation coefficient needed for the CQC rule will be defined as:

$$\rho_{ij} = \frac{\lambda_{ij}}{\sqrt{\lambda_{ii}\lambda_{jj}}} \tag{2.25}$$

The first challenge is to set up a robust procedure to define a PSD function compatible with the assigned RS. In the last decades, great attention has been devoted to develop analytic and numeric techniques aiming at obtaining refined models of RS-compatible PSD functions. Some reference analytical and semi-analytical formulation are presented in the next chapter.

Chapter 3

Analytical definition of a Response Spectrum compatible Power Spectral Density

As stated in Chapter 2, the most rigorous way of modelling the the seismic exitations is to consider zero-mean Gaussian processes that, under some assumptions, can also be assumed as stationary.
Recently, the European codes, by means of the Eurocode 8, have introduced the possibility to design in seismic zones by applying the principles of stocastic analysis. However, the earthquake exitation is usually assigned by means of the Pseudo acceleration RS, without indicating how to evaluate the corresponding PSD [5].
This is not an easy task. There are however some methods in literature able to provide the power spectrum starting from the assigned elastic RS.
A common approach to model earthquakes in a stochastic framework is to define filter equations returning the earthquake excitation as response to a white noise. The most used filter is the Tajimi-Kanai one. Some authors, like Falsone et al [4], proposed a technique to obtain the filter coefficients for Eurocode 8 RS.
Quite interesting techniques for generating spectrum-compatible PSDs are proposed in the works of Martinelli et al [3] and Cacciola et al [**?**], where the authors provided a solution relying on iterative numerical procedures.
An analytical model was instead proposed by Barone et al [5]. By starting from the results proposed by other authors ([14], [4]), they were able able to further generalize the proposed formulation, in order to make it compatible with a very large range of international seismic codes. The required parameters are analytically evaluated as closed-form functions of the seismic codes RS parameters.
The proposed model can be used in place of the RS, so that the practitioner engineer can define the seismic action directly in terms of PSD function and utilize stochastic analysis tools.

3.1 Compatibility condition

A very wide of pseudo-acceleration Response Spectra reported in international building codes can be represented by means of the following four-branches expression:

$$S_a(T) = \begin{cases} S_0[1 + (\alpha - 1)\frac{T}{T_B}] & \text{se } 0 \leq T \leq T_B \\ S_0\alpha & \text{se } T_B \leq T \leq T_C \\ S_0\alpha(\frac{T_C}{T})^{k_1} & \text{se } T_C \leq T \leq T_D \\ S_0\alpha(\frac{T_C}{T_D})^{k_1}(\frac{T_D}{T})^{k_2} & \text{se } T > T_D \end{cases} \tag{3.1}$$

where T is the natural period of the SDOF system, S_0 is the peak ground acceleration, α is the dynamic amplification factor, T_B, T_C and T_D are the periods delimitating the various branches, and k_1 and k_2 are shape factors. The RS defined by (*3.1*) is qualitatively represented in Figure *3.1*. The first branch linearly connects the point at $T = 0$ at the second branch. The second, third and fourth branches of the model corresponds respectively to constant spectral accelerations, velocities and displecements.

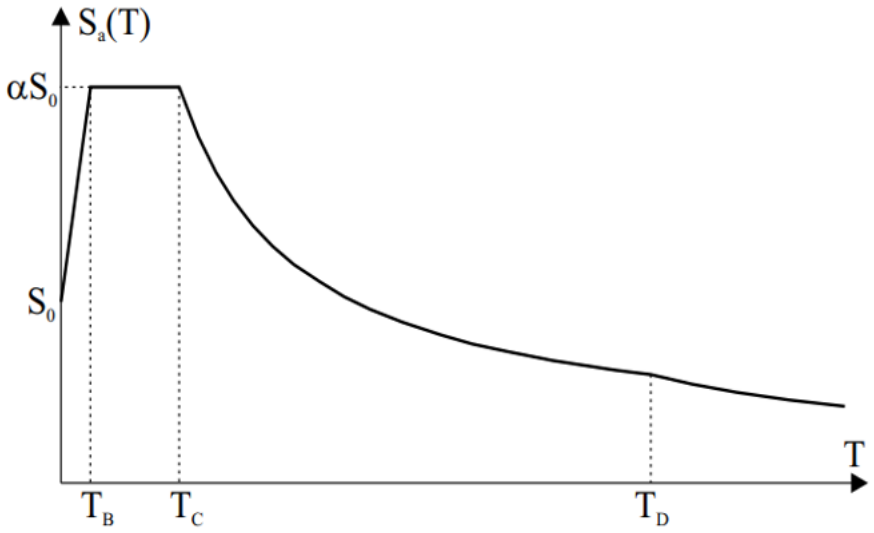

Figure 3.1: Pseudo acceleration Response Spectrum

The goal now is to define a PSD function which is compatible with the codes Response Spectrum. According to Eurocode 8, consistency is achieved when the 50 % fractile values of the peak responses of a SDOF system subjected to the seismic process represented by the PSD coincides, within a tolerance of $+/-10\%$ with the ordinate of the given elastic response spectrum, for a range of periods from 0.2 to 3.5 seconds.
Due to the shapw of the distribution of the response maxima, the 50% fractile can be approximated by the mean value of the peak values. Therefore the pseudo acceleration RS can be evaluated as:

$$S_a(w_i, \xi_i) = \eta_{X_i} {w_i}^2 \sigma_{X_i} \tag{3.2}$$

where η_{X_i} and σ_{X_i} are respectively the peak factor and the standard deviation of the stochastic process X_i of a SDOF oscillator having frequency w_i and damping ξ_i. They are defined as:

$$\eta_{X_i}(T_s, p) = \sqrt{2ln2N_{X_i}[1 - exp[-\delta_{X_i}^1 .2\sqrt{piln(2N_{X_i})}]]} \tag{3.3}$$

where the spread factor δ_{X_i} and the parameter N_{X_i} of the response process X_i are:

$$\delta_{X_i} = \sqrt{1 - \frac{\lambda_{1,X_i}^2}{\lambda_{0,X_i}\lambda_{2,X_i}}} \tag{3.4}$$

$$N_{X_i} = \frac{T_s}{2\pi}\sqrt{1 - \frac{\lambda_{2,X_i}^2}{\lambda_{0,X_i}}}(-lnp)^{-1} \tag{3.5}$$

and

$$\lambda_{n,X_i} = \int_0^{inf} w^n G_{X_i}(\hat{w}) d\hat{w} \tag{3.6}$$

While, for what concerns σ_{X_i}:

$$\sigma_{X_i}^2 = \int_0^{\infty} G_{X_i} d\hat{w} \tag{3.7}$$

Once the PSD and the duration of the input are given, (*3.2*) gives a direct evaluation of the pseudo-acceleration RS. Due to the non linearity of (*3.2*), the inverse problem related to the evaluation of RS consistent PSD is not a trivial problem. As already presented, several methods are available in literature, but either they rely on heavy numerical procedures, or they do not reach a sufficient level of accuracy ([15], [16]).
There are however some authors able to derive quite fast and intuitive semi-analytical procedures for the evaluation of a compatible PSD. Three of these works are reported in the next section.

3.2 Semi-analytical methods

With the time, some direct iterative models able to ensure a good level of compatibility of the results have been developed. In order to have an idea on the possible paths which can be adopted, three of these methods are here briefly presented. Even if each of them relies on different procedures and assumptions, they are equally able to provide quite accurate results.

3.2.1 Der Kiureghian et al (1991)

The following formulation is similar to the one proposed by Kaul [15]. The derivation is based on the concepts of stationary randoma vibrations and assumes that the seismic motion is a wide-band process and the oscillator damping ratio ξ_i is small.
Now, by denoting as $G_{\ddot{u}_g}(w_i)_1$ the first order approximation of the unknown

PSD of the ground acceleration, the mean square response of an oscillator with frequency w_i and damping ξ_i can be approximated by:

$$\lambda_0(w_i)_0 = \frac{\pi G_{\ddot{u}_g}(w_i)_1}{2\xi_i w_i^3} \tag{3.8}$$

Now, by using this approximation in the identity $S_a(w_i, \xi_i) = \eta(w_i)[\lambda_0(w_i)_0]^{1/2}$, where $S_a(w_i, \xi_i)$ are the ordinates of the target Response Spectrum, it is possible to obtain:

$$G_{\ddot{u}_g}(w_i)_1 = \frac{2\xi_i w_i^3}{\pi}\left[\frac{Sa(w_i, \xi_i)}{\eta(w_i)_0}\right] \tag{3.9}$$

Now, for what concerns the peak factor, at the fisrt iteration, the following approximation can be used to compute $\eta(w_i)_0$

$$\eta_0 = \sqrt{2\log(f_0 T_s)} + \frac{\gamma}{\sqrt{2\log(f_0 T_s)}} \tag{3.10}$$

being T_s the duration of the event, $\gamma = 0.577$ the Euler constant, f_0 the average frequency of the process. Now that the first order approximation $G_{\ddot{u}_g}(w_i)_1$ of the PSD is available, it is possible to proceed with the second iteration. The spectral moments of the first order can be computed as:

$$\lambda_m(w_i)_r = \int_0^\infty H_i(\hat{w}, w_i, \xi_i) H_i^{(*)}(\hat{w}, w_i, \xi_i) G_{\ddot{u}_g}(\hat{w})_r d\hat{w} \tag{3.11}$$

Then, by using (*3.3*), the peak factor at the next iteration is obtained.
A second order approximation can be obtained by replacing the terms $\frac{2\xi_i w_i^3}{\pi}$ and η_0 by the new ones, which are $\frac{G_{\ddot{u}_g}(w_i)_1}{\lambda_0(w_i)_1}$ and $\eta_1(w_i)$ respectively:

$$G_{\ddot{u}_g}(w_i)_2 = \frac{G_{\ddot{u}_g}(w_i)_1}{\lambda_0(w_i)_1}\left[\frac{Sa(w_i, \xi_i)}{\eta(w_i)_0}\right]^2 \tag{3.12}$$

By repeating the process, the $r+1$-th approximation of the PSD function is:

$$G_{\ddot{u}_g}(w_i)_{r+1} = \frac{G_{\ddot{u}_g}(w_i)_r}{\lambda_0(w_i)_r}\left[\frac{Sa(w_i, \xi_i)}{\eta(w_i)_r}\right]^2 \tag{3.13}$$

3.2.2 Falsone et al (1999)

The fundamental idea of this formulation is based on the work of Di Paola et al [17]. The center of the procedure is related to the fact tha the frequency axis is subdivided into a set of N discrete intervals of amplitude $\Delta w_k = w_{k+1} - w_k$, inside which the PSDF is considered to be constant:

$$G_{\ddot{u}_g} = \sum_{k=1}^{N} G_k U(\Delta w_k) \tag{3.14}$$

where G_k is the spectral value in the interval Δw_k, while $U(\Delta w_k)$ is the window function equal to one inside the interval and zero outside.
Now, for a SDOF system characterized by a natural frequency w_i and a damping ratio ξ_i, exitated by an input having the PSD function discretized as in (*3.14*), it is possible to compute the spectral moments as follows:

$$\lambda_n = \sum_{k=1}^{N} \int_{w_k}^{w_k+1} w^n |H(\hat{w}, w_i, \xi_i)|^2 d\hat{w} G_k \tag{3.15}$$

where the $H(\hat{w}, w_i, \xi_i)$ is the FRF defined as:

$$H_i(\hat{w}, w_i, \xi_i) = \frac{1}{{w_i}^2 - \hat{w}^2 + 2i\xi_i w_i \hat{w}} \tag{3.16}$$

The innovative idea of the present work is to consider (*3.15*) by varying the system natural frequency w_i with the same step number N as used for the discretization of the PSDF. Then it is possible to rewrite the same equation as:

$$\lambda_m = C_m G \tag{3.17}$$

with $m = 0, 1, 2$. In particular, λ_m are the response spectral moments vectors of order N collecting the N values of the $m - th$ response spectral moments, varying the natural frequency w_i of the system. G is the exitation PSD vector collecting the N values G_k of the exitation PSDF; finally the matrice C_m collects the coefficients given into equations (*3.15*). Having chosen the same step number both for the natural frequency w_i of the SDOF system and for th discretization of the function $G_{\ddot{u}_g}$, matrice C_m is singular, therefore it can be inverted.
Hence, an iterative procedure to construct an analytical approximation of PSDF, starting from the elastic resposnse spectrum, can be implemented by the following steps:

1. trial values of the spectral moments λ_m are assigned
2. the response peak coefficients $\eta_{X_i}(T_s, p)$ are evaluated through (*3.3*), (*3.4*) and (*3.5*) by varying the system natural frequency w_i
3. the response zero order spectral moments $\lambda_{0,X_i} = \sigma^2_{X_i}$ are evaluated by means of (*3.2*)
4. in this way the vector λ_0 is evaluated. Now, by inverting (*3.17*), the first trial of the PSDF, represented by G, is obtained.
5. the first and second order spectral moments are evaluated always by (*3.17*), but considering $m = 1, 2$.
6. having all the required spectral moments, the new peak factor can be evaluated by means of (*3.4*) and (*3.5*)
7. the new response spectrum ordinates obtained are then compared with the target ones. If convergence is not reached, the procedure restarts from point 3.

3.2.3 Cacciola et al (2004)

The last formulation presented is the one proposed by Cacciola et al [18]. The method is based on the direct evaluation of the RS compatible PSD by adopting some approximate assumptions for the spectral moments.
As it was presented before, the evaluation of the PSD $G_{\ddot{u}_g}(w)$ of the ground acceleration, which does not appear explicitly in (*3.2*), requires the evaluation of peak factor and variance of the SDOF system response, both depending on the input PSD itself. However, the following approximate relationship [10] for the variance of the response process can be assumed:

$$\sigma_{X_i}^2 = \frac{G_{\ddot{u}_g}(w)}{{w_i}^4}\Big(\frac{pi}{4\xi} - 1\Big) + \frac{1}{{w_i}^4}\int_0^{w_i} G_{\ddot{u}_g} dw \tag{3.18}$$

While, for what concerns the peak factor:

$$\eta_{X_i}(T_s, p) = \sqrt{2ln2N_{X_i}[1 - exp[-\delta_{X_i}^1 .2\sqrt{\pi ln(2N_{X_i})}]]} \tag{3.19}$$

where the spread factor δ_{X_i} and the parameter N_{X_i} of the response process X_i are

$$\delta_{X_i} = \sqrt{1 - \frac{\lambda_{1,X_i}^2}{\lambda_{0,X_i}\lambda_{2,X_i}}} \tag{3.20}$$

$$N_{X_i} = \frac{T_s}{2\pi}\sqrt{1 - \frac{\lambda_{2,X_i}^2}{\lambda_{0,X_i}}}(-lnp)^{-1} \tag{3.21}$$

and

$$\lambda_{n,X_i} = \int_0^{inf} w^n G_{X_j}(w) dw \tag{3.22}$$

As it can be seen, N_{X_i} e δ_{X_i} are both depending on the system response, but this is not known a priori. However, thanks to the fact that the two parametrs are not too sensitive to the input PSD shape, their approximate evaluation can be obtained by making reference to a white noise input [8]:

$$\delta_{X_i} = \Big[1 - \frac{1}{1-\xi^2}\Big(1 - \frac{2}{pi} arctan\frac{\xi}{\sqrt{1-\xi^2}}\Big)^2\Big]^{1/2} \tag{3.23}$$

$$N_{X_i} = -\frac{T_s}{2\pi}\frac{w_i}{ln(p)} \tag{3.24}$$

Once the actual ground acceleration PSD is approximate by a constant piecewise function, the integral in (*3.18*) can be replaced by a discrete summation, and substituted in (*3.2*), leading to

$$S_a^2(w_i, \xi_i) = \eta_{X_i}^2 G_{\ddot{u}_g}(w_i) w_i \Big(\frac{pi - 4\xi}{4\xi}\Big) + {\eta_{X_i}}^2 \Delta w \Big(\sum_{j=1}^{i-1} G_{\ddot{u}_g}(wj) + G_{\ddot{u}_g}(wi)\Big) \tag{3.25}$$

where $w_i = w_0 + (i - 0.5)\Delta w$ and the peak factor η_{X_i} have to be evaluated for a probability p=*0.5* and for the assigned input duration T_s. The value

of w_0 is chosen as the lowest bound of the existence domain of (*3.18*) consistent with the assumed expressions for the mean zero crossing rate N_{X_i} and the spread factor δ_{X_i}.
Finally (*3.25*) leads to the following direct expression for the ground acceleration PSD:

$$G_{\ddot{u}_g}(w_i) = \frac{4\xi}{w_i pi - 4\xi w_{i-1}} \Big(\frac{S_a^2(w_i, \xi_i)}{\eta_{X_i}^2} - \Delta w \sum_{j=1}^{i-1} G_{\ddot{u}_g}(wj) \Big) \tag{3.26}$$

3.3 Analytical formulation (Barone et al, 2015)

Although the method proposed in (*3.26*) can be adopted to determine a PSD compatible with any building code RS, the numeric iterative procedure has to be entirely repeated for any variation of the RS parameters. This is why, the analytcal model proposed by Barone et al [5] is here presented. In order to define an analytic PSD function, an extensive numerical campaign has been performed by varying the intensity and shape of the assigned RS, as defined in (*3.1*), and evaluating the RS compatible PSD functions using the numeric procedure proposed in (*3.26*). It has been observed that the method always returns numeric PSD functions having the shape qualitatively reported in Figure *3.2*.

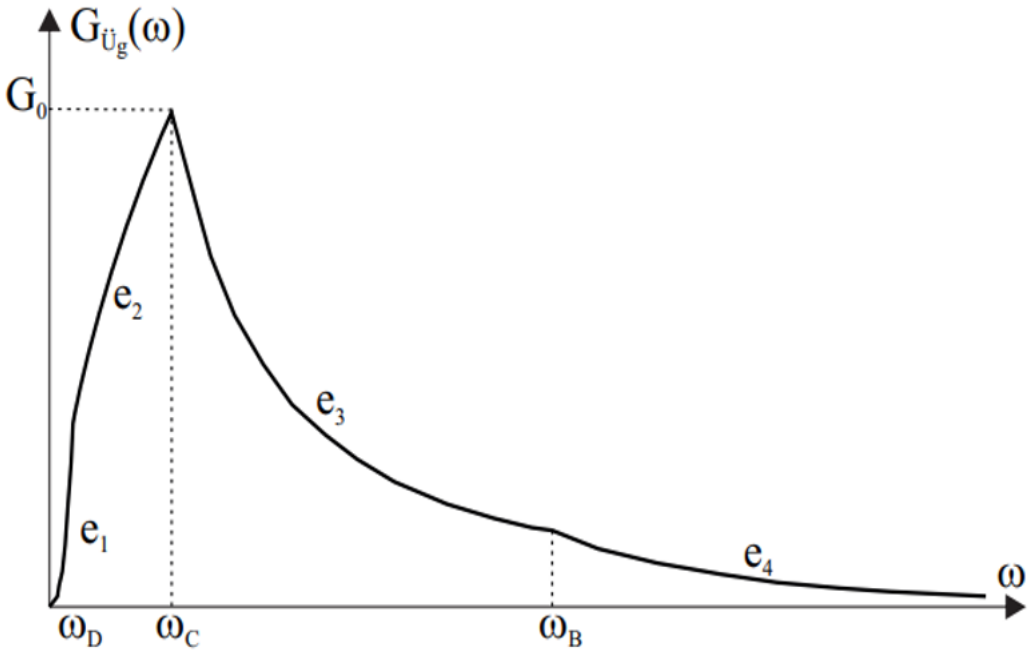

Figure 3.2: RS compatible PSD

This made it possible to describe the PSD function as a four-branches piecewise function having a simple mathematical structure and fully defined once

few parameters are known. Here is the proposed analytical function:

$$G_{\ddot{u}_g}(w) = \begin{cases} G_0(\frac{w_D}{w_C})^{e_2}(\frac{w}{w_D})^{e_1} & \text{se } 0 \leq w \leq w_D \\ G_0(\frac{w}{w_C})^{e_2} & \text{se } w_D \leq w \leq w_C \\ G_0(\frac{w}{w_C})^{e_3} & \text{se } w_C \leq w \leq w_B \\ G_0(\frac{w_B}{w_C})^{e_3}(\frac{w}{w_B})^{e_4} & \text{se } w > w_B \end{cases} \tag{3.27}$$

where G_0 represents the peak value of the PSD function at the frequency $w = w_C$. The proposed model is dependent on 5 parameters, namely G_0 and the four exponents e_1, e_2, e_3, e_4. Therefore, the PSD is fully defined by few parameters. Closed-form expressions for all the parameters can be determined by taking advantage of some simple considerations, as reported in the following paragraph.

3.3.1 Evaluation of the Power Spectrum parameters

For the sake of clarity, the general form of the Response Spectrum of (*3.1*), is herein reported as a function of the circular frequency:

$$S_a(T) = \begin{cases} S_0\alpha(\frac{w_D}{w_C})^{k_1}(\frac{w}{w_D})^{k_2} & \text{se } 0 \leq w \leq w_D \\ S_0\alpha(\frac{w}{w_C})^{k_1} & \text{se } w_D \leq w \leq w_C \\ S_0\alpha & \text{se } w_C \leq w \leq w_B \\ S_0[1 + (\alpha - 1)\frac{w_B}{w}] & \text{se } w > w_B \end{cases} \tag{3.28}$$

To determine the exponent e_1, (*3.26*) is rewritten for the frequency w=w_C:

$$G_0 \frac{{w_D}^{e_2+1}}{w_C^{e_2}} = \frac{\gamma}{w_D}\left[\alpha^2\left(\frac{S_0\left(\frac{w_D}{w_C}\right)^{k_1}}{\eta_{X_i}(w_D)}\right)^2 - \int_0^{w_D} G_{\ddot{u}_g}(w)dw\right] \tag{3.29}$$

where $\gamma = \frac{4\xi}{pi-4\xi}$. Now, by substituting (*3.27*) inside the integral term:

$$G_0 w_C \frac{w_D}{w_C}^{e_2+1}\frac{\gamma + e_1 + 1}{\gamma(e_1+1)} = \alpha^2\left(\frac{S_0\left(\frac{w_D}{w_C}\right)^{k_1}}{\eta_{X_i}(w_D)}\right)^2 \tag{3.30}$$

Then, following the same reasoning but considering a change of variable $w = \frac{w_D}{\rho}$ ($\rho > 1$), the following expression is obtained:

$$G_0 w_C \frac{w_D}{w_C}^{e_2+1}\frac{\gamma + e_1 + 1}{\gamma(e_1+1)} = \alpha^2\left(\frac{S_0\left(\frac{w_D}{w_C}\right)^{k_1}}{\eta_{X_i}(\frac{w_D}{\rho})}\right)^2 \rho e_1 + 1 - 2k_2 \tag{3.31}$$

Therefore, the comparison between (*3.31*) and (*3.30*) leads to:

$$e_1 = \frac{log\frac{\eta^2_{X_i}(\frac{w_D}{\rho})}{\eta^2_{X_i}(w_D)}}{log\rho} + 2k_2 - 1 \tag{3.32}$$

Now, by considering the limit for $\rho \to 1$ of (*3.32*), the exponent e_1 can be expressed in closed form as:

$$e_1 = 2k_2 - 1 - L(w_D) \tag{3.33}$$

where the function $L(w)$ is defined as:

$$L(w) = 2w\frac{d(log(\eta_{X_i}(w_D)}{dw} \tag{3.34}$$

The evaluation of the closed-form expressions for the other parameters is based on the same concepts, but considering points on the other three branches of the PSD. After some algebra, the following set of parameters is obtained:

$$\begin{aligned} e_2 &= 2k_1 - 1 - L(w_C) \\ e_3 &= -1 - \gamma - \beta_2 L(w_C) \\ e_4 &= -1 - \gamma - \beta_3\Big(L(w_B) + 2\frac{\alpha - 1}{\alpha} \\ G_0 &= \frac{\gamma}{\beta_2 w_C}\Big(\frac{\alpha S_0}{\eta^2_{X_i}(w_D)}\Big)^2 \end{aligned} \tag{3.35}$$

while the coefficients β_2 and β_3 are defined as:

$$\begin{aligned} \beta_2 &= \Big(\frac{w_D}{w_C}\Big)^{e_2+1}\frac{\gamma + e_1 + 1}{\gamma(e_1+1)} + \Big(1 - \Big(\frac{w_D}{w_C}\Big)^{e_2+1}\Big)\frac{\gamma + e_2 + 1}{\gamma(e_2+1)} \\ \beta_3 &= \Big(\frac{w_C}{w_B}\Big)^{e_3+1}\beta_2 + \Big(1 - \Big(\frac{w_C}{w_B}\Big)^{e_3+1}\Big)\frac{\gamma + e_3 + 1}{\gamma(e_3+1)} \end{aligned} \tag{3.36}$$

3.3.2 Reduced formulation

The majority of the seismic codes allow to model the ground motion by means of three-branches or two-branches RS as follows [5]:

$$S_a(T) = \begin{cases} S_0[1 + (\alpha - 1)\frac{T}{T_B}] & \text{se } 0 \le T \le T_B \\ S_0\alpha & \text{se } T_B \le T \le T_C \\ S_0\alpha(\frac{T_C}{T})^{k_1} & \text{se } T > T_C \end{cases} \tag{3.37}$$

$$S_a(T) = \begin{cases} S_0\alpha & \text{se } T \le T_C \\ S_0\alpha(\frac{T_C}{T})^{k_1} & \text{se } T > T_C \end{cases} \tag{3.38}$$

Therefore, by setting $w_D \to 0$ for the first case, $w_D \to 0$ and $w_D \to$ inf for the second case, the same reduced formulation can be obtained for the Power Spectrums.
For the three-branches PSd the new formulation reads:

$$G_{\ddot{u}_g}(w) = \begin{cases} G_0(\frac{w}{w_C})^{e_2} & \text{se } 0 < w \le w_C \\ G_0(\frac{w}{w_C})^{e_3} & \text{se } w_C < w \le w_B \\ G_0(\frac{w_B}{w_C})^{e_3}(\frac{w}{w_B})^{e_4} & \text{se } w > w_B \end{cases} \tag{3.39}$$

While, for the two-branches case:

$$G_{\ddot{u}_g}(w) = \begin{cases} G_0(\frac{w}{w_C})^{e_2} & \text{se } 0 < w \leq w_C \\ G_0(\frac{w}{w_C})^{e_3} & \text{se } w > w_C \end{cases} \tag{3.40}$$

with the values of the parameters involved which remain unchanged.
As it will be presented in the next chapters, these simplified formulations turned out to be quite useful. In particular, the use of the two-branches PSD of (*3.40*) in place of the rigorous four-branches formulation allowed to greatly lighten the analytrical formulation of the problem, without having to introduce too strong simplifications for the other parameters involved. Anyway, a comparison with the numerical results obtained by using the four branches PSD will be reported.

Chapter 4

Linear Response Spectrum analysis

Arrived at this point, the knowledge of the PSD function would allow for the full statistical characterization of the response in the nodal space, including the response peak distribution. Nevertheless, the random vibration approch is still not so popular in practice, and tends to be replaced by the more common Response Spectrum method, which combines in a statistical fashion the peak response of the corresponding modal coordinates. The modal superposition technique is widely employed for evaluation of seismic response of structures characterized by elastic behavior. In order to extend the response spectrum technique to multidegree of freedom structures, several rules for the peak value combination of modal responses have been derived on the basis of random vibration theory. The simplest one is the square root of sum of square *SRSS* combination rule [19]. The SRSS rule, ignoring the correlation between modes, provides excellent nodal response estimates only for structures which have well separated natural frequencies and are not too lightly damped and earthquake excitations that contain a wide band of frequencies [**?**]. In these cases only, no appreciable statistic dependence among the peak values of the modal responses exists.
Only in 1981, Wilson et al [20], provided a rational approach to take this correlation into account, namely the CQC rule, where the peak value of the nodal response is obtained as the square root of the sum of products of each couple of peak modal responses scaled by the correspondent cross-modal correlation coefficient. Moreover, Wilson noted that it was possible to approximate the correlation coefficients referring to a stationary white-noise excitation when the duration of the earthquake is long, compared to the periods of modal oscillators, and the power spectrum of the input is smooth over a wide range of frequencies that includes all the frequencies of the significant modal oscillators.

4.1 Linear structures

When the behaviour of the model can be regarded as linear, a modal analysis is the tool commonly adopted for the design of structures in seismic zones. The procedure works in the elastic domain, allowing to transform a differential equations coupled system into a problem with un-coupled differential equations, function of a single variable each. Consequently, the analysis of a MDOF system can be reshaped into a much simpler dynamic problem, in which each differential equation is referred to a SDOF oscillator, and the contribution of each modal response can be analyzed.
As reported by NTC (§7.3.3.1), the linear dynamic analysis involves the following steps:

1. Identification of the modes of the structure. To do so, it is necessary to apply a change of coordinates, switching to the principal coordinate system $y(t)$, such that, $u(t) = \Phi y(t)$, where $u(t)$ represents the displacement solution, while Φ is the modal matrix, whose elements φ_{ij} represents the deformade shape of the i-th oscillator associated to the j-th vibration mode. This new set of coordinates provides the diagonalization of the matrices M and K.

2. definition of the seismic actions provided by means of the Response Spectrum, for each of the vibration modes

3. superposition of each modal contribution by means of the adopted combination rule

From the practical point of view, the primary goal of this kind of analysis is not the evaluation of the solution in time, but the estimation of the maximum value of the responses, like for example the shear at the base, the max displacement at the top, or the max interstory drift. These maximum values can be computed by scaling the elastic RS by means of a factor Γ_j, known as modal participation factor. By means of this coefficient it is posible to either amplify or reduce the acceleration at the base of the fictitous SDOF oscillator under consideration, which will deform according to a specific vibration mode.
Now, the well-known equation of motion for an earthquake-excited discrete linear n-degree of freedom structure with M, C, and K, mass, damping and stiffness matrices, is:

$$M\ddot{u}(t) + C\dot{u}(t) + Ku(t) = -Mv\ddot{u}(t) \tag{4.1}$$

where v is the influence vector. The mode superposition technique involves the following coordinate transformation:

$$u(t) = \Phi y(t) = \sum_{i=1}^{n} \Phi_i y_i(t) \tag{4.2}$$

with $i = 1, 2...n$.
For cassical damped structures, the introduction in (*4.14*) of the coordinate

transformation (*4.2*) and its pre-multiplication by Φ^T yields the following uncoupled system of equations:

$$\ddot{y}(t) + 2\xi_i w_i \dot{y}(t) + {w_i}^2(t) = \Gamma_i \ddot{u}_g(t) \tag{4.3}$$

where Γ_i is the i-th component of the participation factor vector Γ defined as:

$$\Gamma = -\Phi^T M v \tag{4.4}$$

Once the responses of the modal oscillators governed by (*4.3*) have been evaluated, the nodal response can be obtained using (*4.2*). Any generic response parameter $e(t)$ of practical interest can be determined from the modal responses by means of the following relationship:

$$e(t) = b^T u(t) = b^T \sum_{i=1}^{n} \Phi_i y_i(t) = \sum_{i=1}^{n} \psi_i d_i(t) \tag{4.5}$$

where b is the vector collecting the combination coefficients relating the response parameter e(t) to the modal displacements, and

$$\psi_i = b^T \Phi_i \Gamma_i \tag{4.6}$$

In (*4.5*), $d_i(t)$ is the i-th modal response purged of the participation coefficient, i.e., the solution of (*4.16*) for $\Gamma_i = 1$.
Now, in earthquake engineering applications the peak value of the response parameter $e(t)$ is usually deduced by using the response spectrum technique, evaluating the peak values of the "purged" modal coordinates, $max|d_i(t)|$, in the form:

$$max|d_i(t)| = \frac{S_a(w_i, \xi_i)}{{w_i}^2} \tag{4.7}$$

where $S_a(w_i, \xi_i)$ is the ordinate of the pseudo-acceleration response spectrum. In order to deduce the peak value of $e(t)$, several combination rules of modal response peak values have been proposed (Rosenblueth 1951); Wilson et al. 1981; Gupta, 1990). According to the CQC rule of Wilson et al. (1981):

$$max|e(t)| = \sqrt{\frac{\psi_i \psi_j \rho_{ij} S_a(w_i, \xi_i) S_a(w_j, \xi_j)}{{w_i}^2 {w_j}^2}} \tag{4.8}$$

where ρ_{ij} is the correlation coefficient defined as follow:

$$\rho_{ij} = \frac{\lambda_{ij}}{\sqrt{\lambda_{ii}\lambda_{jj}}} \tag{4.9}$$

while λ_{ij},λ_{ii},λ_{jj} are the spectral moments defined as:

$$\lambda_{ij} = Re\Big[\int_0^\infty H_i(\hat{w}, w_i, \xi_i) H_j^*(\hat{w}, w_i, \xi_i) G_{\ddot{u}_g}(\hat{w}) d\hat{w}\Big] \tag{4.10}$$

$$\lambda_{ii} = Re\Big[\int_0^\infty H_i(\hat{w}, w_i, \xi_i) H_i^*(\hat{w}, w_i, \xi_i) G_{\ddot{u}_g}(\hat{w}) d\hat{w}\Big] \tag{4.11}$$

$$\lambda_{jj} = Re\Big[\int_0^\infty H_j(\hat{w}, w_j, \xi_j) H_j^*(\hat{w}, w_j, \xi_j) G_{\ddot{u}_g}(\hat{w}) d\hat{w}\Big] \tag{4.12}$$

and $H_i(\hat{w}, w_i, \xi_i)$ is the Frequency Response Function:

$$H_i(\hat{w}, w_i, \xi_i) = \frac{1}{{w_i}^2 - \hat{w}^2 + 2iw_i\hat{w}} \tag{4.13}$$

The one just presented expresses the rigorous formulation of the CQC combnation rule. However,as it will be presented in the next paragraphs, some approximations can be introduced, both in terms of calculating the correlation coefficient ρ_{ij}, and as regards the number of modalities to be inserted in the combination rule. Now, the presentation of the theories and procedures adopted to provide a closed form solution of ρ_{ij} is devoted to Chapters 6,7 and 8. Here the attention will be now focused on the formulation of the Response Spectrum method proposed by Der Kiureghian et al [21], which explains how to account for the rigid contribution of higher modes and the cross correlation between all mode pairs.

4.2 Response spectrum method

The Response Spectrum method proposed by Der Kiureghian [21] is here recalled.
The goal of the author was to develope a response spectrum analysis method based on the CQC rule, able to give the right importance to the contribution of both the higher and the lower modes, in order to estimate the peak floor acceleration (PFA).
The method accounts for the rigid contribution of truncated higher modes and the cross-correlations between all pairs of modes. The approximation is introduced in the time domain and then formulated in the frequency domain by CQC.
A brief description of the method is reported in the next chapters, highlighting the difference between higher and lower modal contributions.

4.2.1 Peak floor acceleration

The peak floor acceleration (PFA) is an important response quantity in seismic analysis and design of buildings. It is a key engineering parameter when floor diaphragms, non-structural elements or attached equipment are intended to behave as rigid parts, whose natural frequencies are much higher than the dominant frequency of the seismic excitation.
A first contribution to the principles behind the use of the PFA in the design of floor diaphrams was illustrated by Asfura et al [22]. In that work the author proposed a simplified response spectrum method, in which the PFA at the top of the building was computed using the SRSS combination.
More recent works, as Der Kiureghian's [1], relied on the other hand on the concept of random vibration theory to rigorously derive a response spectrum method for computing the PFA in linear and classically damped structures.

The theory benefits from the earlier work of Der Kiureghian and Nakamura [23], where a method for approximating the quasi-static contributions of truncated higher modes in response spectrum analysis by the complete quadratic combination (CQC) rule was proposed.
More recently, a response spectrum method for PFA was developed by Kumari et al [24] where the authors explained how properly accounts for modal cross-correlations and the rigid response of truncated modes.
Their response spectrum formulation required however the knowledge of the relative acceleration response spectra, which is seldom vailable in design situation. In contrast, the theory proposed by Der Kiureghian involves the total acceleration response spectrum, allowing for a simpler formulation, with fewer approximations.

4.2.2 Higher modes truncation

Now, in order to briefly present the method proposed by the author, the equation of motion is here rewritten, by focusing on the response in terms of acceleration:

$$M\ddot{u}(t) + C\dot{u}(t) + Ku(t) = -Mv\ddot{u}(t) \tag{4.14}$$

where the solution $u(t)$ is equal to:

$$u(t) = \sum_{i=1}^{N} \Phi_i \Gamma_i y_i(t) \tag{4.15}$$

As before, Φ_i denotes the i-th modal shape, Γ_i is the participation factor for the i-th mode, while y_i is the solution of the uncoupled system of equation:

$$\ddot{y}(t) + 2\xi_i w_i \dot{y}(t) + {w_i}^2(t) = \Gamma_i \ddot{u}_g(t) \tag{4.16}$$

Now, by taking the second derivative of (*9.10*) and adding the contribution of the ground acceleration, the nodal total acceleration vector is obtained:

$$\ddot{u}^{tot}(t) = \sum_{i=1}^{N} \Phi_i \Gamma_i \ddot{y_i}(t) + v\ddot{u_g}(t) \tag{4.17}$$

This equation describes the usual procedure to compute the nodal total accelerations when working in the time domain, in which the modal relative accelerations are combined together in order to obtain the nodal relative accelerations, adding at the end the ground acceleration.
Now, when all nodes are included in the analysis, the influence vector v can be defined as:

$$v = \sum_{i=1}^{N} \Phi_i \Gamma_i \tag{4.18}$$

By substituting this relation in (*4.17*):

$$\ddot{u}^{tot}(t) = \sum_{i=1}^{N} \Phi_i \Gamma_i \ddot{y}_i^{tot}(t) \tag{4.19}$$

in which

$$\ddot{y}_i^{tot}(t) = \ddot{y}_i(t) + \ddot{u}_g(t) \tag{4.20}$$

is the normalized nodal total acceleration.
Now, in practical nodal analysis, mode shapes and frequencies are available for only the first n modes, where $n \ll N$. Assuming the truncated modes to have frequencies that are much higher than the predominant frequencies of the input excitation, a natural approximation is to neglect the modal relative accelerations $\ddot{y}_i(t)$ for all truncated modes. Several arguments support this assertion. First, when the natural frequency of a mode is much higher than the frequency content of the seismic excitation, the modal response is almost *static*, and the relative acceleration is negligible.
It follows that the relative acceleration term, $\ddot{y}_i(t)$, is negligible if compared with the ground acceleration, meaning that the modal total acceleration $\ddot{y}_i^{tot}(t)$ in (*4.20*) approximately equals the ground acceleration. Using this approximation for the truncated modes in (*4.17*) and making use of (*4.22*):

$$\ddot{u}^{tot}(t) \simeq \sum_{i=1}^{n} \Phi_i \Gamma_i \ddot{y}_i^{tot}(t) + r_{(n)} \ddot{u_g}(t) \tag{4.21}$$

where:

$$r_{(n)} = v - \sum_{i=1}^{n} \Phi_i \Gamma_i \tag{4.22}$$

is the residual vector which transfers to the nodal coordinates the fraction of the ground acceleration that is projected onto the rigid modes.
The contribution of the second term in (*4.21*) is fundamental, because if the summation in (*4.19*) is limited to n, then the contribution of the ground acceleration transmitted by the higher modes would be completely lost.

4.2.3 CQC combination rule

The approximation introduced in (*4.22*), which replaces the modal correlation for all the truncated modes with the ground acceleration, allows to simplify the rigorous formulation of the CQC introduced in the Chapter 4.1. For the case of the total accelaration, the standard CQC rule reads:

$$max|\ddot{u}^{tot}(t)| = \sqrt{\sum_{i=1}^{N} \sum_{j=1}^{N} \Phi_i \Gamma_i \Phi_j \Gamma_j \rho_{ij} S_a(w_i, \xi_i) S_a(w_j, \xi_j)} \tag{4.23}$$

where the correlation coefficient ρij is equal to:

$$\rho_{ij} = \frac{\lambda_{ij}}{\sqrt{\lambda_{ii}\lambda_{jj}}} \tag{4.24}$$

and λ_{ij} is the cross-modal spectral moment defined by:

$$\lambda_{ij} = Re\Big[\int_0^{\inf} H_i(\hat{w}, w_i, \xi_i) H_i^*(\hat{w}, w_i, \xi_i) G_{\ddot{u}_g}(\hat{w}) d\hat{w}\Big] \tag{4.25}$$

Now, by making reference to the concept of total acceleration, the FRF of the i-th mode is equal to:

$$H_i(\hat{w}, w_i, \xi_i) = \frac{{w_i}^2 + 2iw_i\hat{w}}{{w_i}^2 - \hat{w}^2 + 2iw_i\hat{w}} \tag{4.26}$$

Now, the approximation introduced by Der Kiureghian implies the following relations:

$$\begin{aligned} \forall i > n : S_a(w_i, \xi_i) = PGA \\ \forall i, j > n : \rho ij = 1 \\ \forall i \leq n, j > n : \rho ij = \rho ig \end{aligned} \tag{4.27}$$

where ρ_{ig} is the cross-correlation coefficient between the i-th modal response and the ground acceleration.
With this in mind, (*4.23*) becomes:

$$max|\ddot{u}^{tot}(t)| \simeq \Big[\sum_{i=1}^{n}\sum_{j=1}^{n}\Phi_i\Gamma_i\Phi_j\Gamma_j\rho_{ij}S_a(w_i,\xi_i)S_a(w_j,\xi_j) +$$

$$2\sum_{i=1}^{n}\Phi_i\Gamma_i r_{(n)}\rho ig S_a(w_i,\xi_i)PGA + {r_{(n)}}^2 PGA^2\Big]^{\frac{1}{2}} \tag{4.28}$$

Now, to compute the correlation coefficient ρ_{ig} it is sufficient to note that the ground acceleration contribution can be seen as the response of a mode with infinitely large frequency, allowing to simplify the formulation of the spectral moments. associated to the ground acceleration.

In particular:

$$lim_{w_k\to\infty}H_k(\hat{w}, w_k, \xi_k) = 1 \tag{4.29}$$

consequently:

$$\lambda_{ig} = Re\Big[\int_0^{\inf} H_i(\hat{w}, w_i, \xi_i)G_{\ddot{u}_g}(\hat{w})dw\Big] \tag{4.30}$$

$$\lambda_{gg} = Re\Big[\int_0^{\inf} G_{\ddot{u}_g}(\hat{w})dw\Big] \tag{4.31}$$

While nothing changes for what concerns λ_{ij}:

$$\lambda_{ij} = Re\Big[\int_0^{\inf} H_i(\hat{w}, w_i, \xi_i)H_i^*(\hat{w}, w_i, \xi_i)G_{\ddot{u}_g}(\hat{w})dw\Big] \tag{4.32}$$

4.2.4 Total and Pseudo acceleration Response Spectra

The CQC rules presented in (*4.28*) and (*4.23*) are written in terms of the total acceleration response spectrum, which is seldom available in practice as design codes usually specify the pseudo-acceleration response spectrum. However, it is well known that the pseudo-acceleration response spectrum is a good approximation of the total acceleration response spectrum for a wide range of frequency and damping values. The difference between the

two is in the respective FRFs, whereas for the total acceleration response, the FRF is as in (*4.26*); for the pseudo-acceleration response, it is:

$$H_i(\hat{w}, w_i, \xi_i) = \frac{{w_i}^2}{{w_i}^2 - \hat{w}^2 + 2iw_i\hat{w}} \tag{4.33}$$

By comparing the two expressions, it is seen that the two FRFs are nearly identical for low-damped systems. The difference between the two is only significant for high damping values and long periods (small w_i values). These observations suggest that, in many applications, $S_a(w_i, \xi_i)$ in the CQC rule can be replaced with the pseudo-acceleration response spectrum, which is here denote by ${S_a}'(w_i, \xi_i)$. For the cases where this approximation is not valid, say when the damping is high and modal periods are long (e.g., for a base-isolated structure), an improved approximation can be developed, as described in the succeeding paragraphs.
As a measure of the difference between the two spectral ordinates, ${S_a}'(w_i, \xi_i)$ and $S_a(w_i, \xi_i)$ the adimensional parameter γ is introduced:

$$\gamma(w_i, \xi_i) = \frac{S_a(w_i, \xi_i)}{{S_a}'(w_i, \xi_i)} - 1 \tag{4.34}$$

which may be regarded as the percent error when using the pseudo-acceleration in place of the total acceleration.
To correct this error, by inverting the last equation, the total acceleration response spectrum can be derived as $S_a(w_i, \xi_i) = {S_a}'(w_i, \xi_i)[1 + \gamma(w_i, \xi_i)]$.
Sadek et al [25] proposed an analitical formulation for the coefficnet γ, to be used to convert the pseudo acceleration response spectra into the total one:

$$\gamma(w_i, \xi_i) = \beta_i w_i \alpha_i \tag{4.35}$$

with $\alpha_i = -0.268 - 0.205\xi_i$ and $\beta_i = 2.54{\xi_i}^2(2\pi)^{-\alpha_i}$.
The following observations can be made: (1) the results obtained by the random vibration theory are in close agreement with time-history results provided by using the simple formula by Sadek et al, and (2) the error in using the pseudo acceleration response spectrum instead of the total acceleration response spectrum is less than 5 % for values of $\xi \leq 5\%$ and periods shorter than about 7s. For higher damping values and longer periods, the simple correction formula presented above can be used to obtain a more accurate estimate of the total acceleration response spectrum values.

Chapter 5

Dynamics of a frame with rigid cladding panels

As presented at the beginning, the final objective of this work is to define an analytical formulation able to provide the values of the reaction forces which developes at the connections between the primary frame and the cladding panels. The key point is here represented by the fact that the cladding elements are here modelled as rigid entities, disregarding in these way the contributions associated to the vibration modes intrinsic of the panels. The aim of this fifth chapter is therefore to present the general principles behind the dynamics of such model.

5.1 Description of the model

A simple structural scheme, as the one shown in Figure (*5.1*), is considered in this work to investigate the dynamic response of an one-storey precast concrete structure subjected to seismic loads. A rigid cladding panel with total mass m_p is hinged at the base (point A) and connected to a flexible cantilever by means of a rigid truss element. The mass m_f is lumped at the top of the cantilever (point C), to model the effect of the translational inertia forces due to the mass of the roof. Given the fact that the roof diaphragm is rigid, the cantilever can model the whole lateral load resisting system, which, for the type of buildings at hand, is made of columns.
Starting from the definiton of the kinetic and potential energy, the first goal is to write the equation of motion for the frame, accounting for the influence of the cladding panel. The solution in time of the equation of motion will be then used to define the formula for the forces at the connections. As already presented however, the practitioner engineer is not always intersted in the response in time, but due to design necessities, he is more fond of the extreme values of the prameters at stake. To this purpose, two different preocedures are here recalled: the random vibration approach, and the Response Spectrum method based on the modal superposition.

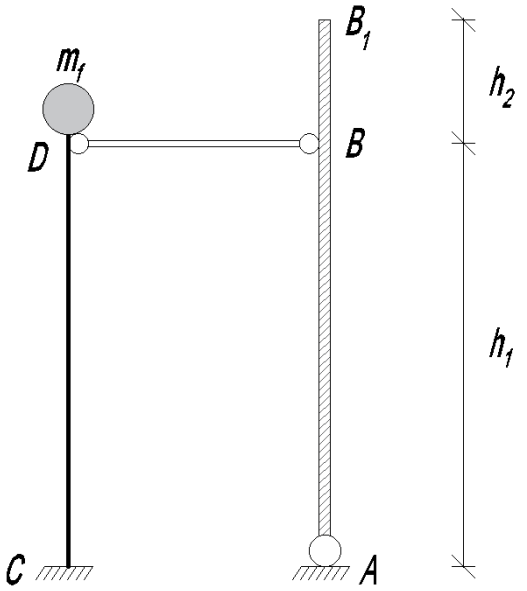

Figure 5.1: Structural sceme: frame + cladding panel

Due to the fact that it allows for a simpler formulation as previously presented, the Response Spectrum method will be the procedure adopted.
A brief description of the model under consideration is here reported. The analysis is refereed to a pre-cast structure, hinged as the base, and enclosed by reinforced concrete elements. The main geometrical characteristics of the panels are:

- $h_p = h_1 + h_2$: total height of the panel $[m]$, with $0 \leq h_2 < h_1$
- m_p: mass of the panel $[ton]$
- $\gamma_p = \frac{m_p}{h_p}$: linear density of the panel $[ton/m]$
- $\eta = \frac{h_2}{h_1}$: aspect ratio of the panel $0 \leq \eta < 1$, with practical values in the range $0 \leq \eta \leq 0.3$
- $I_{Gp} = \frac{1}{12} m_p {h_p}^2$: mass moment of inertia of the panel with respect to its centroid $[tonm^2]$

In terms of the frame only:

- m_f: mass of the frame $[ton]$ (reduced SDOF model)
- k_f: stiffness of the frame $[kN/m]$ (reduced SDOF model)
- $w_f = \sqrt{\frac{k_f}{m_f}}$: natural circular frequency of the frame $[rad/s]$
- $T_f = \frac{2\pi}{w_f}$: natural period of the frame $[s]$
- $\mu = \frac{m_p}{m_f}$: mass ratio

While, for what concerns the total structure:

- $w_s = \sqrt{\frac{k_f}{m_f}}$: natural circular frequency of the frame $[rad/s]$
- $T_s = \frac{2\pi}{w_f}$: natural period of the frame $[s]$

Now, by expressing with $u(t)$ the horizonthal displacemnt of the section B of the frame, with respect to section A, and being $u_g(t)$ the ground motion, it is possible to define, under the small displacement hypothesis, the horizonthal displacement of the panel as:

$$u_p(x,t) = \frac{x}{h_1}u(t) + u_g(t) \tag{5.1}$$

where $x \in [0, h_p]$.
Now that the generalized displacements of the model have been specified, it is possible to apply the D'Alembert principle, finally leading to the equation of motion.
The kinetic energy of the coupled system is:

$$K(t) = \tfrac{1}{2}m_f(\dot{u}(t) + \dot{u}_g(t))^2 + \tfrac{1}{2}\int_0^{h_p}\gamma_p\dot{u}^2(x,t)dx =$$

$$\frac{1}{2}m_f\left[\left(1 + \frac{\mu(1+\eta)^2}{3}\right)\dot{u}^2(t) + 2\left(1 + \frac{\mu(1+\eta)}{2}\right)\dot{u}(t)\dot{u}_g(t) + (1+\mu)\dot{u}_g^2(t)\right] \tag{5.2}$$

On the other hand, the elastic potential energy accounts only for the elastic contribution of the frame:

$$E(t) = \frac{1}{2}k_f u^2(t) \tag{5.3}$$

Therefore, the equation of motion of the undamped system becomes:

$$m_f\left(1 + \frac{\mu(1+\eta)^2}{3}\right)\ddot{q}(t) + k_f q(t) = -m_f\left(1 + \frac{\mu(1+\eta)}{2}\right)\ddot{u}_g(t) \tag{5.4}$$

which can be written in the canonical form as:

$$\ddot{q}(t) + w_s^2 q(t) = -\Gamma(\mu,\eta)\ddot{u}_g(t) \tag{5.5}$$

where:

$$\Gamma(\mu,\eta)\frac{\left(1 + \frac{\mu(1+\eta)}{2}\right)}{\left(1 + \frac{\mu(1+\eta)^2}{3}\right)} \tag{5.6}$$

is the participation factor. While

$$w_s = \sqrt{\frac{k_f}{m_f\left(1 + \frac{\mu(1+\eta)^2}{3}\right)}} \tag{5.7}$$

is the circular frequency of the structure, and consequently the natural period is $T_s = \frac{2\pi}{w_s}$. Now, by introducing the non dimensional parameter χ:

$$\chi(\mu, \eta) = \sqrt{1 + \frac{\mu(1+\eta)^2}{3}} \tag{5.8}$$

which can be seen as a perturbation parameter accounting for the presence of the panel, it is possible to rewrite (*5.7*) and the natural period as:

$$\begin{aligned} w_s &= \frac{w_f}{\chi(\mu, \eta)} \\ T_s &= T_f \chi(\mu, \eta) \end{aligned} \tag{5.9}$$

The solution of the equation of motion will provide the generalized displacement $q(t)$, to be used in the computation of the reaction forces at the connections by means dynamic equilibrium equation of the panel. The inertia force per unit lenght along the element can be defined as:

$$f_I(x, t) = -\gamma \ddot{u}_p(x, t) \tag{5.10}$$

where $\ddot{u}_p(x, t)$ is the second derivative of the horizonthal displacement of the panel, i.e. the relative acceleration of the panel. Now, by making reference to the concept of total acceleration, the expression of the integral equation for the reaction forces at the base $F_A(t)$ becomes:

$$F_A(t) = \int_0^{h_p} (-\gamma_p) \left(-1 + \frac{x}{h_1}\right) \left[\frac{x}{h_1} \ddot{u}(t) + \left(1 - \frac{x}{h_1}\right) \ddot{u}_g(t)\right] dx \tag{5.11}$$

While, for the force $F_B(t)$ at the top:

$$F_B(t) = \int_0^{h_p} (\gamma_p) \left(\frac{x}{h_1}\right) \left[\frac{x}{h_1} \ddot{u}(t) + \left(1 - \frac{x}{h_1}\right) \ddot{u}_g(t)\right] dx \tag{5.12}$$

By substituting (*5.1*) into (*5.11*) and (*5.12*):

$$F_A(t) = \frac{1}{6}(1+\eta)(1-2\eta) m_p \ddot{u}(t) + \frac{1}{2}(1-\eta) - \frac{1}{6}(1+\eta)(1-2\eta) m_p \ddot{u}_g(t) \tag{5.13}$$

$$F_B(t) = \frac{1}{3}(1+\eta)^2 m_p \ddot{u}(t) + \frac{1}{2}(1+\eta) - \frac{1}{3}(1+\eta)^2 m_p \ddot{u}_g(t) \tag{5.14}$$

Now, by introducing:

$$\begin{aligned} \alpha_A &= \frac{1}{6}(1+\eta)(1-2\eta) \\ \beta_A &= \frac{1}{2}(1-\eta) - \frac{1}{6}(1+\eta)(1-2\eta) \\ \alpha_B &= \frac{1}{3}(1+\eta)^2 \\ \beta_B &= \frac{1}{2}(1+\eta) - \frac{1}{3}(1+\eta)^2 \end{aligned} \tag{5.15}$$

the final form for the reaction forces can be written as:

$$F_A(t) = \alpha_A m_p \ddot{u}(t) + \beta_A m_p \ddot{u}_g(t) \tag{5.16}$$

$$F_B(t) = \alpha_B m_p \ddot{u}(t) + \beta_B m_p \ddot{u}_g(t) \tag{5.17}$$

5.2 Random vibration approach

As presented at the beginning, the advantage of a stochastic analysis is related to the fact that it allows for a complete statistical characterziation of the response. As it will be briefly presented in the following lines however, this kind of approach tends to over-complicate the formulation of the problem, not allowing for a handy analitical formulation.
A proof of this statement can be obtained by considering the simple case of the steady state response under an armonic ground motion:

$$\ddot{u}_g = \hat{a}_g exp(jwt) \tag{5.18}$$

where $\hat{a}_g$ is the magnitude of the motion.
and the solution for a dynamical system perturbated by $\ddot{u}_g$ is:

$$u(t) = \hat{u} exp(jwt) \tag{5.19}$$

Now, the equation of motion of the structure including the contribution of the damping is:

$$\ddot{u}(t) + 2i\xi w_s \dot{u}(t) + w_s^2 u(t) = -\Gamma(\mu, \eta)\ddot{u}_g(t) \tag{5.20}$$

By substituting (*5.19*) inside (*5.20*), the following relation yields:

$$\hat{u} = -\Gamma(\mu, \eta) H(\hat{w}, w_s, \xi)\hat{a}_g \tag{5.21}$$

where $H_i(\hat{w}, w_i, \xi_i)$ is the Frequency Response Function

$$H(\hat{w}, w_s, \xi) = \frac{1}{{w_i}^2 - \hat{w}^2 + 2iw_i\hat{w}} \tag{5.22}$$

Finally, the acceleration of the frame can be computed as:

$$\ddot{u} = -\hat{w}^2\hat{u}exp(jwt) = \Gamma(\mu, \eta)\hat{w}^2 H(\hat{w}, w_s, \xi)\hat{a}_g exp(jwt) \tag{5.23}$$

Such expression can be replaced inside equation (*5.16*) and (*5.17*), obtaining:

$$F_A(t) = (\alpha_A \Gamma(\mu, \eta)\hat{w}^2 H(\hat{w}, w_s, \xi) + \beta_A) m_p \hat{a}_g exp(jwt) \tag{5.24}$$

$$F_B(t) = (\alpha_B \Gamma(\mu, \eta)\hat{w}^2 H(\hat{w}, w_s, \xi) + \beta_B) m_p \hat{a}_g exp(jwt) \tag{5.25}$$

where:

$$H_{F_i} = (\alpha_i \Gamma(\mu, \eta)\hat{w}^2 H(\hat{w}, w_s, \xi) + \beta_i) \tag{5.26}$$

with $i = A, B$ is the FRF of the cladding panel reaction forces.
As it can be seen, the FRF obtained includes both the elastic contribution of the acceleration of the structure, and the contribution from the ground acceleration.
However, some problems arise when it comes to compute the spectral moments. In particcular, being $G_{\ddot{u}_g}(\hat{w})$ the Power Spectral density representing

the ground motion defined by Barone et al, the bilateral PSD of the cladding panel reaction force is defined as:

$$G_q(\hat{w}) = \frac{\Gamma^2}{w_s^4}|H(\hat{w}, w_s, \xi)|^2 G_{\ddot{u}_g}(\hat{w}) \tag{5.27}$$

Now, by means of the random vibration theory, the maximum value of the response parameter is:

$$max|F_i| = \sigma_{F_i}^2 \eta_{F_i} \tag{5.28}$$

where:

$$\sigma_{F_i}^2 = 2w_s m_p^2 \int_0^{\inf} |H(\hat{w}, w_s, \xi)|^2 G_{\ddot{u}_g}(\hat{w}) d(\hat{w}) \tag{5.29}$$

while:

$$\eta_{F_i}(T_s, p) = \sqrt{2ln2N_{F_i}[1 - exp[-\delta_{F_i}^1 .2\sqrt{piln(2N_{F_i})}]]} \tag{5.30}$$

where the spread factor δ_{F_i} and the parameter N_{F_i} of the response process F_i are defined as:

$$\delta_{F_i} = \sqrt{1 - \frac{\lambda_{1,F_i}^2}{\lambda_{0,F_i}\lambda_{2,F_i}}} \tag{5.31}$$

$$N_{F_i} = \frac{T_s}{2pi}\sqrt{1 - \frac{\lambda_{2,F_i}^2}{\lambda_{0,F_i}}}(-lnp)^{-1} \tag{5.32}$$

and

$$\lambda_{n,F_i} = 2w_s m_p^2 \int_0^{\infty} (\hat{w})^n |H_{F_i}|^2 G_{\ddot{u}_g}(\hat{w}) dw \tag{5.33}$$

with $i = A, B$ and $n = 0, 1, 2$
The key aspect here is related to the fact that, as already observed, each spectral moment argument is characterized by the square of the FRF. This means that, due to the way in which the FRF has been modelled (*5.26*), the square of the FRF will give rise to thre e different contributions, in particular:

$$\begin{aligned}\lambda_{n,F_i} = \Bigg[&\Big[\int_0^{\infty} \Big(\alpha_i \Gamma(\mu, \eta)\hat{w}^2 H(\hat{w}, w_s, \xi)\Big)^2 G_{\ddot{u}_g}(\hat{w}) d\hat{w}\Big] \\ &+ \Big[\int_0^{\infty} 2\Big(\alpha_i \beta_i \Gamma(\mu, \eta)\hat{w}^2 H(\hat{w}, w_s, \xi)\Big) G_{\ddot{u}_g}(\hat{w}) d\hat{w}\Big] \\ &+ \Big[\int_0^{\infty} \beta_i^2 G_{\ddot{u}_g}(\hat{w}) d\hat{w}\Big]\Bigg] 2w_s m_p^2\end{aligned} \tag{5.34}$$

The first term represents the usual contribution associated to the frame acceleration. Then two additional contributions appear:

- the cross term represented by the product between the two previous contributions

- the contributiona associated to the groun motion

These last two terms tend to make the formulation heavier, especially when the ratio between the spectral quantities is involved, as it happens for example for the computation of the parameters δ_{F_i} and N_{F_i}. This is why an alernative path is followed in this work, which is the Resposne Spectrum method proposed by Der Kiureghian, which will be briefly recalled in the next paragraph and adapted to this particular case.

5.3 Response Spectrum method

As already presented in Chapter 4, the Response Spectrum method proposed by Der Kiureghian states that for modes with frequencies which are much higher than the predominant frequency of the input exitation, the modal response can be considered almost static, meaning that the relative acceleration is negligible wrt the ground acceleartion.
The same kind of reasoning can be applied also for the problem under consideration. By recalling the formula of the inertia forces acting along the panels, these are given by two contributions:

- the acceleration of the panel

- the ground acceleration

as reported here:

$$f_I(x,t) = -\gamma \ddot{u}_p(x,t) = -\gamma \frac{x}{h_1}\ddot{u}(t) + \ddot{u}(t) \tag{5.35}$$

Now, in order to rewrite the problem like for the case of a multi-modal system, the ground acceleration can be seen as the contribution of a mode with infinite frequency. Doing so, the maximum value of the reaction forces at the connection can be computed by superimposing the contribution of the mode associated the acceleration of the panel and the one associated to the ground acceleration only, by applying the CQC rule.

$$E[max|F_i(t)|] = (\alpha_i^2 max|\ddot{u}(t)|^2 + \beta_i^2 max|\ddot{u}_g(t)|^2) + 2\alpha_i\beta_i\rho_{1g} max|\ddot{u}(t)|max|\ddot{u}_g(t)|)^{\frac{1}{2}} \tag{5.36}$$

where $i = A, B$. Now, by imposing:

$$max|\ddot{u}(t)| = S_a(w_s, \xi_s) \tag{5.37}$$

and

$$max|\ddot{u}_g(t)| = PGA \tag{5.38}$$

(*5.36*) can be rewritten as:

$$E[max|F_i(t)|] = m_p\Big[\alpha_i^2 S_a(T_s,\xi_s)^2 + \beta_i^2 PGA^2 + 2\alpha_i\beta_i\rho_{ig}S_a(T_s,\xi_s)PGA\Big]^{\frac{1}{2}} \tag{5.39}$$

where ρ_{ig} is the correlation coeffcient relating the mode associated to the natural frequency of the structure with the fictitous mode associated to the ground motion:

$$\rho_{ig} = \frac{\lambda_{ig}}{\sqrt{\lambda_{ii}\lambda_{gg}}} \tag{5.40}$$

and $\lambda_i g$, $\lambda_i i$, $\lambda_g g$ are respectively the covariance, the variance of the response total acceleration and the variance of the ground acceleration, defined as:

$$\lambda_{ig} = Re\Big[\int_0^{\inf} H_i H_g G_{\ddot{u}_g}(\hat{w})dw\Big] \tag{5.41}$$

$$\lambda_{ii} = Re\Big[\int_0^{\inf} H_i H_i^* G_{\ddot{u}_g}(\hat{w})dw\Big] \tag{5.42}$$

$$\lambda_{gg} = Re\Big[\int_0^{\inf} H_g H_g^* G_{\ddot{u}_g}(\hat{w})dw \tag{5.43}$$

As already presented, the parameter H_i represents the kernel function, in this case associated to the total acceleration:

$$H_i = H_i(\hat{w}, w_i, \xi_i) = \frac{{w_i}^2 + 2iw_i\hat{w}}{{w_i}^2 - \hat{w}^2 + 2iw_i\hat{w}} \tag{5.44}$$

Now, since $\lim_{w_i\to\infty} H_i(\hat{w}, w_i, \xi_i) = 1$, the expression of the spectral moments in (*5.41*) and (*5.43*) can be simplified:

$$\lambda_{ig} = Re\Big[\int_0^{\inf} H_i G_{\ddot{u}_g}(\hat{w})dw\Big] \tag{5.45}$$

$$\lambda_{gg} = Re\Big[\int_0^{\inf} G_{\ddot{u}_g}(\hat{w})dw\Big] \tag{5.46}$$

One of the goal of this thesis is therefore to find an analitical solution for the above mentioned spectral moments. Thanks to the handy formulation of the PSD provided by [5] this does not represent a big issue for the spectral quantity λ_{gg}. The same does not hold however for the remaining two integrals, in which the presence of both the PSD and the FRF requires the introduction of some simplifications.
In the next three Chapters, three different formulations will be presented. Despite relying on different theories and assumptions, they share the same goal, i.e. providing a closed form analytical solution for the computation of ρ_{ig}.
Chapter 6 reports some approximated formulations based on the white noise rapresentation of the seismic input.
Chpater 7 relies on the Multiple Timescale Analysis theory proposed by Denoel. While the formulation in Chapter 8 is based on some initial approximations introduced on both the shape of the PSD and on the FRF in order to simplify the computations.
At the end of each chapter, a comparison between the anlytical solutions and the numerical results obtained by means of the software Matlab are reported.

Chapter 6

Correlation coefficients - White Noise approximation

As already presented before, when the duration of the earthquake is long, and the input spectra is smooth over a wide frequency range, it is possible to approximate the correlation coefficients making reference to a stationary white noise exitation.
The formulations proposed by Der Kiureghian [8] and Moshen [7] are here presented
Both authors characterized the seismic hazard $\ddot{u}_g(t)$ in the frequency domain by making use of the analytical PSD model proposed by Kanaj-Tajimi in hypothesis of white noise. They followed however different procedures to obtain the final analytical formulation.

6.1 Der Kiureghian (1979)

The response spectrum analysis method based on the CQC rule proposed by der Kiureghian et al is here recalled, where the author studied the stationary responses of single- and multi-degree-of-freedom structures subjected to stationary input excitations.
In particular, by using a modal superposition procedure, closed form solutions for the first three spectral moments as response to white-noise inputs are derived. These solutions account for the correlation between modal responses of multi-degree structures.
Now, the *m-th* order spectral moment $\lambda_{m,ij}$ associated to the *i-th* and *j-th* modes is defined as:

$$\lambda_{m,ij} = Re\Big[\int_0^{\inf} \hat{w}^n H_i(\hat{w}, w_i, \xi_i) H_j^*(\hat{w}, w_i, \xi_i) G_{\ddot{u}_g}(\hat{w}) dw\Big] \tag{6.1}$$

where $H_i(\hat{w}, w_i, \xi_i)$ is the FRF associated to the *i-th* mode:

$$H_i(\hat{w}, w_i, \xi_i) = \frac{1}{{w_i}^2 - \hat{w}^2 + 2i w_i \hat{w}} \tag{6.2}$$

For the aim of this work, only the spectral moments of order zero are needed, e.g.

$$\lambda_{0,ij} = Re\Big[\int_0^{\inf} H_i(\hat{w}, w_i, \xi_i) H_j^*(\hat{w}, w_i, \xi_i) G_{\ddot{u}_g}(\hat{w}) dw\Big] \tag{6.3}$$

6.1.1 Response to white noise

Der Kiureghian initially limited his studies to the basic case of white noise exitation, where $G_{\ddot{u}_g}(\hat{w}) = G_0$ is a constant.
Now, by using the *Residue Theorem of integration*, he analytically evaluated the solution of the integral (*6.3*), obtaining:

$$\lambda_{0,ij} = \frac{2\pi G_0}{K_{ij}} (\xi_i w_i + \xi_j w_j) \tag{6.4}$$

where:

$$K_{ij} = (w_i^2 - w_j^2)^2 + 4\xi_i \xi_j w_i w_j (w_i^2 + w_j^2) + 4(\xi_i^2 + \xi_j^2) w_i^2 w_j^2 \tag{6.5}$$

The results obtained in (*6.4*) and (*6.5*) were then used inside the formula for the correlation coefficient:

$$\rho_{0,ij} = \frac{\lambda_{ij}}{\sqrt{\lambda_{ii} \lambda_{jj}}} \tag{6.6}$$

obtaining the following analytical solution:

$$\rho_{0,ij} = \frac{8\sqrt{\xi_i \xi_j w_i w_j} (\xi_i w_i + \xi_j w_j) w_i w_j}{K_{ij}} \tag{6.7}$$

For small damping and for closely spaced modes, (*6.7*) can be reduced, through a first-order approximation, to:

$$\rho_{0,ij} = \frac{2\sqrt{\xi_i \xi_j} \Big[(w_i + w_j)^2 (\xi_i + \xi_j) + (w_i^2 - w_j^2)(\xi_i \xi_j)\Big]}{4(w_i - w_j)^2 + (\xi_i + \xi_j)^2 (w_i + w_j)^2} \tag{6.8}$$

These approximate expressions provide reasonable accuracy for damping values as large as 0.20, and that they should be adequate for most practical applications.

6.1.2 Response to filtered white noise

Formally, filtered white noise can be seen as the response of an oscillator to a white-noise input. It is often used to represent the input into a structure supported by a single-degree primary system which itself is subjected to a white-noise excitation. A common example is represented by the case of a structure situated on a soil layer which is excited by earthquake motions; More generally, however, the filtered white noise may be used as a convenient model for a large class of excitations.

For such cases, the PSD function can be expressed by making use of the analytical PSD model proposed by Kanaj-Tajimi in hypothesis of white noise:

$$G_{\ddot{u}_g}(w) = G_0 \frac{w_g^4 + 4\xi_g w_g^2 w^2}{(w_g^2 - w^2)^2 + 4\xi_g w_g^2 w^2} \tag{6.9}$$

where w_g and ξ_g are filter constants, and G_0 the normalized PSD of the underlying white noise.
This represents the Power Spectral Density of the absolute acceleration response of a single-degree-of-freedom system to a white-noise base acceleration, where w_g and ξ_g are the circular natural frequency and the damping coefficient, respectively.
By proper selection of w_g and ξ_g, (*6.9*) may be used to represent excitations with varying power spectral density shapes.
However, if on one hand, the filtered Kanaj-Tajimi model is able to provide a more general formulation, on the other hand it produces far more complex spectral moments expressions. Although approximate expressions for small damping are possible, such results are not expected to be simple enough to justify their use in place of the exact expressions.
For the aim of this work however, the only correlation coefficient required is the one correlating the fundamental mode of the structure and the groun motion. This allows in particular to compute the correlation coefficient expoliting the analytical formulation obtained in hypothesis of white noise (*6.7*), but making use on the other hand of the consideration of Kanaj-Tajimi for the more general filtered white noise model.
The first step is to substitute the contribution of the hypothetical $j-th$ mode of the structure, with the mode associated to the ground motion ($w_j \to w_g$ and $\xi_j \to \xi_g$), obtaining:

$$\rho_{0,ig} = \frac{8\sqrt{\xi_i \xi_g w_i w_g}(\xi_i w_i + \xi_g w_g) w_i w_g}{K_{ig}} \tag{6.10}$$

and

$$K_{ig} = (w_i^2 - w_g^2)^2 + 4\xi_i \xi_g w_i w_g (w_i^2 + w_g^2) + 4(\xi_i^2 + \xi_g^2) w_i^2 w_g^2 \tag{6.11}$$

While in the hypothesis of small damping ξ_i and $w_j \approx w_g$, a similar approximation as the one of (*6.12*) can be obtained:

$$\rho_{0,ig} = \frac{2\sqrt{\xi_i \xi_g}\Big[(w_i + w_g)^2(\xi_i + \xi_g) + (w_i^2 - w_g^2)(\xi_i \xi_g)\Big]}{4(w_i - w_g)^2 + (\xi_i + \xi_g)^2 (w_i + w_g)^2} \tag{6.12}$$

For what concerns the parameters w_g and ξ_g, Kanai (5) and Tajimi (7) have suggested $w_g = 5\pi$ and $\xi_g = 0.6$ for modeling ground acceleration response during earthquakes. However, other values can be adopted.
For example, it is possible to associate to w_g the value of the largest circular frequency compatible with the sampling rate of the accelerations ($w_g = 100\pi$).

Finally, a further analytical approximation for the correlation coefficient could be introduced by imposing $w_g \to \infty$, obtaining:

$$\rho_{0,ig} = \frac{4\xi_i\sqrt{\xi_i\xi_g}}{\xi_i^2 + 2\xi_i\xi_g + \xi_g^2 + 4} \tag{6.13}$$

A more refined formulation can be considered also for what concerns the modelling of the damping contribution, by providing the value of the damping coefficient ξ_i as a function of the natural period T_i of the structure:

$$\xi_i = \begin{cases} 0.05 & \text{for } T_i > T_C \\ 0.6 + (0.05 - 0.6)\frac{(T_i - T_B)}{(T_C - T_B)} & \text{for } T_i > T_B \\ 0.6 & \text{for } T_i > 0 \end{cases} \tag{6.14}$$

6.2 Moshen (2016)

By following the steps of Der Kiureghian, Moshen et al [7] too addressed the prediction of the median peak floor total acceleration (PFA) demand in spatial elastic structures subjected to seismic excitation. By using the response spectrum technique, several approximations and simplifications concerning the correlation between modal contributions, peak factors, and cross-spectral moments are discussed, leading to the proposed modified modal combination rules.
As before, here the focus will be centered on the correlation coefficient ρ_{ij}:

$$\lambda_{0,ij} = Re\Big[\int_0^{\inf} H_i(\hat{w}, w_i, \xi_i) H_j^*(\hat{w}, w_i, \xi_i) G_{\ddot{u}_g}(\hat{w}) dw\Big] \tag{6.15}$$

being H_i the transfer function ffor the total acceleration:

$$H_i(\hat{w}, w_i, \xi_i) = \frac{w_i^2 + 2iw_i\hat{w}}{{w_i}^2 - \hat{w}^2 + 2iw_i\hat{w}} \tag{6.16}$$

and $G_{\ddot{u}_g}(w)$ the Kanaj-Tajimi PSD:

$$G_{\ddot{u}_g}(w) = G_0 \frac{w_g^4 + 4\xi_g w_g^2 w^2}{(w_g^2 - w^2)^2 + 4\xi_g w_g^2 w^2} \tag{6.17}$$

Through the application of the Cauchy's residue theorem, the integral (*6.15*) can be solved, yielding:

$$\lambda_{0,ij} = G_0 \pi w_j w_i w_g \left[\frac{\sum_{m=0}^{2}\sum_{n=0}^{2}\xi_i^m\xi_j^n\zeta_{0,mn}(w_i,w_j)}{4\xi_g D_4} + \frac{2w_g\sum_{m=0}^{4}\sum_{n=0}^{2}\xi_i^m\xi_j^n\Psi_{0,mn}(w_i,w_j)}{D_1}\right] \tag{6.18}$$

where the parameters D_1, D_4, $\zeta_{0,mn}(w_i, w_j)$ and $\Psi_{0,mn}(w_i, w_j)$ in the summands are functionals sorted with respect to the exponent of the damping ratios, m and n, which allows to linearize the CQC combination rule with respect to the damping coefficients. $\zeta_{0,mn}(w_i, w_j)$ and $\Psi_{0,mn}(w_i, w_j)$ represent the generic components in position mn of the functional matrices Ξ

and Ψ.
At the denominator of (*6.26*), D_1 and D_4 are defined as:

$$\begin{aligned} D_1 &= K(w_g,\xi_g,w_i,\xi_i)K(w_g,\xi_g,-w_i,\xi_i)K(w_i,\xi_i,-w_j,\xi_j) \\ D_4 &= K(w_g,\xi_g,w_i,\xi_i)K(w_g,\xi_g,-w_j,\xi_j) \end{aligned} \tag{6.19}$$

where $K{=}K(w_m,\xi_m,w_n,\xi_n)$ is equal to:

$$K = \Big(w_m^2 - w_n^2\Big)^2 + 4w_m w_n\Big(-w_m^2\xi_m\xi_n + w_m w_n\xi_m^2 + w_m w_n\xi_n^2 - w_n^2\xi_m\xi_n\Big) \tag{6.20}$$

While for what concerns the functionals appearing at the the numerator:

$$\zeta_{0,mn}(w_i,w_j) = \begin{cases} -\zeta_{1,mn}(w_i,w_j) - 2\xi_g\hat{\zeta}_{1,mn}(w_i,w_j) & \text{if } m+n \text{ is even} \\ \zeta_{1,mn}(w_i,w_j) - 2\xi_g\hat{\zeta}_{1,mn}(w_i,w_j) & \text{if } m+n \text{ is odd} \end{cases} \tag{6.21}$$

$$\Psi_{0,mn}(w_i,w_j) = \begin{cases} \frac{\Psi_{1,mn}(w_i,w_j)}{2} & \text{if } m=0 \\ \frac{\Psi_{1,mn}(w_i,w_j) - \hat{\Psi}_{1,mn}(w_i,w_j)}{2} & \text{if } m>0 \end{cases} \tag{6.22}$$

Now, the components of the matrix Ξ are characterized by the following relations:

$$\begin{cases} \zeta_{1,01}(w_i,w_j) = -\zeta_{1,01}(w_i,w_j) \\ \zeta_{1,02}(w_i,w_j) = \zeta_{1,20}(w_i,w_j) \\ \zeta_{1,12}(w_i,w_j) = -\zeta_{1,21}(w_i,w_j) \\ \hat{\zeta}_{1,01}(w_i,w_j) = -\hat{\zeta}_{1,01}(w_i,w_j) \\ \hat{\zeta}_{1,02}(w_i,w_j) = \hat{\zeta}_{1,20}(w_i,w_j) \\ \hat{\zeta}_{1,12}(w_i,w_j) = -\hat{\zeta}_{1,21}(w_i,w_j) \end{cases} \tag{6.23}$$

It should be noted that the off-diagonal elements of Ξ and $\hat{\Xi}$ are determined by considering the sign changing between the frequencies w_i and w_j of their off-diagonal counterpart. All the other elements can be expressed as:

$$\begin{cases} \zeta_{1,00}(w_i,w_j) = w_i w_j\Big(w_g^2 X(w_j,\phi_3',-\phi_2) + w_i^2 X(w_j,-\phi_1,\phi_3')\Big) \\ \zeta_{1,01}(w_i,w_j) = 2w_i w_g\xi_g\Big(-w_g^2 X(w_j,2\phi_3',3) + w_i^2 X(w_j,2\phi_1,\phi_2)\Big) \\ \zeta_{1,02}(w_i,w_j) = 4w_i w_j w_g^2 X(w_i,-\phi_1,\phi_3') \\ \zeta_{1,11}(w_i,w_j) = -4\phi_3' w_g^6 + 16\phi_1 w_i^2 w_j^2 w_g^2\xi_g^2 + 8\phi_2 w_g^4\xi_g^2(w_i^2+w_j^2) \\ \zeta_{1,12}(w_i,w_j) = -8w_j w_g^3\xi_g X(w_j,2\phi_1,\phi_2 \\ \zeta_{1,22}(w_i,w_j) = -16\phi_1 w_i w_j w_g^4 \\ \hat{\zeta}_{1,00}(w_i,w_j) = -w_i w_j\xi_g\Big(w_g^2 X(w_j,1,-2) + w_i^2 X(w_j,4\xi_g^2,1)\Big) \\ \hat{\zeta}_{1,01}(w_i,w_j) = w_i w_g\Big(w_g^2 X(w_j,-4\xi_g^2,1) - w_i^2 X(w_j,(4\xi_g^2)^2,1)\Big) \\ \hat{\zeta}_{1,02}(w_i,w_j) = -4w_i w_j w_g^2 X(w_i,4\xi_g^2,1) \\ \hat{\zeta}_{1,11}(w_i,w_j) = 4w_g^2\xi_g\Big(w_g^2 X(w_j,2\phi_2',1) + w_i^2 X(w_j,(4\xi_g^2)^2,\phi_2')\Big) \\ \hat{\zeta}_{1,12}(w_i,w_j) = 4w_i w_j w_g^3 X(w_i,(4\xi_g^2)^2,\phi_2') \\ \hat{\zeta}_{1,22}(w_i,w_j) = -64w_i w_j w_g^4\xi_g^3 \end{cases} \tag{6.24}$$

The $zero-th$ spactral moment of the ground is instead defined as:

$$\lambda_{0,gg} = G_0 \pi w_g \Big(\xi_g + \frac{1}{4\xi_g^2} \Big) \tag{6.25}$$

6.2.1 First order approximation of the zero-th order moment

For the zeroth cross-spectral moment, the expansion of the sums in (*6.18*) to the first degree of the exponent of the damping ratios yields:

$$\lambda_{0,ij}^{(1)} = G_0 \pi w_j w_i w_g \left[\frac{\sum_{m=0}^{1} \sum_{n=0}^{1} \xi_i^m \xi_j^n \zeta_{0,mn}(w_i, w_j)}{4\xi_g D_4} \right]$$

$$+ G_0 \pi w_j w_i w_g \left[\frac{2w_g \sum_{m=0}^{1} \sum_{n=0}^{1} \xi_i^m \xi_j^n \Psi_{0,mn}(w_i, w_j)}{D_1} \right] \tag{6.26}$$

This expression is equivalent to a successively first-order Taylor series expansion of the numerator of $\lambda_{0,ij}$ at $\xi_i = 0$ and $\xi_j = 0$.
Now, by considering the limit $\lim_{w_j \to \infty}$ it is possible to compute the cross-spectral moment between the $i-th$ modal acceleration and the ground acceleration, $\lambda_{0,ig}^{(1)}$:

$$\lambda_{0,ij}^{(1)} = \frac{G_0 \pi w_i w_g}{4\xi_g} \frac{w_i^3 - w_i w_g^2 + 4w_i^3 \xi_g^2 + \xi_i \Big(4w_i^2 w_g \xi_g + 4w_g^3 \xi_g + 16 w_i^2 w_g \xi_g^3 \Big)}{K(w_g, \xi_g, -w_i, \xi_i)} \tag{6.27}$$

6.2.2 Hybrid approximation of the zero-th order moment

A further simplified formulation of (*6.18*) can be obtained by exploiting the concept of *hybrid approximation* of the zero-th order spectral moment.
In particular, by introducing the functionals $\xi_0(w_i, w_j)$, $\Psi_{0,10}(w_i, w_j)$ and $\Psi_{0,01}(w_i, w_j)$, it is possible to compute the spactral moment $\lambda_{0,ij}^{(1')}$, which is a hybrid type of a first order and a zero-th order approximation of $\lambda_{0,ij}$:

$$\lambda_{0,ij}^{(1')} = G_0 \pi w_j w_i w_g \left[\frac{\xi_0(w_i, w_j)}{4\xi_g D_4} + \frac{2w_g \psi_{0,10}(w_i, w_j) + \xi_j \psi_{0,01}(w_i, w_j)}{D_1} \right] \tag{6.28}$$

where:

$$\xi_0(w_i, w_j) = w_i w_j \Big[w_i^2 \Big(w_j^2 (4\xi_g^2 + 1) - w_g^2 \Big) - w_j^2 w_g^2 + w_g^2 \Big(1 - 8\xi_g^2 \Big) \Big] \tag{6.29}$$

$$\Psi_{0,10}(w_i, w_j) = w_j \Big[2w_i^6 w_g^2 + w_j^6 w_g^2 + 4w_i^6 w_g^2 + w_i^2 w_j^2 w_g^4 \xi_g^2 - w_i^4 w_g^2 \Big(2w_g^2 + w_j^2 (1 + 8\xi_g^2 - 16\xi_g^4) \Big) \Big] \tag{6.30}$$

$$\Psi_{0,01}(w_i, w_j) = w_i^3 w_g^6 + 4w_i^9 \xi_g^2 + w_i^2 w_g^2 (1 - 4\xi_g^2)^2 + 2w_i^5 w_g^4 (-1 + 4\xi_g^2) \tag{6.31}$$

As before, the cross spectral moment between mode i and the ground acceleration $\ddot{u}_g$ is derived by replacing the contribution of the *j-th* mode with the one of the ground acceleration, obtaining:

$$\lambda_{0,ig}^{(1')} = \frac{G_0 \pi w_i w_g}{4\xi_g} \frac{w_i^3 - w_i w_g^2 + 4w_i^3 \xi_g^2}{K(w_g, \xi_g, -w_i, \xi_i)} \tag{6.32}$$

Now that the required spectral moments are obtained, by exploiting the results obtained in (*6.28*) and (*6.32*) through the hybrid approximation procedure, and by recalling (*6.25*), it is possible to compute the coefficint of correlation as:

$$\rho_{MO} = \frac{\lambda_{0,ig}^{(1')}}{\sqrt{\lambda_{0,ij}^{(1')} \lambda_{gg}}} \tag{6.33}$$

6.3 Results comparison

In this section the analytical formulation proposed by der Kiureghian et al and Moshen et al are compared with the results numerically obtained by means of Matlab.
Matlab allows to evaluate the integral solution by using different procedures. What was done here was to exploit the *trapz* command, which automatically implement the so called "trapezoidal quadrature rule" to estimate the area subtended by a curve.
The main steps adopted in Matlab are here briefly recalled. By making reference to the transfer function for the total acceleration (*6.16*) and to the 4-branches PSD formulation proposed by Barone et al, the spectral moments are umerically evaluate as:

$$\lambda_{ig}^{num} = trapz\Big[H_i(\hat{w}, w_i, \xi_i) G_{\ddot{u}_g}(\hat{w}) dw\Big] \tag{6.34}$$

$$\lambda_{ii}^{num} = trapz\Big[H_i(\hat{w}, w_i, \xi_i) H_i^*(\hat{w}, w_i, \xi_i) G_{\ddot{u}_g}(\hat{w}) dw\Big] \tag{6.35}$$

$$\lambda_{gg}^{num} = trapz\Big[G_{\ddot{u}_g}(\hat{w}) dw\Big] \tag{6.36}$$

Finally, the numerical correlation coefficient can be evaluate as:

$$\rho_{0,ig}^{num} = \frac{\lambda_{ig}^{num}}{\sqrt{\lambda_{ii}^{num} \lambda_{gg}^{num}}} \tag{6.37}$$

For what concerns instead the results proposed by Der kiureghian et al, the three possible formulation are here recalled. The most rigorous formulation for the correlation coefficient, here denoted as ρ_{WN}, yields:

$$\rho_{WN} = \frac{8\sqrt{\xi_i \xi_g w_i w_g}(\xi_i w_i + \xi_g w_g) w_i w_g}{K_{ig}} \tag{6.38}$$

and

$$K_{ig} = (w_i^2 - w_g^2)^2 + 4\xi_i \xi_g w_i w_g (w_i^2 + w_g^2) + 4(\xi_i^2 + \xi_g^2) w_i^2 w_g^2 \tag{6.39}$$

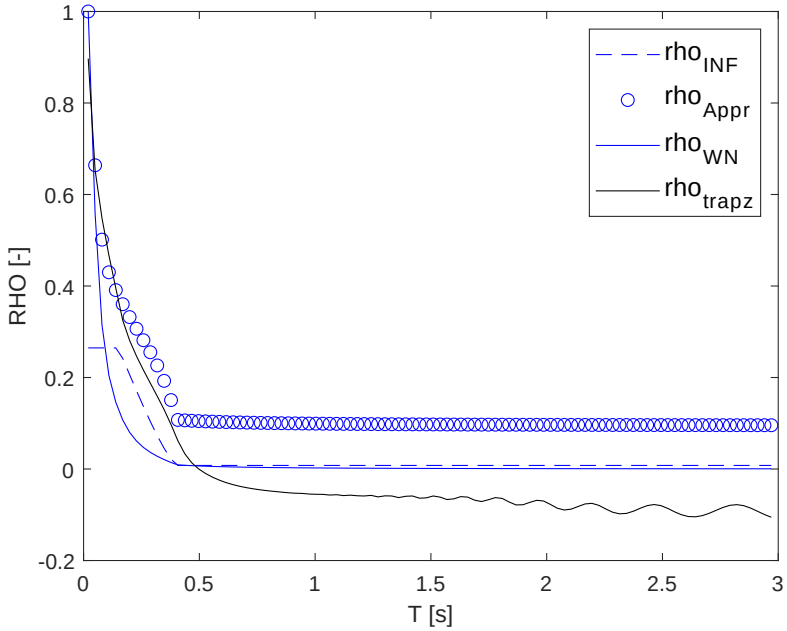

Figure 6.1: Corr. coeff. in hypothesis of white noise (Der Kiureghian)

In the case of small damping, and $w_j \approx w_g$, the approximated solution ρ_{Appr} can be adopted:

$$\rho_{Appr} = \frac{2\sqrt{\xi_i \xi_g}\Big[(w_i + w_g)^2(\xi_i + \xi_g) + (w_i^2 - w_g^2)(\xi_i \xi_g)\Big]}{4(w_i - w_g)^2 + (\xi_i + \xi_g)^2(w_i + w_g)^2} \tag{6.40}$$

A further analytical approximation ρ_{INF} is finally obtained by enforcing $w_g \to \infty$:

$$\rho_{INF} = \frac{4\xi_i\sqrt{\xi_i \xi_g}}{\xi_i^2 + 2\xi_i\xi_g + \xi_g^2 + 4} \tag{6.41}$$

The comparison of the results in the time domain is reported in Figure *6.1*. The more rigorous formulation ρ_{WN} is the one presenting the more regular behaviour. However, if compared with the numerical results, it tends to underestimate the valus of ρ_{ig} at low values of the natural periods, where instead the approximate formulation ρ_{Appr} is able to provide quite better results.

For what concerns the formulation proposed by Moschen, the results can be viewed in Figure *6.2*. Unlike the previous case, the proposed formulation overestimates the value of ρ_{ig} along the whole domain, providing also quite a regular behaviour. Finally, Figure *6.3* gathers together all the formulations presented in this Chapter. The results provided by Moschen are the ones able to better follow the behaviour of the numerical results along the domain. However, in the high frequency range, the best approach is the one proposed by Der Kiureghian, by means of (*6.40*).

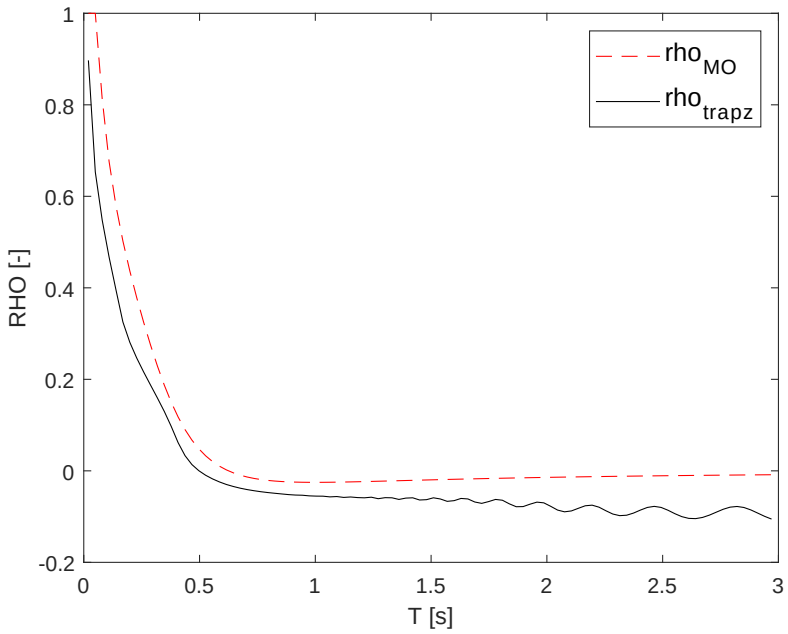

Figure 6.2: Corr. coeff. in hypothesis of white noise (Moschen)

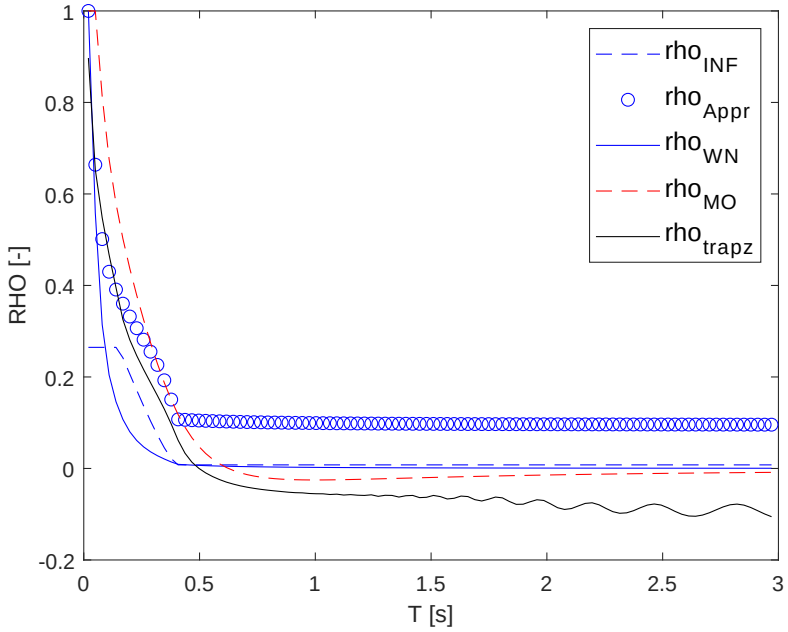

Figure 6.3: Corr. coeff. in hypothesis of white noise

6.4 White noise validity

Summing up, the two methods provide closed form solutions for the first three moments of the power spectral density of response to the classes of white-noise and filtered white-noise inputs.
The formulations yield good results for the prediction of median PFA demands of tallspatial structures with closely spaced modes.
There are situations however, in which this kind of approximation is not able provide reliable solutions, due to the fact that it tends to underestimate the contribution of higher modes.
In particular, the ineffectiveness of the white-noise input assumption for evaluation of correlation coefficients has been widely recognized for both the following two cases:

1. nodal frequencies that lie outside the range of the significant frequency content of the input [8]

2. system response dominated by high frequency modes [26]

Der Kiureghian himself investigated the influence of PSD shape on correlation coefficient evaluation, using a PSD derived from the U.S.Nuclear Regulatory Commission response spectrum by adopting a rough approach [23], and the effect of input narrow-bandedness by employing the well-known Kanai-Tajimi PSD. They stated that (1) the white noise model tends to underestimate the modal correlations when either of the two modes has a frequency higher than 30 rad/s and (2) narrow-bandedness of the input excitation has a profound influence on the correlation coefficients, for modes with frequencies higher than the predominant frequency of the input excitation. Therefore in the next two chapters two analytical solution are presented, disregarding the hypothesis of white noise approximation and providing the correlation coefficients consistent with the input PSD.

Chapter 7

Correlation coefficients - Multiple timescale analysis

The aim of this chapter is to present the basic principles behind the Multiple Timescale Spectral Analysis approach proposed by Denoel [6]. It will be seen how, the principle proposed, once applied to the case study, will allow to obtain a very handy and elegant formulation for the computation of the required spectral moments. After a brief introduction to the theory background, the implementation of the model is presented.
As already presented, the spectral analysis is a useful tool to study many common engineering situation, as for example the response of linear or slightly non linear oscillators, MDOF systems under stationary loadings, or even transients excitations. For all these kinds of problems, the procedure to adopt in order to obtain the final solution involves the integration of the spectra over the frequency space. Due to the fact that in many applications, frequency domain may be multi-dimensional, the application of standard derivation technique may be prohibitive. However, many of the above mentioned engineering problems involve a clear timescale separation. In these problems, a proper exploitation of the peculiarity allows to decrease the order of integration by one, at least. In particular, when the order of integration drops to zero, this offers the possibility to derive analytical solutions, which is the goal of this work.
Now, by supposing to work in the R^{j-1} frequency domain, then the spectral analysis goal is to determine the *j-th* cumulant of the response:

$$k^{(j)} = \int .. \int_{R^{(j)}} G_x(w^{(j)}) dw^{(j)} \tag{7.1}$$

being $G_x(w^{(j)})$ the *j-th* order spectrum of the response.

Now, the existence of multiple timescales in the response translates into the existence of several well-distinct peaks in the spectra. This aspect was first taken into account by Davenport [27] who suggested to decompose the response in two components, the background and the resonant one. In the adoption of a numerical integration scheme, this allowed to greatly reduce the number of integration points to the sole natural frequencies of

the (possibly very large) structural model.
The first to propose a fully analytical solution was instead Preumont [28], who suggested to replace the loading by a piecewise constant approximation which finally results in a semi-analytical approach, thanks to some closed-form integrations. The work of Denoel can be considered a step halfway between the two procedures.

7.1 Timescale separation

The work by Denoel is proposed for the cases in which the timescale of the loading $G_p(w^{(j)})$ is different from the one of the system, where the latter ones are generally attributed to the poles in the kernel function $H(w^{(j)})$. However, as it will be presented later, with some manipulations and simplifications, the analytical approximation will be able to cover the whole frequency domain, also those zones in which the kernel pole is not so distant from the characteristic frequency of the loading.
Now, by focusing on the case under analysis, in which the structure is modeled as a 1 DOF linear oscillator, the frequency domain reduces to the dimension R^1, therefore the functions entering the problem recover the usual dependencies:

$$\begin{cases} G_p = G_{\ddot{U}_g} = G_{\ddot{U}_g}(\hat{w}) \\ G_X = G_X(\hat{w}, w_i, \xi_i) \\ K = K(\hat{w}, w_i, \xi_i) = H(\hat{w}, w_i, \xi_i) H^*(\hat{w}, w_i, \xi_i) \end{cases} \tag{7.2}$$

The first step of the method consists in locating the different peaks in $G_X(w^j)$. The resonant behaviour of the kernel function will manifest in corrispindence of one point only, i.e. the natural frequency of the structure. Sharp peaks are local contributions to the integral while wideband spectral regions result in global contributions.
However depending on their nature, the peaks might be classified into different families. For the problem under consideration, two categories of peaks can be identified:

1. background component
2. resonant component

7.1.1 Background component

The background component corresponds to the peak of the loading spectrum $G_p(\hat{w})$. Depending on the relative smallness of the characteristic frequency of the loading $\hat{\alpha}$ and that of the structure w_i, the behaviour of the kernel function may change. For example, in the case where $w_i >> \hat{\alpha}$, the local behaviour of the kernel function can be approximated as constant in correspondence of the origin, corresponding to the quasi static solution of a linear oscillator. On the other hand, for $w_i < \hat{\alpha}$, the local behaviour of the kernel

can be represented by the inertia regime solution. The approximation can be written in the general form:

$$\hat{K}(\hat{w}) = K_0 \hat{w}^{p_i} \tag{7.3}$$

where:

1. for $w_i >> \hat{\alpha}$, $p_i = 0$
2. for $w_i < \hat{\alpha}$, $p_i = 4$

Now, the contribution k_b associated to the background component is:

$$k_b = \int_0^{\inf} \hat{K}(\hat{w}) S_p(\hat{w}) d\hat{w} = K_0 \int_0^{\inf} \hat{w}^{p_i} S_P(\hat{w}) d\hat{w} \tag{7.4}$$

7.1.2 Resonant component

The subtraction of the background approximation k_b from the initial problem creates the following residual:

$$\int_0^{\inf} \hat{K}(\hat{w}) S_p(\hat{w}) d\hat{w} = K_0 \int_0^{\inf} \hat{w}^{p_i} \Big[K(\hat{w}, w_i, \xi_i) - \hat{K}(\hat{w}) \Big] G_{\ddot{U}_g}(\hat{w}) d\hat{w} \tag{7.5}$$

This term does not feature any significant contribution in the background domain anymore, therefore the resonant components are found to be the remaining ones in the residual. The analysis of the different contributions to this integral has to be performed specifically for each problem. Following the same considerations from above, the most important contributions are attributable to the regions of the frequency space where the poles of $H(\hat{w}, w_i, \xi_i)$ are located; they correspond to resonant components. In those regions, the loading spectrum $G_{\ddot{U}_g}(\hat{w})$ might be very small, which thus results in a small resonant component.
Depending on the original expression of the kernel $H(\hat{w}, w_i, \xi_i)$ and the loading spectrum $G_{\ddot{U}_g}(\hat{w})$, other regions of the domain may contribute more significantly. They correspond to smaller values of the factor in the square brackets, but much larger values of the loading spectrum. These components are classified as mixed background/ resonant components. There is a priori no means to rank the relative importance of these terms, it is thus recommended to carefully identify and study the different possible contributions. However, for the purposes of this thesis, the contribution related to the mixed background/resonant components will be disregarded.
In the following lines, a brief introduction to the procedure is reported.
In particular, by assuming the integral equation 7.5 to have a contribution in the neighbour of the frequuency $\hat{w} = \Omega_j$, extending over a more or less short bandwidth Δ_j, a new set of coordinates $\hat{\eta}$ is then introduced, in order to set the focus of the analysis on this contribution only: $\hat{w} = \Omega_j + \Delta_j \hat{\eta}$. Now, the equation 7.5 can be rewritten as:

$$f_1(\hat{w}(\hat{\eta}), w_i, \xi_i) = \Big[K(\hat{w}(\hat{\eta}), w_i, \xi_i) - \hat{K}(\hat{w}(\hat{\eta})) \Big] G_{\ddot{U}_g}(\hat{w}) |J_{\hat{w}}| d\hat{\eta} \tag{7.6}$$

Up till now, no approximations have been introduced. The center of method is now to derive a local approximation of the product:

$$\Big[K(\hat{w}(\hat{\eta}), w_i, \xi_i) - \hat{K}(\hat{w}(\hat{\eta}))\Big] G_{\ddot{U}_g}(\hat{w}) \tag{7.7}$$

The *Padè approximant* is usually available for this kind of task. It consists in the approximation of an analitic function with a rational one. The method is similar to the Taylor Series Expansion, in which the Padè approximant can be expressed as a truncation of a continous function, whose limits is the function itself.
Integration along at least one direction might be thus performed explicity, which thus drops by one the dimensionality of the integral.

7.2 Implementation of the procedure

Now that the basic principles behind the Multi time-scale analysis have been pointed out, it is possible to present the implementation of the model for the case under investigation. As already mentioned, the goal is to define an analytical approximation for the spectral moments entering the formula for the correlation coefficient:

$$\lambda_{ii} = Re\Big[\int_0^{\inf} H_i(\hat{w}, w_i, \xi_i) H_i^*(\hat{w}, w_i, \xi_i) G_{\ddot{u}_g}(\hat{w}) dw\Big] \tag{7.8}$$

$$\lambda_{ig} = Re\Big[\int_0^{\inf} H_i(\hat{w}, w_i, \xi_i) G_{\ddot{u}_g}(\hat{w}) dw\Big] \tag{7.9}$$

$$\lambda_{gg} = Re\Big[\int_0^{\inf} G_{\ddot{u}_g}(\hat{w}) dw\Big] \tag{7.10}$$

where $H_i(\hat{w}, w_i, \xi_i)$ is the Frequency Response Function associated to the absolute acceleration::

$$H_i(\hat{w}, w_i, \xi_i) = \frac{w_i^2 + 2i\hat{w}w_i\xi}{{w_i}^2 - \hat{w}^2 + 2iw_i\hat{w}} \tag{7.11}$$

While, for what concerns the adopted Power Spectral Density $G_{\ddot{u}_g}(\hat{w})$, the piecewise formulation proposed by Barone et al, compatible with the codes RS, is chosen:

$$G_{\ddot{u}_g}(w) = \begin{cases} G_0(\frac{w_D}{w_C})^{e_2}(\frac{w}{w_D})^{e_1} & \text{se } 0 \le w \le w_D \\ G_0(\frac{w}{w_C})^{e_2} & \text{se } w_D \le w \le w_C \\ G_0(\frac{w}{w_C})^{e_3} & \text{se } w_C \le w \le w_B \\ G_0(\frac{w_B}{w_C})^{e_3}(\frac{w}{w_B})^{e_4} & \text{se } w > w_B \end{cases} \tag{7.12}$$

However, in order to decrease as much as possibily the complexity of the formulation,the two-branched version of the PSD formulation proposed by Barone et al [5] is used:

$$G_{\ddot{u}_g}(w) = \begin{cases} G_0(\frac{w}{w_C})^{e_2} & \text{se } 0 \le w \le w_C \\ G_0(\frac{w}{w_C})^{e_3} & \text{se } w > w_C \end{cases} \tag{7.13}$$

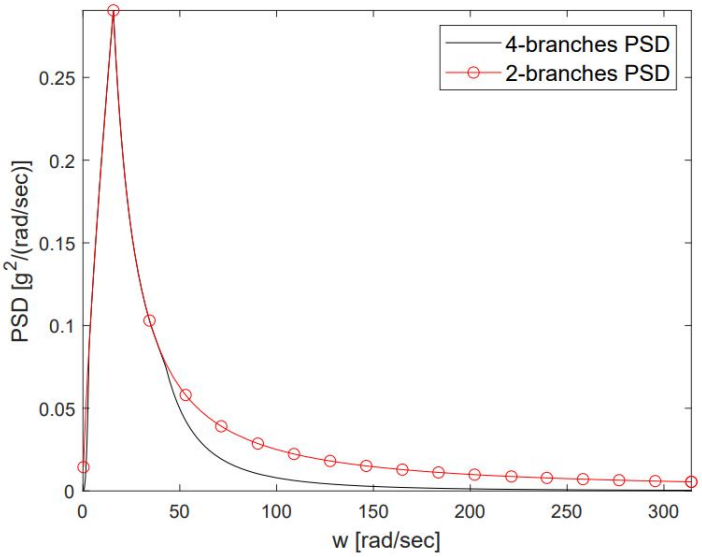

Figure 7.1: PSD comparison

A comparison between the two formulations reported in (*7.12*) and (*7.13*) is presented in Figure (*7.1*) The two branches formulation can be used for the same reason for which the majority of the codes allow to model the RS with a 2 piece formulation instead of the usual one with 4 branches. Now the next paragraph will be organized in the following way. Starting from the variance of the response, the implementation of the multi timescale analysis will be presented for the three different frequency domain:

1. Case 1: $w_i > w_C$
2. Case 2: $w_i = w_C$
3. Case 3: $w_i < w_C$

Then the same will be done for the cross spectral moment λ_{ig}.
The results which will be presented in the next paragraphs have been obtained with the help of the software *WX MAXIMA*. *Maxima* is a *CAS* (Computer Algebra System). A *CAS* can perform symbolic algebraic manipulations. This is particularly handy when manipulating large polynomials. The symbolic manipulation includes differentiation, integration, Taylor series, Laplace transforms, ordinary differential equations, systems of linear equations and polynomials, yielding high precision numeric results by using exact fractions, arbitrary precision integers, and variable precision floating point numbers.

7.3 Variance of the response λ_{ii}

The variance of the response has the form:

$$\lambda_{ii} = Re\Big[\int_0^{\inf} H_i(\hat{w}, w_i, \xi_i) H_i^*(\hat{w}, w_i, \xi_i) G_{\ddot{u}_g}(\hat{w}) dw\Big] \tag{7.14}$$

where the PSD function $G_{\ddot{u}_g}(\hat{w})$ is amplified by the product between the FRF and its conjugate:

$$H_i(\hat{w}, w_i, \xi_i) \times conj\Big[H_i(\hat{w}, w_i, \xi_i)\Big] = \frac{w_i^4 + 4i\hat{w}^2 w_i^2 \xi^2}{(w_i{}^2 - \hat{w}^2)^2 + 4i\hat{w}^2 w_i^2 \xi^2} \tag{7.15}$$

Now, in order to soften the formulation, the contribution of the damping at the numerator has been neglected. In the frequency domain, the behaviour of the Kernel function is therefore represented by the following curve:

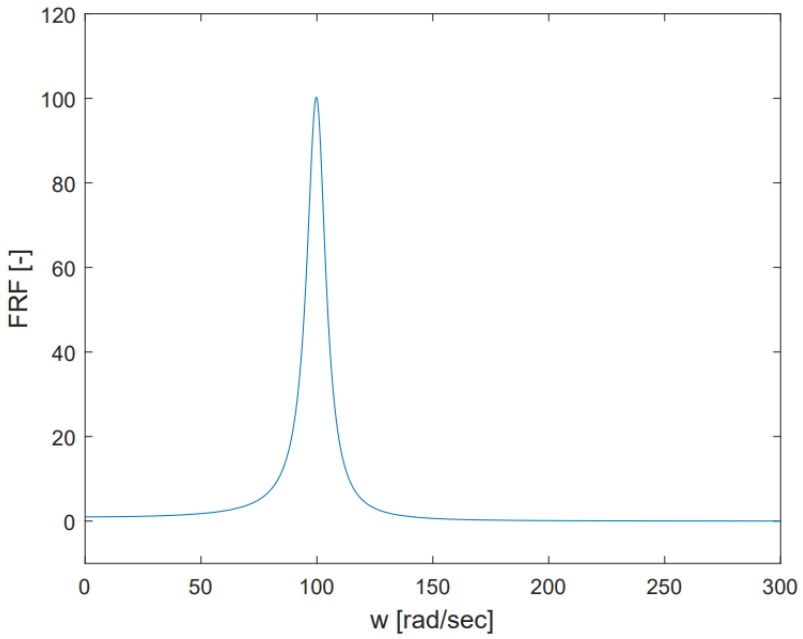

Figure 7.2: Kernel function - $w_i > w_c$

In conclusion, the aim of this paragraph is to define a simplified analitical formulation for the following integral:

$$\lambda_{ii} = \int_0^{\inf} \frac{w_i^4}{(w_i{}^2 - \hat{w}^2)^2 + 4i\hat{w}^2 w_i^2 \xi^2} G_{\ddot{u}_g}(\hat{w}) d\hat{w} \tag{7.16}$$

7.3.1 Case 1: $w_i > w_C$

For the case under consideration, by assuming a value of the natural frequency equal to $w_i = 4w_C$, the curve representing the behaviour of the integrand in the frequency domain is:

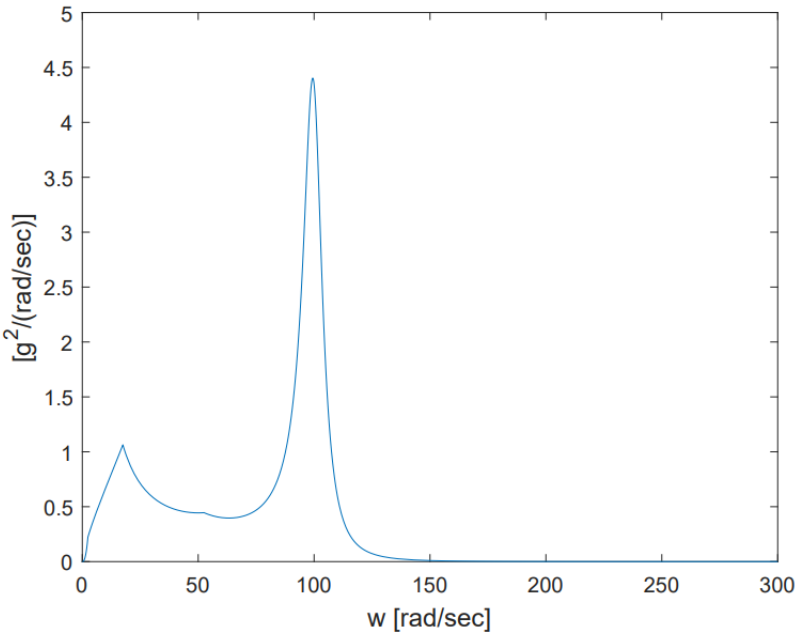

Figure 7.3: Response PSD - $w_i > w_c$

A clear separation of the timescale can be observed, allowing to apply the principles proposed by Denoel. In particular:

1. the lower peak represents the background response associated to the PSD

2. the higher peack is related to the resonant response

Now, the background contribution can be obtained simply by observing that:

$$\lim_{\hat{w}\to 0} H_i H_i^{(*)} = \lim_{\hat{w}\to 0} \frac{w_i^4}{(w_i{}^2 - \hat{w}^2)^2 + 4i\hat{w}^2 w_i^2 \xi^2} = 1 \tag{7.17}$$

where $H_i = H_i(\hat{w}, w_i, \xi_i)$, and $H_i^{(*)}$ represents its complex conjugate. Consequently, in order to obtain the final solution, it is sufficient to integrate the piecewise expression of the PSD along the frequency domain. This is possible however only in those ragion of the domain in which the approximation (*7.17*) holds. This is why the integration domain will be limited from the top to natural frequency w_i only, and not extended to $+\infty$:

$$\begin{aligned} \lambda_{ii,b} &= \int_0^{w_i} G_{\ddot{u}_g}(\hat{w}) d\hat{w} = \int_0^{w_C} G_0 (\frac{w}{w_C})^{e_2} d\hat{w} + \int_{w_C}^{w_i} \frac{w}{w_C})^{e_3} d\hat{w} \\ &= \frac{G_0 \left(\frac{w_i^{e_3+1}}{e_3+1} - \frac{w_C^{e_3+1}}{e_3+1} \right)}{e_2+1} + \frac{G_0 w_C}{e_2+1} \end{aligned} \tag{7.18}$$

The focus can be now centerned on the resonant contribution. The first step is to compute the residual r_1 of the kernel function, in order to disregard

the contribution already accounted for in the background integral:

$$r_1 = \left[H_i H_i^{(*)}\right] - 1 = \frac{\hat{w}^4 + 2\hat{w}^2 w_i^2 + 4i\hat{w}^2 w_i^2 \xi^2}{(w_i{}^2 - \hat{w}^2)^2 + 4i\hat{w}^2 w_i^2 \xi^2} \tag{7.19}$$

whose behaviour in the frequency domain is:

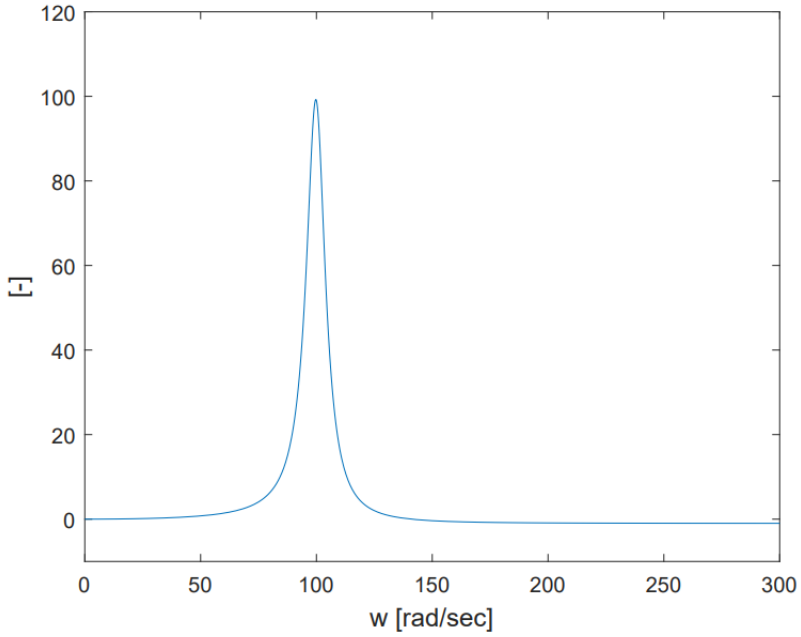

Figure 7.4: Residual function r_1

The resonant contribution is now represented by the integral equation:

$$\lambda_{ii,r} = \int_0^{\inf} \frac{\hat{w}^4 + 2\hat{w}^2 w_i^2 + 4i\hat{w}^2 w_i^2 \xi^2}{(w_i{}^2 - \hat{w}^2)^2 + 4i\hat{w}^2 w_i^2 \xi^2} G_{\ddot{u}_g}(\hat{w}) d\hat{w} \tag{7.20}$$

As it can be seen, no practical analytical solution is available for $\lambda_{ii,r}$ in this form. To solve the problem, the approximation proposed by Padè is introduced. First of all it is necessary to introduce a new variable η, in such a way that: $\hat{w} = w_1(1+\xi\eta)$, where w_1 is the frequency abscissa of the peak, which is evaluated by imposing the stationarity of the residual:

$$\frac{dr_1}{d\hat{w}} = 0 \tag{7.21}$$

Three solutions are provided:

$$\begin{cases} w_1 = w_i\sqrt{1-2\xi^2} \\ w_2 = 0 \\ w_3 = -w_i\sqrt{1-2\xi^2} \end{cases} \tag{7.22}$$

The trivial solution w_2 and the negative solution w_3 are disregarded, therefore the attention is focused on w_1. By replacing the new set of coordinates

inside (*7.19*) , a new formulation for the residual r_1, here recalled as q_1, is obtained:

$$q_1 = -\frac{4\eta^4\xi^8 + 16\eta^3\xi^7 + (16\eta^2 - 4\eta^4)\xi^6 - 16\eta^3\xi^5 + (\eta^4 - 16\eta^2 - 4)\xi^4 + 4\eta^3\xi^3 + (4\eta^2 + 4)\xi^2 - 1}{4\eta^4\xi^8 + 16\eta^3\xi^7 + (16\eta^2 - 4\eta^4)\xi^6 - 16\eta^3\xi^5 + (\eta^4 - 16\eta^2 - 4)\xi^4 + 4\eta^3\xi^3 + 4(\eta^2 + 1)\xi^2} \tag{7.23}$$

By plotting q_1 in the stretched domain (*7.5*), where the new variable on the ascissa is η, it can be seen how the peak of "r1" is now centered in zero:

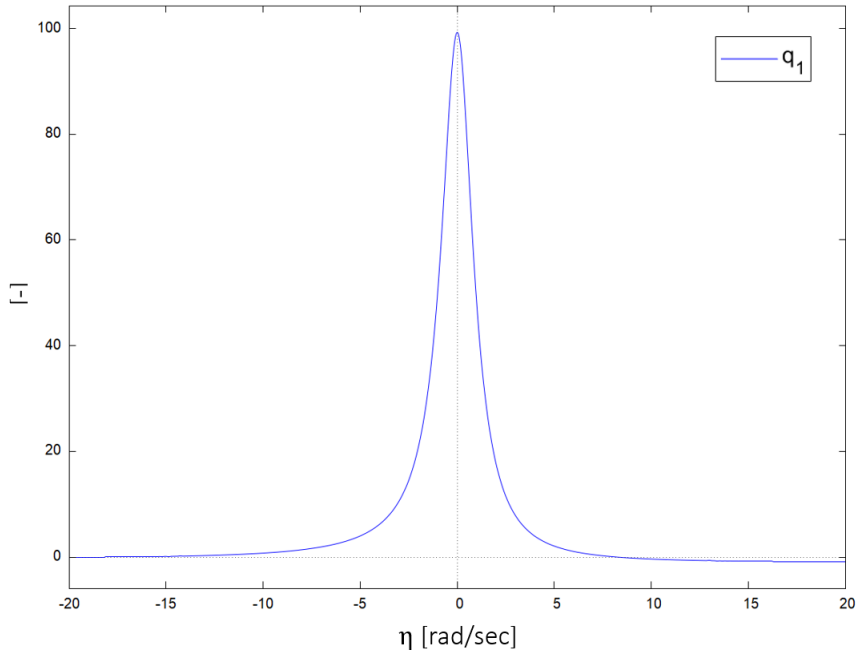

Figure 7.5: Residual function in the frequency stretched domain

This allows now to introduce the concept of Padè approximant. As presented before, Padé approximants are rational polynomial derived typically from a Taylor series expansion. The infinite terms of a Taylor series are made into a polynomial rational function (i.e. polynomial over a polynomial).
In order to have a clearer view of what was dose, a brief explaination of the steps adopted in *wxMaxima* is here reported in the case of the simple sinusoidal function $sin(x)$. The line of code adopted in *wxMaxima* is:

$$pade\Big[taylor\Big(sin(x), x, 0, 3\Big), 2, 2\Big] \tag{7.24}$$

The function $taylor()$ generates a taylor series. In the example above, the code is generating a taylor series for $sin(x)$ with the variable x centered at 0 by using 3 terms. This taylor series is an input for the Pade approximation, where the arguments $2, 2$ are the degrees of numerator and denominator requested for the final rational approximating polynomials.
at the end the output is: $\left[\frac{6x}{x^2+6}\right]$ The same procedure was followed for the case under analysis. Formula (*7.47*) in the stretched coordinate is given as

input, and the program is asked to generate a rational polynomial approximation with a degree 0 at the numerator and a degree 2 at the denominator, leading to:

$$p_1 = \frac{4\xi^4 - 4\xi^2 + 1}{-4\xi^4 + 4\eta^2\xi^2 + 4\xi^2} \tag{7.25}$$

where p_1 represents the Padè approximant of the residual r_1. The formulation provided by *MAXIMA* is able to approximate quite well the original form of the residual. A comparison in the stretched domain between q_1 and p_1 is here reported:

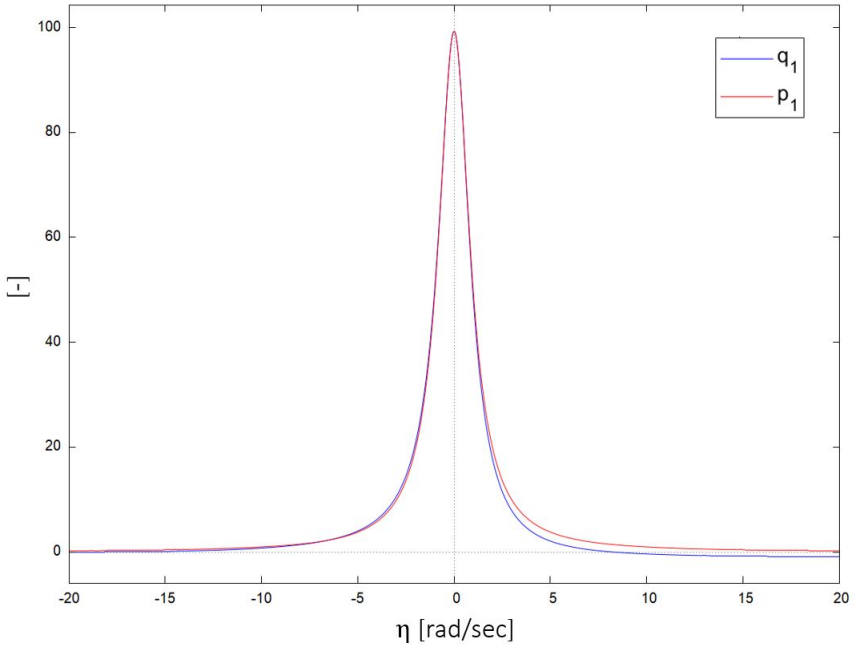

Figure 7.6: Comparison between q_1 and p_1

Now, by comparing the formulation obtained by means of the Padè approximation and the original one in (*7.19*), it is evident how the latter is more handy, allowing now to analitically evaluate its integral.
In particular, by introducing the Jacobian of the differential problem, $\frac{d\hat{w}}{d\eta} = \xi w_1$, the integral solution of (*7.25*) is:

$$\int_{-\infty}^{\infty} p_1 \xi w_1 d\eta = \frac{\pi w_i \sqrt{1-2\xi^2}\left(4\xi^4 - 4\xi^2 + 1\right)}{2\sqrt{4\xi^2 - 4\xi^4}} \tag{7.26}$$

Now it's only a matter of multiplying the solution (*7.26*) by the value of the PSD in correspondence of the peak. This is possible since the behaviour of the PSD can be usually considered as constant accros a resonance peak, as a result of the timescale separation.
Therefore, the final solution yields:

$$\lambda_{ii,r} = \frac{\pi w_i \sqrt{1-2\xi^2}\left(4\xi^4 - 4\xi^2 + 1\right)}{2\sqrt{4\xi^2 - 4\xi^4}} G_{\ddot{u}_g}(w_1) \tag{7.27}$$

and by considering that $w_i > w_C$:

$$G_{\ddot{u}_g}(w_1) = G_0\left(\frac{w_1}{w_C}\right)^{e_3} \tag{7.28}$$

Finally, by gathering together both the background $\lambda_{ii,b}$ and the resonant contributions $\lambda_{ii,r}$, the anlytical solution for λ_{ii} is:

$$\begin{aligned}\lambda_{ii} = &\frac{\pi w_i \sqrt{1-2\xi^2}\left(4\xi^4 - 4\xi^2 + 1\right)}{2\sqrt{4\xi^2 - 4\xi^4}} G_{\ddot{u}_g}(w_1) \\ &+ \frac{G_0\left(\frac{w_i^{e_3+1}}{e_3+1} - \frac{w_C^{e_3+1}}{e_3+1}\right)}{e_2+1} + \frac{G_0 w_C}{e_2+1}\end{aligned} \tag{7.29}$$

7.3.2 Case 2: $w_i < w_C$

As for the case $wi > w_C$, the variance of the response is represented by the following integral:

$$\lambda_{ii} = \int_0^{\inf} \frac{w_i^4}{(w_i{}^2 - \hat{w}^2)^2 + 4i\hat{w}^2 w_i^2 \xi^2} G_{\ddot{u}_g}(\hat{w}) d\hat{w} \tag{7.30}$$

However, when the frequency of the structure is lower than the characteristic frequency of the loading, the behaviour of the response PSD in the frequency domain is quite different, as it can be appreciated in Figure *7.8*, where the graph was plotted considering a fictitous value for the structural frequency $w_i = \frac{1}{2} w_C$

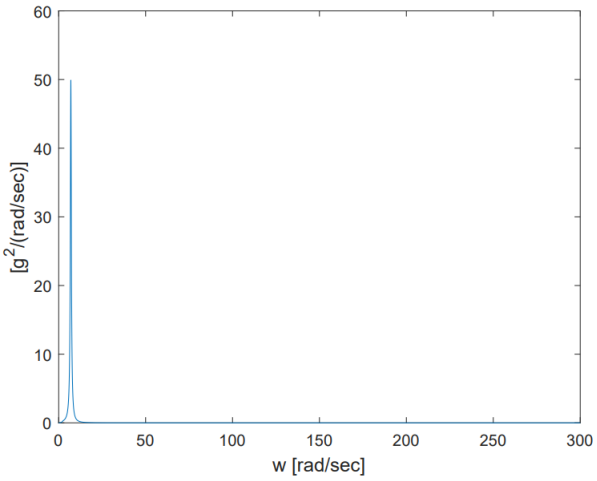

Figure 7.7: Output PSD - $w_i < w_c$

What happens now is that there is not a clear timescale separation as observed in the previuos case, since only a single peak appears. However, in order to solve the problem, the theory proposed by Denoel can still be used, as long as some approximations are introduced. In particular:

1. the background component will be now neglected

2. the Padè approximant will be applied directly to the Kernel function.

So, since the background component is disregarded, there would be no need to compute a residual component, therefore the r_1 function will coincide in this case with the kernel function itself:

$$r_1 = H_i H_i^{(*)} = \frac{w_i^4}{(w_i{}^2 - \hat{w}^2)^2 + 4i\hat{w}^2 w_i^2 \xi^2} \tag{7.31}$$

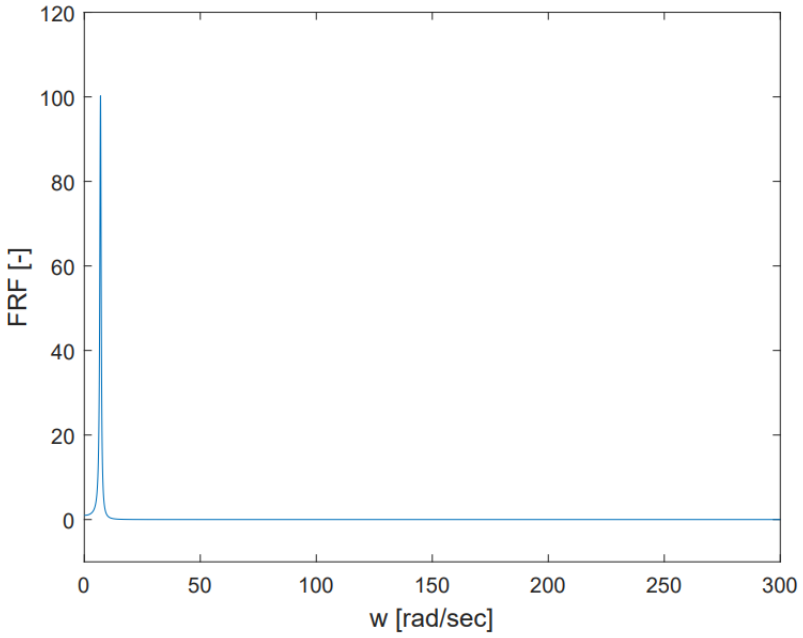

Figure 7.8: Kernel function: wi<wc

By adopting a change of variable of the type: $\hat{w} = w_1(1 + \xi\eta)$, (*7.31*) can be rewritten in terms of the new coordinate η:

$$q_1 = \frac{1}{4\eta^4\xi^8 + 16\eta^3\xi^7 + (16\eta^2 - 4\eta^4)\xi^6 - 16\eta^3\xi^5 + (\eta^4 - 16\eta^2 - 4)\xi^4 + 4\eta^3\xi^3 + 4(\eta^2 + 1)\xi^2} \tag{7.32}$$

As before, w_1 represents the abscissa coordinate in correspondence of the peak, computed by imposing the stationarity of r_1: $\frac{dr_1}{d\hat{w}} = 0$. The positive solution $w_1 = w_i\sqrt{1 - 2\xi^2}$ is adopted.
The change of variable will cause a translation of the peak in correspondence of the origin (Figure *7.9*),

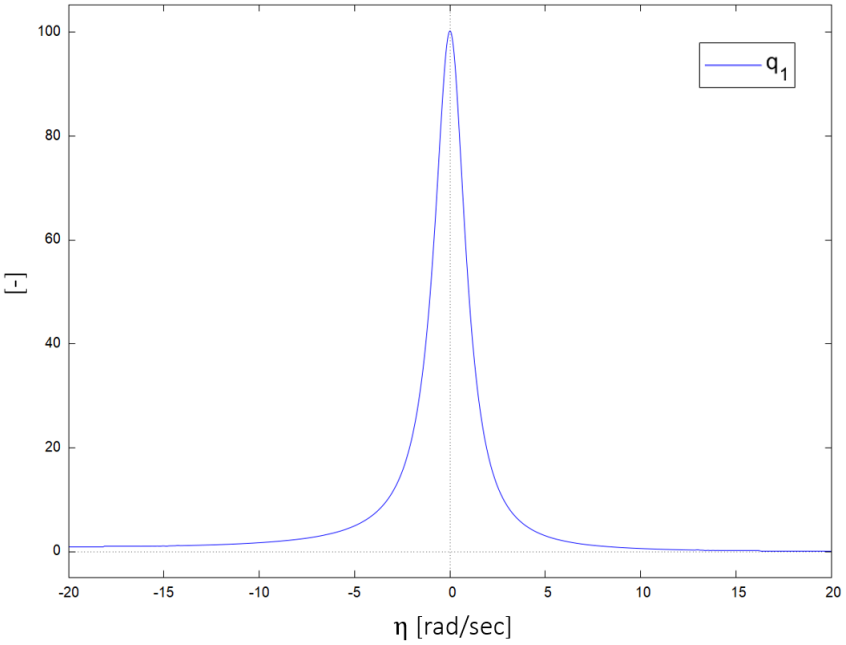

Figure 7.9: q_1 function: wi<wc

By exploiting now the algebraic capacity of *WX MAXIMA*, it is possible to compute the rational polynomial rapresentation of (*7.32*) exploiting the Padè approximation:

$$pade\Big[taylor\Big(q_1(\eta),\eta,0,2\Big),0,4\Big] \tag{7.33}$$

obtaining:

$$p_1 = \frac{1}{\eta^2\Big(16\xi^6 - 16\xi^4 + 4\xi^2\Big) - 4\xi^4 + 4\xi^2} \tag{7.34}$$

A comparison between p_1 and q_1 is reported in Figure *7.10*.
As before, by introducing the Jacobian of the differential problem, $\frac{d\hat{w}}{d\eta} = \xi w_1$, the integral solution of (*7.25*) is:

$$\int_{-\infty}^{\infty} p_1 \xi w_1 d\eta = \frac{\pi w_i \ \xi\sqrt{1-2\xi^2}}{\sqrt{4\xi^2 - 4\xi^4}\sqrt{16\xi^6 - 16\xi^4 + 4\xi^2}} \tag{7.35}$$

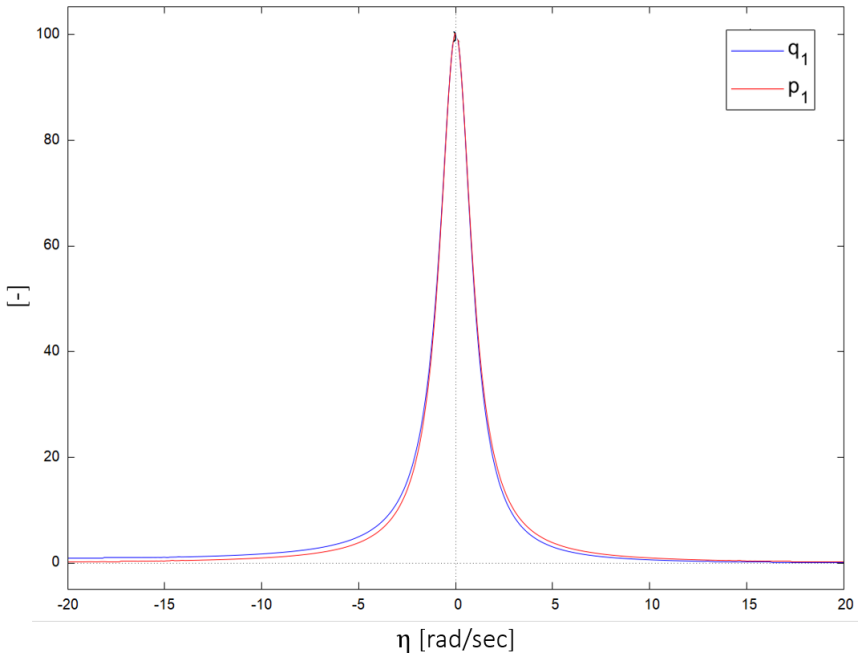

Figure 7.10: q_1 function: wi<wc

The final analytical solution for $\lambda_i i$ is obtained by multiplying (*7.36*) times the value of the PSD in correspondence of the kernel peak, i.e.

$$\lambda_i i = \frac{\pi w_i \ \xi\sqrt{1-2\xi^2}}{\sqrt{4\xi^2-4\xi^4}\sqrt{16\xi^6-16\xi^4+4\xi^2}} G_{\ddot{u}_g}(w_1) \tag{7.36}$$

and since $w_i < w_C$:

$$G_{\ddot{u}_g}(w_1) = G_0\left(\frac{w_1}{w_C}\right)^{e_2} \tag{7.37}$$

where $e_2 = \frac{2}{3}$.

7.3.3 Case 3: $w_i = w_C$

The procedure adopted when the frequency of the structure equals the one of the loading follows the one for the case of $wi < wc$. As before, in the frequency domain, the argument of the integral function shows a unique peak, meaning that also in this case, the contribution associated to the peak of the PSD is absorbed by the resonant one (Figure *7.11*). The background contribution can be neglected, and the Padè approximation is directly applied on the kernel function

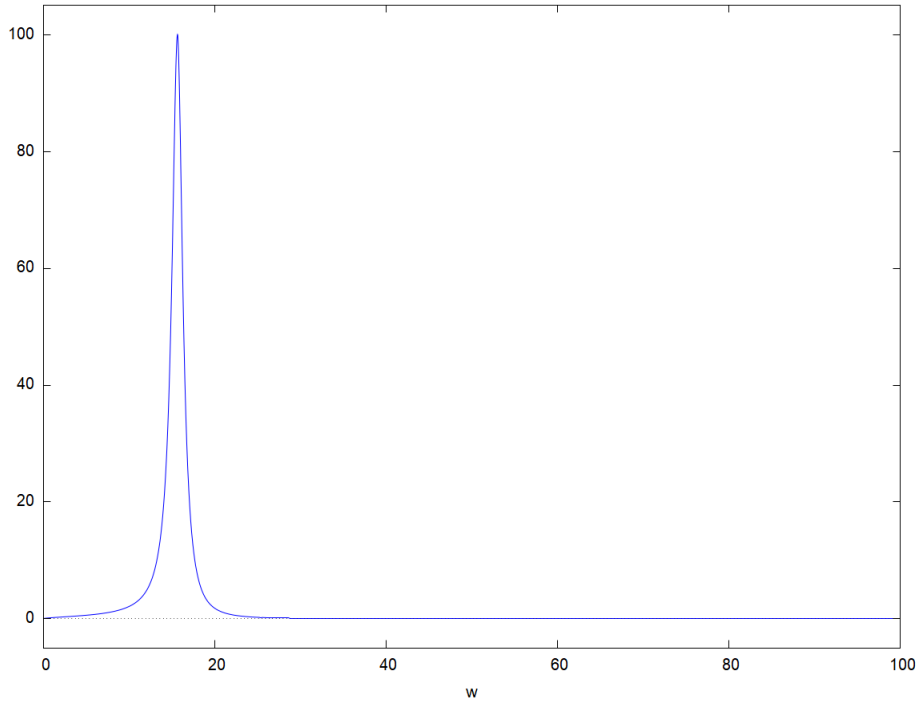

Figure 7.11: Output PSD - $w_i = w_c$

By following the same steps adopted in the previous case $w_i < w_C$, the Padè method provides the following rational approximation:

$$p_1 = \frac{1}{\eta^2\left(16\xi^6 - 16\xi^4 + 4\xi^2\right) - 4\xi^4 + 4\xi^2} \tag{7.38}$$

Therefore the final analytical solution for the spectral moment $\lambda_i i$ reads:

$$\lambda_i i = \frac{\pi w_i \ \xi\sqrt{1-2\xi^2}}{\sqrt{4\xi^2 - 4\xi^4}\sqrt{16\xi^6 - 16\xi^4 + 4\xi^2}} G_{\ddot{u}_g}(w_1) \tag{7.39}$$

In conclusion, for the different frequency sub-domains, the analytical formulations for the spectral moment λ_u is:
for $w_i \leq w_C$

$$\lambda_{ii} = \frac{\pi w_i \ \xi\sqrt{1-2\xi^2}}{\sqrt{4\xi^2 - 4\xi^4}\sqrt{16\xi^6 - 16\xi^4 + 4\xi^2}} G_{\ddot{u}_g}(w_1) \tag{7.40}$$

while, for $w_i > w_C$:

$$\lambda_{ii} = \frac{\pi w_i \sqrt{1-2\xi^2}\left(4\xi^4 - 4\xi^2 + 1\right)}{2\sqrt{4\xi^2 - 4\xi^4}} G_{\ddot{u}_g}(w_1) + \frac{G_0\left(\frac{w_i^{e_3+1}}{e_3+1} - \frac{w_C^{e_3+1}}{e_3+1}\right)}{e_2+1} + \frac{G_0 w_C}{e_2+1} \tag{7.41}$$

7.4 Cross spectral moment λ_{ig}

The cross spectral moment λ_{ig} between the $i-th$ mode of the structure and the ground acceleration is defined as:

$$\lambda_{ig} = \int_0^\infty Re\Big[H_i(\hat{w}, w_i, \xi_i)\Big] G_{\ddot{u}_g}(\hat{w}) d\hat{w} \tag{7.42}$$

where:

$$Re\Big[H_i(\hat{w}, w_i, \xi_i)\Big] = \frac{w_i^4 - \hat{w}^2 w_i^2 + 4i\hat{w}^2 w_i^2 \xi^2}{({w_i}^2 - \hat{w}^2)^2 + 4i\hat{w}^2 w_i^2 \xi^2} \tag{7.43}$$

whose behaviour in the frequency domain is:

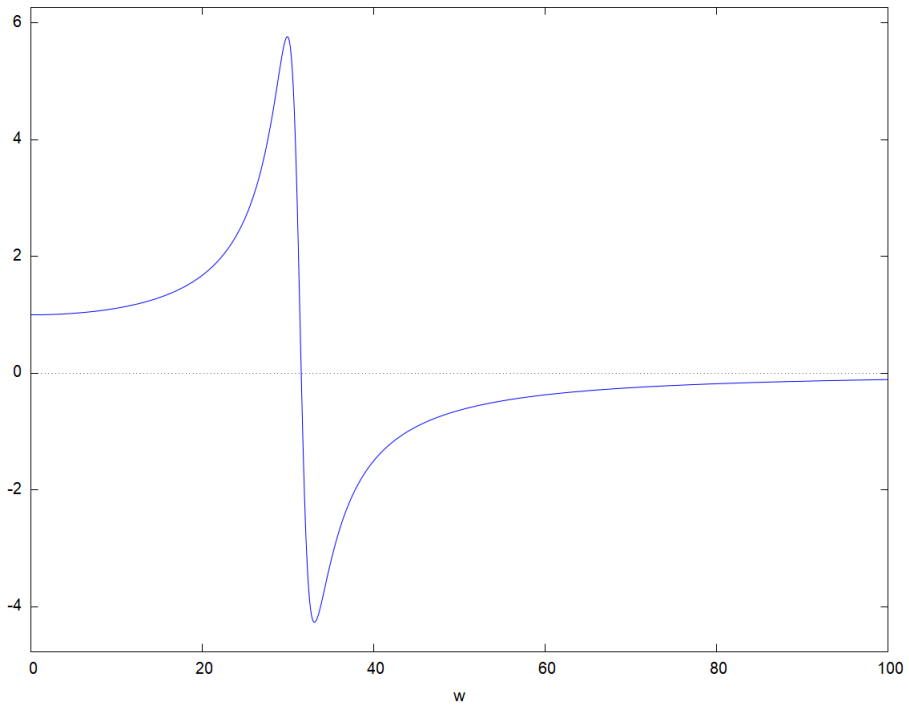

Figure 7.12: Frequency response function

Exactly as before, depending on the relation between forcing frequency w_C and natural frequency w_i, different considerations and approximations will be made.

7.4.1 Case 1: $w_i > w_C$

By adopting a value $wi = 4wc$ for the natural frequency , the intagrand function in the frequency domain has the following behaviour:

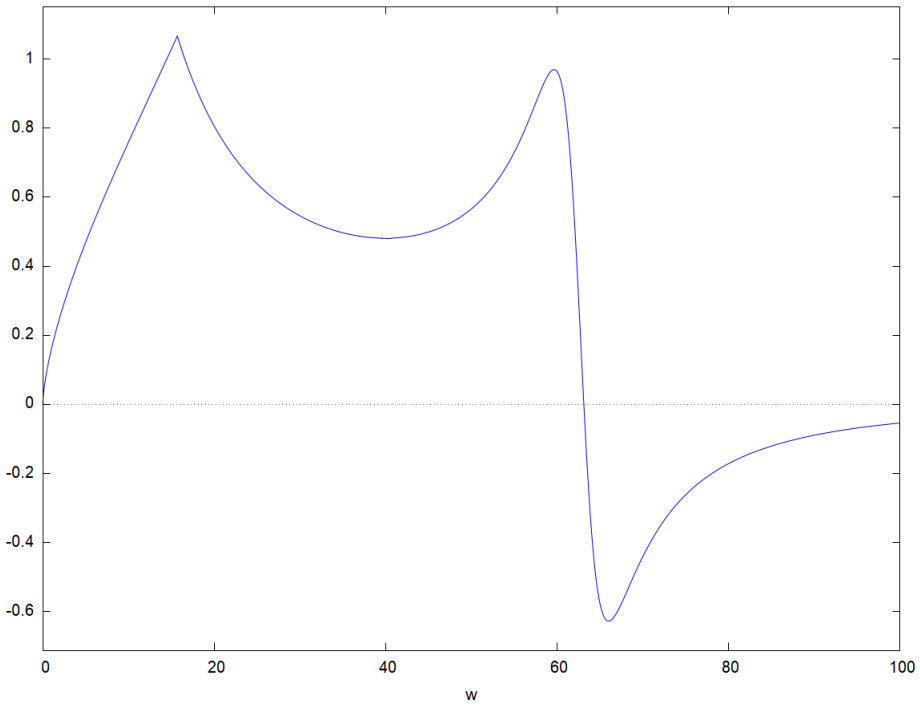

Figure 7.13: Cross spectral moment integrand function

The peak located in the low frequency domain represents the background contribution associated to the PSD. While the resonant component developes in the neighbour of the natural frequency w_i. The main diffrenece wrt the previus case is related to the fact that the cross spectral moment λ_{ig} shows a double peak in correspondence of the natural frequency of the system. This however do not represent a problem, and the results provided by the Padè approximant remain valid.
For what concerns the background component, as before, the way of reasoning exploits the fact that the PSD goes to zero as w goes to ∞, while the leading order term of the kernel function (*7.43*), i.e. its limit as w goes to 0, is 1.
Consequently, the background component λ_{ig} is:

$$\begin{aligned}\lambda_{ii,r} &= \int_0^{w_i} G_{\ddot{u}_g}(\hat{w})d\hat{w} = \int_0^{w_C} G_0(\frac{w}{w_C})^{e_2}d\hat{w} + \int_{w_C}^{w_i}(\frac{w}{w_C})^{e_3}d\hat{w} \\ &= \frac{G_0\left(\frac{w_i^{e_3+1}}{e_3+1} - \frac{w_C^{e_3+1}}{e_3+1}\right)}{e_2+1} + \frac{G_0 w_C}{e_2+1}\end{aligned} \tag{7.44}$$

The next step is to compute the residual contribution r_1 of the kernel func-

tion:

$$r_1 = Re\Big[H_i\Big] - 1 = \frac{\hat{w}^2 w_i^2 - w_i^4}{4w_i^2\hat{w}^2\xi^2 + w_i^4 - 2\hat{w}^2 w_i^2} \tag{7.45}$$

The peaks of the residual function are located in correspondence of the points which ensure the stationarity of r_1. Therefore, by imposing $\frac{dr_1}{d\hat{w}} = 0$, four different results are provided. In the positive frequency domain the solutions are:

$$\begin{cases} w_1 = \frac{w_i}{\sqrt{2\xi+1}} \\ w_2 = \frac{iw_i}{\sqrt{2\xi-1}} \end{cases} \tag{7.46}$$

Now, the procedure to follow in order to define a handy analitical formulation of the residual is the same of the one presented in section 7.3.1, only that now it must be repeated for both the peaks involved.
The first peak analysed is the positive one. By introducing the variable η, and by adopting the new strained coordinate $\hat{w} = w_1(1+\xi\eta)$, (*7.45*) can be rewritten as:

$$q_1 = -\frac{\eta^4\xi^3 + \Big(4\eta^3 - 2\eta^2\Big)\xi^2 + \Big(5\eta^2 - 4\eta\Big)\xi + 2\eta - 2}{8\eta^2\xi^4 + (\eta^4 + 4\eta^2 + 16\eta)\xi^3 + (4\eta^3 - 4\eta^2 + 8\eta + 8)\xi^2 + (4\eta^2 - 8\xi + 8)\xi} \tag{7.47}$$

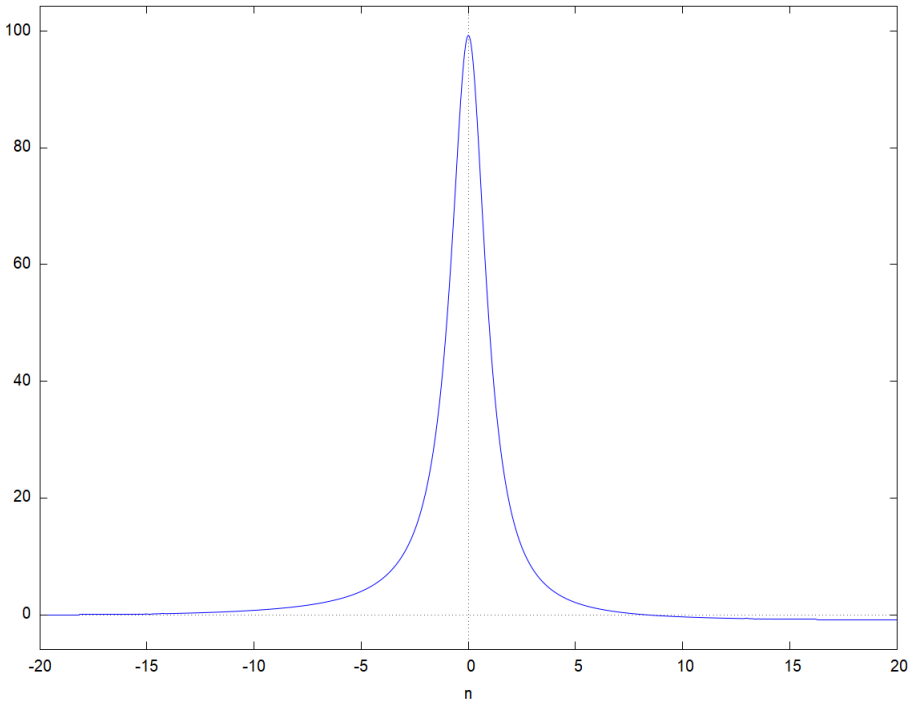

Figure 7.14: residual behaviour in the strained coordinates

The new strained coordinate moves the peak of the residual in zero (Figure *7.14*) which enables the reader to apply the rational approximation proposed by Padè. In particular:

$$p_1 = pade\Big[taylor\Big(q_1(\eta), \eta, 0, 2\Big), 0, 2\Big] \tag{7.48}$$

obtaining:

$$p_1 = \frac{1}{\eta^2\Big(8\xi^3 + 8\xi^2 + 2\xi\Big) + 4\xi^2 + 4\xi} \tag{7.49}$$

which approximates very well the behaviour of the residual function q_1 in correspondence of the peak (Figure *3.40*)

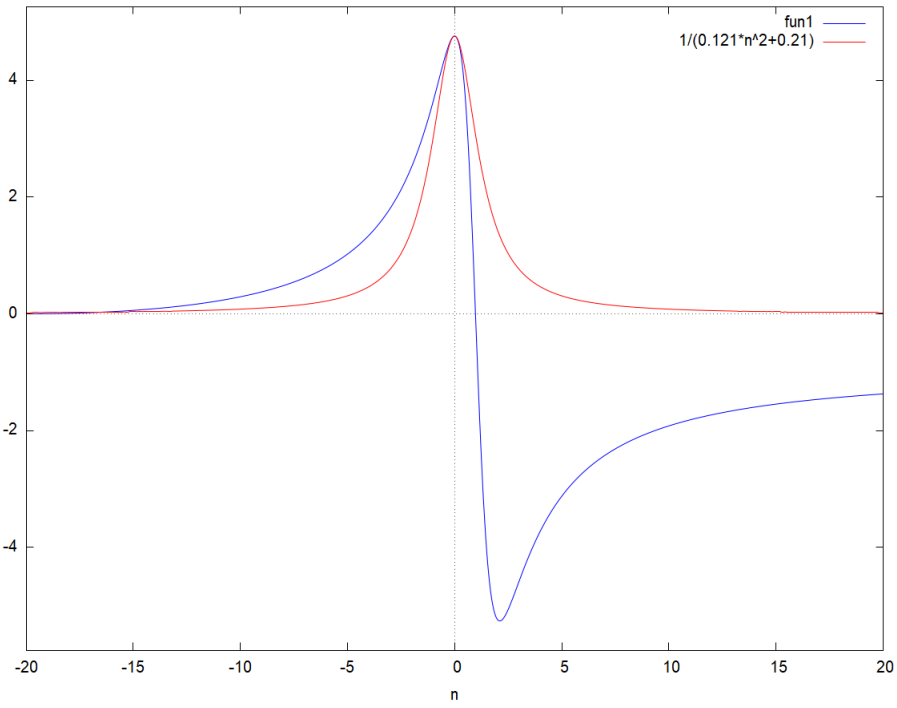

Figure 7.15: Formulation comparison in the strained domain

It is now possible to evaluate the anlytical solution of (*7.49*):

$$\int_{-\infty}^{\infty} p_1 \xi w_1 d\eta = \frac{\pi w_i \ \xi}{\sqrt{4\xi^2 + 4\xi}\sqrt{2\xi + 1}\sqrt{8\xi^3 + 8\xi^2 + 2\xi}} \tag{7.50}$$

By multiplying the solution (*7.63*) by the value of the PSD in correspondence of the peak, the final analytical solution for the first resonant component is obtained:

$$\lambda_i i = \frac{\pi w_i \ \xi}{\sqrt{4\xi^2 + 4\xi}\sqrt{2\xi + 1}\sqrt{8\xi^3 + 8\xi^2 + 2\xi}} G_{\ddot{u}_g}(w_1) \tag{7.51}$$

and since $w_i > w_C$:

$$G_{\ddot{u}_g}(w_1) = G_0\Big(\frac{w_1}{w_C}\Big)^{e_2} \tag{7.52}$$

where $e_2 = \frac{2}{3}$.
The same way of reasoning is applied to the second resonant contribution. The formulation for the residual coincides with the previous one:

$$r_2 = Re\Big[H_i\Big] - 1 = \frac{\hat{w}^2 w_i^2 - w_i^4}{4w_i^2\hat{w}^2\xi^2 + w_i^4 - 2\hat{w}^2 w_i^2} \tag{7.53}$$

only that now the change of variable makes reference to the abscissa of the negative peak, $\hat{w} = w_2(1 + \xi\eta)$. In the stretched domain, (*7.53* becomes:

$$q_2 = -\frac{\eta^4\xi^3 + \Big(4\eta^3 + 2\eta^2\Big)\xi^2 + \Big(5\eta^2 + 4\eta\Big)\xi + 2\eta + 2}{8\eta^2\xi^4 + (-\eta^4 - 4\eta^2 + 16\eta)\xi^3 + (-4\eta^3 - 4\eta^2 - 8\eta + 8)\xi^2 + (-4\eta^2 - 8\xi - 8)\xi} \tag{7.54}$$

Finally, the $0, 2$ Padè approximation of the residual q_2 reads:

$$p_2 = -\frac{1}{\eta^2\Big(8\xi^3 - 8\xi^2 + 2\xi\Big) - 4\xi^2 + 4\xi} \tag{7.55}$$

whose behaviour in the strained domain is represented in Figure *3.40*

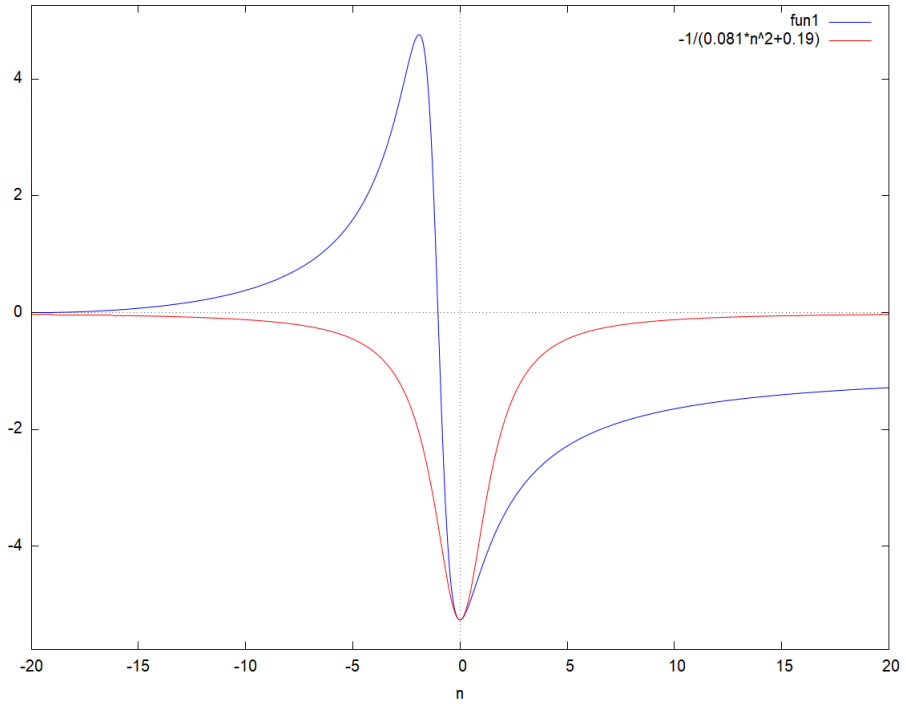

Figure 7.16: Formulation comparison in the strained domain

It is now easy to analytically evaluate the integral solution of (*7.55*):

$$\int_{-\infty}^{\infty} p_2\xi w_2 d\eta = -\frac{i\pi w_i\ \xi}{\sqrt{4\xi^2 - 4\xi}\sqrt{2\xi - 1}\sqrt{8\xi^3 - 8\xi^2 + 2\xi}} \tag{7.56}$$

The multiplication of the equation with the value of the PSD in correspondence of the peak yields the final solution:

$$\lambda_{ij,r2} = -\frac{i\pi w_i\ \xi}{\sqrt{4\xi^2 - 4\xi}\sqrt{2\xi - 1}\sqrt{8\xi^3 - 8\xi^2 + 2\xi}} G_{\ddot{u}_g}(w_2) \tag{7.57}$$

where:

$$G_{\ddot{u}_g}(w_2) = G_0\Big(\frac{w_2}{w_C}\Big)^{e_2} \tag{7.58}$$

7.4.2 Case 1: $w_i < w_C$

For all the cases in which the value of the natural frequency of the system is smaller than the forcing frequency w_C, the behaviour of the integrand in (*7.42*), by assuming a value of $w_i = \frac{1}{2}w_C$, is:

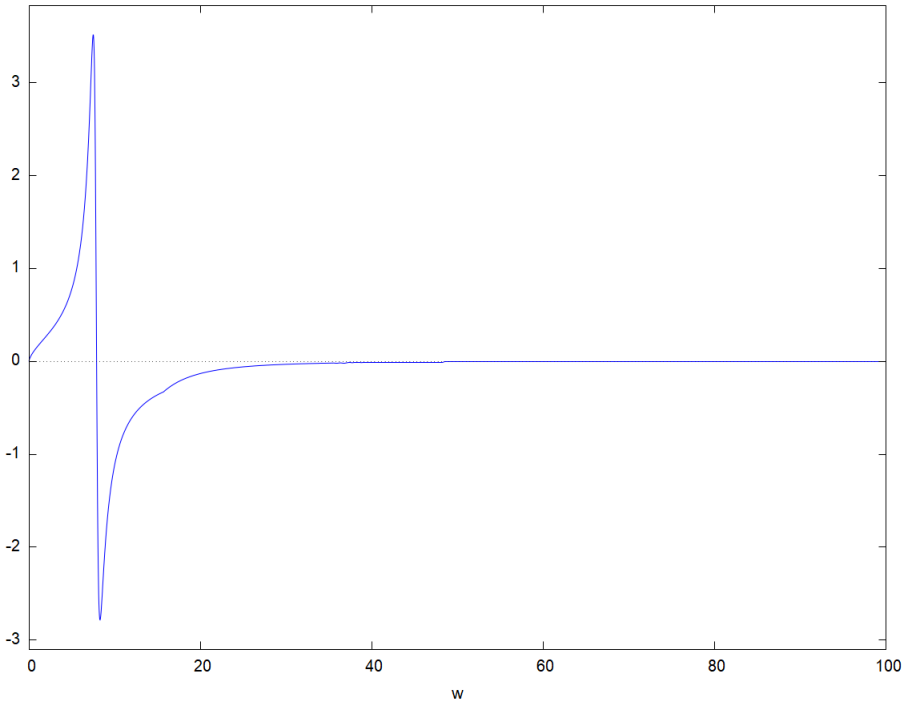

Figure 7.17: Cross spectral moment integrand function

Unlike the previous case, the timescale sepration is not so evident, and the only peaks visible are the ones associated to the kernel function. Due to this, no background contribution is here considered, and the attention is focused on the kernel function only.
Therefore:

$$r_1 = Re\Big[H_i(\hat{w}, w_i, \xi_i)\Big] = \frac{w_i^4 - \hat{w}^2 w_i^2 + 4i\hat{w}^2 w_i^2 \xi^2}{({w_i}^2 - \hat{w}^2)^2 + 4i\hat{w}^2 w_i^2 \xi^2} \tag{7.59}$$

whose behaviour in the frequency domain is represented in Figure *7.18* The imposition of the stationarity of r_1 allows to retrieve the coordinates of the peaks of the kernel function:

$$\begin{cases} w_1 = \frac{w_i}{\sqrt{2\xi+1}} \\ w_2 = \frac{iw_i}{\sqrt{2\xi-1}} \end{cases} \tag{7.60}$$

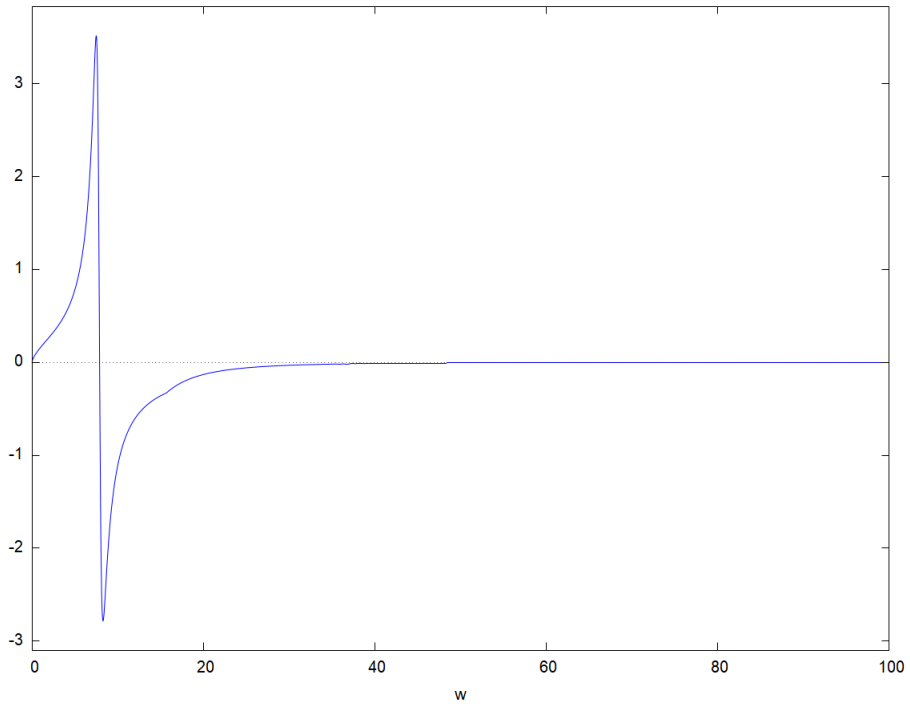

Figure 7.18: r1

Starting from the positive peak, the change of variable $\hat{w} = w_1(1 + \xi\eta)$ generates the following equation:

$$q_1 = -\frac{8\eta^2\xi^4 + (4\eta^2 + 16\eta)\xi^3 + (-2\eta^2 + 8\eta + 8)\xi^2 + (-\eta^2 - 4\xi + 8)\xi - 2\eta + 2}{8\eta^2\xi^4 + (\eta^4 + 4\eta^2 + 16\eta)\xi^3 + (4\eta^3 - 4\eta^2 + 8\eta + 8)\xi^2 + (4\eta^2 - 8\xi + 8)\xi} \tag{7.61}$$

The polynomial Padè approximation reads:

$$p_1 = \frac{4\xi^2 + 4\xi + 1}{4\xi^2 + 2\eta^2 + 4\eta} \tag{7.62}$$

whose integration provides:

$$\int_{-\infty}^{\infty} p_1 \xi w_1 d\eta = \frac{\pi w_i \sqrt{\xi}}{\sqrt{4\xi^2 + 4\xi + 1}\sqrt{2\xi + 1}\sqrt{4\xi^2 + 4\xi}\sqrt{2}} \tag{7.63}$$

The final analytical solution for the first resonant integral is:

$$\lambda_{ij,r1} = -\frac{\pi w_i \sqrt{\xi}}{\sqrt{4\xi^2 + 4\xi + 1}\sqrt{2\xi + 1}\sqrt{4\xi^2 + 4\xi}\sqrt{2}} G_{\ddot{u}_g}(w_1) \tag{7.64}$$

By following the same procedure for the negative peak:

$$\lambda_{ij,r1} = -\frac{i\pi w_i \sqrt{\xi}}{\sqrt{4\xi^2 - 4\xi + 1}\sqrt{2\xi - 1}\sqrt{4\xi^2 - 4\xi}\sqrt{2}} G_{\ddot{u}_g}(w_2) \tag{7.65}$$

7.4.3 Case 1: $w_i = w_C$

The solution for the case $w_i = w_C$ can be sought by applying almost the same considerations adopted in section 7.4.2. Figure *7.19* shows the behaviour of the integrand function of (*7.42*). No background component can be clearly highlighted, therefore the formulation is centered on the resonant components only.

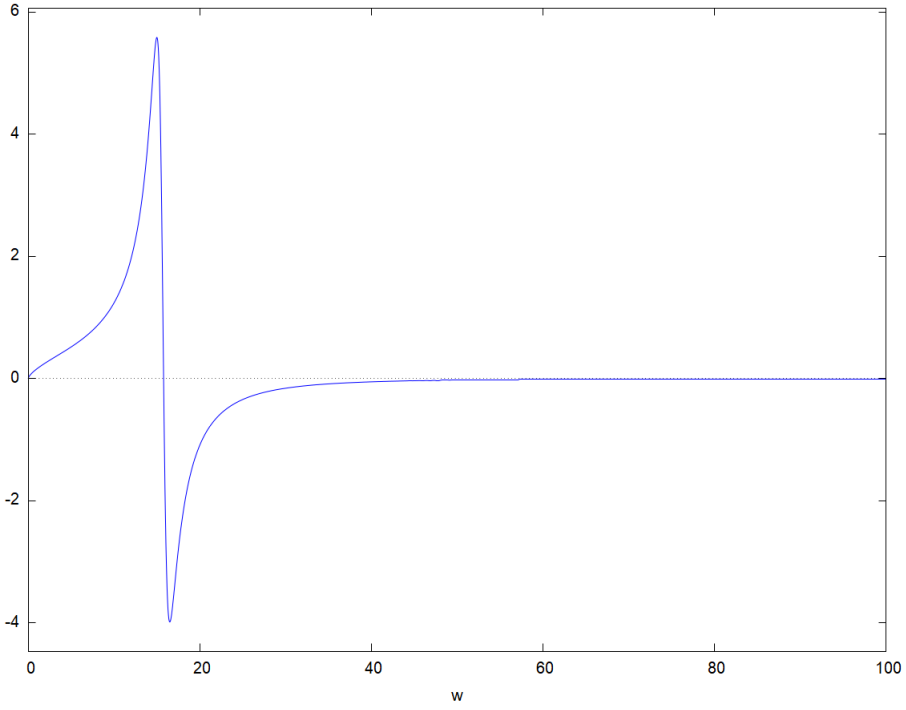

Figure 7.19: Integrand function

The procedure is identical to the one presented for the case of $w_i < w_C$, therefore for the sake of brevity, only the final analytical solution of the two resonant contribution is here reported.
For what concerns the positive peak located at $w_1 = \frac{w_i}{\sqrt{2\xi+1}}$:

$$\lambda_{ij,r1} = -\frac{\pi w_C \sqrt{\xi}}{\sqrt{4\xi^2+4\xi+1}\sqrt{2\xi+1}\sqrt{4\xi^2+4\xi}\sqrt{2}} G_{\ddot{u}_g}(w_1) \tag{7.66}$$

While, for the peak at $w_2 = \frac{iw_i}{\sqrt{2\xi-1}}$:

$$\lambda_{ij,r2} = -\frac{i\pi w_C \sqrt{\xi}}{\sqrt{4\xi^2-4\xi+1}\sqrt{2\xi-1}\sqrt{4\xi^2-4\xi}\sqrt{2}} G_{\ddot{u}_g}(w_2) \tag{7.67}$$

7.5 Spectral moment λ_{gg}

The variance of the ground motion λ_{gg} is defined as:

$$\lambda_{gg} = Re\Big[\int_0^{\inf} G_{\ddot{u}_g}(\hat{w})dw\Big] \tag{7.68}$$

However, the handy analytical formulation for $G_{\ddot{u}_g}(\hat{w})$ provided by Barone et al allows for a trivial evaluation of the integral solution:

$$\lambda_{gg} = \frac{G_0 w_C}{e_3 + 1} - \frac{G_0 w_C}{e_2 + 1} \tag{7.69}$$

7.6 Results comparison

A comparison between the analytical solution obtained and the numerical results provided by Matlab is here reported. It is interesting to see how each formulation is able to actually get close to the correct solution only inside the sub-frequency domain for which it was developed, leading to wrong results elsewhere.
This is observed in Figure *3.40*, in which the results obtained by means of the trapezoidal rule from Matlab are compared with the analytical ones, where:

- ρ_{DN_1} is the correlation coefficient computed by considering the formulation for the low freqeuncy domain, $0 \leq w < w_C$;
- ρ_{DN_3} is the correlation coefficient computed by considering the formulation for the high freqeuncy domain, $w > w_C$;

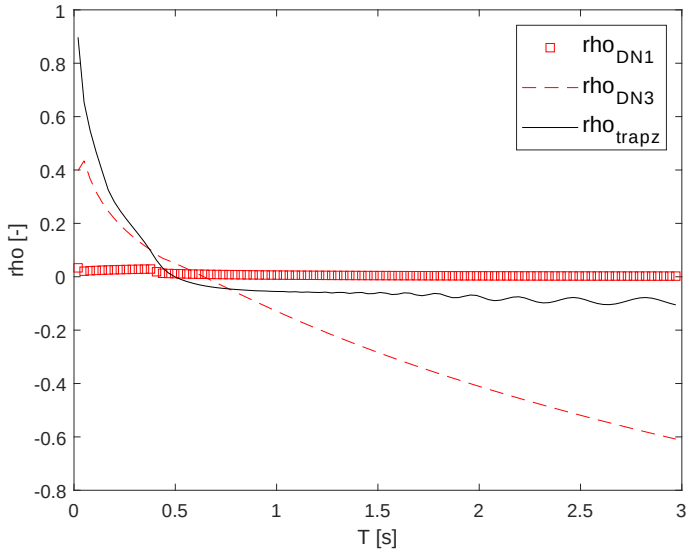

Figure 7.20: Results comparions: Multiple timescale separation

As expected, the two formulation are able to provide reasonable outputs only inside the domains inside which they have been designed, underestimating the reference solution in the remaining domain.
Finally, by putting the results together, the overall behaviour of the solution based on the Timescale Separation method is reported in Figure *7.21*. The analytical solution tend to underestimate the results in the high frequency

domain (low periods), similarly to what happened using the White Noise approximation by Der Kiureghian et al.

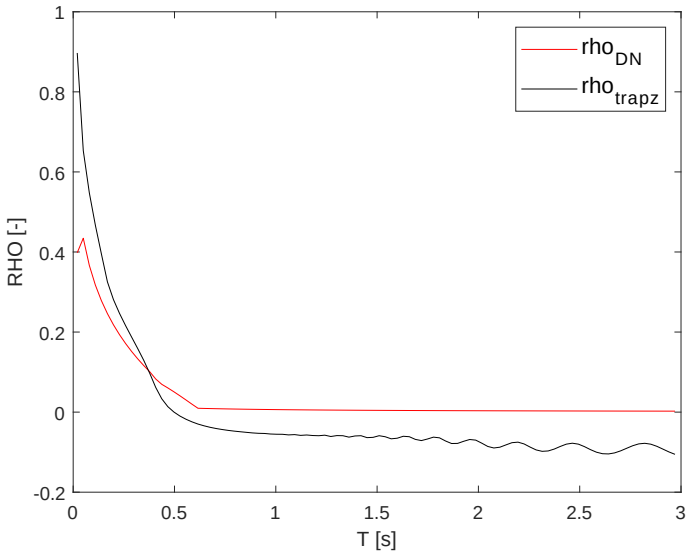

Figure 7.21: Results comparions: Multiple timescale separation

Chapter 8

Correlation coefficients - Analytical simplified formulation

One last formulation aimed to analytically evaluate the correlation coefficient ρ_{ij} is here presented.
The goal of the method is simply to study term by term formula of the spectral moments, evaluating separately the integral analytical solution of each contribution, and finally assembling everything together to obtain the whole solution. This to say that the method is not interested in what happens in the frequency or in the time domain, or in the relations which exist between kernel and forcing function, as it happened instead in the case of the Multiple timescale separation procedure.
From the mathematical point of view, such a rigorous procedure will provide a more burdensome final formulation. However the advantages are related to the fact that a lot of terms are identically shared by the different spectral moments, meaning that the related calculations can be developed one time only. The method fully relies on the computational capacities of the software *WX MAXIMA*. As presented in Chapter 7.3, *MAXIMA* is a *Computer algebra System* which allows allows to perform symbolic algebraic calculations, which turned out to be quite useful for the manipulations of the large polynomials functions involving spectral and cross spectral moments, needed in the formula for ρ_{ij}, which is here recalled:

$$\rho_{0,ig} = \frac{\lambda_{ig}}{\sqrt{\lambda_{ii}\lambda_{gg}}} \tag{8.1}$$

Despite its dexterity however, the software alone was not able to handle the complexity of the formulation, causing the solution of the problem, i.e. the integration of the spectral quantities, impossible to be obtined without introducing some approximations. As before, if on one hand the solution for λ_{gg} is trivial, the same does not hold for λ_{ii} and λ_{ig}.
In order to have an idea of the heaviness of the problem, the following lines will show the expanded version of the spectral quantities entering (*8.1*).
By starting from the numerator, the expression for λ_{ig} reads:

$$\lambda_{ig} = \int_0^\infty Re\Big[H_i(\hat{w}, w_i, \xi_i)\Big] G_{\ddot{u}_g}(\hat{w}) d\hat{w} \tag{8.2}$$

where:

$$Re\Big[H_i(\hat{w}, w_i, \xi_i)\Big] = \frac{w_i^4 - \hat{w}^2 w_i^2 + 4\hat{w}^2 w_i^2 \xi^2}{(w_i{}^2 - \hat{w}^2)^2 + 4i\hat{w}^2 w_i^2 \xi^2} \tag{8.3}$$

While, for what concerns the PSD function, the formulation proposed by Barone is:

$$G_{\ddot{u}_g}(w) = \begin{cases} G_0(\frac{w_D}{w_C})^{e_2}(\frac{w}{w_D})^{e_1} & \text{se } 0 \le w \le w_D \\ G_0(\frac{w}{w_C})^{e_2} & \text{se } w_D \le w \le w_C \\ G_0(\frac{w}{w_C})^{e_3} & \text{se } w_C \le w \le w_B \\ G_0(\frac{w_B}{w_C})^{e_3}(\frac{w}{w_B})^{e_4} & \text{se } w > w_B \end{cases} \tag{8.4}$$

As already presented, the goal of the method is to split each integral equation in single components, developing the product between FRF and PSD for each of the frequency subdomains:

$$\begin{aligned}
\lambda_{ij} = {} & G_0 \frac{w_s^4 w_D^{e_2-e_1}}{w_C^{e_2}} \int_0^{w_D} \frac{\hat{w}^{e_1}}{(w_i{}^2 - \hat{w}^2)^2 + 4i\hat{w}^2 w_i^2 \xi^2} d\hat{w} \\
& - G_0 \frac{w_s^2 w_D^{e_2-e_1}}{w_C^{e_2}} \int_0^{w_D} \frac{\hat{w}^{e_1+2}}{(w_i{}^2 - \hat{w}^2)^2 + 4i\hat{w}^2 w_i^2 \xi^2} d\hat{w} \\
& + 4G_0 \frac{4w_s^2 w_D^{e_2-e_1}}{w_C^{e_2}} \int_0^{w_D} \frac{\xi^2 \hat{w}^{e_1+2}}{(w_i{}^2 - \hat{w}^2)^2 + 4i\hat{w}^2 w_i^2 \xi^2} d\hat{w} \\
& + G_0 \frac{w_s^4}{w_C^{e_2}} \int_0^{w_D} \frac{\hat{w}^{e_2}}{(w_i{}^2 - \hat{w}^2)^2 + 4i\hat{w}^2 w_i^2 \xi^2} d\hat{w} \\
& - G_0 \frac{w_s^2}{w_C^{e_2}} \int_0^{w_D} \frac{\hat{w}^{e_2+2}}{(w_i{}^2 - \hat{w}^2)^2 + 4i\hat{w}^2 w_i^2 \xi^2} d\hat{w} \\
& + 4G_0 \frac{4w_s^2}{w_C^{e_2}} \int_0^{w_C} \frac{\xi^2 \hat{w}^{e_2+2}}{(w_i{}^2 - \hat{w}^2)^2 + 4i\hat{w}^2 w_i^2 \xi^2} d\hat{w} \\
& + G_0 \frac{w_s^4}{w_C^{e_3}} \int_0^{w_D} \frac{\hat{w}^{e_3}}{(w_i{}^2 - \hat{w}^2)^2 + 4i\hat{w}^2 w_i^2 \xi^2} d\hat{w} \\
& - G_0 \frac{w_s^2}{w_C^{e_3}} \int_0^{w_D} \frac{\hat{w}^{e_3+2}}{(w_i{}^2 - \hat{w}^2)^2 + 4i\hat{w}^2 w_i^2 \xi^2} d\hat{w} \\
& + 4G_0 \frac{4w_s^2}{w_C^{e_3}} \int_0^{w_C} \frac{\xi^2 \hat{w}^{e_3+2}}{(w_i{}^2 - \hat{w}^2)^2 + 4i\hat{w}^2 w_i^2 \xi^2} d\hat{w} \\
& + G_0 \frac{w_s^4 w_B^{e_3-e_4}}{w_C^{e_3}} \int_0^{w_B} \frac{\hat{w}^{e_4}}{(w_i{}^2 - \hat{w}^2)^2 + 4i\hat{w}^2 w_i^2 \xi^2} d\hat{w} \\
& - G_0 \frac{w_s^2 w_B^{e_3-e_4}}{w_C^{e_3}} \int_0^{w_B} \frac{\hat{w}^{e_4+2}}{(w_i{}^2 - \hat{w}^2)^2 + 4i\hat{w}^2 w_i^2 \xi^2} d\hat{w} \\
& + 4G_0 \frac{4w_s^2 w_B^{e_3-e_4}}{w_C^{e_3}} \int_0^{w_B} \frac{\xi^2 \hat{w}^{e_4+2}}{(w_i{}^2 - \hat{w}^2)^2 + 4i\hat{w}^2 w_i^2 \xi^2} d\hat{w}
\end{aligned} \tag{8.5}$$

The same reasoning is applied to the variance λ_{ii}, which now involves the

product between the conjugates of the FRF function.

$$H_i(\hat{w}, w_i, \xi_i) * conj\Big[H_i(\hat{w}, w_i, \xi_i)\Big] = \frac{w_i^4 + 4i\hat{w}^2 w_i^2 \xi^2}{({w_i}^2 - \hat{w}^2)^2 + 4i\hat{w}^2 w_i^2 \xi^2} \tag{8.6}$$

The following expression yields:

$$\begin{aligned}
\lambda_{ii} = {} & G_0 \frac{w_s^4 w_D^{e_2-e_1}}{w_C^{e_2}} \int_0^{w_D} \frac{\hat{w}^{e_1}}{({w_i}^2 - \hat{w}^2)^2 + 4i\hat{w}^2 w_i^2 \xi^2} d\hat{w} \\
& + 4G_0 \frac{4w_s^2 w_D^{e_2-e_1}}{w_C^{e_2}} \int_0^{w_D} \frac{\xi^2 \hat{w}^{e_1+2}}{({w_i}^2 - \hat{w}^2)^2 + 4i\hat{w}^2 w_i^2 \xi^2} d\hat{w} \\
& + G_0 \frac{w_s^4}{w_C^{e_2}} \int_0^{w_D} \frac{\hat{w}^{e_2}}{({w_i}^2 - \hat{w}^2)^2 + 4i\hat{w}^2 w_i^2 \xi^2} d\hat{w} \\
& + 4G_0 \frac{4w_s^2}{w_C^{e_2}} \int_0^{w_C} \frac{\xi^2 \hat{w}^{e_2+2}}{({w_i}^2 - \hat{w}^2)^2 + 4i\hat{w}^2 w_i^2 \xi^2} d\hat{w} \\
& + G_0 \frac{w_s^4}{w_C^{e_3}} \int_0^{w_D} \frac{\hat{w}^{e_3}}{({w_i}^2 - \hat{w}^2)^2 + 4i\hat{w}^2 w_i^2 \xi^2} d\hat{w} \\
& + 4G_0 \frac{4w_s^2}{w_C^{e_3}} \int_0^{w_C} \frac{\xi^2 \hat{w}^{e_3+2}}{({w_i}^2 - \hat{w}^2)^2 + 4i\hat{w}^2 w_i^2 \xi^2} d\hat{w} \\
& + G_0 \frac{w_s^4 w_B^{e_3-e_4}}{w_C^{e_3}} \int_0^{w_B} \frac{\hat{w}^{e_4}}{({w_i}^2 - \hat{w}^2)^2 + 4i\hat{w}^2 w_i^2 \xi^2} d\hat{w} \\
& + 4G_0 \frac{4w_s^2 w_B^{e_3-e_4}}{w_C^{e_3}} \int_0^{w_B} \frac{\xi^2 \hat{w}^{e_4+2}}{({w_i}^2 - \hat{w}^2)^2 + 4i\hat{w}^2 w_i^2 \xi^2} d\hat{w}
\end{aligned} \tag{8.7}$$

By comparing however Eq.8.3 with (*8.6*), it can be noted how, except for one term, the two expression are the same. This means that by exploiting the results obtained for λ_{ig}, no other computations are needed for λ_{ii}. This is the advantage of not treating all the terms together, as it was instead done in the case of the Multiple time-scale separation.

Now, the achievement of a handy analytical solution of the above integrals is impeeded mainly by two reasons:

1. the number of subdomains in which the PSd function is subdivided. More branches means different formulations, and so highr computational cost

2. the role played the exponential coefficients e1,e2,e3,e4: these are not integer coefficients, and heavily affect the complexity of the integration procedure

To try to limit the inconveniences produced by these aspects, three approximations are introduced:

1. semplification of the PSD formulation

2. approximation of the exponential coefficients

3. omission of the viscous contribution (damping) when possible

For what concerns the PSD function, exactly as done in Chapter 7, the first step is to reduce the number of branches from four to two, obtaining:

$$G_{\ddot{u}_g}(w) = \begin{cases} G_0(\frac{w}{w_C})^{e_2} & \text{se } 0 \leq w \leq w_C \\ G_0(\frac{w}{w_C})^{e_3} & \text{se } w > w_C \end{cases} \tag{8.8}$$

The second, and maybe the strongest approximation, is instead related to the exponential coefficients. In particular it turned out that the only possible way to reach a solution with *wxMaxima* was to consider integer exponential numbers. Moreover the degree of the polynomial expressions at both numerator and denominator had to be as low as possible, otherwise no analytical solution could be reached by the program. Consequently, the chosen values for e_1 and e_2 are: $e_1 = 1$ and $e_2 = -1$, leading to:

$$G^{appr}_{\ddot{u}_g}(\hat{w}) = \begin{cases} G_0(\frac{w}{w_C})^{1} & \text{se } 0 \leq w \leq w_C \\ G_0(\frac{w}{w_C})^{-1} & \text{se } w > w_C \end{cases} \tag{8.9}$$

Now, a comparison between the 4 branches PSD proposed by Barone et al, and the approximated one adopted in this work is reported in Figure *8.1* As it can be seen, consistent differences arise especially in the high frequency domain, leading to a higher energy contenct for the 2-branches formulation. This is why, as it will be presented later, the final analytical solution built upon on Eq 2 branches PSD, will be eventually revised by using specific correction coefficients, in charge of accounting for the differences between the two areas eneveloped.
By exploiting these approximations, the analytical solution for each spectral moment is treated in the next sections.

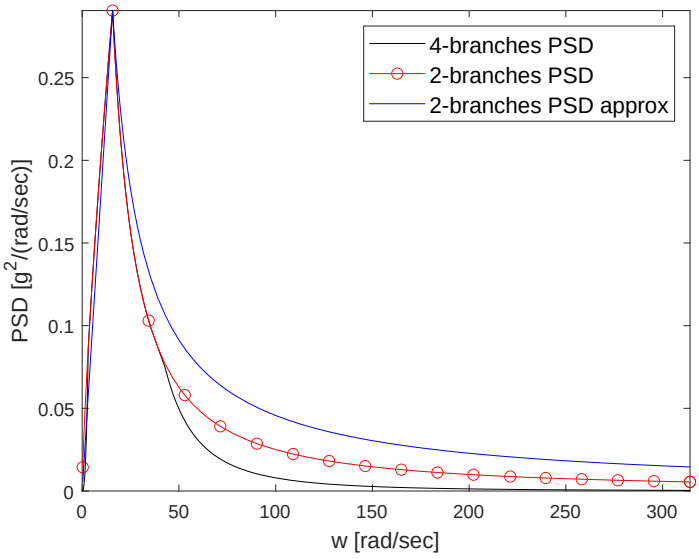

Figure 8.1: 4 branches vs 2 branches approximate PSD formulation

8.1 Cross spectral moment: λ_{ig}

As presented in the previous paragraphs, in order to lighten the formulation, the contribution of damping is neglected when possible. In particular the behaviour of the kernel function is not much affected by the contribution of χ at the numerator when its value is small enough, therefore it can be omitted. Thanks to this, the formulation of the integral in the two subdomians becomes, for $0 \leq w \leq w_C$:

$$\lambda_{ig} = \frac{G_0}{w_c} \int_0^{w_C} \frac{\hat{w}(w_i^4 - \hat{w}^2 w_i^2)}{({w_i}^2 - \hat{w}^2)^2 + 4i\hat{w}^2 w_i^2 \xi^2} d\hat{w} \tag{8.10}$$

while, for $w > w_C$:

$$\lambda_{ig} = G_0 w_C \int_{w_C}^{\infty} \frac{\frac{1}{\hat{w}}(w_i^4 - \hat{w}^2 w_i^2)}{({w_i}^2 - \hat{w}^2)^2 + 4i\hat{w}^2 w_i^2 \xi^2} d\hat{w} \tag{8.11}$$

Now, by exploiting the computational capacity provided by *WX MAXIMA*, the following analytical solution for each subdomain is obtained.
For $0 \leq w \leq w_C$:

$$\begin{aligned}\lambda_{ij} = \frac{G_0 w_s^4}{w_C} \Bigg[& \frac{100 arctg\left(\frac{200\sqrt{399}w_C^2 - 199\sqrt{399}w_s^2}{399 w_s^2}\right)}{\sqrt{399} w_s^2} + \frac{100 arctg\left(\frac{199}{\sqrt{399}}\right.}{\sqrt{399} w_s^2} \\ & - \frac{\log\left(|100 w_C^4 - 199 w_C^2 w_s^2 + 100 w_s^4|\right)}{4 w_s^2} - \frac{199 arctg\left(\frac{200\sqrt{399}w_C^2 - 199\sqrt{399}w_s^2}{399 w_s^2}\right)}{2\sqrt{399} w_s^2} \\ & + \frac{\log(100 w_s^4)}{4 w_s^2} - \frac{199 arctg(\frac{199}{\sqrt{399}})}{2\sqrt{399} w_s^2} \Bigg]\end{aligned} \tag{8.12}$$

And for $w > w_C$:

$$\begin{aligned}\lambda_{ij} = (G_0 w_C) \Bigg[& \frac{199 arctg\left(\frac{200\sqrt{399}w_C^2 - 199\sqrt{399}w_s^2}{399 w_s^2}\right)}{4} - \log\left(w_C^4\right) \\ & - \frac{199 arctg\left(\frac{200\sqrt{399}w_C^2 - 199\sqrt{399}w_s^2}{399 w_s^2}\right)}{2\sqrt{399}} - \frac{\sqrt{399}\log(100) - 199\pi}{4\sqrt{399}} \\ & - \frac{50\pi}{\sqrt{399}} - \frac{199 arctg\left(\frac{200\sqrt{399}w_C^2 - 199\sqrt{399}w_s^2}{399 w_s^2}\right)}{2\sqrt{399}} \Bigg]\end{aligned} \tag{8.13}$$

However, as anticipated before, if on one hand the approximated 2-branches PSD fomrulation reduces the complexity of the problem, on the ther hand it overestimates the energy content of the event. This is why, in order to try to solve this issue, two correction coefficients are introduced, ε and γ. They are computed simply as the ratio between the area subtended by the

exact 4-branches formulation, and the 2-branches approxmated one.
In particular, for $0 \leq w \leq w_C$:

$$\gamma = \frac{\int_0^{w_D} (\frac{w_D}{w_C})^{e_2} (\frac{w}{w_D})^{e_1} d\hat{w} + \int_{w_D}^{w_C} (\frac{w}{w_C})^{e_2} d\hat{w}}{\int_0^{w_C} (\frac{w}{w_C})^{e_2} d\hat{w}} \tag{8.14}$$

And for $w > w_C$:

$$\varepsilon = \frac{\int_{w_C}^{w_B} (\frac{w}{w_C})^{e_3} d\hat{w} + \int_{w_B}^{\infty} (\frac{w_B}{w_C})^{e_3} (\frac{w}{w_B})^{e_4} d\hat{w}}{\int_{w_C}^{\infty} \frac{w}{w_C})^{e_3} d\hat{w}} \tag{8.15}$$

Both coefficients are characterized by the fact that, regardless the characteristic of the site, their range of variability is very limited, allowing to adopt fixed values for both, i.e., $\gamma = 1.15$ and $\varepsilon = 0.5$.
It is now possible to gather together all the contributions, scaled by the correspondent correction factor. The final expression for λ_{ij} is:

$$\begin{aligned}
\lambda_{ij} = \left(\frac{100 G_0 w_s^2}{w_C \sqrt{399}}\right) \Bigg[& \frac{1}{200}\Big(\gamma + \varepsilon \frac{w_C^2}{w_S^2}\Big) \arctan\Big(\frac{200\sqrt{399} w_C^2 - 199\sqrt{399} w_s^2}{399 w_s^2}\Big) \\
& - \frac{1}{200}\Big(\epsilon \frac{w_C^2}{w_S^2}\Big)\Big(50\pi\Big) - \Big(\frac{1}{200}\gamma\Big) \arctan\Big(\frac{199}{\sqrt{399}}\Big) \\
& \Big(\frac{\sqrt{399}}{400}\Big)\Big(-\gamma + \epsilon \frac{w_C^2}{w_S^2}\Big) \log\Big(|100 w_C^4 - 199 w_C^2 w_s^2 + 100 w_s^4|\Big) \\
& - \Big(\frac{\sqrt{399}}{100}\Big)\Big(\epsilon \frac{w_C^2}{w_S^2}\Big) \log\Big(w_C\Big) - \Big(\gamma \frac{\sqrt{399}}{400}\Big) \log\Big(100 w_s^4\Big) \\
& - \Big(\frac{\sqrt{1}}{400}\Big)\Big(\epsilon \frac{w_C^2}{w_S^2}\Big) \log\Big(\sqrt{399} \log(100) - 199\pi\Big) \Bigg]
\end{aligned} \tag{8.16}$$

8.2 Variance of the response: λ_{ii}

As already presented before, no further calculatons are needed for λ_{ii}. By recalling (*8.17*, it is evident how the solution obtained for λ_{ig}, can be here exploited as well. Now, in order to limit the computational costs, the damping contribution at the numerator is here disregarded as well. This is equivalent to make reference to the concept of pseudo acceleration instead of total acceleration response spectrum. However, as it was already seen, the pseudo-acceleration response spectrum is a good approximation of the total one for a wide range of frequency and damping values, and the difference between the two is only significant for high damping values and long periods (small w_i values).

Doing so, the new integral equation for λ_{ig} becomes:

$$\begin{aligned}\lambda_{ii} = & G_0 \frac{w_s^4 w_D^{e_2-e_1}}{w_C^{e_2}} \int_0^{w_D} \frac{\hat{w}^{e_1}}{({w_i}^2 - \hat{w}^2)^2 + 4i\hat{w}^2 w_i^2 \xi^2} d\hat{w} \\ & + G_0 \frac{w_s^4}{w_C^{e_2}} \int_0^{w_D} \frac{\hat{w}^{e_2}}{({w_i}^2 - \hat{w}^2)^2 + 4i\hat{w}^2 w_i^2 \xi^2} d\hat{w} \\ & + G_0 \frac{w_s^4}{w_C^{e_3}} \int_0^{w_D} \frac{\hat{w}^{e_3}}{({w_i}^2 - \hat{w}^2)^2 + 4i\hat{w}^2 w_i^2 \xi^2} d\hat{w} \\ & + G_0 \frac{w_s^4 w_B^{e_3-e_4}}{w_C^{e_3}} \int_0^{w_B} \frac{\hat{w}^{e_4}}{({w_i}^2 - \hat{w}^2)^2 + 4i\hat{w}^2 w_i^2 \xi^2} d\hat{w}\end{aligned} \tag{8.17}$$

While the solution provided by *WX MAXIMA*, scaled by the correspondent correction coefficients, yields:

$$\begin{aligned}\lambda_{ii} = & \left(\frac{100 G_0 w_s^2}{w_C \sqrt{399}}\right) \Bigg[\frac{1}{200}\Big(\gamma + \varepsilon \frac{w_C^2}{w_S^2}\Big) \arctan\Big(\frac{200\sqrt{399} w_C^2 - 199\sqrt{399} w_s^2}{399 w_s^2}\Big) \\ & - \frac{1}{200}\Big(\epsilon \frac{1}{400} \frac{w_C^2}{w_S^2}\Big)(199\pi) - \Big(\gamma \arctan\Big(\frac{199}{\sqrt{399}}\Big)\Big) \\ & \Big(\frac{\sqrt{399}}{400}\Big)\Big(\epsilon \frac{w_C^2}{w_S^2}\Big) \log\Big(|100 w_C^4 - 199 w_C^2 w_s^2 + 100 w_s^4|\Big) \\ & - \Big(\frac{\sqrt{399}}{100}\Big)\Big(\epsilon \frac{w_C^2}{w_S^2}\Big) \log\Big(w_C\Big) - \Big(\gamma \frac{\sqrt{399}}{400}\Big) \log\Big(100 w_s^4\Big) \\ & - \Big(\frac{\sqrt{1}}{400}\Big)\Big(\epsilon \frac{w_C^2}{w_S^2}\Big) \log\Big(\sqrt{399}\log(100)\Big)\Bigg]\end{aligned} \tag{8.18}$$

8.3 Variance of the forcing function: λ_{gg}

For this last case, the solution of the integral equation is quite straightforward, since it involves only the formulation related to the forcing function. Just one trick must be introduced. In particular, as it is defined, the integral to infinity of the PSD in the second frequency sub-domain would cause the solution to diverge. To solve the problem, the involved sub-domian is limited from above by a fictitous high frequency value w_max, which in this case can be taken equal to the maximum frequency sampling rates, e.g., $\pi 100 Hz$. Finally:

$$\lambda_{gg} = \begin{cases} \int_0^{w_C} G_{\ddot{u}_g}^{appr}(\hat{w}) d\hat{w} = \frac{G_0 w_C}{2} & \text{se } 0 \leq w \leq w_C \\ \int_{w_C}^{w_{max}} G_{\ddot{u}_g}^{appr}(\hat{w}) d\hat{w} = G_0 w_C \Big(log(|w_{max}|) - log(|w_C|)\Big) & \text{se } w > w_C \end{cases} \tag{8.19}$$

8.4 Comparison of the results

The plot presented in Figure *8.2* shows the behaviour of the correlation coefficient rho_{WX} computed with the proposed analytical formulation. De-

spite the use of quite heavy approximations, the results provides a good matching with the numerical procedure adopted in Matlab.

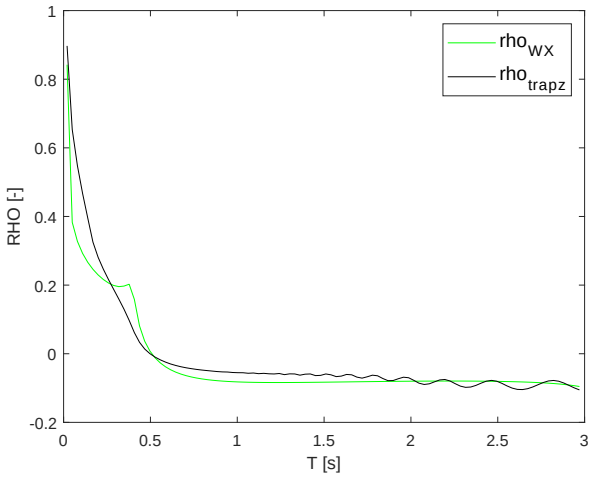

Figure 8.2: Results comparison: Analytical approximate formulation

Chapter 9

Comparison between the implemented formulations

In this Chapter, the results obtained by means of the response spectrum method are presented.
The procedure was implmented using the software *Matlab*, thanks to the lines of code provided by Prof Luca Martinelli. By adopting the various formulations to determine the correlation coefficients for the CQC rule, the aim of this section is to validate the results in terms of the reaction forces arising at the connections between frame and panels. To do so, the results obtained by means of the RS method will be compared with the reference numerical solutions obtained through the direct integration of the equation of motion. This will be done by considering the seismic actions generated by the EC8 prescribed Response Spectrum, type 1. The analysis will be carried out for the following type of soils:

- Soil type A
- Soil type B
- Soil type C
- Soil type D
- Soil type E

Then, for each soil type, 5 different damping ratios will be assigned to the structural system, i.e.:

- $\xi = 2\%$
- $\xi = 5\%$
- $\xi = 10\%$
- $\xi = 15\%$
- $\xi = 20\%$

In the next section, the main steps used to implement the above mentioned time history analysis on the *Matlab* software will be highlighted.

9.1 Time history analysis

The requirement for a time history analysis is based on the fact that the seismic action input is provided in terms of ground acceleration time history. In particular, the accelerogram of a real seismic event is the most accurate rappresentation of an earthquake, since it contains a lot of useful info about the characteristics of the sisma itself, as well as the nature of the waves which propagates from the epicenter.
The use of accelerograms is recomended for the dynamic analysis of irregular buildings, for the design of complex structures or to evaluate the response in terms of deformability and stability. However, recordings of the ground motion are not always available, this is why codes and provisions allow to rely on alternative methods. In particular, depending on the needs and of the available informations, the seismic motion can be obtained three different categories of accelerograms:

- real recordings
- sintetic recordings obtained from sismologic models
- artificial recordings

9.1.1 Artificial accelerograms

Simulated accelerograms are signals which are generated through both deterministic and stocastic methods, able to simulate physical process conneceted to the motion of the ground, as for example the genesys of the earthqueke, the waves propagation and the superficial response of the site. As underlines by EC8, the artificially generetaed signals must be such that their resultant elastic response spectrum has to be coherent with the target response spectrum adopted in design. The coherency has to be checked by veryfing that the difference between the average of the spectral ordinates obtained from the different accelerograms, is not lower than the 10% of the elstic spectrum ones. This condition must be verified in the bigger of the intervals, $0.15s - 2.0s$ and $0.15s - 2T$, where T is the fundamental period of the structure in the elastic field. Now, the most used artificial accelerograms are the ones originated by the Software *SIMQKE* [Vanmarcke and Gasparini, 1976], which generates one or more signals starting from a reference spectrum. The acelerograms are obtained on the base of a trapezoidal enevelope, Figure *9.1*, where the duration of the differente branches, increasing constant and decreasing, are fixed by the user:

- TRISE: beginning of the stationary part
- TLVL: duration of the stationary part ($\geq 10s$)
- DUR : total duration of the accelerogram

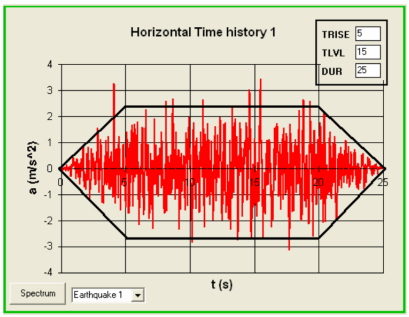

Figure 9.1: SIMQKE: Trapezoidal envelope of the accelerograms

For the purpose of this work, the accelerograms are generated with $TRISE = 5s$, $TLVL = 5s$, $DUR = 20s$.

9.1.2 Solution of the equation of motion

The aim of this section is to briefly present the procedure adopted to compute the solution in time of the response of a single DOF oscillator.
The main point here is related to the fact that th analysis in the time domain is complex and time consumig. This is why the solution was searched in an alternative way, by switching from the time to the frequency domain. This allows for an easier and faster analysis, and once the problem is solved in the frequency domain, by going back to the time domain, it is possible to obtain the solution in time.

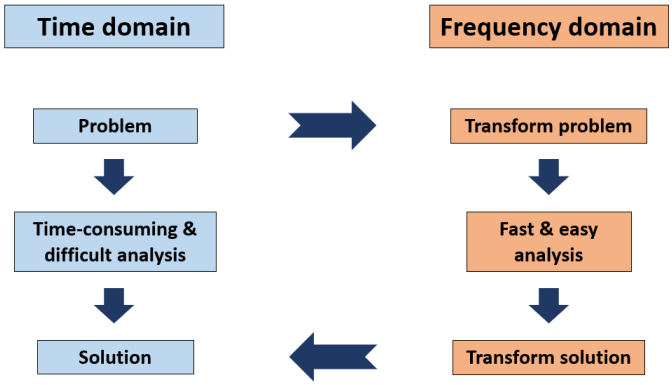

Figure 9.2: Time vs Frequency domain analysis

Briefly, discrete time signals can be decomposed into a linear combination of sinusoidal functions (Fourier series):

$$p(t_i) = \sum_{n=-\infty}^{\infty} a_n \cos\left(n\frac{2\pi}{T}t_i\right) + b_n \cos\left(n\frac{2\pi}{T}t_i\right) \tag{9.1}$$

where:

- T is the fundamental period

- $\sqrt{\left(a_n^2 + b_n^2\right)}$ is the amplitude of the single harmonic

- $\tan\theta = \frac{b_n}{a_n}$ is the amplitude of the single armonic

Now, in the frequency domian the signals can be represented by means of the so called "spectrum", in which the amplitude of each harmonic component is reported as a function of the frequency. In the continous domain, these coefficients can be computed with different methods. The most used way is the one which calls upon the orthogonality of the harmonics to identify how much the signal $p(t)$ resembles a given sinusoids of frequency $w_n = \frac{2\pi}{T}$:

$$P(f) = \int_{-\infty}^{\infty} p(t)\exp(-i2\pi ft)dt \tag{9.2}$$

Now, in the time domain, the response $x(t)$ of a MDOF system is computed as:

$$x(t) = \int_{-\infty}^{\infty} h(t-\tau)p(\tau)d(\tau) \tag{9.3}$$

where $h(t)$ is the impulse response function. By applying the Fourier transform operator to both the terms of (*9.3*), the solution in the frequency domain is:

$$X(\hat{w}) = H(\hat{w})P(\hat{w}) \tag{9.4}$$

where $H(\hat{w})$ is the frequency response function.
The same procedure was followed using the software Matlab. In particular by using the command *easyFFT* it was possible to compute the Fourier Transform for each accelerograms $p(t)$:

$$P(w) = easyFFT\Big[p(t)\Big] \tag{9.5}$$

Now, by means of the concept of FRF, the response solution of the structure, both in terms of displacements and total acceleration are obtained as:

$$U(w) = H(\hat{w})P(\hat{w}) \tag{9.6}$$

$$\ddot{U}(w) = H(\hat{w})P(\hat{w}) \tag{9.7}$$

where:

$$H(\hat{w}, w_i, \xi_i) = \frac{1}{{w_i}^2 - \hat{w}^2 + 2iw_i\hat{w}} \tag{9.8}$$

$$H(\hat{w}, w_i, \xi_i) = \frac{{w_i}^2 + 2iw_i\hat{w}}{{w_i}^2 - \hat{w}^2 + 2iw_i\hat{w}} \tag{9.9}$$

Now, to come back in the time domain, the inverse Fourier Transform, by means of the comand *ifft*, is applied to the two solution (*9.6*) and (*9.7*):

$$u(t) = ifft\Big[U(w)\Big] \tag{9.10}$$

$$\ddot{u}(t) = ifft\Big[\ddot{U}(w)\Big] \tag{9.11}$$

This allows to obtain, for each accelerogram, the time history of the reaction forces $F_a(t)$ and $F_b(t)$ as:

$$F_A(t) = \alpha_A m_p \ddot{u}(t) + \beta_A m_p \ddot{u}_g(t) \tag{9.12}$$

$$F_B(t) = \alpha_B m_p \ddot{u}(t) + \beta_B m_p \ddot{u}_g(t) \tag{9.13}$$

being $\ddot{u}_g(t)$ the peak ground acceleration.
Now, the goal of the work is to define the response spectrum method for both forces. In the following, the procedure is briefly explained.
By starting from (*9.12*) and (*9.13*), the first step is to compute the maximum values of $F_a(t)$ and $F_b(t)$ inside each accelerogram:

$$F_{A_{p_k}}^{T_j} = max[F_{A_{p_k}}^{T_j}(t)] \tag{9.14}$$

$$F_{B_{p_k}}^{T_j} = max[F_{B_{p_k}}^{T_j}(t)] \tag{9.15}$$

where the subscript p_k is referred to the accelerogram considered, while the pedix T_j is the period of the structure for which the Frequency response Functions have been computed. By averaging now the maximum values of the forces on the all the accelerograms considered, the ordinate of the response spectra for that particular value of the period T_j is obtained:

$$RS_{F_A}(T_j) = mean[F_{A_{p_k}}^{T_j}] \tag{9.16}$$

$$RS_{F_B}(T_j) = mean[F_{B_{p_k}}^{T_j}] \tag{9.17}$$

The procedure will be repeated for any value T_j of intereseted.
Finally, by considering the ratio between (*9.16*) and (*9.17*), the correspondent non dimensional Response Spectrum are obtained:

$$RS_{F_A}^{ND}(T_j) = \frac{RS_{F_A}}{max[RS_{F_A}]} \tag{9.18}$$

$$RS_{F_B}^{ND}(T_j) = \frac{RS_{F_B}}{max[RS_{F_B}]} \tag{9.19}$$

The same steps which lead to (*9.16*) and (*9.17*) are used to compute the total accelertion and the pseudo accelertion RS generated by the accelerograms. In particular, inside each accelerogram:

$$\ddot{u}_{p_k}^{T_j} = max[\ddot{u}_{p_k}^{T_j}(t)] \tag{9.20}$$

$$u_{p_k}^{T_j} = max[u_{p_k}^{T_j}(t)] \tag{9.21}$$

As before, by averaging out the maximum values between all the signals, the spectral ordinates are computed.
For the total acceleration RS:

$$RS_{\ddot{u}}(T_j) = mean[\ddot{u}^{T_j}] \tag{9.22}$$

While, in terms of displacements:

$$RS_u(T_j) = mean[u_{p_k}^{T_j}] \tag{9.23}$$

The pseudo acceleration RS can be then obtained by scaling (*9.23*) by the square of the natural frequency w^2 :

$$RS_a(T_j) = w^2 RS_u(T_j) \tag{9.24}$$

These further steps allowed for the comparison between the the target RS provided by EC8 and the resulting ones generated from the accelerograms. This will be useful in order to have a measure on how reliable the reference results provided by the time histories are, since as it will be seen, they are the ones more affected by the change of the damping ratio.

9.2 Result presentation

This section will be devoted to present the results obtained by considering the different cases of soil types and damping ratios ξ. The various formulations adopted are here recalled, indicating the namethey have been associated to in the plotting phase:

- *TH*: time history analysis
- *TRAPZ*: CQC results obtained by means of numerical evaluation of the correlation coefficient
- *WN*: CQC results obtained in hypothesis of white noise input (Der Kiureghian - (*6.8*))
- WN_{APPR}: CQC results obtained in hypothesis of white noise input (Der Kiureghian - (*6.12*))
- WN_{INF}: CQC results obtained in hypothesis of white noise input (Der Kiureghian - (*6.13*))
- *MO*: CQC results obtained in hypothesis of white noise input (Moschen - Eq 6.37)
- *DN*: CQC results obtained by exploiting the Multiple Timescale Separation method (Denoel)
- *WX*: CQC results obtained by exploiting the computational capacities of the software *wxMaxima*.

For the above mentioned procedures, the comparison of the solutions will be done in terms of:

- Aceleration response spectrum (limited to the results coming from the time history analysis
- Reaction forces Response Spectrum
- Non dimensional reaction forces Response Spectrum

By starting from the Type 1 EC8 Response Spectrum, for every class of soil, the results for the different damping ratios are reported. Then the same will be done for the Type 2 EC8 RS.

9.3 EC8 type 1 Response Spectrum

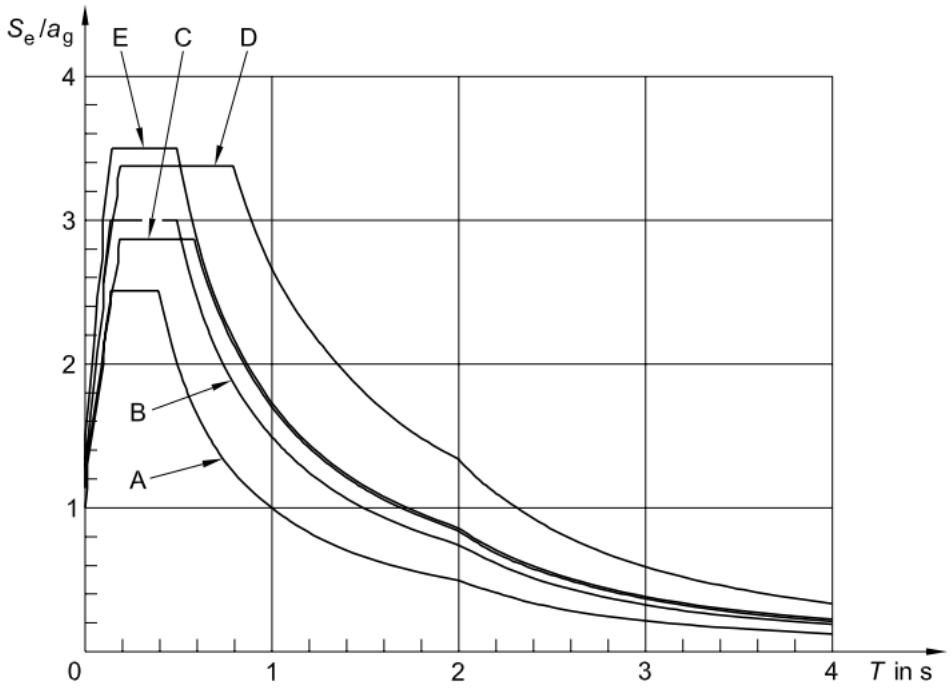

Figure 9.3: EC8 Type 1 Response Spectrum

The Eurocode 8, depending on the characteristics of the most significant earthquakes contributing to the local hazard, recomends two elastic spectral shape:

- Type 1: high and moderate seismicity regions ($M_s > 5.5$)
- Type 2: low seismicity regions for near field earthquakes ($M_s \leq 5.5$)

where M_s is the magnitude of the surface travelling waves.
(Questo lo potremmo usare come intro nel Capitolo del tipo 2) Se i terremoti che contribuiscono in misura maggiore al rischio sismico definito per il sito al fine di valutare il rischio probabilistico hanno una magnitudo di onde di superficie, Ms, non maggiore di 5,5, si raccomanda di adottare lo spettro di Tipo 2. Now, for the Type 1 RS, the five spectral shapes for the different soil classes are reported in Figure *9.3*. The spectra are normalized wrt to the peak ground acceleration.

9.3.1 Soil class A

By starting from the comparison in terms of acceleration RS, two aspects characterize the results. In particular, for small values of ξ, the time history response spectrum provides higher ordinates than the target one. The opposite happens on the other hand by increasing the damping ratio. A

rather good correspondence is found instead for the case of $\xi = 0.05$.
This is due to the fact the accelerograms taking part in the time analysis are generated in such a way to be compatible with the 5% damped response spectrum. The value of ξ used for the comparison enters the formulation only as the damping ratio of the structural system, without affecting the intensity of the accelerograms. It is clear that, by generating time histories accelerations with a damping coefficient equal to the one of the structure, the correspondence of the results would be garanteed.
This could not be done however, due to the fact that in the non linear field, the accelerograms by definition must be generated considering a 5% damped RS. Therefore, in order to allow for a comparison between the elastic and the elasto-plastic results, a 5% damping was adopted to generated the time history also in the elastic field.

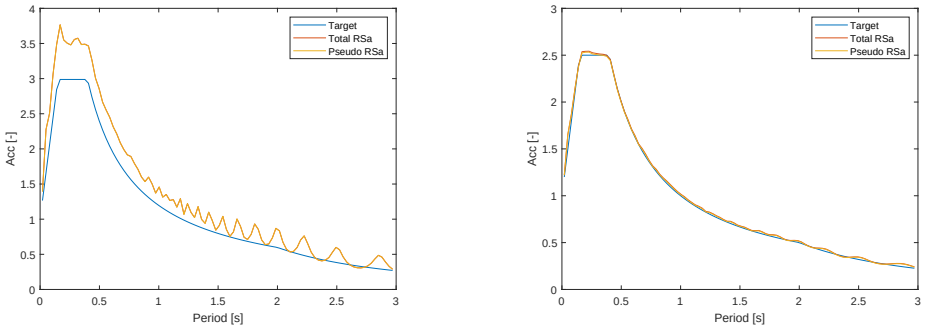

(a) $\xi = 0.02$ (b) $\xi = 0.05$

Figure 9.4: Soil type A: Response Spectrum comparison

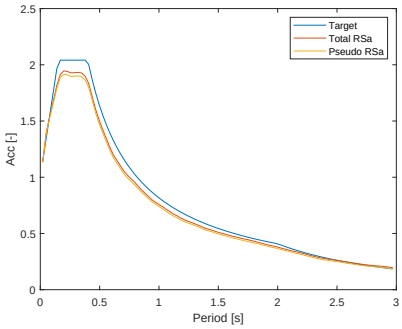

(c) $\xi = 0.10$

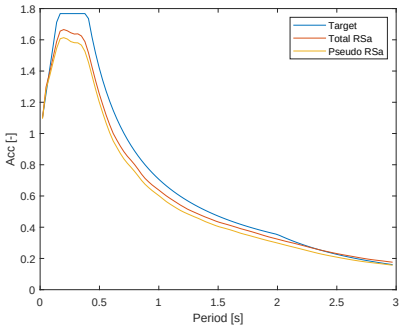

(d) $\xi = 0.15$

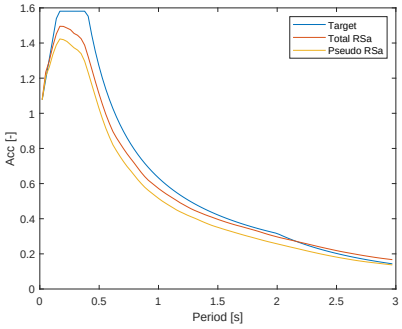

(e) $\xi = 0.20$

Figure 9.4: Soil type A: Response Spectrum comparison

The second aspect is instead related to the correlation between the pseudo and the total acceleration RS. As expected, the two coincide when the damping contribution is negligible. However, when the value of ξ increases, the total acceleration provides higher results. This is the reason why, being interested in the most unfavorable case, the time history results which will be reported make reference to the concept of total acceleration.

For what concerns the reaction forces, the considerations made before for the acceleration outputs will remain valid. In particular, as it can be seen from Fig.9.5, for small damping, the time history RS envelopes all the other results. Things change instaed for small values of ξ.
Now, the presentation of the results will be organized as follow:

1. comparison between the time history analysis and the Response Spectrum method results

2. comparison between the different formulations adopted for the Response Spectrum results

Time history vs CQC results

What happens in general is that, for small contributions of damping, the higher results are the ones provided by time domain analysis. As it happened however for the case of the acceelration RS, the time history results tend to be more affected by the increment in damping than the other formulations. This is why, from values of ξ higher than 10%, the TH results are overcome by other solutions.
What happens in general is that:

- in the high frequency domain, the TH results are limited from above by the provided by Moschen et al (MO), and from the bottom by WN

- in the low frequency domain instead, it is WX to reprsent the lower limit, while WN_{APPRX} provides the upper boundary

This behaviour is more evident in the diagrams associated to F_A. For what concerns the force at the top F_B, a more irregular trend developes in the intermediate domain $0.5T - T$.

Response spectrum method outputs

Now, by focusing on the comparison between the results provided by the CQC, some further considerations can be done. For what concerns F_B, it can be appreciated how in general, it is the formulation proposed by Denoel to better fit the CQC reference results provided by the trapezoidal integration scheme by Matlab. The same holds for F_A, even if less rigorously.
Of all the analytical formulations, Moschen's was the only one overestimating the value of ρ_{ig} along the whol domain (Figure *6.2*), and this is consequently reflected on the forces at the connections. On the opposite, in the high frequenct domain, the formula provided by Der Kiureghian is the one providing lower results.

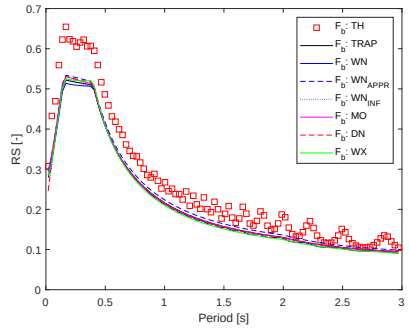

(a) $\xi = 0.02$

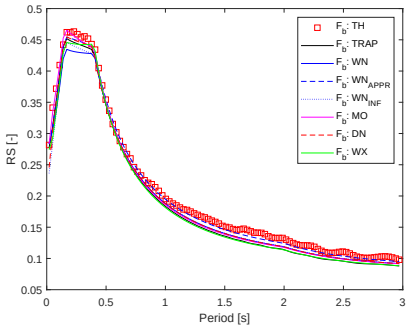

(b) $\xi = 0.05$

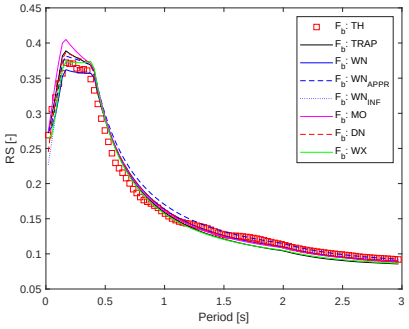

(c) $\xi = 0.10$

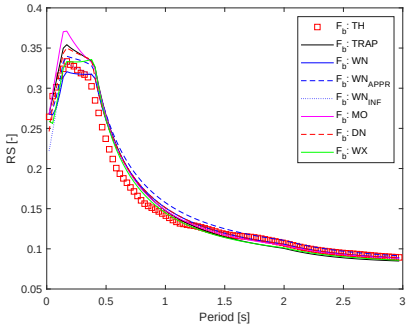

(d) $\xi = 0.15$

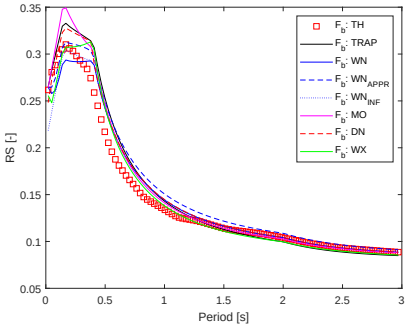

(e) $\xi = 0.20$

Figure 9.5: Soil type A: Reaction force F_b Response Spectrum

The same holds for the formulation obtained by exploiting the capacity of *WX MAXIMA*.
In conclusion, for small values of ξ, the different formulations show a rather good correspondence between the results. Things are different for higher damping ratios. In this case the formulations based on the assumptions of low damped structures clearly underestimate the results.

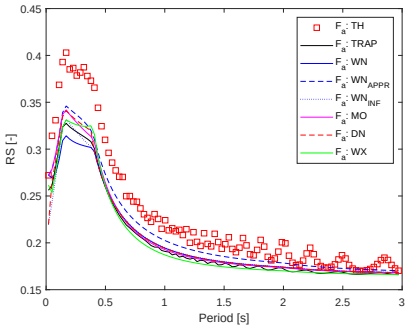

(a) $\xi = 0.02$

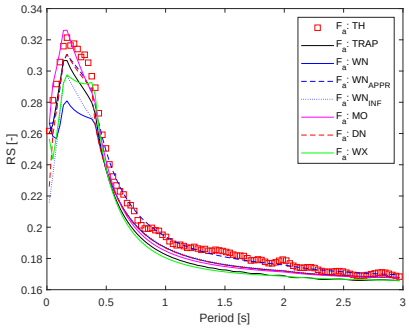

(b) $\xi = 0.05$

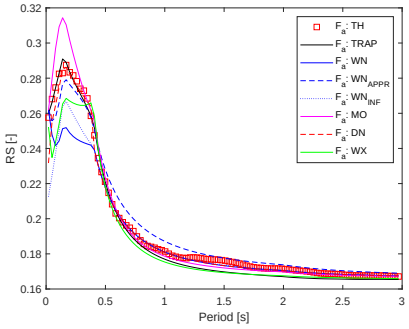

(c) $\xi = 0.10$

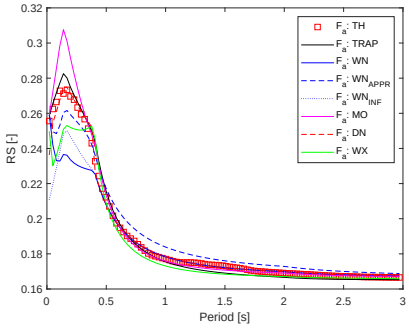

(d) $\xi = 0.15$

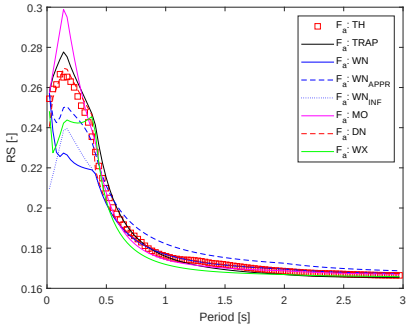

(e) $\xi = 0.20$

Figure 9.6: Soil type A: Reaction force F_a Response Spectrum

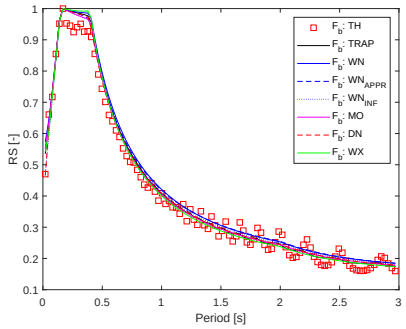

(a) $\xi = 0.02$

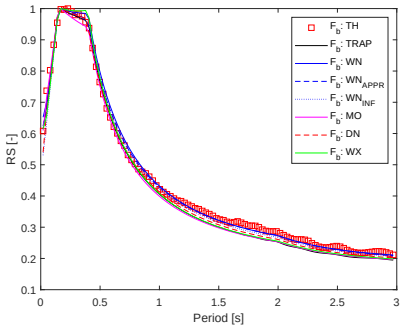

(b) $\xi = 0.05$

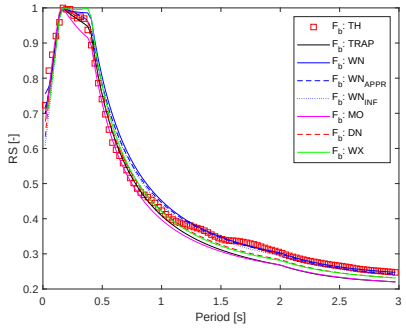

(c) $\xi = 0.10$

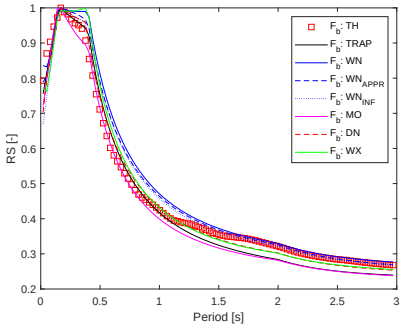

(d) $\xi = 0.15$

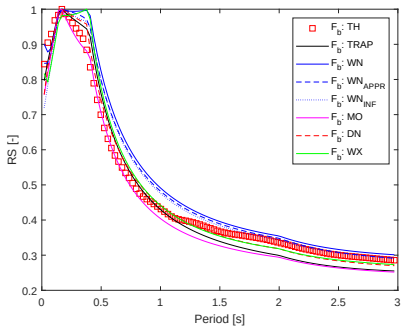

(e) $\xi = 0.20$

Figure 9.7: Soil type A: Reaction force F_b Adimensional Response Spectrum

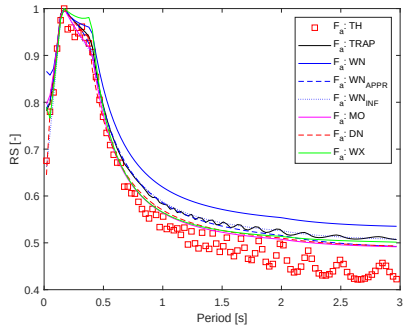

(a) $\xi = 0.02$

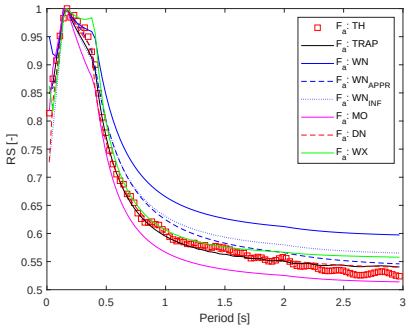

(b) $\xi = 0.05$

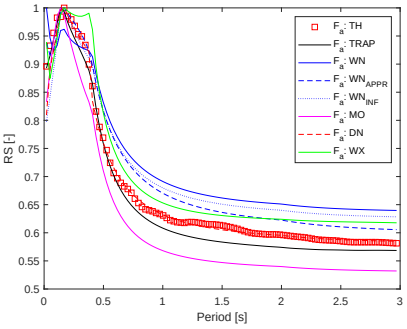

(c) $\xi = 0.10$

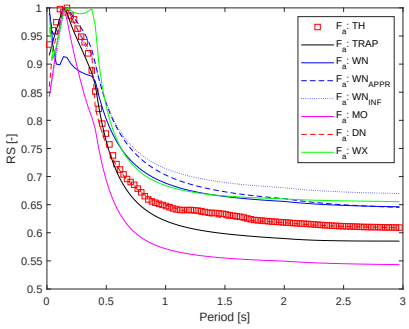

(d) $\xi = 0.15$

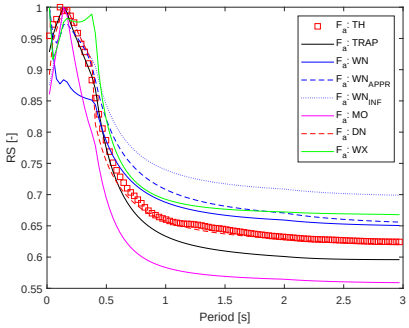

(e) $\xi = 0.20$

Figure 9.8: Soil type A: Reaction force F_a Adimensional Response Spectrum

9.3.2 Soil class B

The considerations presented for the Soil class A remain valid also for the other types of soils, where the shape of the Response Spectrum does affect the overall behaviour of the results. The time history solutions are the ones more influenced by the change in the damping ratio, providing the highest results for small values of χ, and then quickly decreasing as the damping contribution increase. For what concerns the different RS method formulations, in the high frequency domain, the results obtained by exploiting Denoel's theory (DN) represent an upper limit for the soultions. On the contrary, the results by Der Kiureghian (WN) tend to underestimate the values of F_A and F_B.

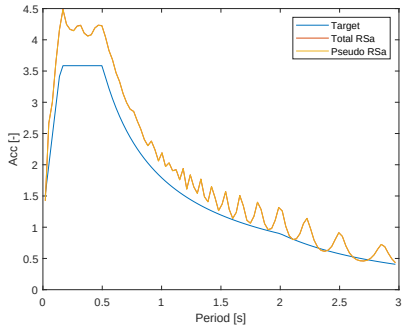

(a) $\xi = 0.02$

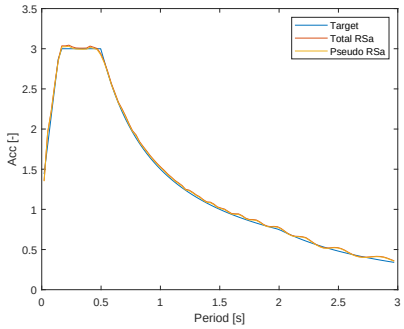

(b) $\xi = 0.05$

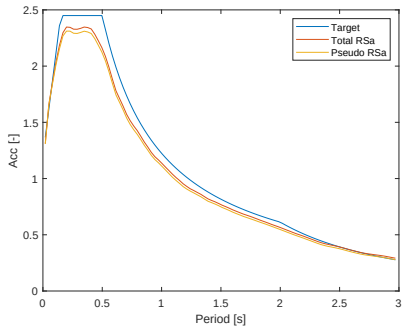

(c) $\xi = 0.10$

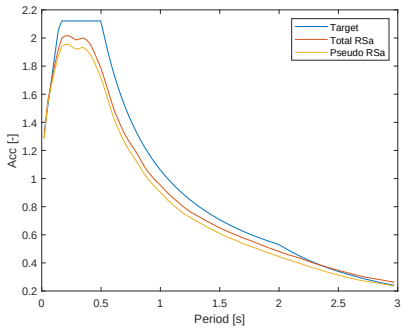

(d) $\xi = 0.15$

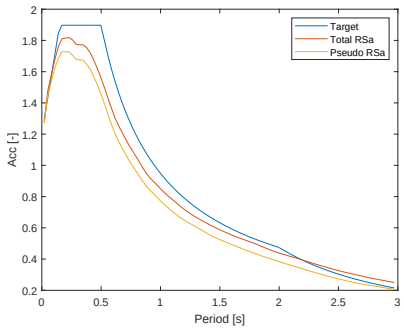

(e) $\xi = 0.20$

Figure 9.9: Soil type B: Response Spectrum comparison

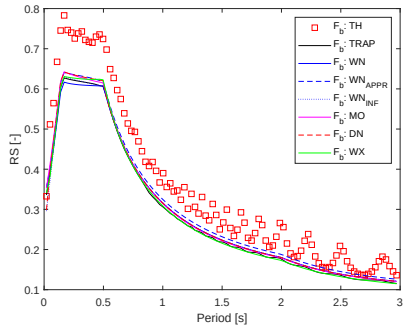

(a) $\xi = 0.02$

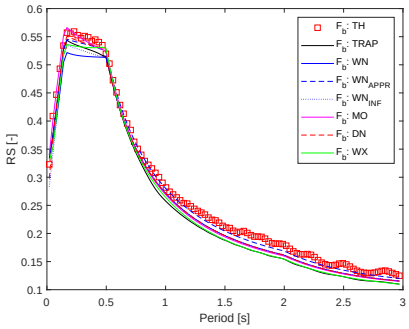

(b) $\xi = 0.05$

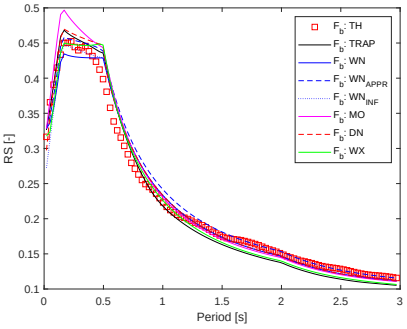

(c) $\xi = 0.10$

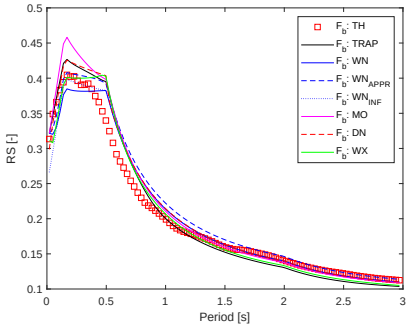

(d) $\xi = 0.15$

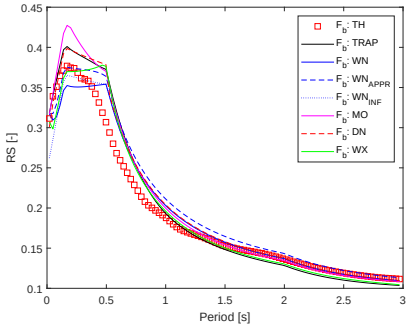

(e) $\xi = 0.20$

Figure 9.10: Soil type B: Reaction force F_b Response Spectrum

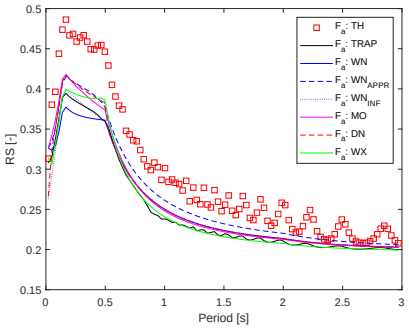

(a) $\xi = 0.02$

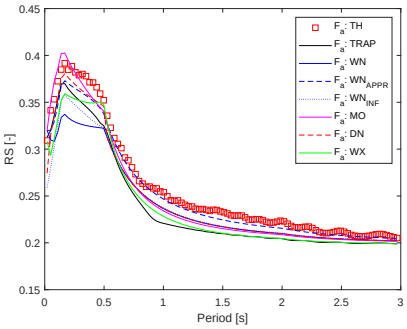

(b) $\xi = 0.05$

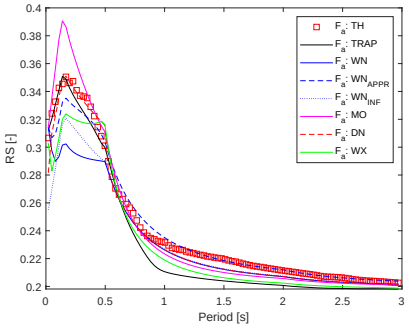

(c) $\xi = 0.10$

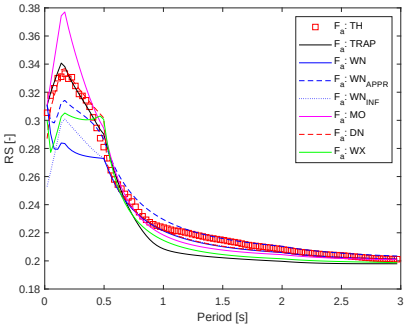

(d) $\xi = 0.15$

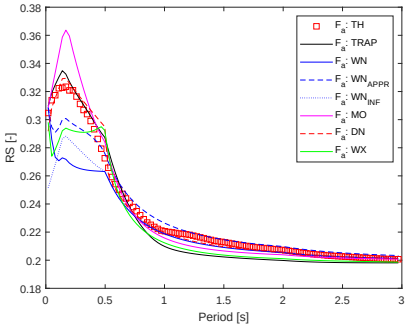

(e) $\xi = 0.20$

Figure 9.11: Soil type B: Reaction force F_a Response Spectrum

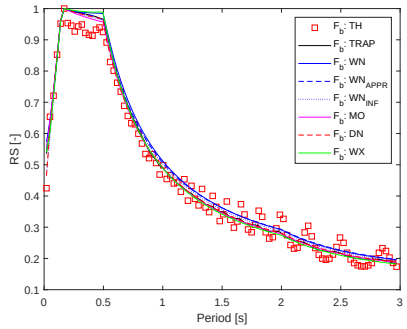

(a) $\xi = 0.02$

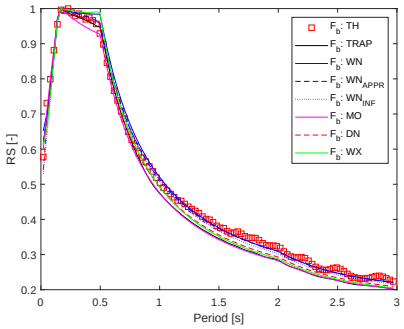

(b) $\xi = 0.05$

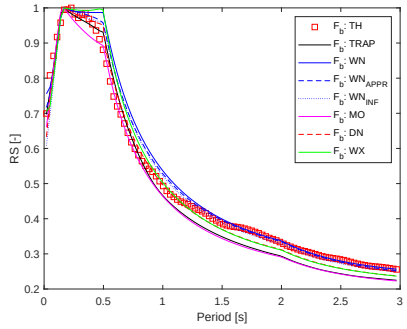

(c) $\xi = 0.10$

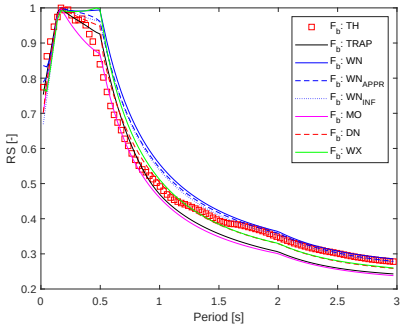

(d) $\xi = 0.15$

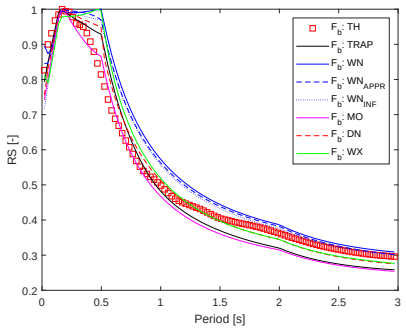

(e) $\xi = 0.20$

Figure 9.12: Soil type B: Reaction force F_b Adimensional Response Spectrum

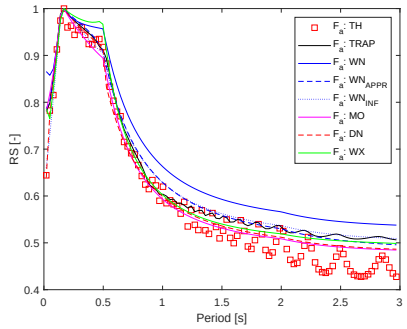

(a) $\xi = 0.02$

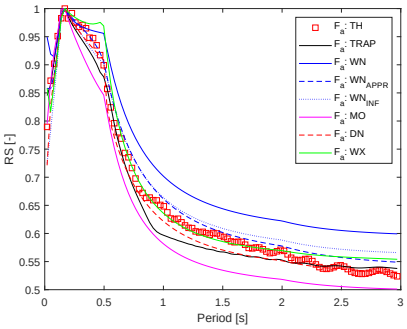

(b) $\xi = 0.05$

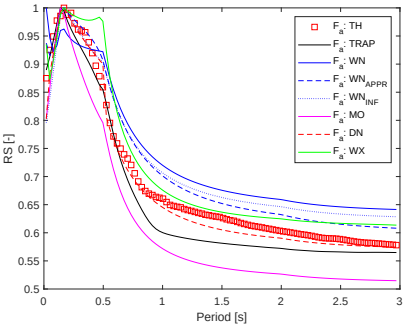

(c) $\xi = 0.10$

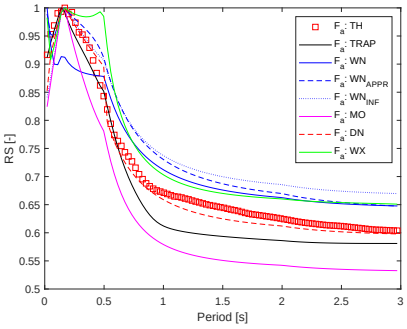

(d) $\xi = 0.15$

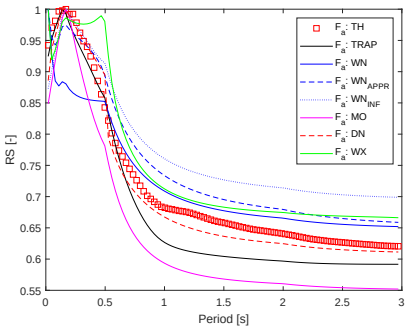

(e) $\xi = 0.20$

Figure 9.13: Soil type B: Reaction force F_a Adimensional Response Spectrum

9.3.3 Soil class C

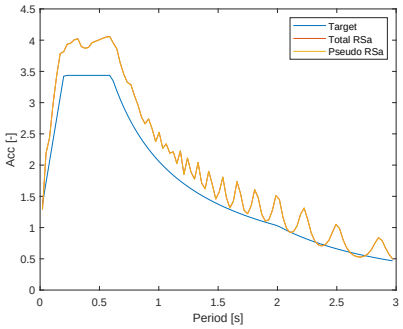

(a) $\xi = 0.02$

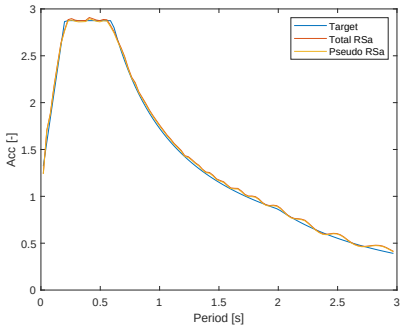

(b) $\xi = 0.05$

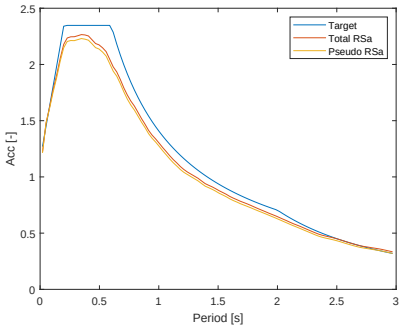

(c) $\xi = 0.10$

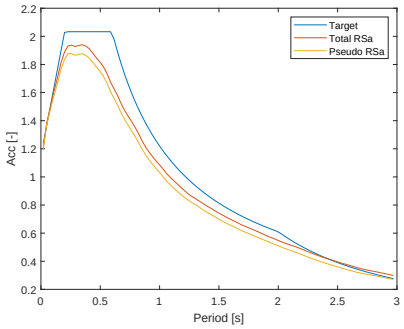

(d) $\xi = 0.15$

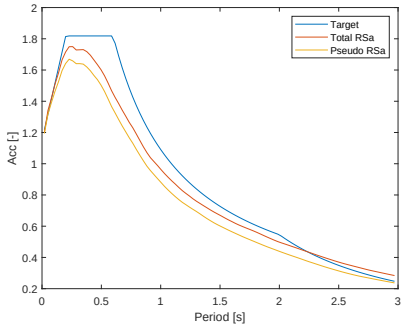

(e) $\xi = 0.20$

Figure 9.14: Soil type C: Response Spectrum comparison

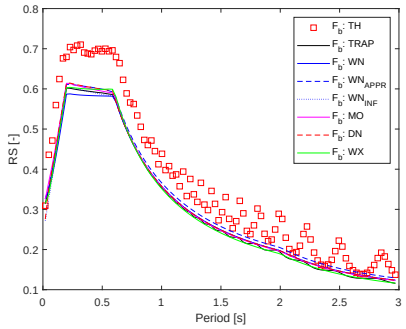

(a) $\xi = 0.02$

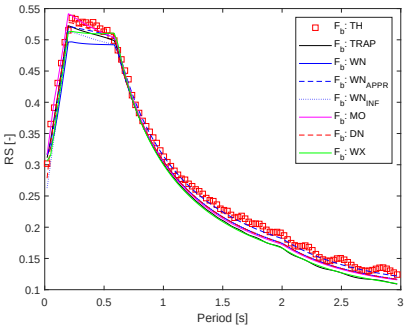

(b) $\xi = 0.05$

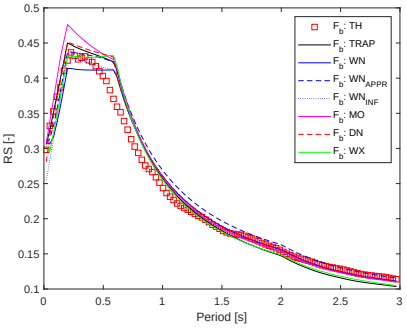

(c) $\xi = 0.10$

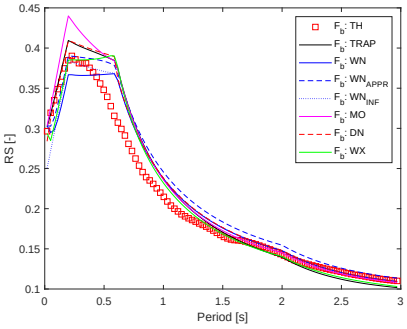

(d) $\xi = 0.15$

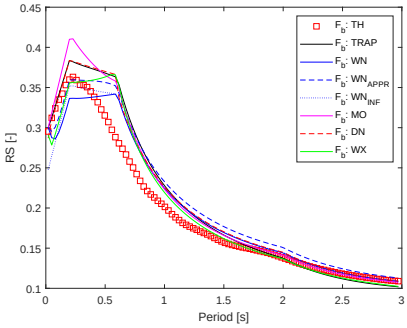

(e) $\xi = 0.20$

Figure 9.15: Soil type C: Reaction force F_b Response Spectrum

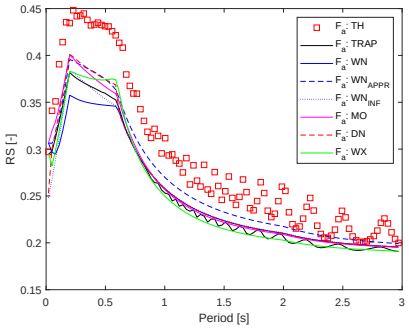

(a) $\xi = 0.02$

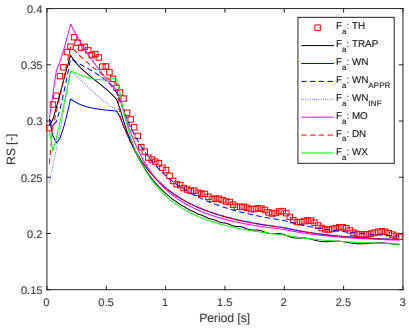

(b) $\xi = 0.05$

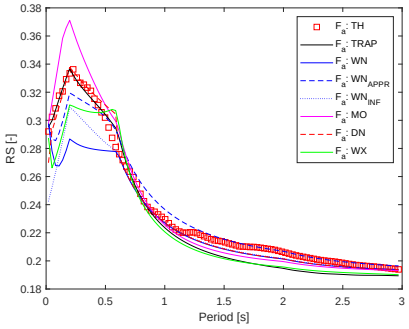

(c) $\xi = 0.10$

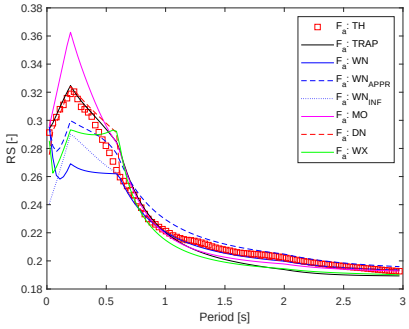

(d) $\xi = 0.15$

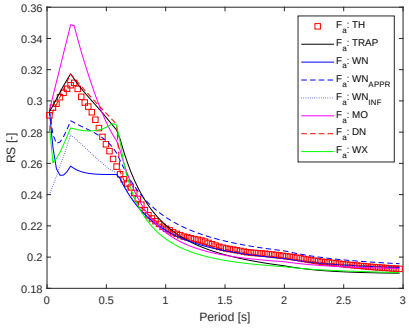

(e) $\xi = 0.20$

Figure 9.16: Soil type C: Reaction force F_a Response Spectrum

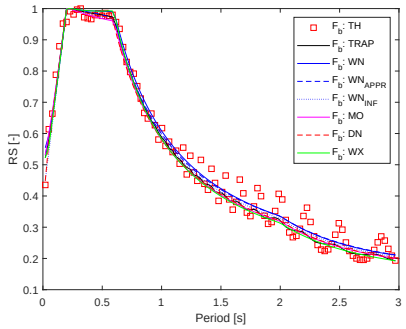

(a) $\xi = 0.02$

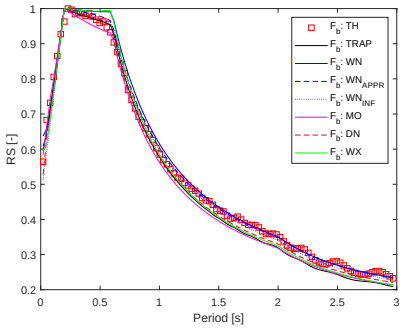

(b) $\xi = 0.05$

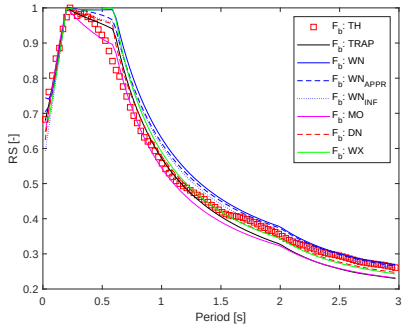

(c) $\xi = 0.10$

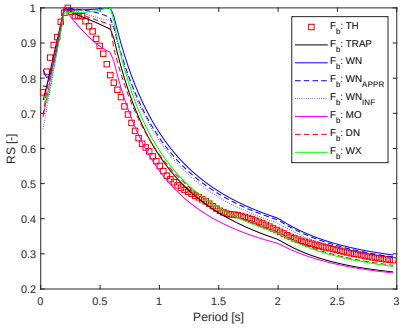

(d) $\xi = 0.15$

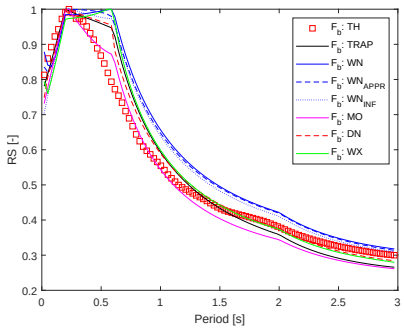

(e) $\xi = 0.20$

Figure 9.17: Soil type C: Reaction force F_b Adimensional Response Spectrum

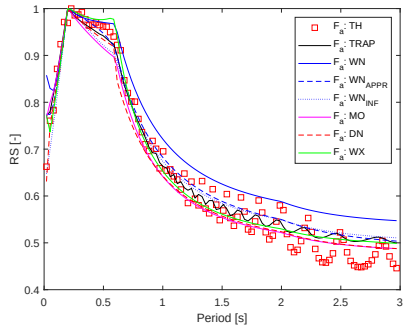

(a) $\xi = 0.02$

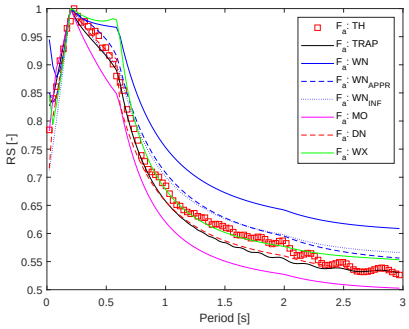

(b) $\xi = 0.05$

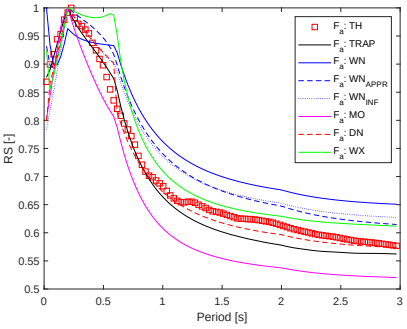

(c) $\xi = 0.10$

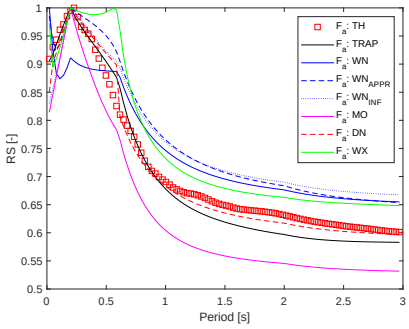

(d) $\xi = 0.15$

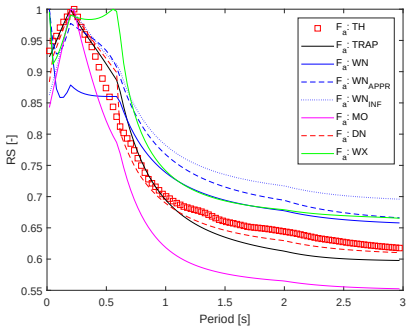

(e) $\xi = 0.20$

Figure 9.18: Soil type C: Reaction force F_a Adimensional Response Spectrum

9.3.4 Soil class D

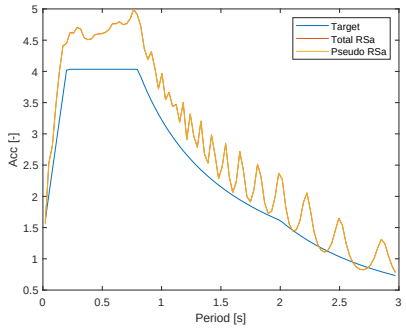

(a) $\xi = 0.02$

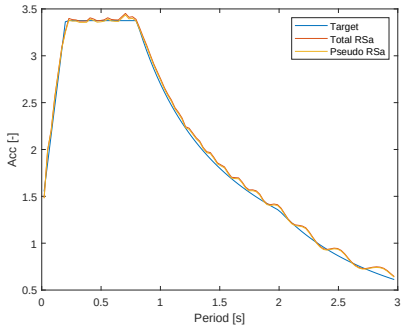

(b) $\xi = 0.05$

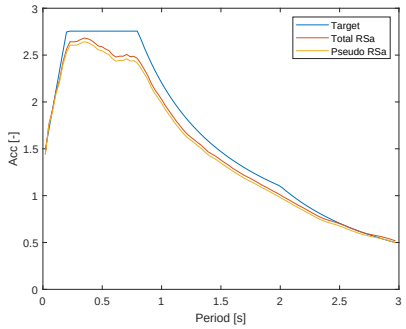

(c) $\xi = 0.10$

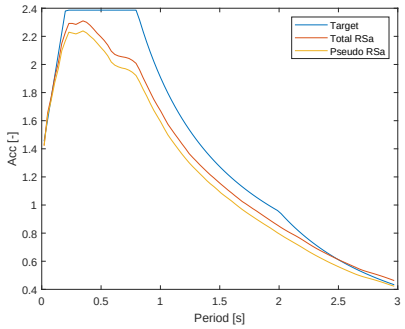

(d) $\xi = 0.15$

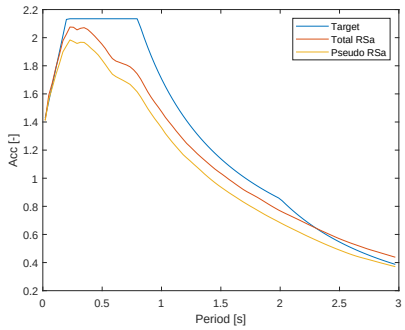

(e) $\xi = 0.20$

Figure 9.19: Soil type D: Response Spectrum comparison

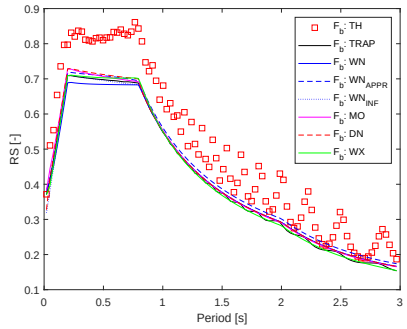

(a) $\xi = 0.02$

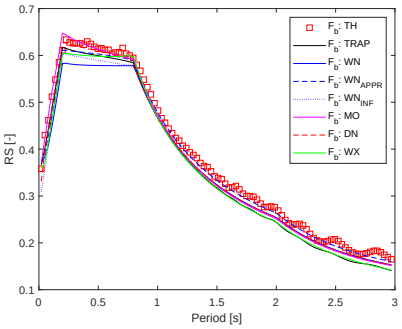

(b) $\xi = 0.05$

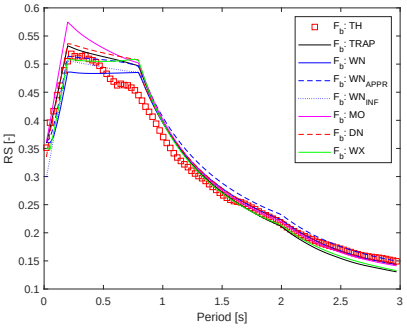

(c) $\xi = 0.10$

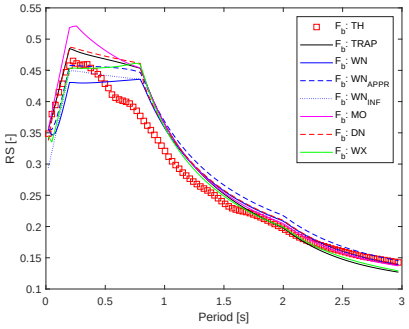

(d) $\xi = 0.15$

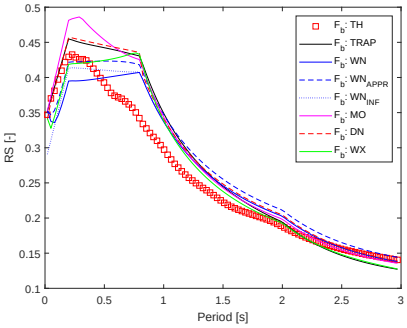

(e) $\xi = 0.20$

Figure 9.20: Soil type D: Reaction force F_b Response Spectrum

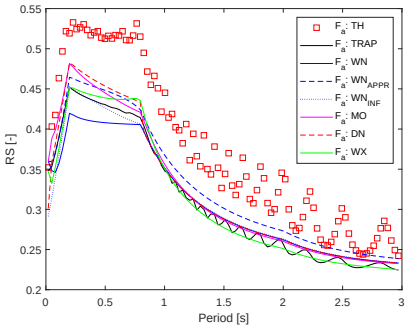

(a) $\xi = 0.02$

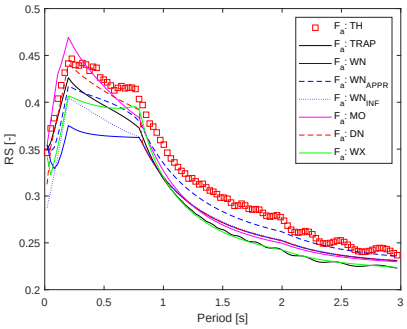

(b) $\xi = 0.05$

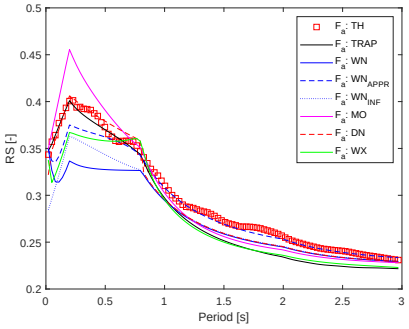

(c) $\xi = 0.10$

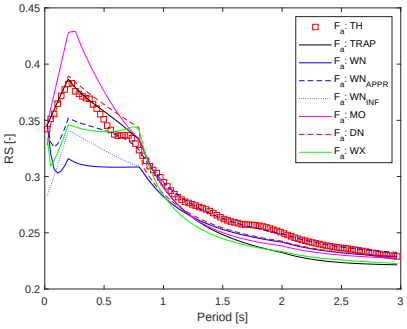

(d) $\xi = 0.15$

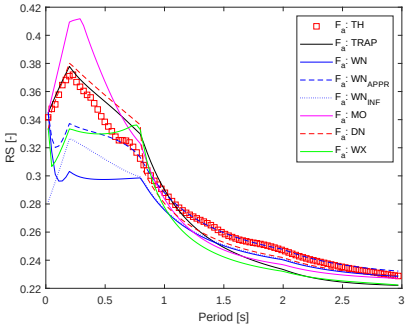

(e) $\xi = 0.20$

Figure 9.21: Soil type D: Reaction force F_a Response Spectrum

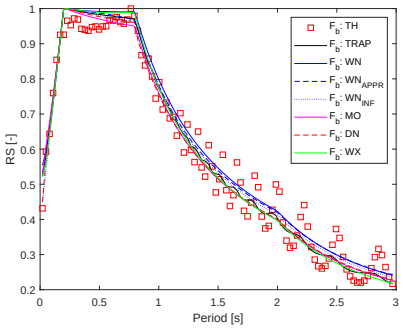

(a) $\xi = 0.02$

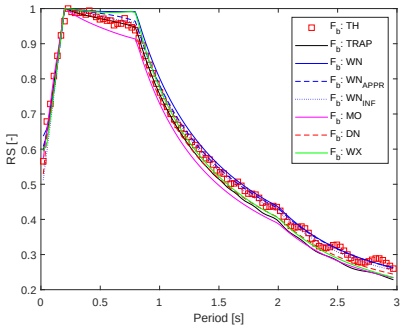

(b) $\xi = 0.05$

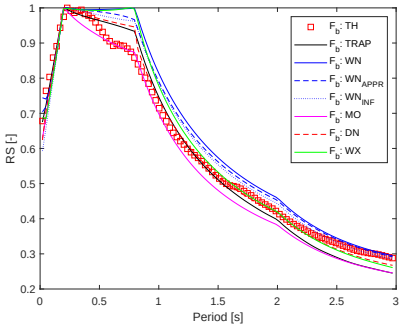

(c) $\xi = 0.10$

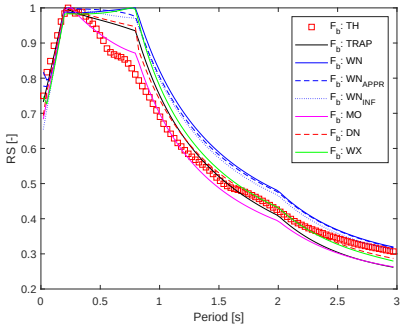

(d) $\xi = 0.15$

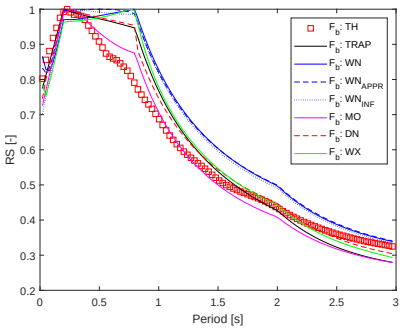

(e) $\xi = 0.20$

Figure 9.22: Soil type D: Reaction force F_b Adimensional Response Spectrum

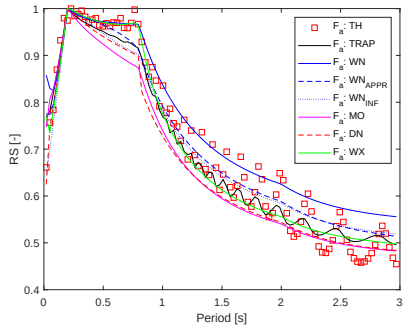

(a) $\xi = 0.02$

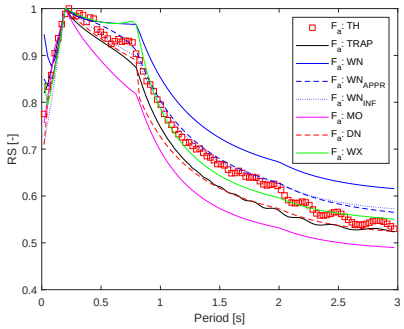

(b) $\xi = 0.05$

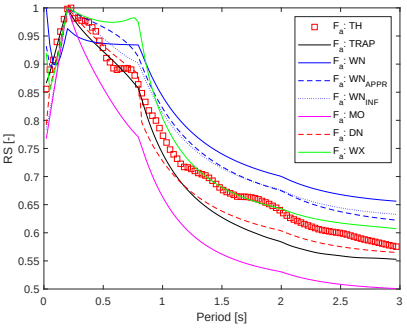

(c) $\xi = 0.10$

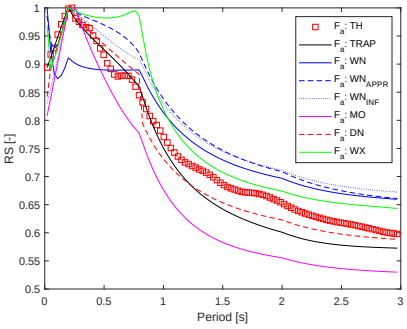

(d) $\xi = 0.15$

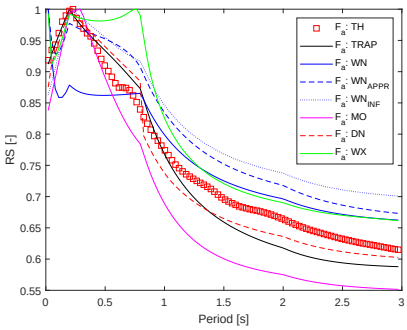

(e) $\xi = 0.20$

Figure 9.23: Soil type D: Reaction force F_a Adimensional Response Spectrum

9.3.5 Soil class E

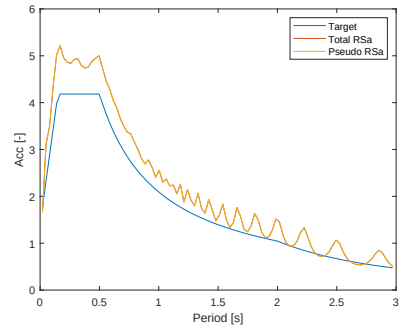

(a) $\xi = 0.02$

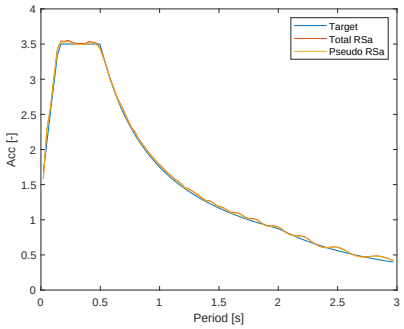

(b) $\xi = 0.05$

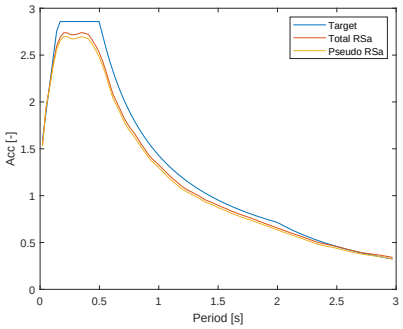

(c) $\xi = 0.10$

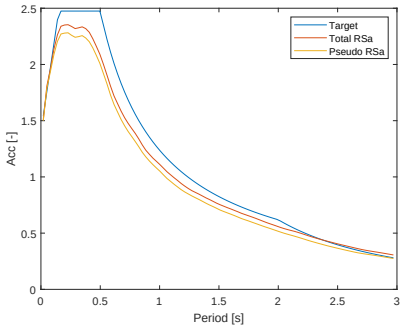

(d) $\xi = 0.15$

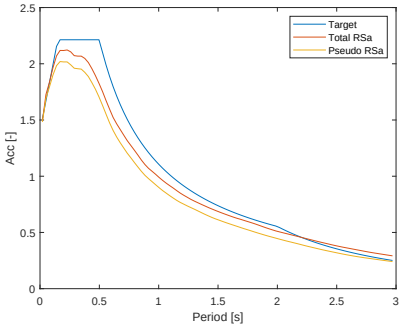

(e) $\xi = 0.20$

Figure 9.24: Soil type E: Response Spectrum comparison

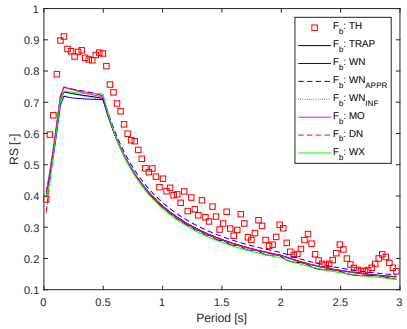

(a) $\xi = 0.02$

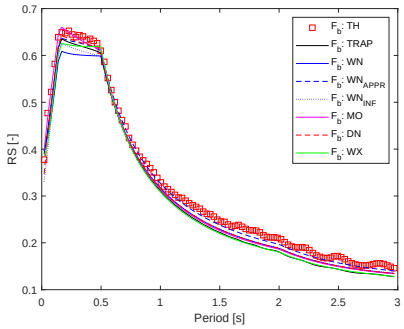

(b) $\xi = 0.05$

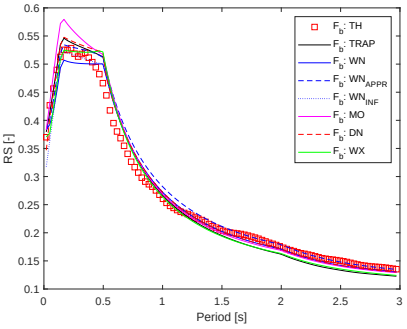

(c) $\xi = 0.10$

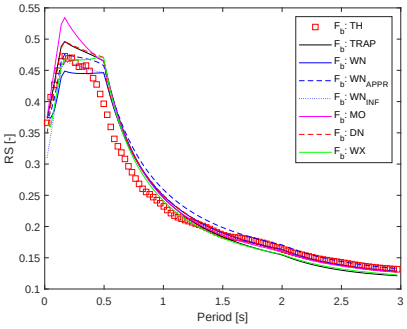

(d) $\xi = 0.15$

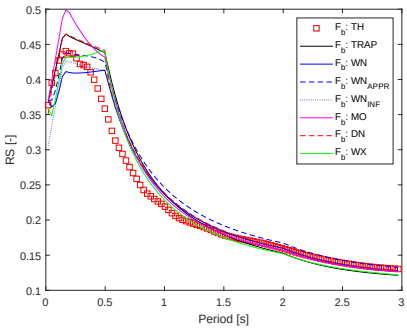

(e) $\xi = 0.20$

Figure 9.25: Soil type E: Reaction force F_b Response Spectrum

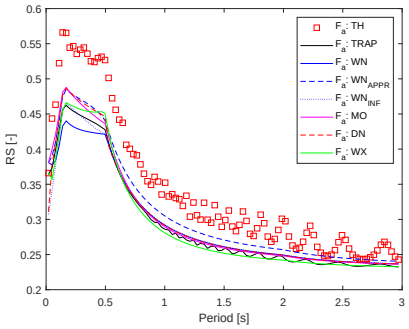

(a) $\xi = 0.02$

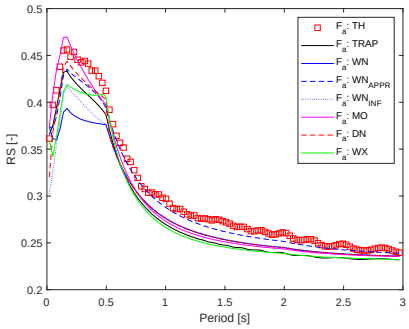

(b) $\xi = 0.05$

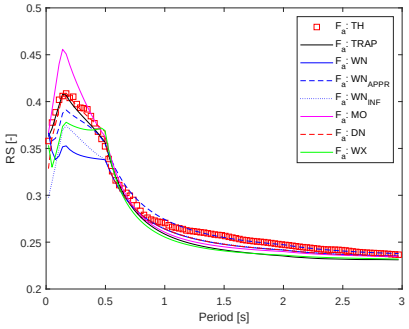

(c) $\xi = 0.10$

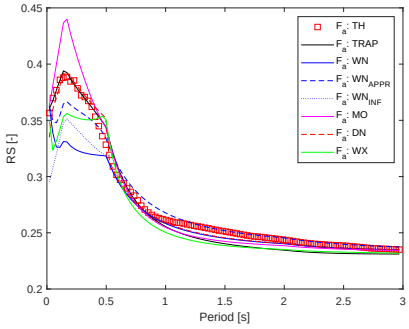

(d) $\xi = 0.15$

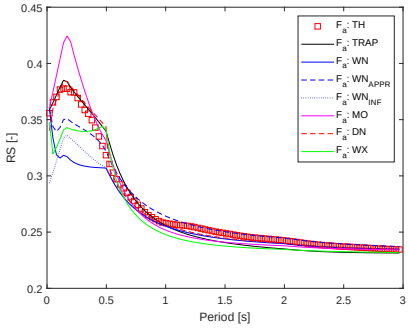

(e) $\xi = 0.20$

Figure 9.26: Soil type E: Reaction force F_a Response Spectrum

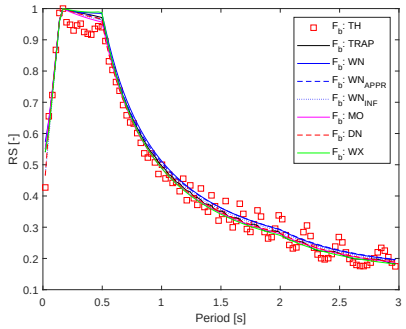

(a) $\xi = 0.02$

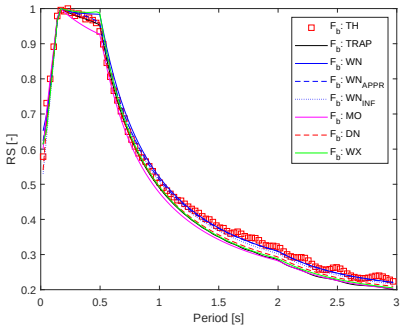

(b) $\xi = 0.05$

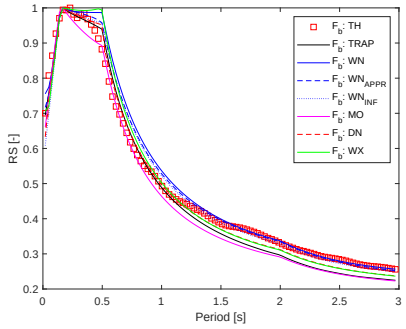

(c) $\xi = 0.10$

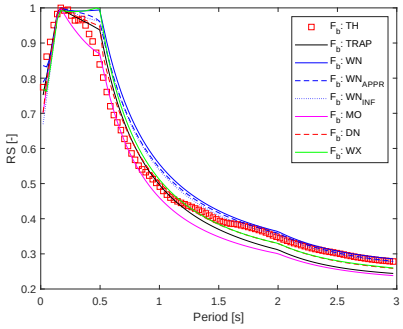

(d) $\xi = 0.15$

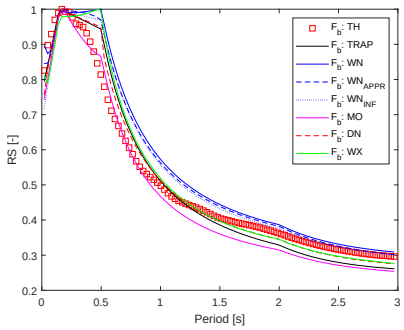

(e) $\xi = 0.20$

Figure 9.27: Soil type E: Reaction force F_b Adimensional Response Spectrum

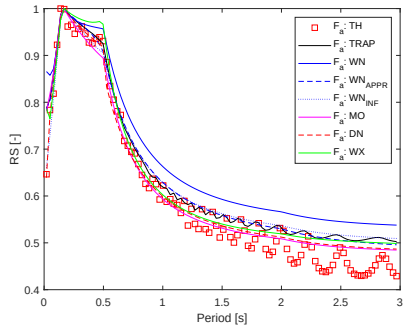

(a) $\xi = 0.02$

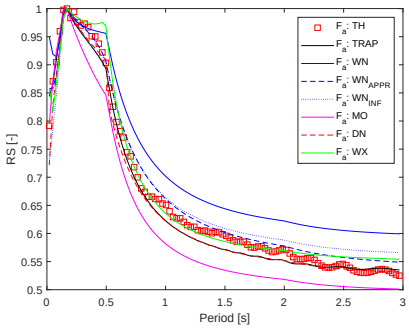

(b) $\xi = 0.05$

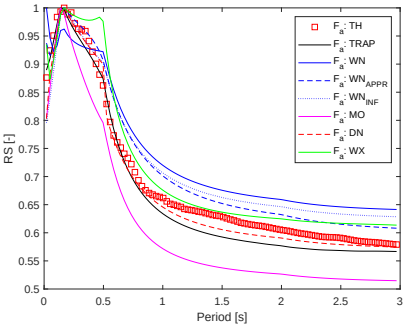

(c) $\xi = 0.10$

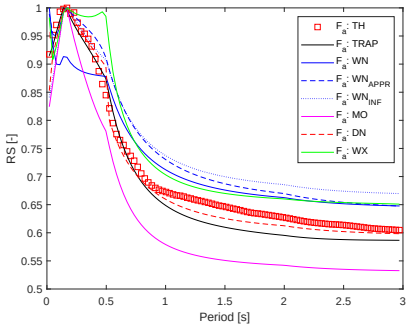

(d) $\xi = 0.15$

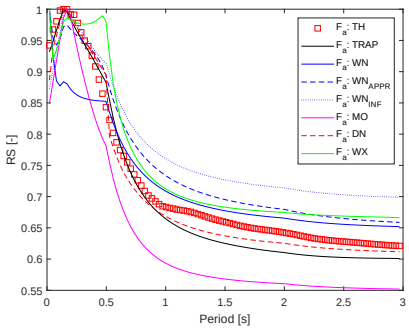

(e) $\xi = 0.20$

Figure 9.28: Soil type E: Reaction force F_a Adimensional Response Spectrum

Chapter 10

Validation of the results via Finite Element modelling

The results presented in the previous chapter proved how the Response Spectrum method is able to provide very good results in terms of maximum values, if compared with the numerical solutions provided by the rigorous time history analysis. The lack of precision in some cases is due to the fact that the different formulations adopted to compute the correlation coefficients are based sometimes on assumptions which cannot be satisfied for all the ranges of frequencies and damping values examined. Keeping this in mind, and depending on the problem to deal with, the most proper formulation can be adopted. There is however a far more heavy assumption upon which the results presented in the previous chapter are based, i.e. the modeling of the cladding panel as a fully rigid element.
On one hand this assumption allowed to simplify the implementation by hand of the Response Spectrum method in a software like Matlab.
On the other hand however, it neglects the dynamics of the panel, disregarding all the effects coming from it's vibration modes, which affect the elements in reality.
This is why, in order to validate the Response Spectrun method results presented in Chapter 9, a Finite Elelment model, through the use of the software *Straus7*, has been defined, which will serve as a reference solution.
The next paragraphs will be therefore devoted to present the results obtained through the ise of *Straus7*, discussing the modeling choices adopted, and the structural cases considered.
At the ened, the outputs coming from 3 analysis will be extracted and used as a reference:

1. Natural frequency analysis: providing the frequencies of the model modes of vibration

2. Spectral response analysis: providing the maximum solutions of the analyses quantities

3. Time history analysis: providing the solution in time

10.1 Finite Element modelling

The aim of this section is to present the principal choices and assumptions upon which the different FE models in Straus7 were built. Reference is made to the industrial structure depicted in Figure *10.1*, where the attention is focused on the behavior along one direction only, but obviously the same consideration holds also for the other direction.

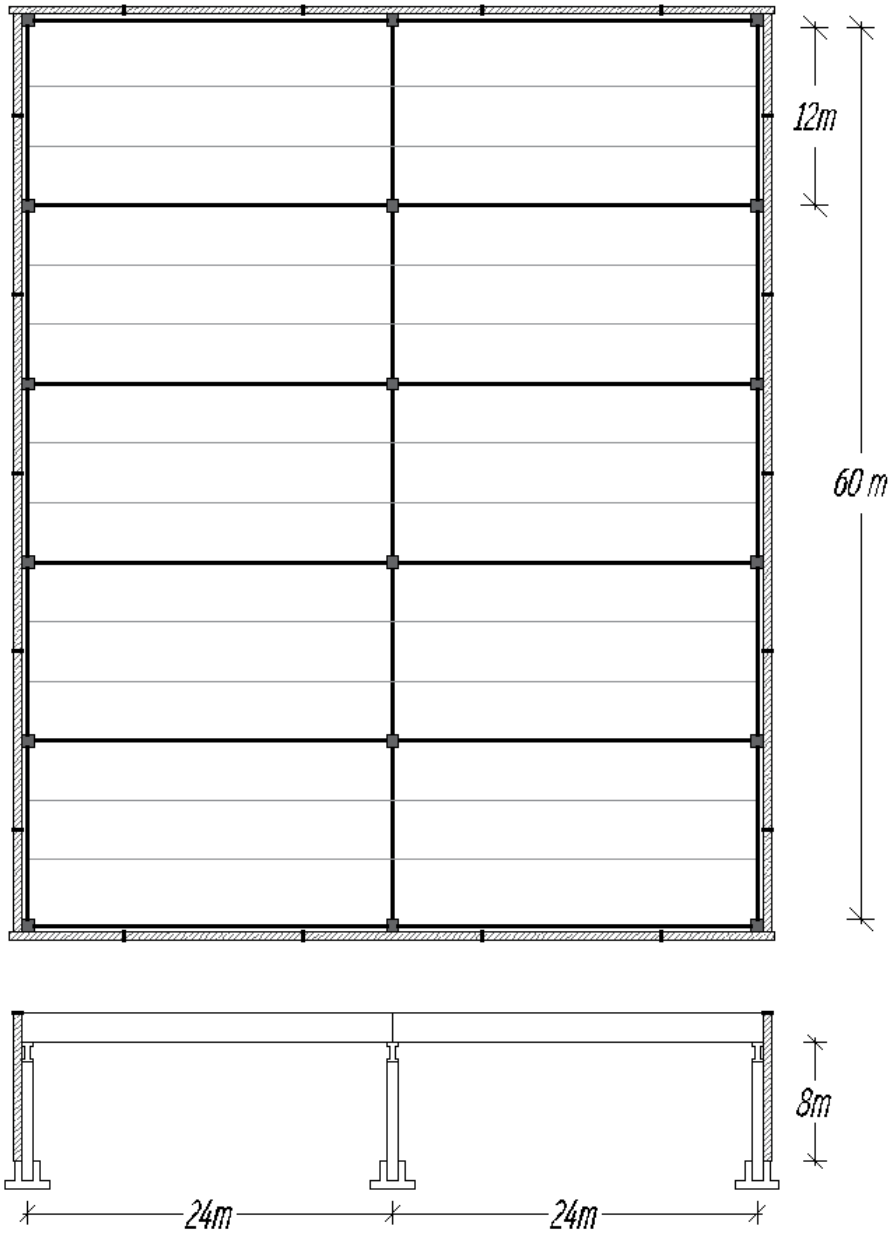

Figure 10.1: In plan and side structural view

The structure is characterized by five spans (campate), with square $60x60cm$ columns, closed at the edges by 14cm thick panels. The distance between

the columns is equal to 12m, in both directions
Now, by exploiting the in plant simmetry, the behavior of the single campata in the x direction can be reproduced a scheme like the one reported in Figure 3, made by:

- two internal columns
- a boarder column
- A portion of the panel determined on the bases of its influence area on the boarder column

The main modelling aspects are reported in the following sections.

10.1.1 Modeling of the columns

The columns in Straus7 are created with the following characteristics:

- section geometry: 600mm x 600mm
- height: 8000mm
- material: Concrete $f_c = 40MPa$

Column 600×600 mm	
Area	3.6E+04 mm^2
Inertia	1.08E+10 mm^4
Elastic modulus	$34920 \frac{N}{mm^2}$
Flexural stiffnes	$2209 \frac{N}{mm}$

Table 10.1: Characteristic of the column

The self weight of the element is here considered negligible if compared with the axial force generated by the roof, therefore the specific density is fixed equal to zero. Finally, the parameters of interest are reported in Table *10.1*. The columns are fixed at the base, while at the top they are linked together by a pinned rigid link.
They are subdivided into a number of 16 beam elements. This was necessary to better capture the non linear behavior of the element in the non linear field.

10.1.2 Modeling of the panel

The panel is modeled as a beam element, with the following characteristics:

- section geometry: $140mm \times 12000mm$
- height: 10000mm
- material: Concrete $f_c = 40MPa$

where 12000mm represents the influence lenght of the panel associated to the edge column. The main geometrical and mechanical properties are reported in Table *10.2*. In order to model the panel as a rigid entity, its elastic modulus E has been amplified by a factor equal to 1000. As it will be treated in the next sections however, this won't be enough to cancel out the intrinsic vibration modes of the element. This is why, further measures will be later introduced.
The element is hinged at the base, and pinned to the boarder column at the top. Also in this case, a discretization in different sub-elements is adopted. This was necessary first of all to introduce the node needed to model the

connection with the boarder column, and second of all for a better comprehension of the behavior of the forces along the height of the panel.

Rigid cladding panel	
Area	3.6E+04 mm^2
Inertia	1.08E+10 mm^4
Elastic modulus	$34920\frac{N}{mm^2}$
Flexural stiffnes	$2209\frac{N}{mm}$
η	0.25

Table 10.2: Characteristic of the panel

Modelling of the cladding connections

As presented before, the columns at the top are linked together by a pinned rigid link. The same holds also for the rigid connections between the edge column and the panel. The disadvantage of doing so is related to the fact that *Straus7* does not allow to compute the reaction forces inside a rigid link. This is why, the seismic force generated inside the connection will be obtained indirectly from the shear force diagram acting in the cladded panel in correspondence of the anchoring point.
In particular, F_B will be computed as:

$$F_B = T^+_{CONN} - T^-_{CONN} \tag{10.1}$$

where T^+_{CONN} and T^-_{CONN} are the shear forces at the anchoring device coming from above and below.

10.1.3 Modeling of the structural masses

The final step now remaining is to account for the structural masses involved. As presented before, the self weight of the columns is here neglected. The same cannot be done however for the weight of the structural elements supported by the columns themselves. In particular, for and industrial structure like this, a roof system made by ????? is considered.
The influence of such configuration can be accounted by considering a specific weight of $350\frac{kg}{m^2}$. Doing so, the axial force generated on each column can be obtained by multiplying this value for the associated influence area:

$$N_{COLUMN} = 350\frac{kg}{m^2} \times 12m \times 12m \simeq 100Tonn \tag{10.2}$$

At the end 3 point masses have been applied on top of each column, as represented in Figure **??**. The last contribution is the one associated to the panel. To account for it, a specific weight of $2,86\frac{kN}{m^3}$ is adopted.

Therefore, by considering an influence length of the panel equal to 12m, the weight of the panel is equal to $48 Tonn$. The final model on *Straus7* is depicted in Figure *10.2*, where the red dots represent the lumped masses applied on top of the columns.

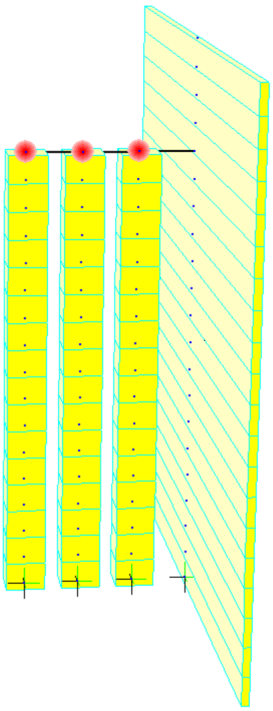

Figure 10.2: FE model

10.2 Results validation

As already presented, the validity of the model implemented in *Matlab* will be evalauted via the comparison with the outputs obtained in *Straus7* by running the following analysis:

1. Natural frequency analysis (NFA)
2. Spectral response analysis (SRA)
3. Time history analysis (THA)

Now, in order to account for the cracking process which affects the structure during a seismic event, the eleastic modulus of the structural elements, in these case the columns, have been reduced to 50% of its value. This to say that, all the results which will be presented from now on, make reference to structural elements with an elestic modulus equal to $\frac{E}{2} = 17145\frac{N}{mm^2}$

10.2.1 Natural frequency analysis

By performing a *Natural Frequency Analysis* in *Straus7*, the solutions for the first 10 modes of vibration are obtained. The first mode of the structure, whose deformed shape is reported in Figure *10.3*, is the one associated to the dual system frame and panel, whose period of vibration is equal to $T_{S_1} = \frac{1}{f_1} = \frac{1}{7.11Hz} = 1.40sec.$ On the other hand, in the Matlab code, the period of vibration of the SDOF dual system, was computed by amplifying the natural period of the frame times an infulence factor χ, accounting for the presence of the cladding panel.
In particular, being K_f and m_f the stiffness and mass of the structural model, equal to:

$$\begin{aligned} K_f &= 3\frac{3EI}{H_{col}^3} = 6627\frac{N}{mm} \\ m_f &= 3 \times 100Tonn = 300Tonn \end{aligned} \tag{10.3}$$

then the natural period of the frame is equal to:

$$T_f = \sqrt{\frac{m_f}{K_f}} = 1.337sec \tag{10.4}$$

In order to account for the presence of the panel, the following coefficient is introduced:

$$\chi(\mu, \eta) = \sqrt{1 + \frac{\mu(1+\eta)^2}{3}} = 1.0408 \tag{10.5}$$

being $\mu = \frac{m_p}{m_f}$ the ratio between the mass of the panel and the mass of the frame. For the case under analysis, $\chi(\mu, \eta) = ...$ Therefore, the natural period of the dual system is equal to:

$$\begin{aligned} w_s &= \frac{w_f}{\chi(\mu, \eta)} = 4.5164\frac{rad}{sec} \\ T_s &= T_f\chi(\mu, \eta) = 1.3912sec \end{aligned} \tag{10.6}$$

Despite some differences in the results, there is a quite good correspondnce between the two models.
It is now interesting to examine the remaining vibration modes provided by *Straus7*. This is important because even if their influence in terms of participation mass may seem negligible, their contributions to the overall response of the structure can strongly affect the final results.
The second, third and fouth modes are associated to a vertical behaviour of the structure (Figure *3.40*)

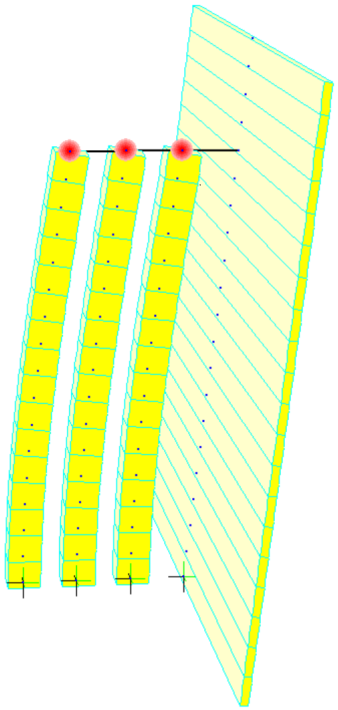

Figure 10.3: First mode of vibration

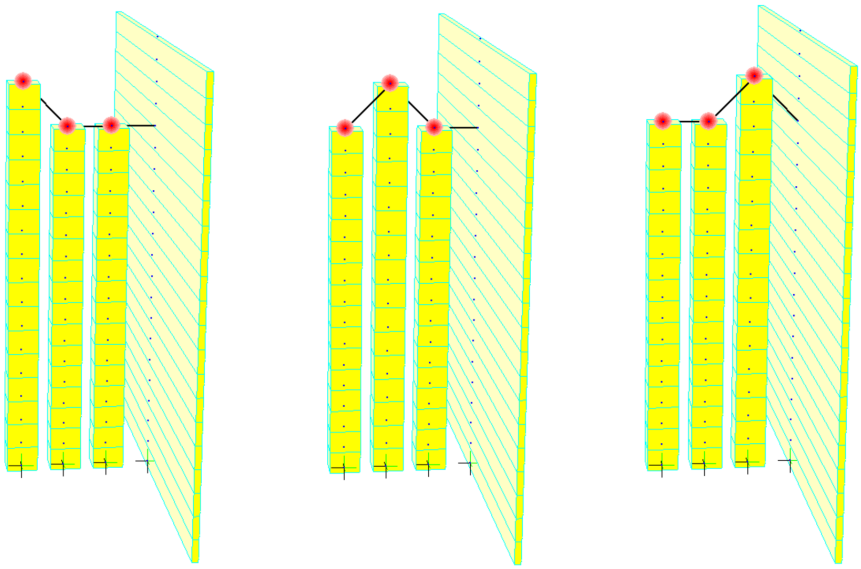

(a) f_2=19.77 Hz (b) f_3=19.77 Hz (c) f_4=19.77 Hz

Figure 10.4: Vertical vibration modes

The remaining six modes are associated to the deformation mechanisms of the panel, as represented in Figure *10.5*. Their mass participation is relatively low, however they can be responsible for spurious oscillations in the time history solution, thus affecting the results in terms of maximum values. In order to avoid this problem, for the case of linear analysis, *Straus7* gives the designer the possibility to select which modes to be accounted for in the analysis.
This is not the best solution though. The reason is that the panel in *Straus7* was not modelled as a rigid entity, being its elastic modulus a finite quentity, which could not be set too high in order to avoid ill-conditioning of the system.
This means that, being the panel flexible, lower values of the internal forces are to be expected if the higher vibrational modes are completely disregarded. A solution is to adopt a different damping formulation wrt the viscous one proposed by default by the software.
Therefore, a Rayleigh model is selected. This will allow to filter out the spurious effects due to the higher modes.

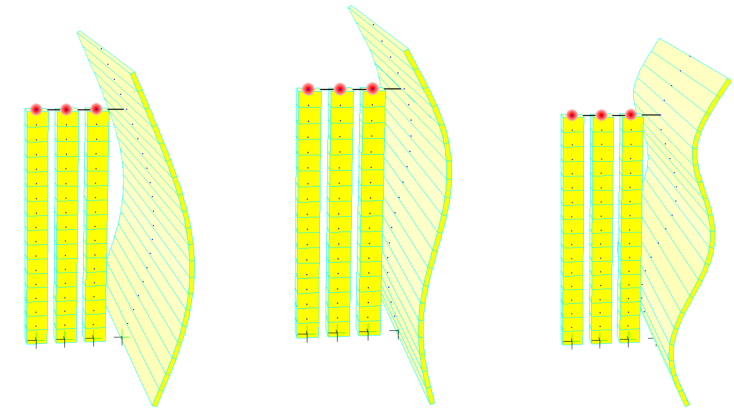

(a) f_5=104.31Hz

(b) f_6=325.09Hz

(c) f_7=576.93Hz

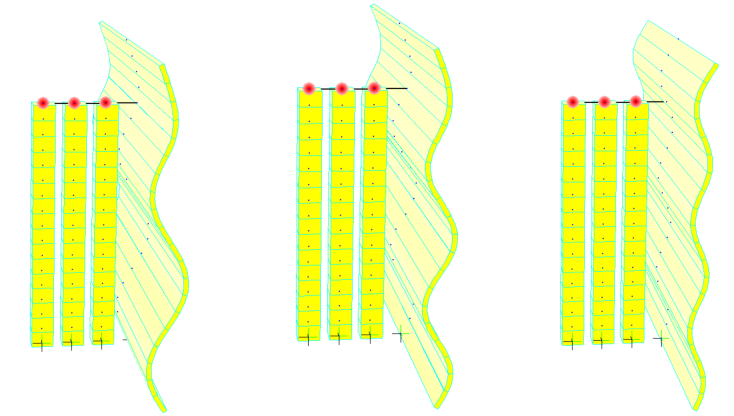

(d) f_8=1093.71Hz

(e) f_9=1842.9Hz

(f) f_{10}=2731.94Hz

Figure 10.5: Vibration modes of the panel

10.2.2 Rayleigh damping model

The implmentation of the damping model in *Straus7* passes through the following window:

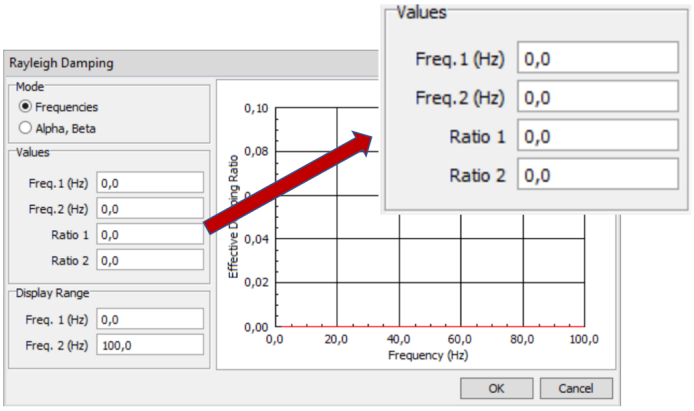

Figure 10.6: Implementation of the Rayleigh model of damping

Everything is based on the values adopted in the four slots highlighted in the zoom. The software requests two values of frequencies: f_1 and f_2. Then it asks for the damping ratios to associate to these two frequencies, where f_1 represents the frequency of the dual system, while f_2 represents a fictitous frequency, defined as ????
The model works in such a way to overdamp every frquency component which stands outside this range.
Therefore, by adopting a value of $f_1 = 0.71Hz$, $f_2 = 0.15Hz$, and fixing both damping ratios at $\chi = 0.05$, the behaviour of the coefficient χ in the frequency domain is:

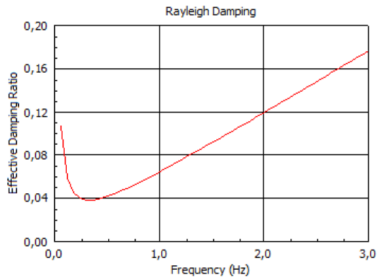

(a) Frequency range: 0 - 3 Hz

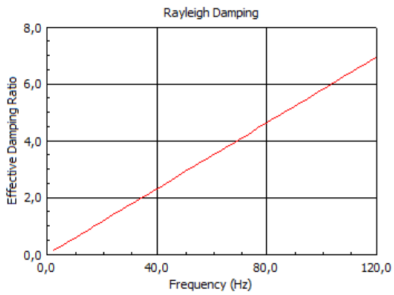

(b) Frequency range: 0 - 120 Hz

Figure 10.7: Rayleigh damping curve

The first vibration mode will behave with a 5% damping ratio. While for what concerns the contributions associated to the deformation of the panel, the first mode has a frequency component of around 100Hz., corresponding to a damping factor close to 6.

10.2.3 Spectral analysis

The aim of this section is to analyze the results in terms of the maximum reaction forces arising in the panel at the base (F_A) and at the connection point with the frame (F_B). The goal is to validate the results obtained by means of the RS method in matlab with the outputs coming from the Finite Element Spectral analysis. A EC8 compatible pseudo acceleration RS, for a soil class A and PGA of 0.261g, is here adopted.
As already presented, in *Straus7* the above mentioned reaction forces are derived from the shear diagram acting along the element (Figure *10.8*). In particular, by denoting with F_A^{ST} and F_B^{ST} the outputs provided by *Straus7*:

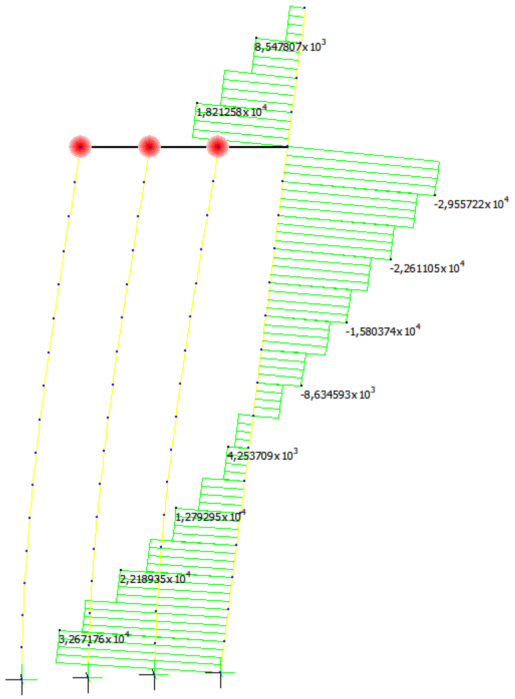

Figure 10.8: Shear forces along the panel

$$\begin{aligned} F_B^{ST} &= T_{CONN}^{+} - T_{CONN}^{-} = 4.8510^4 N \\ F_A^{ST} &= T_{BASE} = -3.2710^4 N \end{aligned} \tag{10.7}$$

On the other hand, for what concenrs the Response Spectrum method implemented in Matlab, the results for the different formulations are reported in Table *10.3*. The absolute values of the forces will be considered.
The results given by the formulation of Moshchen and Der Kiureghian define respectively an upper and lower bound of the solution domain. The value of F_B^{ST} falls exactly inside this range. For what concerns the reaction at the base, the results are in general higher than the one provided by *Straus7*.
It is interesting to see how the change in the natural period of the structure due to the change in the sectional dimensions strongly affects only the

reaction force at the top. On the other hand, the reaction at the base, as expected, does not vary too much.
Summing up, the model in Matlab tend to overestimate the values of the final solutions. Nevertheless, a good correspondnece between the two methods in terms of absolute values is reached.

Formulation	F_A [N]	F_B [N]
TH	3.42E+04	4.75E+04
$TRAP$	3.43E+04	4.77E+04
WN	3.44E+04	4.88E+04
WN_{APPR}	3.54E+04	5E+04
WN_{INF}	3.47E+04	4.92E+04
MO	3.44E+04	4.85E+04
DN	3.47E+04	4.92E+04
WX	3.38E+04	4.68E+04

Table 10.3: Spectral analysis outputs

10.2.4 Linear transient analysis

As already presented at the beginning, the aim of this work is not to find a solution in time of the assigned problem. It is however interesting to verify if the rigid panel assumption adopted in Matlab is able to provide relaible results also in terms of time history analysis.
The solution in *Straus7* is obtained by exploiting the Linear Transient Analysis Solver. The same damping model introduced for the case of the Spectral analysis is adopted.
On the other hand, the solutions in Matlab have been obtained through the use of two procedures:

1. Frequency domain analysis, manually implemented by Prof. Luca Martinelli

2. Direct integration of the equation of motion in time, manually implmented by Prof. Francesco Foti

The results make reference to the ground acceleration time history represented in Figure *10.9* As presented in Chapter 9, the adopted accelerogram has been obtained thanks to the software *SIMQKE*. The signal is compatible to the same Response Spectra used for the Spectral Analysis in the previous section (Soil type A, PGA 0.25g).

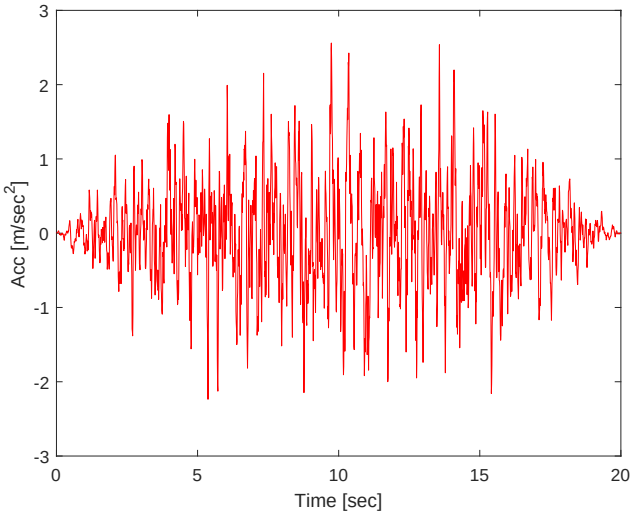

Figure 10.9: Acceleration time history - Soil type:A, PGA:0.25g

In Figure *10.10* and Figure *10.11* the solutions in terms of F_A and F_B are presented, where the results denoted with *TH* are the ones obtained through the time history analysis, *FDA* are the solution of the Frequency domain Analysis, while *Straus* refers to the outputs provided by the software *Straus7*.
It is evident how the solution in *Straus7* matches quite well the two obtained via Matlab. This is possible thanks to the damping model adopted in the FE model, which allows to filters out the higher vibration modes associated to the panel, which are not accounted in the formulation of Matlab.

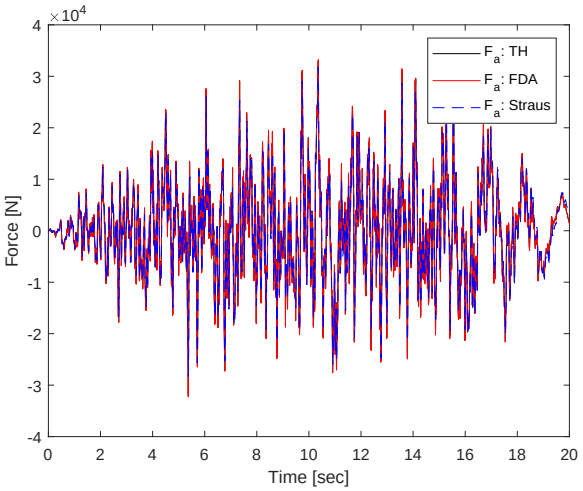

Figure 10.10: Time history solution - F_b

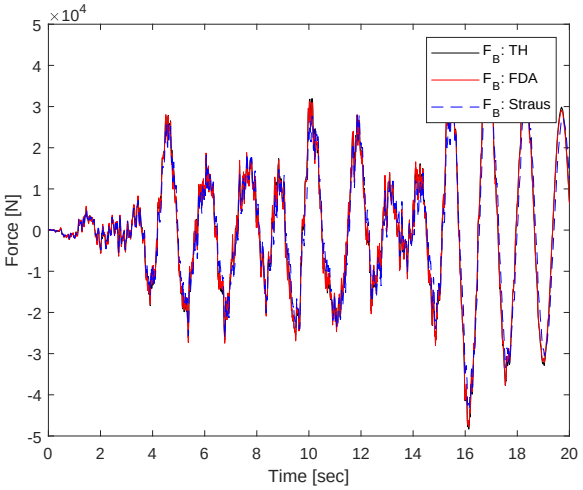

Figure 10.11: Time history solution - F_b

10.2.5 Further cases

Now, the same procedure presented in the previous paragarphs, is here repeated for different values of the natural period of the structure, in such a

way to widen the range of validity of the model. In particular, by changing the section of the columns, and keeping all the other parameters fixed, the following cases have been analysed:

- Section $500 \times 500\ cm^2$
- Section $700 \times 700\ cm^2$
- Section $800 \times 800\ cm^2$

The comparison of the results in terms of natural periods of the dual system is reported in Table 10.4. A very good correspondence of values is garanteed, with the models in *Straus7* which tends to be a little stiffer.
For what concerns the solutions provided by the Spectral analysis, the outputs are reported in Table *10.5*, Table *10.6*, and Figure *3.40 respsctively*. Table *10.5* and *10.6* indicate, for each case, (1) the numerical solution in terms of forces at the connections provided by *Straus7*, (2) the maximum and minimum values of F_A and F_B obtained by means of the different formulations in *Matlab*.

Section	*Straus7*	*Matlab*
500×500	2.082 sec	2.003 sec
600×600	1.401 sec	1.391 sec
700×700	1.031 sec	1.022 sec
800×800	0.789 sec	0.783 sec

Table 10.4: Comparison between the natural periods

Section	*Straus7* [N]	FA_{MIN} [N]	FA_{MAX} [N]
500×500	3.15E+04	3.34E+04 (WX)	3.45E+04 (WN_{APPRX})
600×600	3.27E+04	3.38E+04 (WX)	3.54E+04 (WN_{APPRX})
700×700	3.45E+04	3.48E+04 (WX)	3.66E+04 (WN_{APPRX})
800×800	3.61E+04	3.60E+04 (WX)	3.86E+04 (WN_{APPRX})

Table 10.5: Spectral analysis: Reaction at the base

Section	*Straus7* [N]	FB_{MIN} [N]	FB_{MAX} [N]
500×500	3.51E+04	3.37E+04 (WX)	3.68E+04 (WN_{APPRX})
600×600	4.93E+04	4.68E+04 (WX)	5.0E+04 (WN_{APPRX})
700×700	6.42E+04	6.35E+04 (DN)	6.67E+04 (WN_{APPRX})
800×800	8.96E+04	8.5E+04 (WX)	8.85E+04 (DN)

Table 10.6: Spectral analysis: Reaction at the top

For what concerns the reaction at the base, the RS method provides results which are always higher than the numerical ones. While in the case of F_B, the solutions from *Straus7* are almost perfectly included in the interval of values provided by Matlab.
Finally, the comparison between the results in time are reported in Figure *10.12*, Figure *10.13* and Figure *10.14*.
The solution in time coming from Finite Element Analysis fits quite well the ones manually implemented in Matlab.
In addition to the outputs related to the reaction forces, the plots in Fig 10.14 show the solution in terms of absolute acceleration of the node in correspondnece of the anchorage point between the panel and the connection. Also in this case the correspondence between the different analysis is quite good.

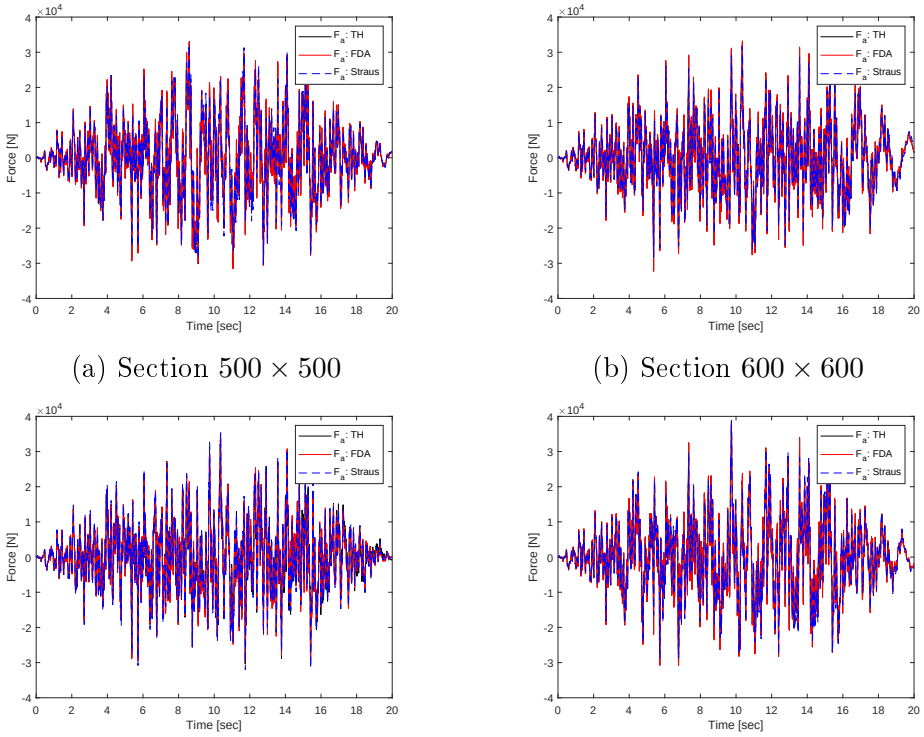

(a) Section 500 × 500

(b) Section 600 × 600

(c) Section 700 × 700

(d) Section 800 × 800

Figure 10.12: Time history outputs: Reaction force at the base

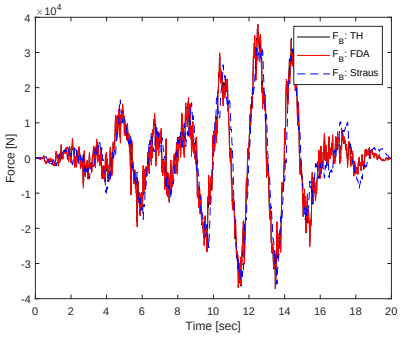

(a) Section 500 × 500

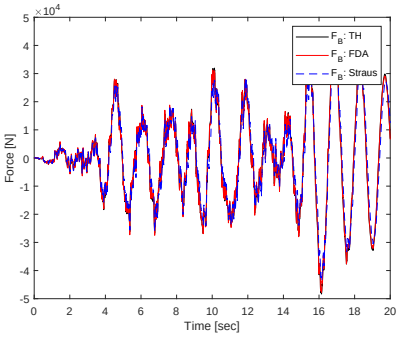

(b) Section 600 × 600

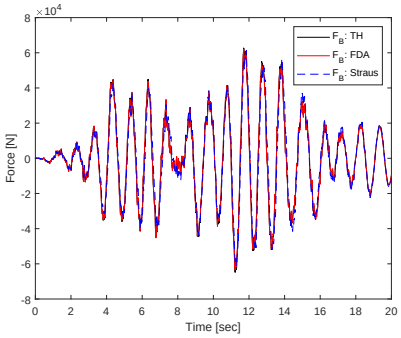

(c) Section 700 × 700

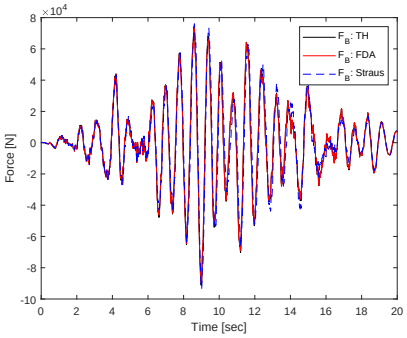

(d) Section 800 × 800

Figure 10.13: Time history outputs: Reaction force at the top

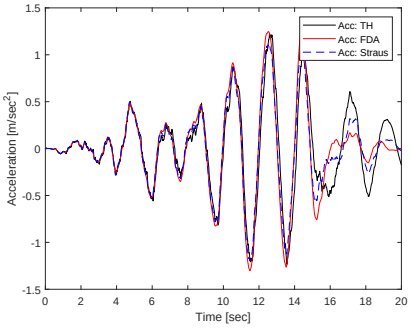

(a) Section 500 × 500

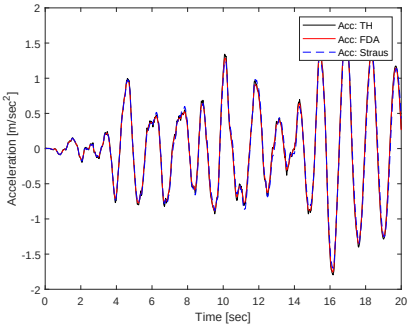

(b) Section 600 × 600

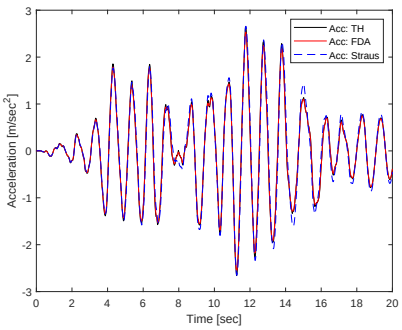

(c) Section 700 × 700

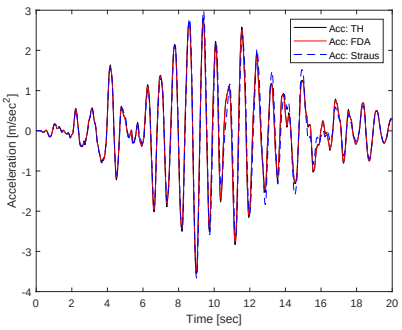

(d) Section 800 × 800

Figure 10.14: Time history outputs: Acceleration at the connection point

In conclusion, a very good correspondence characterize the results obtained through the different formulations. This on one hand confirms goodness of the outputs provided by the RS procedure implemented in Matlab, and on the other hands it validates the models built in *Straus7*, which will be later used for the analysis in the non linear field.

Chapter 11

Post elastic behaviour

As mentioned at the beginning of this work, the behaviour of pre-cast systems is highly non linear, therefore a proper study of the post elastic phase of such structure is fundamental in order to properly characterise their seismic response. The methods based on a linear analyis, both static and dynamic, account for the non linear post-elastic behaviour of the structure in a synthetic way, by means of the concept of behaviour factor q, which allows to reduce the elastic Response Spectrum, or through the parameter Θ, which considers the geometrical non linearities. These methods are not able however to catch the changes in the structural response which arise during the degradation process affecting the building, due especially to the plasticization of the structural elements. This is why, by using such simplified procedures, it is not possible to identify the possible collapse mechanism and the corresponsing distribution of stresses, giving rise to the necessity to rely on a non linear type of analysis.
A non linear dynamic analysis is for sure the one able to provide the most reliable results, due to the fact that seismic response of a structure is always dynamically non linear. This method however is not so widespread, first of all due to the difficulties in the choices of the structural variable to adopt in the post-elastic field, and secnd for its high computational costs.
The right compromise between the semplifications offered by an elastic analysis and the complexities of a dynamic non linear study is represented by the non linear static analysis.
This is a design procedure based on the concept of structural capacity, whose computational costs are much lower than the rigouros time history procedure, which is very oftern limited as a final assesement step. This is exactly what was done in his work, where the outputs coming from the non linear time history analysis are used as reference results.
While, for what the concerns the design phase, this second part of the thesis has the goal to validate the RS method formulation when the structure enters the non linear field.
To do so, the remaining part of the work will be organized in three chapters. The following paragraphs of Chaptr 11 will present the results obtained by means of a non linear time history analysis implemented in *Straus7*.
Chapter 12 will be devoted to the validation of the RS method in the non

linear field. To do so, the results of the non linear static Pushover analysis will be exploited. Finally, a comparison with the existing design rules proposed by the Codes will be presented.
A summary of the results and the final considerations will be presented in Chapter 13.

11.1 Structural schemes

Before entering in the detail of the non linear time history analysis, la seguente sezione presenterà i differenti modelli strutturali che verranno analizzati. Le analisi in campo non lineare sono state condotte adottando 16 diversi modelli strutturali, facendo variare le seguenti caratteristiche del sistema: (1) sezione dei pilastri, (2) numero dei pilastri, (3) altezza dei pilastri, (4) rapporto $\eta = \frac{h_1}{h_2}$. This was done first of all in order to study the influence of the different parameters on the behaviour of the structure, and second of all, in such a way to obtain a wide range of structural periods, which will thus correspond to different Spectral ordinates.
An acronym will be associated to each model, which will be later used for the legend in the results diagrams, where:

- "C" indicates the number of columns
- "h" indicates the height of the columns
- "η" representes the ratio h_1/h_2

Model 1 (C3h8η0.25)

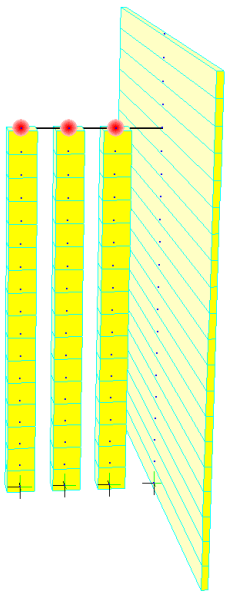

Section: 600×600 mm
n° of columns: 3
Heigth of columns: 8m
η : 0.25
$T_s = 1.41sec$
$f_s = 0.7Hz$

Figure 11.1: Model 1 - structural scheme

Model 2 (C1h8η0.25)

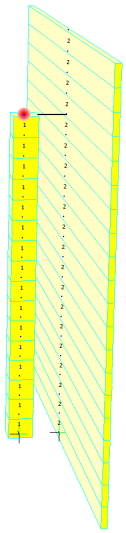

Section: 600×600 mm
n° of columns: 1
Heigth of columns: 8m
η : 0.25
$T_s = 1.51sec$
$f_s = 0.66Hz$

Figure 11.2: Model 2 - structural scheme

Model 3 (C3h8η0.1)

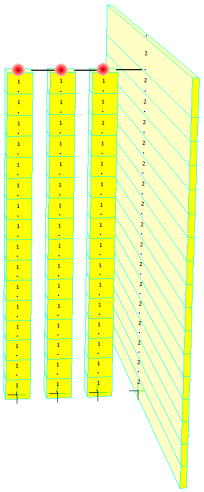

Section: 600×600 mm
n° of columns: 3
Heigth of columns: 8m
η : 0.25
$T_s = 1.38sec$
$f_s = 0.72Hz$

Figure 11.3: Model 3 - structural scheme

Model 4 (C1h8η0.1)

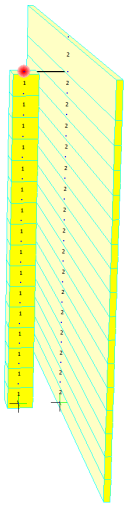

Section: 600×600 mm
n° of columns: 1
Heigth of columns: 8m
η : 0.1
$T_s = 1.47sec$
$f_s = 0.68Hz$

Figure 11.4: Model 4 - structural scheme

Model 5 (C3h10η0.25)

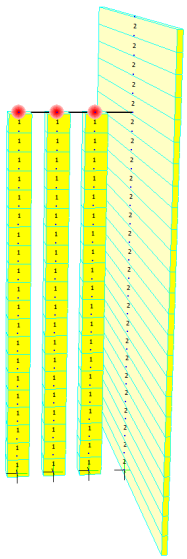

Section: 600×600 mm
n° of columns: 3
Heigth of columns: 10m
η : 0.25
$T_s = 1.98sec$
$f_s = 0.505Hz$

Figure 11.5: Model 5 - structural scheme

Model 6 (C1h10η0.25)

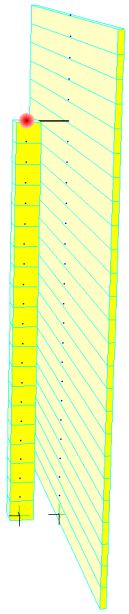

Section: 600×600 mm
n° of columns: 1
Heigth of columns: 10m
η : 0.25
$T_s = 2.15sec$
$f_s = 0.463Hz$

Figure 11.6: Model 6 - structural scheme

Model 7 (C3h10η0.1)

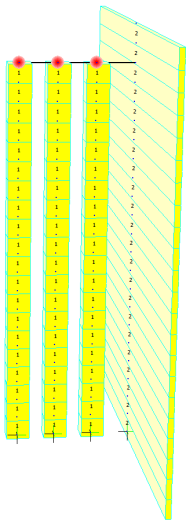

Section: 600×600 mm
n° of columns: 3
Heigth of columns: 10m
η : 0.1
$T_s = 1.95sec$
$f_s = 0.512Hz$

Figure 11.7: Model 7 - structural scheme

Model 8 (C1h10η0.1)

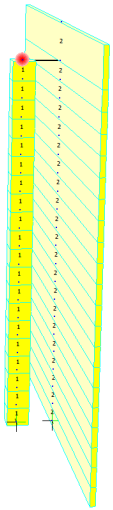

Section: 600×600 mm
n° of columns: 1
Heigth of columns: 10m
η : 0.1
$T_s = 2.08sec$
$f_s = 0.48Hz$

Figure 11.8: Model 8 - structural scheme

Model 9 (C3h8η0.25)

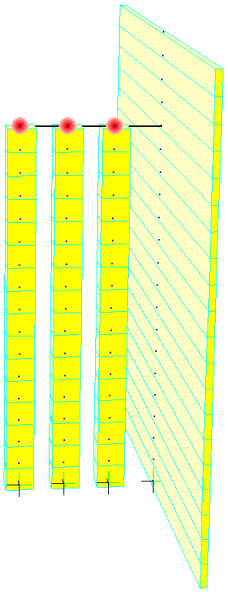

Section: 700×700 mm
n° of columns: 3
Heigth of columns: 8m
η : 0.25
$T_s = 11.03sec$
$f_s = 0.969Hz$

Figure 11.9: Model 9 - structural scheme

Model 10 (C1h8η0.25)

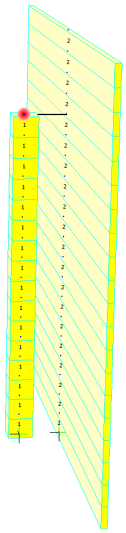

Section: 700×700 mm
n° of columns: 1
Heigth of columns: 8m
η : 0.25
$T_s = 1.11sec$
$f_s = 0.9Hz$

Figure 11.10: Model 10 - structural scheme

Model 11 (C3h8η0.1)

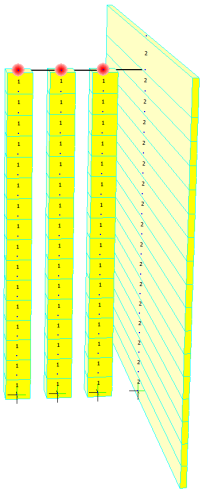

Section: 700×700 mm
n° of columns: 3
Heigth of columns: 8m
η : 0.25
$T_s = 1.02sec$
$f_s = 0.98Hz$

Figure 11.11: Model 11 - structural scheme

Model 12 (C1h8η0.1)

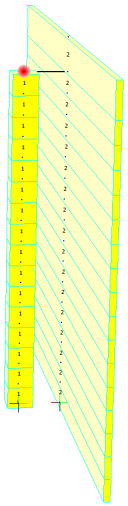

Section: 700×700 mm
n° of columns: 1
Heigth of columns: 8m
η : 0.1
$T_s = 1.08sec$
$f_s = 0.93Hz$

Figure 11.12: Model 12 - structural scheme

Model 13 (C3h10η0.25)

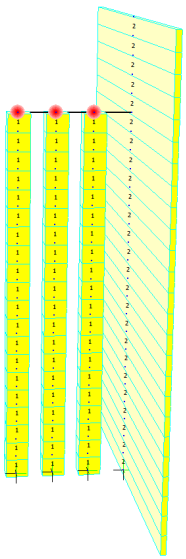

Section: 700×700 mm
n° of columns: 3
Heigth of columns: 10m
η : 0.25
$T_s = 1.45sec$
$f_s = 0.69Hz$

Figure 11.13: Model 13 - structural scheme

Model 14 (C1h10η0.25)

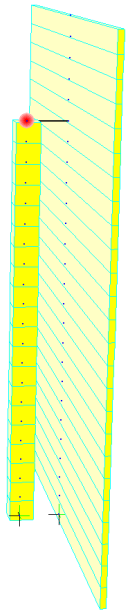

Section: 700×700 mm
n° of columns: 1
Heigth of columns: 10m
η : 0.25
$T_s = 1.59sec$
$f_s = 0.63Hz$

Figure 11.14: Model 14 - structural scheme

Model 15 (C3h10η0.1)

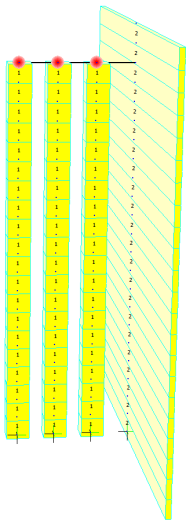

Section: 700×700 mm
n° of columns: 3
Heigth of columns: 10m
η : 0.1
$T_s = 1.43sec$
$f_s = 0.7Hz$

Figure 11.15: Model 15 - structural scheme

Model 16 (C1h10η0.1)

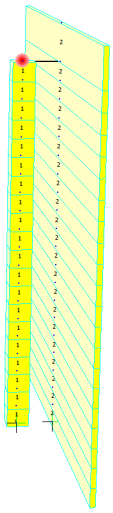

Section: 700×700 mm
n° of columns: 1
Heigth of columns: 10m
η : 0.1
$T_s = 1.51sec$
$f_s = 0.66Hz$

Figure 11.16: Model 16 - structural scheme

11.1.1 Plastic hinge model

In both static and dynamic analysis, the non-linear behavior of the model is reproduced by introducing the concept of plastic hinge. Doing so, the constitutive relationship of the structural elements is represented by the corresponding moment-curvature diagram.
This constitutive law depends on the following characteristics:

- Cross section dimensions
- Reinforcement ratio
- Concrete constitutive model
- Axial force in the element

Section 600×600 **mm**

The evaluation of the Moment-Curvature diagram was performed by using the sofware *MathCad 15*. The characteristics of the section are reported in Figure *11.17*. For what concerns the concrete, a type 40/50 was used, adopting the following constituve laws:

- Confined concrete: Mander law
- Unconfined concrete: Modified Mander law

The tensile strength of the concrete was here taken into account.
For what concerns the reinforcments, a B450C steel class was chosen. A total number of 16Φ20 are distributed along the section, in such a way to

obtain a reinforcement ratio $\rho = 1\%$. The concrete cover is equal to 30mm, and Φ10 transversal reinforcements are used. Finally, by considering a distributed load coming from the roof system of around 350 kg/m2, an axial force of 100 Tonn was considered acting in the columns.
The cross section model implemented in *MathCad15* is reported in Figure *3.40*.

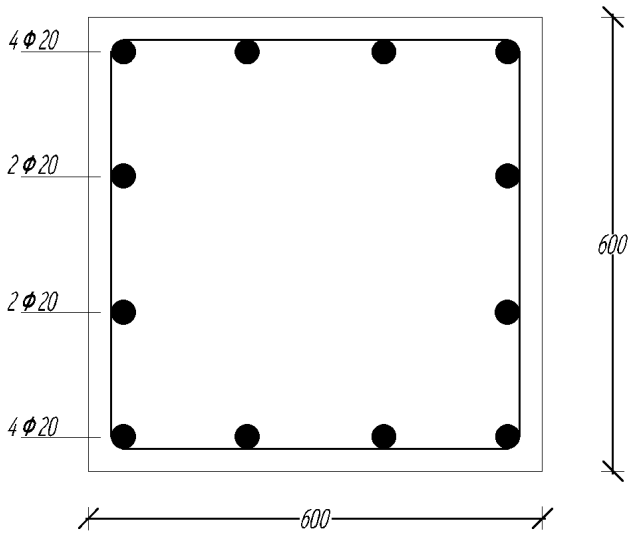

Figure 11.17: 600 × 600 mm column cross section

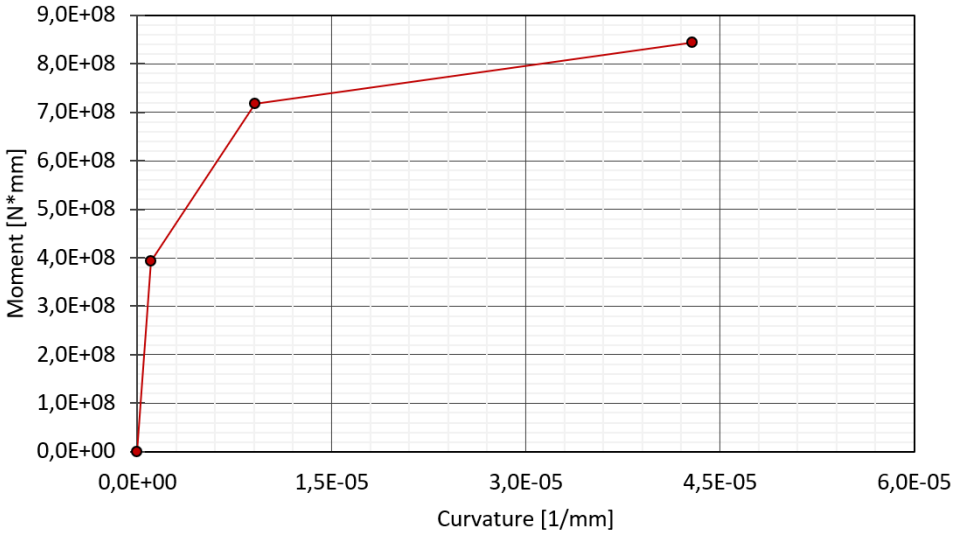

Figure 11.18: Section 600 × 600: trilinear M-χ diagram

The tri-linearized Moment-Curvature diagram provided by the software is reported in Figure *11.18*.
The same procedure has been followed for the 700 × 700 mm case. The characteristic of the section are reported in Figure *11.19*. The correspondent M-χ diagram is reported in Figure *11.20*.

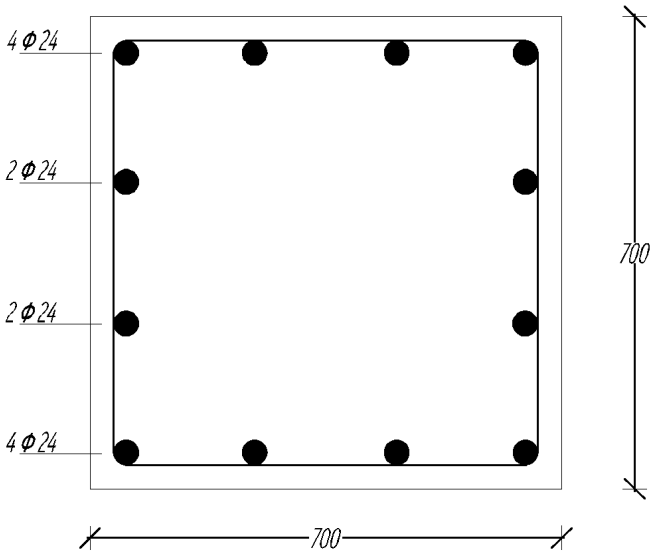

Figure 11.19: 700 × 700 mm column cross section

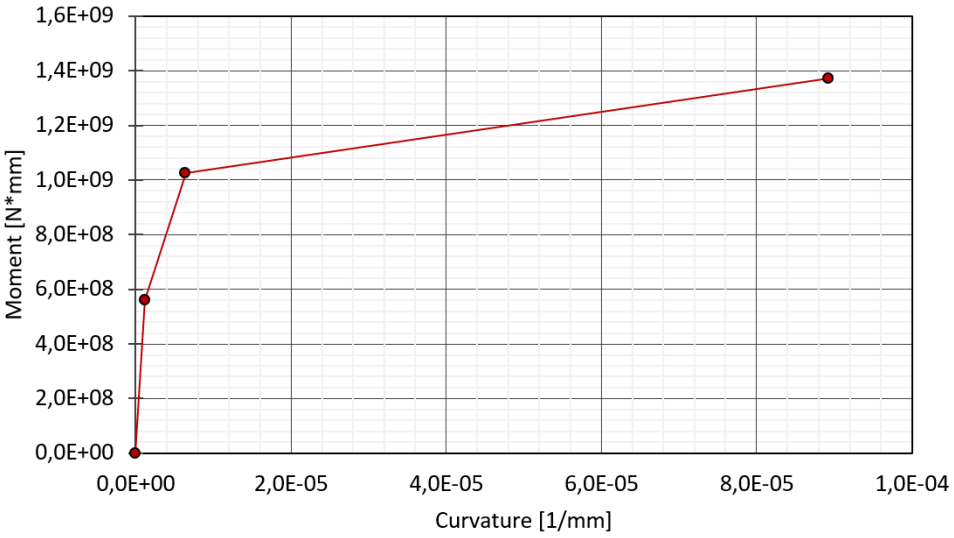

Figure 11.20: Section 700 × 700: trilinear M-χ diagram

11.2 Non linear time history anaysis analysis

The non linear dynamic analysis consists in the evaluation of the seismic response by means of the direct integration of the equation of motion, adopting a non linear model of the structure, where the inputs are acceleretion time histories, defined as in 3.2.3.6 of NTC. The goal is to evaluate the dynamic behaviour of the structure in the non linear field, allowing for the comparison between required uctility and available ductility at every time instant, checking the integrity of the structural elements against non ductile mechanisms.
Unlike static analysis, this method does not require the prior determination

of the global seismic demand; the latter is in fact evaluated during the analysis of the structural response. Compared to linear dynamic analysis, which provides only an estimate of the peak response using SRSS and CQC, the non-linear dynamic analysis allows the exact evaluation of the maximum seismic response, providing extremely accurate results; this accuracy however must be paid for with the need to define the non-linear behavior of the structure in a more complete way, also including the description of its cyclic behavior.
To this purpose, the dynamic non-linear analyses are performed with a Takeda model (Takeda et al. 1970 1 REF) for the columns. While for what concerns the damping model, as in the linear case, a Rayleigh formulation is used. The difference now is related to the damping ratios adopted, which in this case are equal to 2% (Figure *11.21*), in order to account for the dissipation of the phenomena associated to the cracking of the concrete. For what concerns the definition of the seismic input, la maggior parte dei codici di progettazione sismica , incluso l'EC8, specificano che devono essere utilizzate almeno 3 registrazioni. Aggiungono poi che se vengono utilizzate meno di sette registrazioni, la massima strutturale deve essere utilizzato come base per la progettazione, invece se si utilizza sette o più di sette registrazioni, è possibile valutare effetti medi e non massimi sulla risposta strutturale. The results presented in the next section represesnt the average over seven accelerograms.

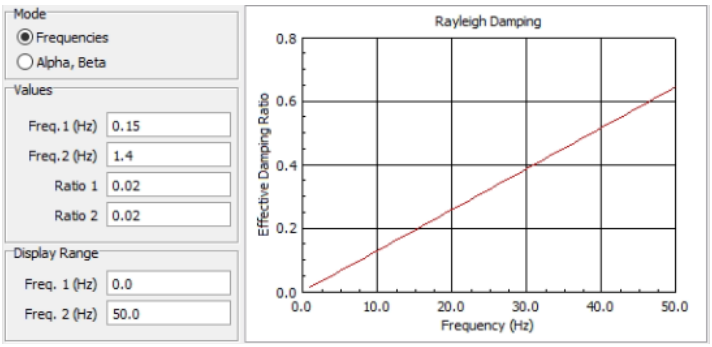

Figure 11.21: Non linear dynamic analysis: Damping model

11.2.1 Presentation of the results

The results obtined by performing the non linear dynamic analysis by means of *Straus7* are here reported. For the 16 structural models, the outputs extracted are the following:

- Reaction force F_A at the base
- Reaction force F_B at the top connection
- Absolute acceleration at the connection
- Column top displacement
- Column base shear

In order to lighten the treatment of the problem, the solution in terms of time history results have been proposed for one model only (Model 1). Then, for each case, a comparison between the non linear time history analysis results in terms of maximum values, and the elastic ones provided by the Response Spectrum method is reported.

Non Linear Time History Analysis - Time history solutions

In this section, the time history solutions for the output of interest are presented. The results refer to Model 1 (C3h8η0.25), which was subjected to a RS compatible accelerogram (EC8, Soil type A), with a PGA equal to 0,3g.
A comparison between the elastic solutions (Linear Time History Analysis - LTHA) and the non linear ones (Non Linear Time History Analysis - NLTHA) is proposed.

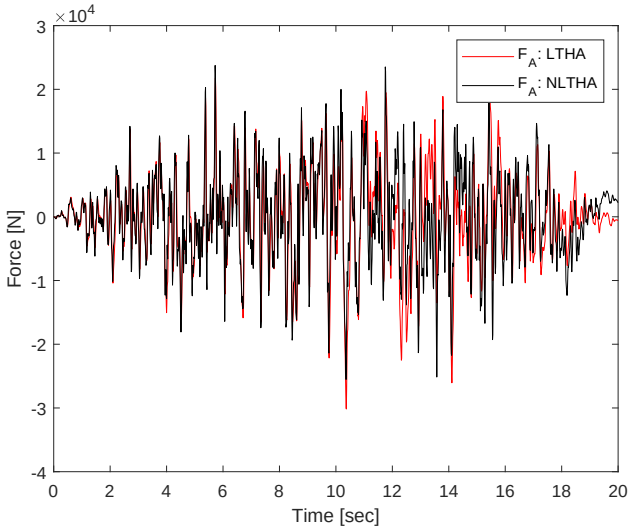

Figure 11.22: Reaction force F_A

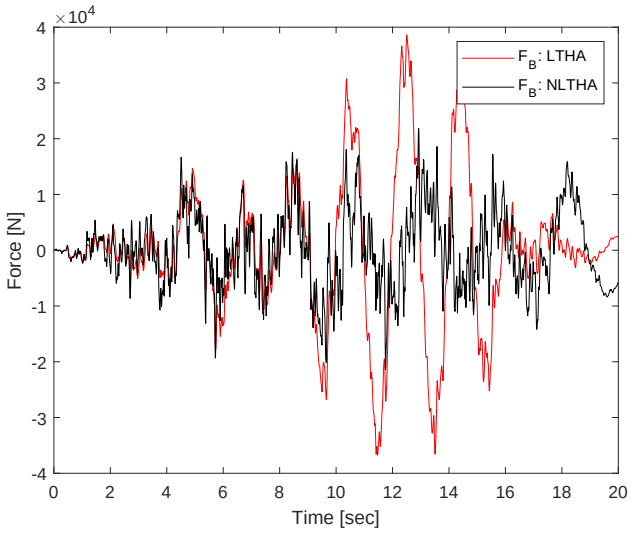

Figure 11.23: Reaction force F_B

Starting from the elastic solutions, the results confirm the direct proportionality between the time history outputs in terms of F_B, acceleration, shear and displacements, with the respective graphs having practically the same shape. The only exception is represented by F_A, which presents a greater dependence on the ground ground acceleration.
Even if less rigorously, this proportionality remains valid also for the non linear solutions.
For what concerns the comparison between the two analysis, the solutions are almost coincident during the first instant of the seismic event. The reaching of the yielding point causes a modification of the natural period of the structure. This is well represented in the graphs, where the period between each peak tends to elongate as time passes.

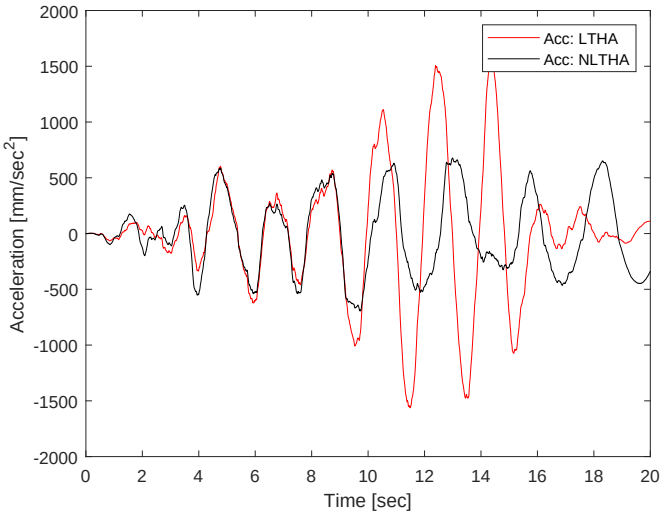

Figure 11.24: Absolute acceleration

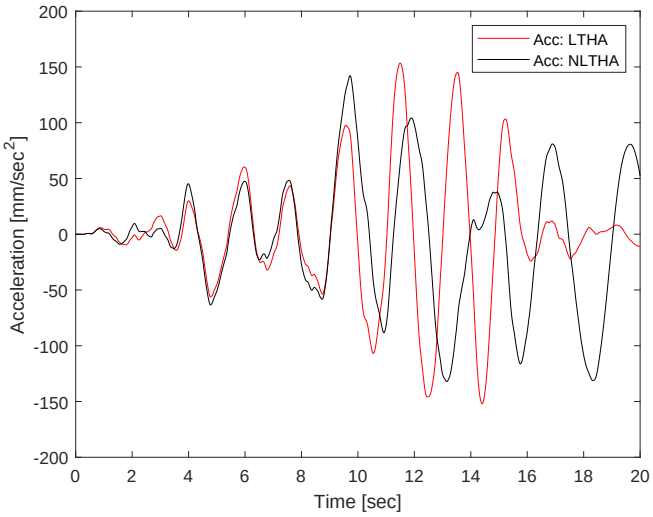

Figure 11.25: Column top displacement

Finally, for what concerns the differences in terms of maximum values, both F_B, the acceleration and the shear force at the column base are strongly influenced by the stiffness reduction after yielding. This on the other hand does not involve the reaction F_A and the displacements. This is due to the fact that the reaction F_A is mainly depending on the ground acceleration, which is not influenced by the stiffness reduction of the structure after yielding. While, for what concerns the displacements, lower stiffness means lower forces, but obviously it means also more flexibility, and the two effects tend to compensate.

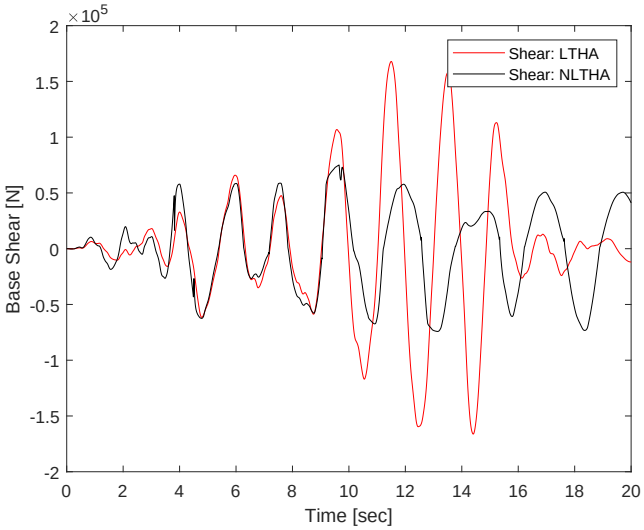

Figure 11.26: Column base shear

Non Linear Time History Analysis - Maximum values

This last section is devoted to the presentation of the results obtained by means of the parametric anaysis conducted by considering the 16 different models. For each output the solutions are oranized into two diagrams, the first one for the case of the 600x600 column cross section, and the secondo one for the 700× case.

Reaction force at the base F_A

If compared with the elastic results, the reaction force at the base is the output less affected by the plasticization phenomena influencing the models. This is due to the fact that the force F_A is mainly depending on the ground acceleration, which is not influenced by the stiffness decrease of the system. The stiffness reduction has effects on the structural acceleration only, but since here it's contribution is low, the outputs coming from the two analysis are quite similar, even for high PGA.
For what concerns the influence of the characteristics of the models, higher columns means higher shear reactions at the base. On the other hand, it's interesting to see how the solution it's not affected by the type of cross section, providing quite the same for both 600*600 and 700*700. The same holds for the height of the panel in terms of η.

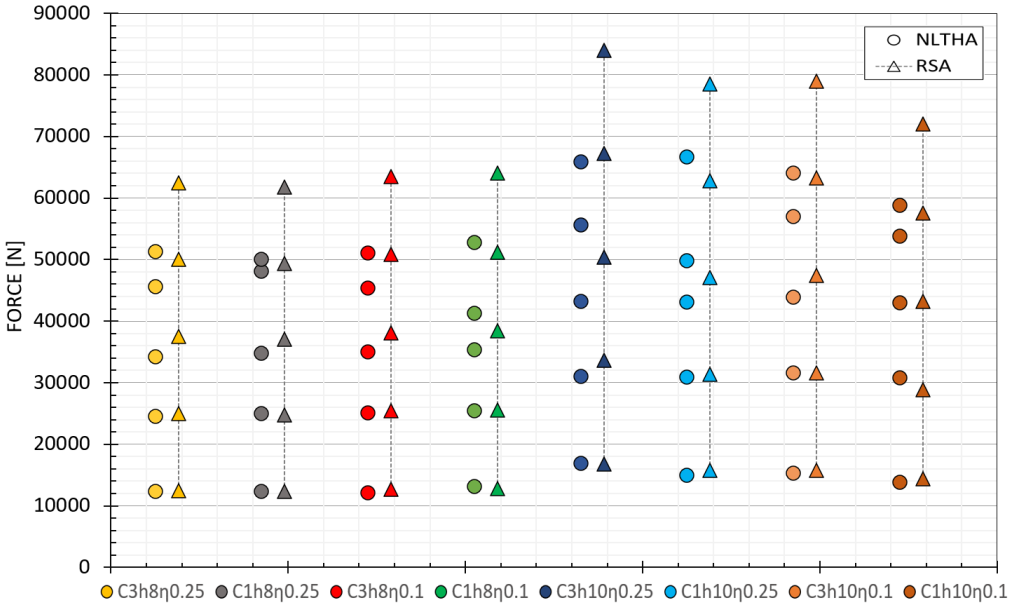

Figure 11.27: Section 600 × 600: Reaction force F_A

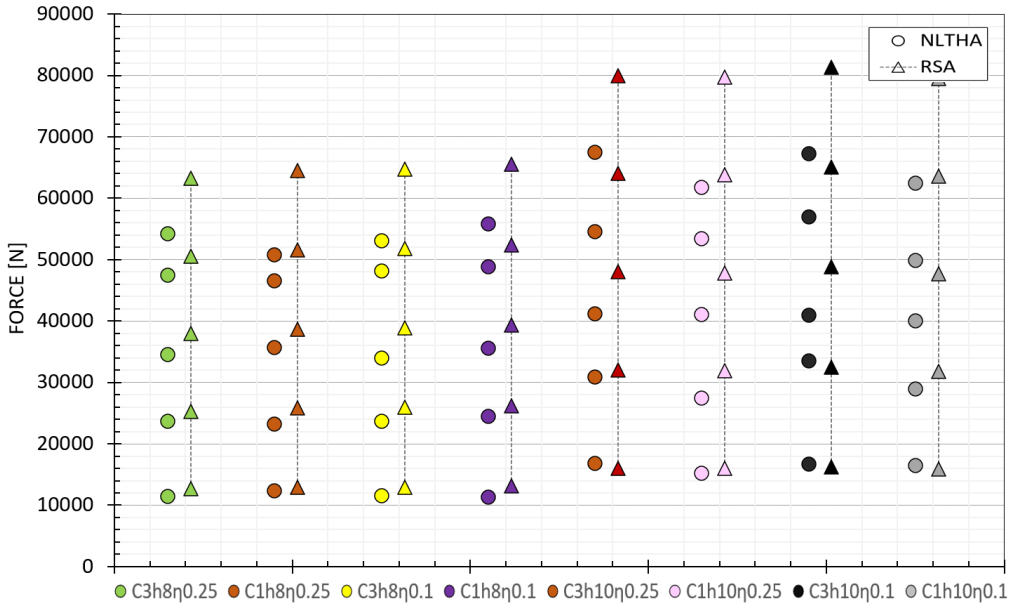

Figure 11.28: Section 700 × 700: F_A

Reaction force F_B

For what concerns the reaction force at the upper connection, the opposite reasoning wrt to what was said before for FA must me made.
In this case the main dependency of the force is related to the absolute acceleration of the structure, which is in turn strongly influenced by the stiffness decrease after yielding. This explains why the NLTHA provides far lower results for high PGAs

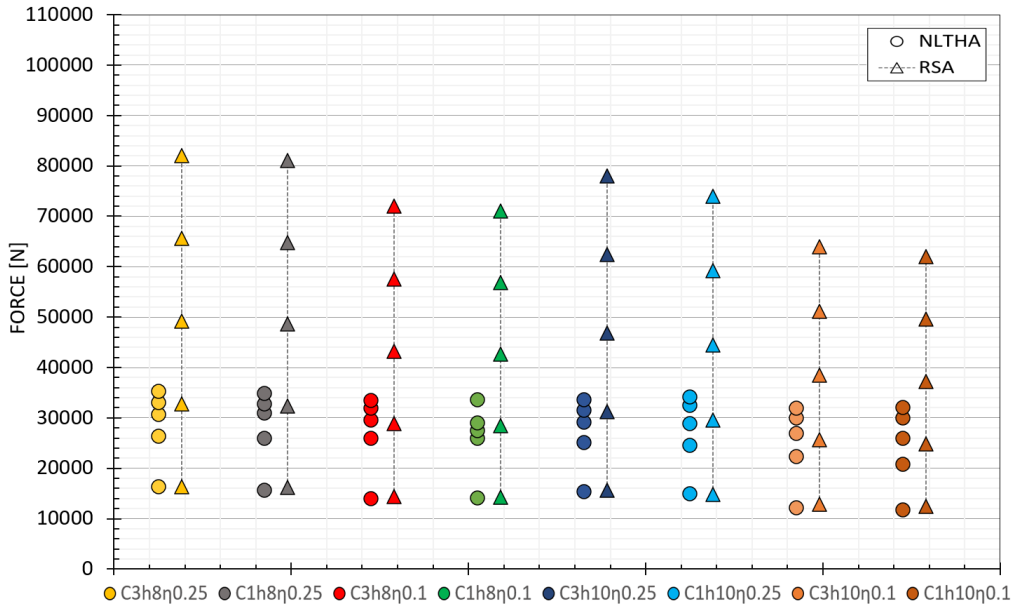

Figure 11.29: Section 600 × 600: Reaction force F_B

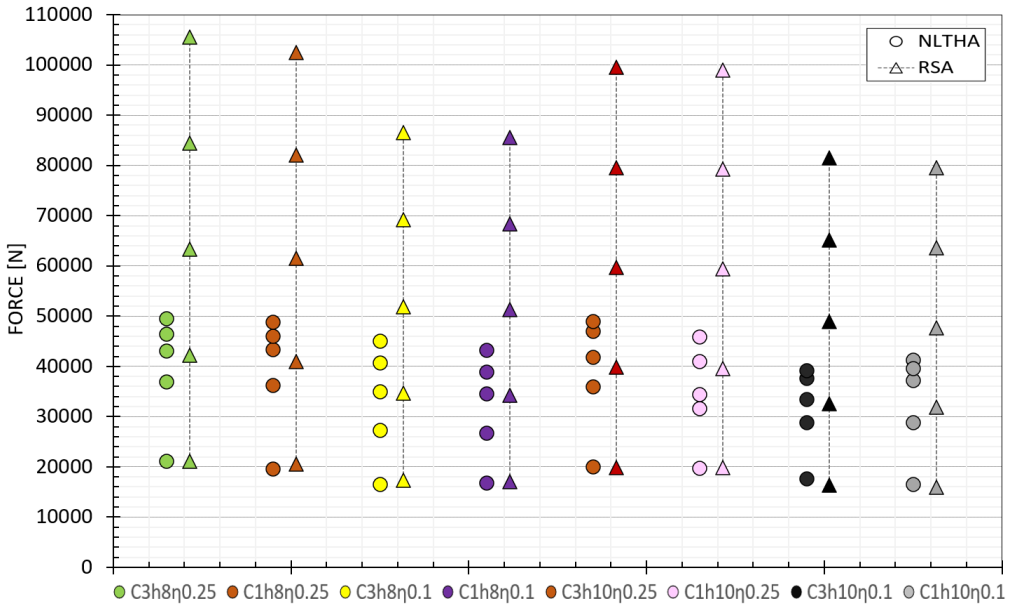

Figure 11.30: Section 700 × 700: Reaction force F_B

It's interesting to notice how F_B is the parameter with the strongest dependency on the value of η. The higher results obtained with ETA=0.25 are justified by the fact that, as shown in *(5.15)*, the higher η and the higher α_B, and consequently the higher the mass contributing to F_B.

Column absolute acceleration

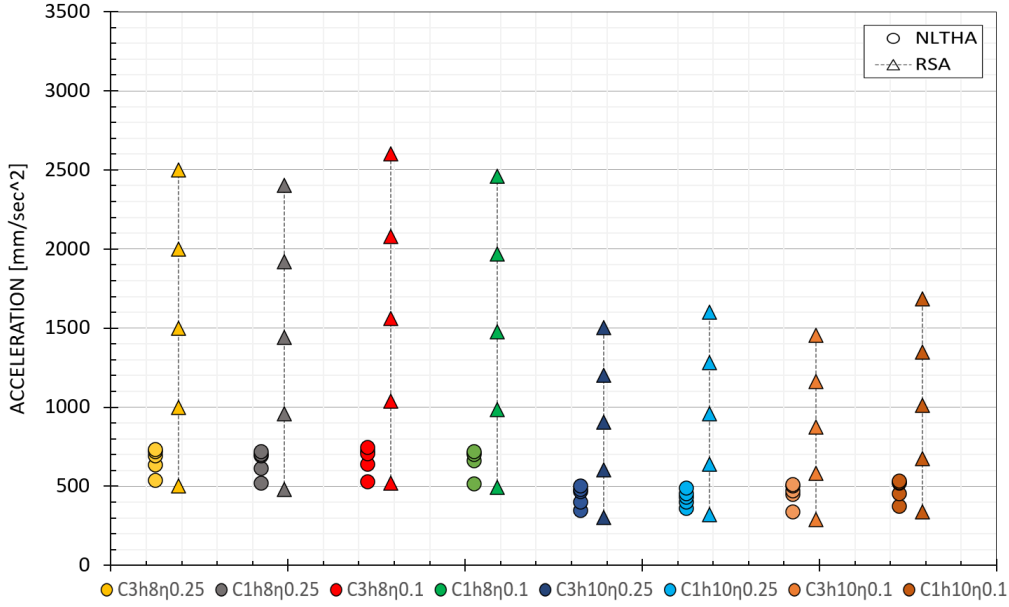

Figure 11.31: Section 600 × 600: Absolute acceleration

Unlike the previously presented reaction forces, the structural acceleration depends on one parameter only, i.e., the stiffness of the model. As it can be observed, the higher value of $\ddot{u}(t)$ is obtained for Model 11 (C3h8η0.1), having the lowest natural period. On the other hand, the lower value of acceleration is provided by Model 7 ((C3h8η0.1)), with the lowest period. The correspondence with the elastic solutions is assured only for the first value of the PGA (0.1g). The maximum acceleration experienced in the plastic field is not higher than the 50% of such value. Then plasticization phenomena does not allow the acceleration to go any further.

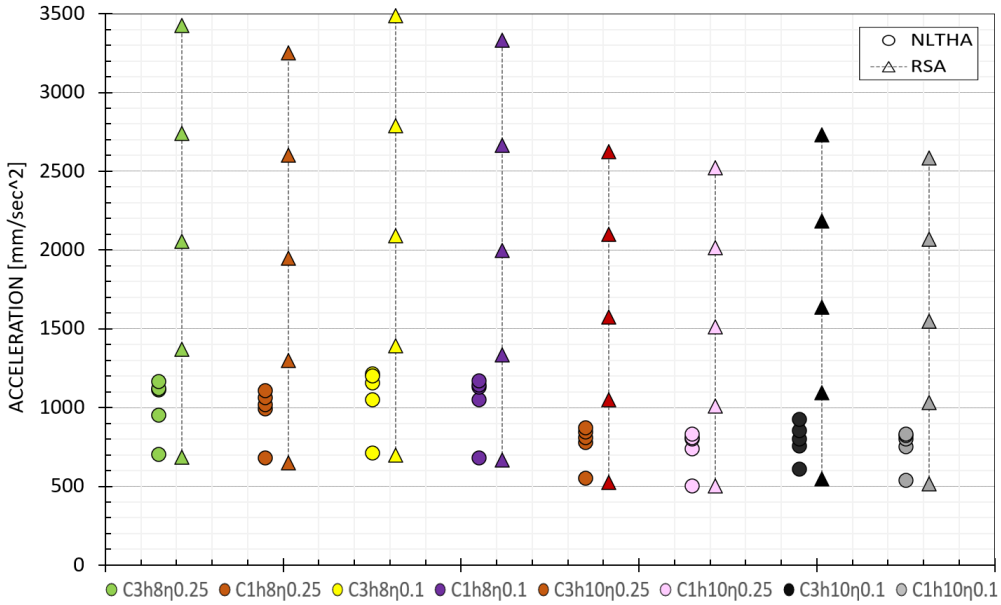

Figure 11.32: Section 700 × 700: Absolute acceleration

Column base shear

What was said before in the case of the acceleration remains valid for this case too. This is due to the fact that the relation between shear at the base and acceleration is linear in the elastic field. The two parameters are linked together by the mass of the system, in this case, the mass of the column. To this purpose, it was interesting to study the results in terms of the mass obtained as the ratios between shear V_C and acceleration $\ddot{u}_C$ of the column, to understand the influence of the panel on the model. It turned out that trend of the results can be described, in approximated way, by the following relation:

$$m_? = \frac{V_C}{\ddot{u}_C} = m_{top} + \frac{1}{n}(\alpha_B \cdot m_p) \tag{11.1}$$

being m_{top} the mass the mass due to the weight of the roof supported by each column, m_p the mass of the panel, n the number of columns and α_B the mass coefficient defined as in *(5.15)*. This relation maintains a certain validity also when the structure enters the elasto-plastic behavior, meaning that these result has a double significance:

1. they confirm the validity of the mass coefficients formulation introduced in (*5.15*) also in the non linear field

2. it gives a fast indications on how to account for the mass of the panel when modeling the adjacent columns

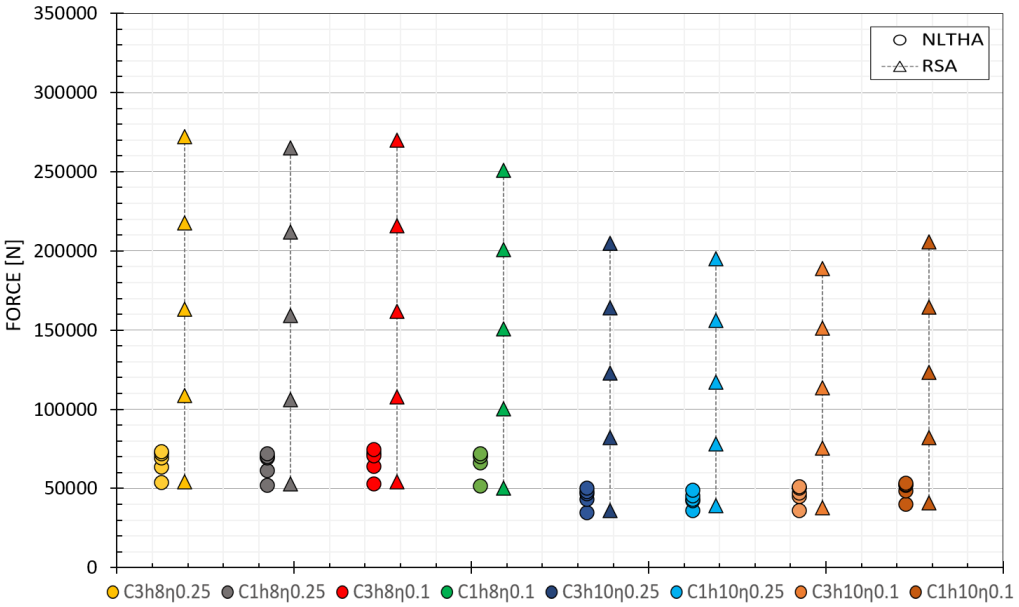

Figure 11.33: Section 600 × 600: Column base shear

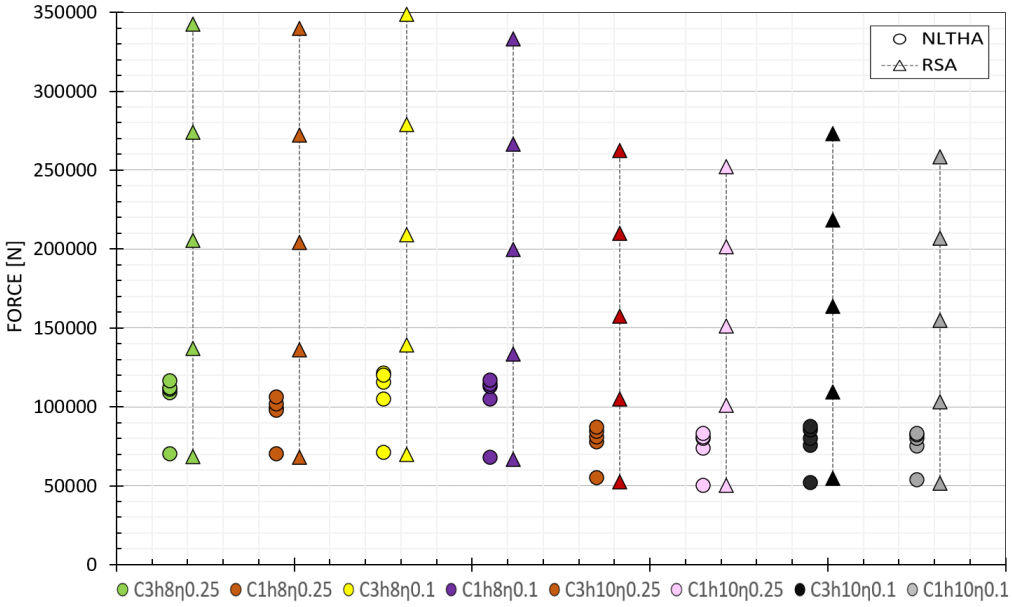

Figure 11.34: Section 700 × 700: Column base shear

Column top displacement

Finally, concerning the outputs in terms of displacements, as it can be seen form the graphs, it is not possible to highlight a clear dependence of the solutions on the characteristics of each model. The only parameter which has a clear influenece on the results is the cross section dimensions, with the 700 × 700 columns providing lower values of displacements. For what concerns the comparison between the linear and non linear solutions, the two analysis tends to provide quite close results until a 0.3g PGA. After plasticization occurs, the NLTHA solutions tend to be smaller.

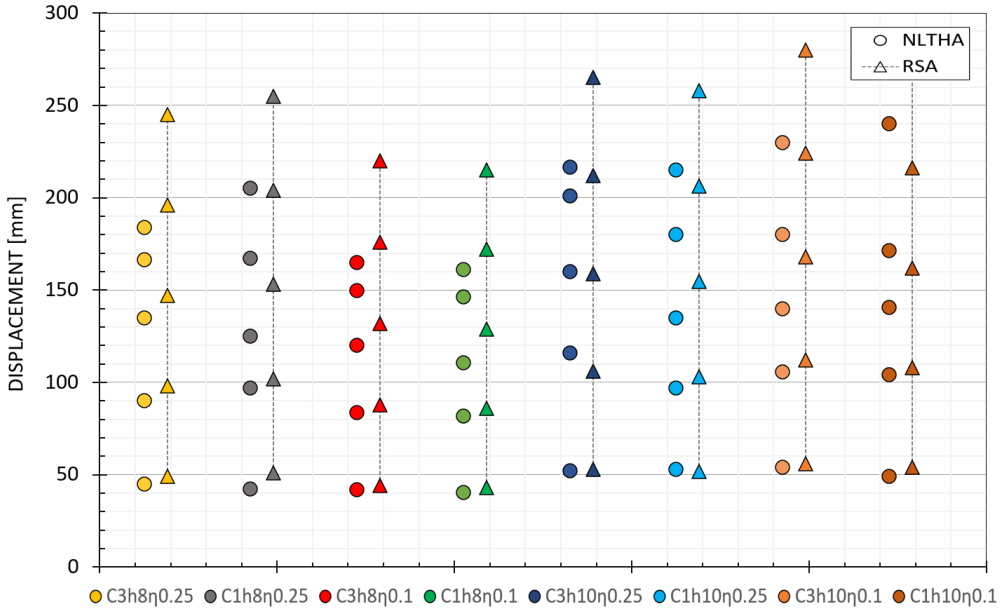

Figure 11.35: Section 600600: Column top displacement

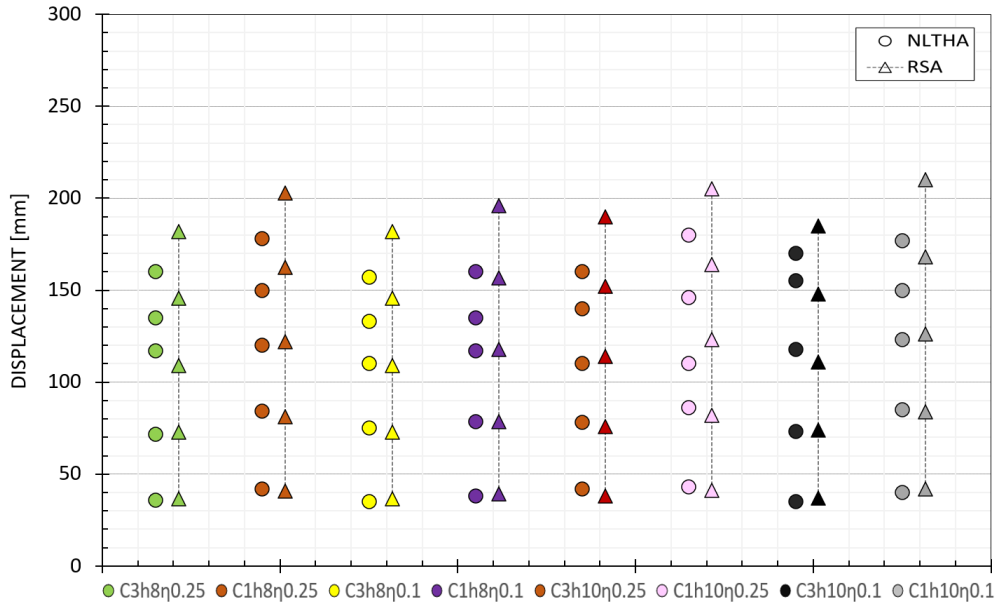

Figure 11.36: Section 700 × 700: Column top displacement

Chapter 12

Design proposal

The aim of this final Chapter is to verify the validity of the Response Spectrum method presented in Chapter 6 also when the structural behaviour is non linear. The elastic analysis provided very good results, the goal now is to see what happens when plasticiaztion occurs. The implementation of the RS spectrum will require however the knowledge of the real performance of the structure under the seismic event. These information are obtained by means of quite complex preliminary analysis, whose implementation is not so immediate. This is why the first part of the Chapter will be devoted to present the main steps to be followed. A brief presentation of the design rules specified by EC8 will be treated in the final section. The comparison between with the results obtained through the implemented Response Spectrum Method will be provided.

12.1 Performance Based Response Spectrum Method (PBRSM)

The name adopted for the procedure is related to the fact that, as presented before, the implementation of the method relies on the preliminary evaluation of the performance of the structure. This requires quite complex formulations the practitioner engineer is not always familiar with. This is why, due to its intrinsic complexity, this method can be used as a final assessment stage, in place of the more demanding and time consuming non linear time history analysis.

12.1.1 Complete Quadrature rule revision

By focusing on the reaction force at the top connection, the peak values of the response are evaluated through the following combination rule:

$$E[max|F_B(t)|] = m_p\Big[\alpha_B^2\ddot{u}_{max}^2 + \beta_B^2 PGA^2 + 2\alpha_B\beta_B\rho_{ig}\ddot{u}_{max}PGA\Big]^{\frac{1}{2}} \quad (12.1)$$

Where $\ddot{u}_{max}$ is the maximum absolute acceleration of the structure, α_B and β_B are the mass coefficients, PGA represents the peak ground acceleration,

and ρ_{ig} is the correlation coefficient. Now, the question is: "How to evaluate the acceleration of the structure when plasticization phenomena occur?" One way is the one associated to the definition of the behavior factor "q", as presented in the building codes. This is for sure the fastest way, however this procedure defines the capacity of the structure in a very approximate way, without accounting for the real features of the model.
Now, even if the performance acceleration could have been obtained by less demanding procedure, the validation of the method will be carried out by taking advantages of the results provided by the NLTHA of Straus, adopting the most rigorous approach possibile. There is another parameter in (*12.1*) worth mentioning however: the correlation coefficient ρ_{ig} Yes because ρ_{ig} depends on the natural period and on the damping ratio of the system These two parameters will not coincide however with the ones adopted in the elastic case, but they must be computed in accordance to the real performance of the structure in the plastic regime. To this purpose, a non linear static analysis has been implemented

12.1.2 Non linear static analysis

Demand, capacity and performance are the three guiding words of nonlinear analysis as a whole: the demand is a measure of the earth's seismic motion or its effects on structure. Capacity, on the other hand, is the ability of the structure and of all its structural elements to resist to the seismic question. It is therefore represented with a curve that defines the global behavior of the building, the so called *Pushover curve* (Figure *12.1*). Finally, performance represents the extent to which capacity absorbs demand, therefore it indicates the real expected performance of the structure and is obtained from the intersection of the curve of capacity (pushover curve), with the demand curve (response spectrum).

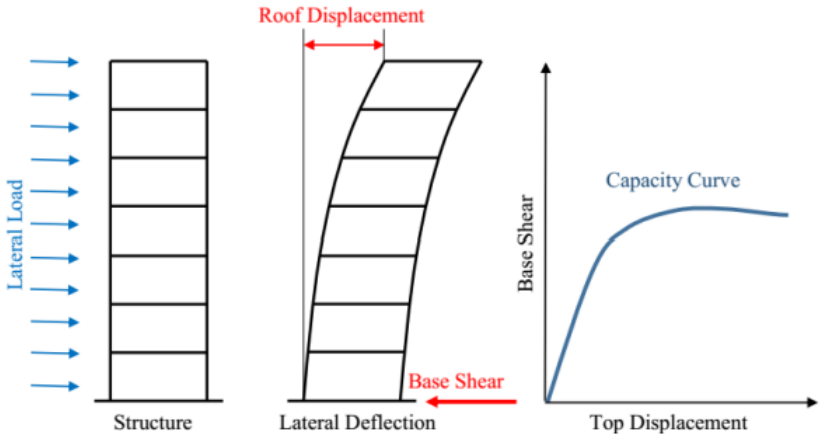

Figure 12.1: Pushover analysis scheme

At the end, this intersection point, known as the performance point PP, is checked with respect to the point that represents the design limit state. The facility must have the ability to withstand simic demand in order for performance to be compatible with project objectives. The pushover analysis involves gradually applying horizontal displacements to the structure. These displacements are scaled in a progressive way so as to make the shear reaction at the base of the pillars grow monotonously, until the collapse is reached.

12.1.3 Pushover analysis implementation

The evaluation of the capacity of the model could be obtained by implementing the Pushover analysis in Straus7. This would have been the most rigorous way. In order to lighten the computational costs however, a different approach was followed, and the Pushover analysis was performed with the use of MathCad7.
Thanks to the lines of code provided by Prof dal Lago, by specifying the characteristics of each model, the software is able to provide the capacity curve for each case. The advantage of such approach are related to the fact that it does not require a FE modeling of the structure.
In the following lines, the main steps behind the definition of the capacity curve will be presented for one of the analysed structural models (Model 1). The monotonic capacity curve is rapresented by 3 linear branches made by 2 points, aside from the origin: the yelding and the cracking point. The post-yelding branch is condidered constant. The load associated to cracking (P_{cr}) is obtained by imposing the decompression limit of the concrete cross-section, assuming the section, due to previous events was already cracked (as in *(12.2)*. The axial load (N) is required for this stage, which is determined by multiplying the distributed mass (wich includes/contain the proper portion of cladding pannel mass)by the size of the single column. The cracking displacement is obtained by taking innto consideration the elastic deformation of the plain-cross section, as in *3.40*

$$P_{cr} = \frac{Nh}{6H} \tag{12.2}$$

$$d_{cr} = P_{cr} \cdot \frac{H^3}{3E_{cm}I_{plain}} \tag{12.3}$$

where h is the section depth, H is the clear span column, E_{cm} is the mean Young modulus of concrete and I_{plain} is the gross second moment of the area of the idealised cross-section. The yelding load P_y is obtained by imposing the rotation and traslation equilibria to the cross-section under imposed axial load N and yelding strain ε_y of the extreme bar layer (*12.4*). The yelding displacement d_y is obtained by numerically solving the differential equation of the inelastic line, integrating the curvature distribution over the beam twice.

$$P_y = M_y(N; \varepsilon_y)/H \tag{12.4}$$

Now that all the ingredients are available, the capacity curve can be drawn. The process will be subdivided into three phases:

1. Phase 1: $d < d_{cr}$
2. Phase 2: $d_{cr} < d < d_y$
3. Phase 3: $d > d_y$

The P-d law adopted for each phase is:

$$P(d) = \begin{cases} P_{cr}\frac{d}{d_{cr}} & \text{if } d < d_{cr} \\ P_{cr} + (d - d_{cr})\frac{P_y - P_{cr}}{d_y - d_{cr}} & \text{se } d_{cr} < d < d_y \\ P_y + (d - d_y)\frac{P_u - P_y}{d_u - d_y} & \text{se } d > d_y \end{cases} \tag{12.5}$$

The resulting capacity curve is represented in Figure *12.2*

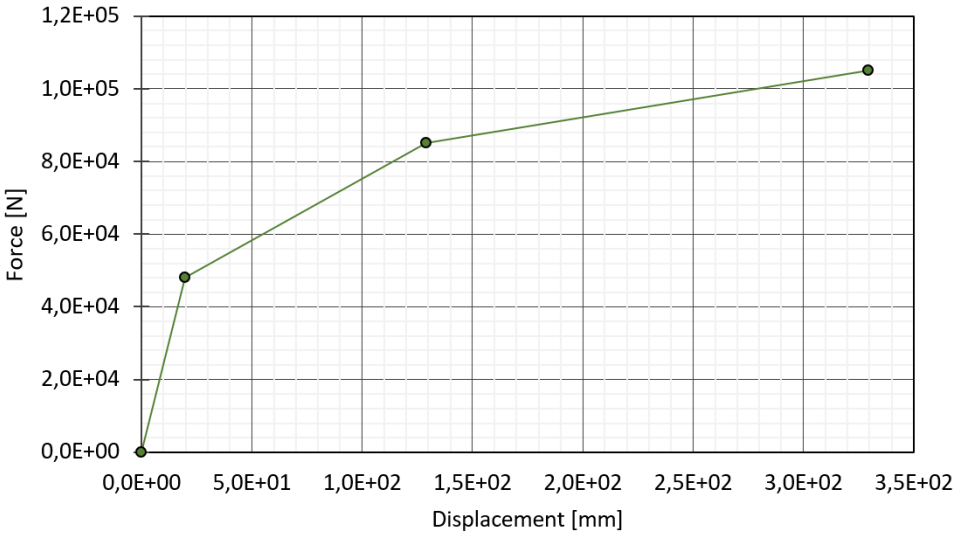

Figure 12.2: Load-Displacement curve: 1st order contributions

12.1.4 Contribution of the second order effects

Now, the capacity curve in Figure *12.2* has been obtained without accounting for the geometrical non linearities of the model. There are in particular two types of contributions which affect these kind of structural schemes: (1) the 2nd order effects associated to the frame, (2) the second order effects generated due to the presence of the claddings. A schematic representation of the problem is reported in Figure *12.3*

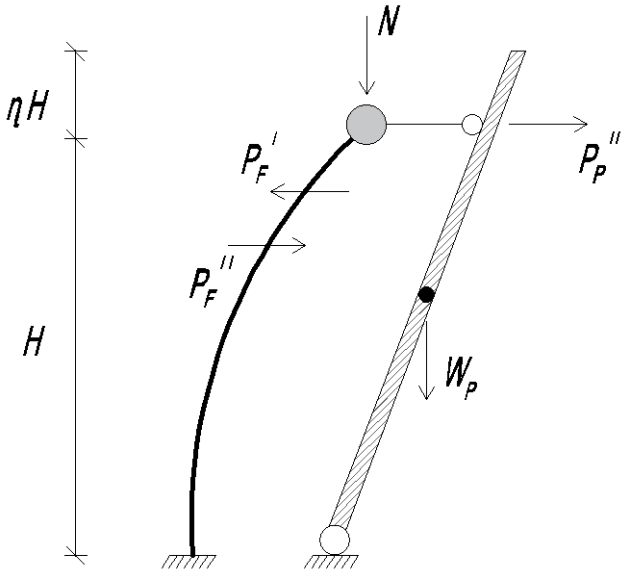

Figure 12.3: Dual system: Second order effects

Due to these 2nd order contributions, the final value of the shear force at the column base is equal to:

$$P(d) = P_F^I + P_F^{II} + P_P^{II} \tag{12.6}$$

where P_F^I is the first order shear reaction defined as in (*12.5*) , while P_F^{II} and P_P^{II} are the second order contributions associated to the frame and the panel.
For what concerns P_F^{II}, being N the axial load acting in the column, the buckling force generated inside the element is:

$$P_F^{II} = N\frac{d}{H} \tag{12.7}$$

The new curve obtained by considering the presence of P_F^{II} is reported in Figure *12.4*

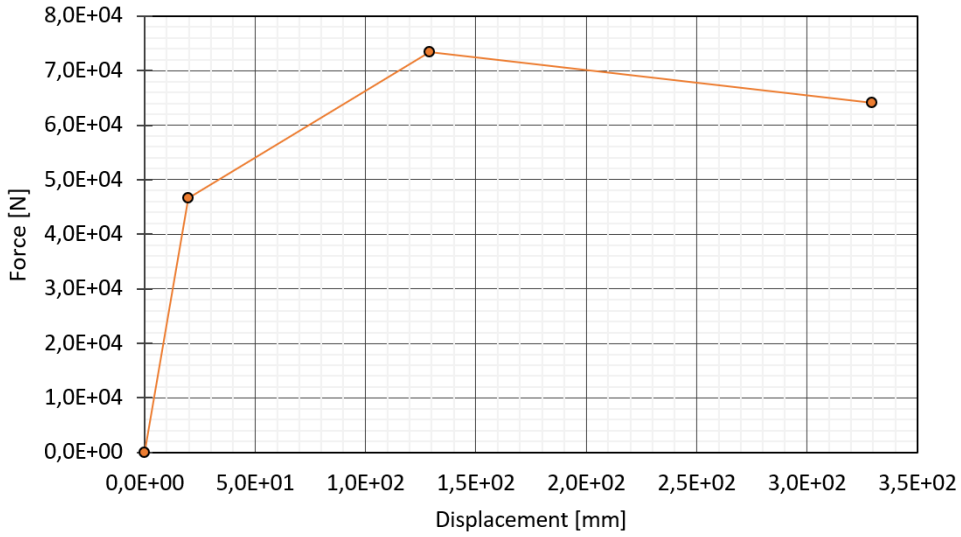

Figure 12.4: Load-Displacement curve with frame 2nd order effects

A further 2nd order contribution is generated by the cinematic of the cladding.
In particular, by focusing on the panel only, the rigid rotation of the element produces a bending action in A as the product of W_P times its level arm δ. Such moment must be equilibrated by the contribution of the reaction force at the connection as:

$$W_p \delta = P_P^{II} H \tag{12.8}$$

being δ the horizonthal displacement of the panel center of mass, which is obtained starting from the displacement d of the frame as:

$$\delta = d\frac{1+\eta}{2} \tag{12.9}$$

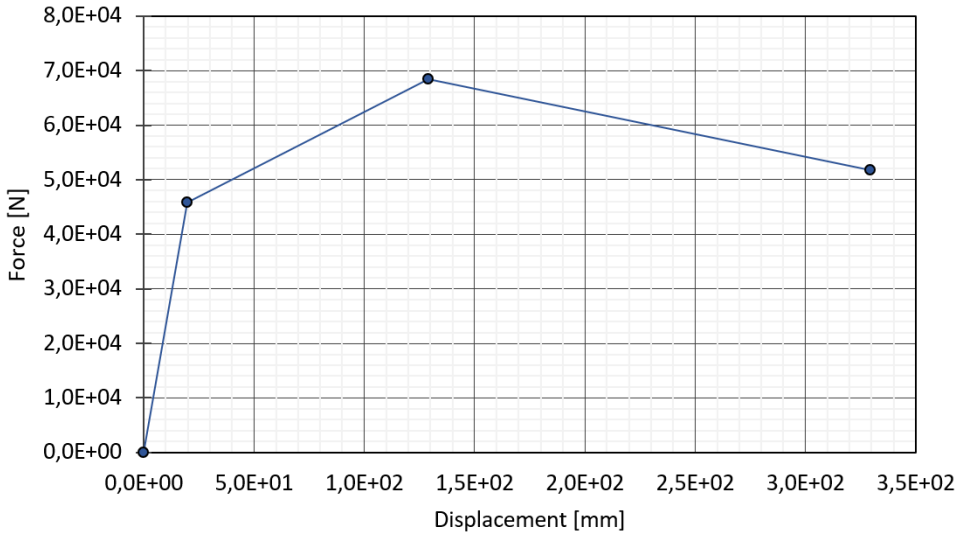

Figure 12.5: Load-Displacement curve: frame and panel 2nd order effects

Summing up, P_P^{II} is equal to:

$$P_P^{II} = W_P \frac{d(1+\eta)}{2H} \tag{12.10}$$

The final capacity curve is represented in Figure *12.5*. A comparison between the diagrams obtained for the three different cases is instead proposed in Figure *12.6*.

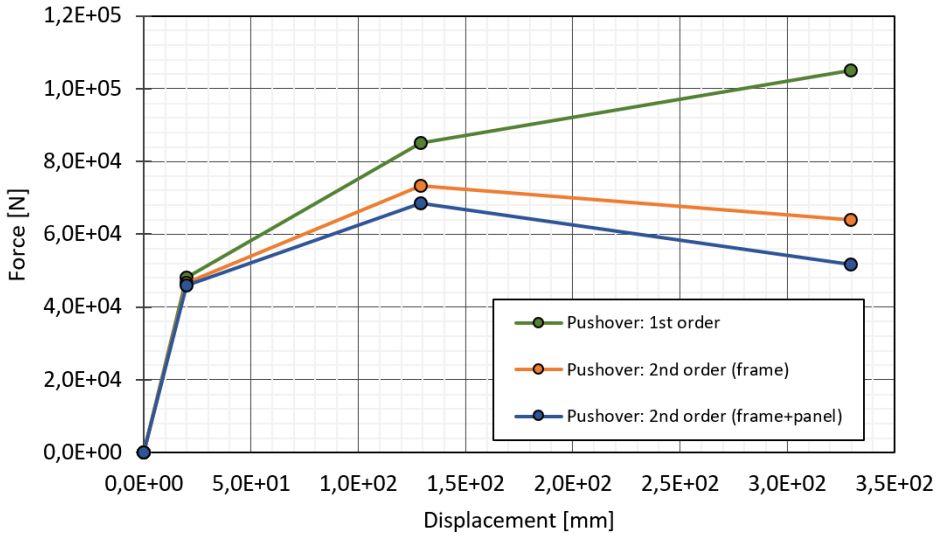

Figure 12.6: Load-Displacement curves comparison

12.1.5 Equivalent damping ratio and period

As a further step to the definition of the capacity curve, the CSM requires the definition of the equivalent viscous damping curve The formulation proposed in the work of Dal lago et al [9] is here briefly recalled. Everything is centered around the computation of the dissipated energy at each loading cycle. To do so, the evolution of the stiffness of the system after yielding is needed, this is why the *Takeda Law of hysteresis* has been adopted. [29] This rule is not the same for the 3 linear brances: in the uncracked branch, the energy dissipation is null; in the cracked elastic branch the energy dissipation is shown in Figure 12.7; in the plastic branch the energy dissipation is shown in Figure 12.8

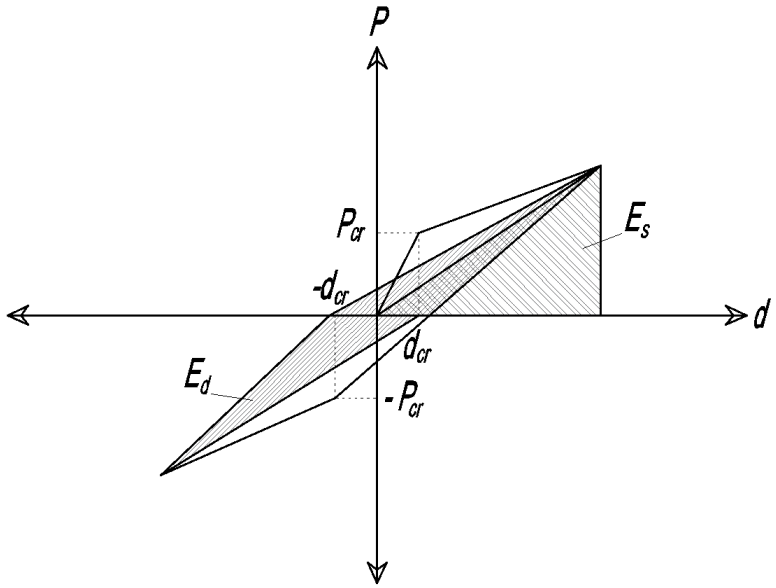

Figure 12.7: Energy dissipation along the elastic branch

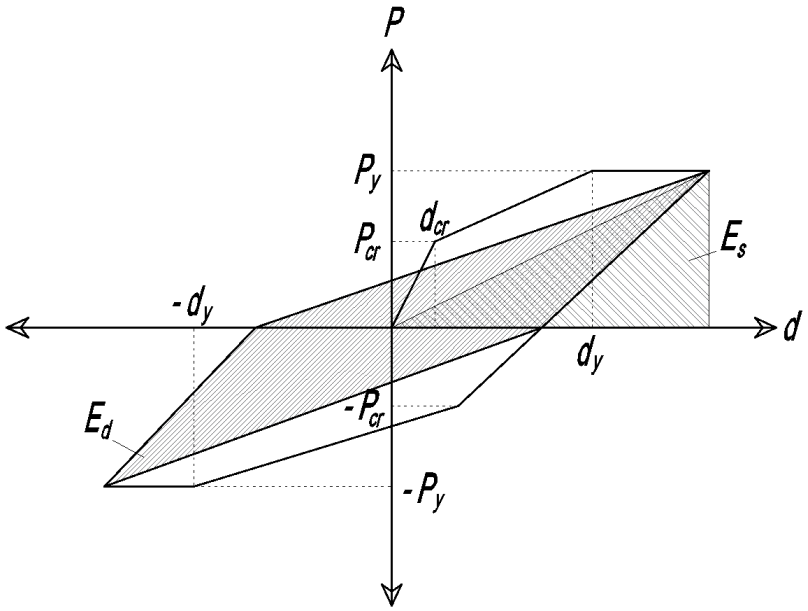

Figure 12.8: Energy dissipation along the plastic branch

What remains to be computed is the stiffness of the frame during the unloading phase K_{unload}. In particular:

- if the displacement d is lower than d_y:

$$K_{unload} = \frac{P(d) + P(d_{cr})}{d + d_{crack}} \tag{12.11}$$

- if the displacement d is higher than d_y, then the Takeda law of hysteresis must be implemented:

$$K_{unload} = \frac{P(d_y) + P(d_{cr}}{d_y + d_{crack}} \cdot \left(\frac{d_y}{d}\right)^{0.4} \tag{12.12}$$

The dissipated energy by the frame E_d can be now computed as:

$$E_d = \begin{cases} 0 & \text{if } d < d_{cr} \\ 2P\Big(d - \frac{P}{K_{unload}}\Big) & \text{se } d > d_{cr} \end{cases} \tag{12.13}$$

The equaivalent damping ratio ξ_{eq} cab be finally defined as:

$$\xi_{eq} = \xi_0 + \frac{E_d}{4\pi E_s} \tag{12.14}$$

being ξ_0 the initial damping ratio, assumed here equal to 2% in order to account for the cracking of the concrete, and E_s is the elastic deformation energy defined as:

$$E_s = d\Big(\frac{P_{max} + |P_{min}|}{4}\Big) \tag{12.15}$$

with P_{max} and P_{min} the maximum positive and negative load reached during that cycle. The equaivalent period T_{eq} is obtained by following the same kind of reasoning. By entering the curves with the value of the performance displacement, it is possible to determine the corresponding values of T_{eq} and χ_{eq} to be used to compute the correlation coefficients ρ_{ig}.
The results, in terms of performance displacements, are reported for each one of the analysed models, in the next section.

12.1.6 Implementation of the Complete Quadratic Rule

Now that all the ingredients are ready, it is possible to enter the CQC rule in order to evaluate the maximum values of the force at the top connection. Before doing so, another aspect must be tackled.
As presented before, the cinematic of the panel is responsible for some second order effects which alter the load displacement curve of the model. These second order effects however, do not affect the capacity of the structure only, but they produce another contribution, which has a direct influence on the reaction forces at the connections. This contribution does not depend on the acceleration of the model, meaning that it represents a static component of F_B.
This to say that, the overall force at the upper connection F_B is equal to:

$$F_B = F_B^{DYN} + F_B^{ST} \tag{12.16}$$

where F_B^{DYN} is the dynamic component of the force defined as

$$F_B^{DYN} = m_p \Big[\alpha_B^2 \ddot{u}_{CSM}^2 + \beta_B^2 PGA^2 + 2\alpha_B \beta_B \rho_{ig} \ddot{u}_{CSM} PGA \Big]^{\frac{1}{2}} \tag{12.17}$$

On the other hand, the static component is equal to:

$$F_B^{ST} = W_P \frac{d_{CSM}(1+\eta)}{2H} \tag{12.18}$$

being $\ddot{u}_{CSM}$ and d_{CSM} the performance acceleration and performance displacements. The results in terms of performance displacements have been already presented. What remains to do is to evaluate the performance acceleration. The steps to be followed are here summarized for the case of Model 1, making reference to a PGA of 0.3g.
The first step requires the evaluation of the performance displacement under the considered sesimc motion. Therefore, by entering Figure (*3.40*) with a 0.3 PGA, the corresponding displacement turned out o be equal to $u_P = 115mm$. The performance shear correspondent to a displacement to such displacement can be now computed exploiting the results of the Pushover analysis. By following the same procedure adopted before, the performance shear is defined by enering the Capacity Curve with the value of the perfomance dipalcement (Figure *12.9*), obtaing $F_P = 65000N$.
At last, the value of the performance acceleration is computed as:

$$\ddot{u}_{CSM} = \frac{F_{CSM}}{M} \tag{12.19}$$

being M the mass of the dual system frame-panel.

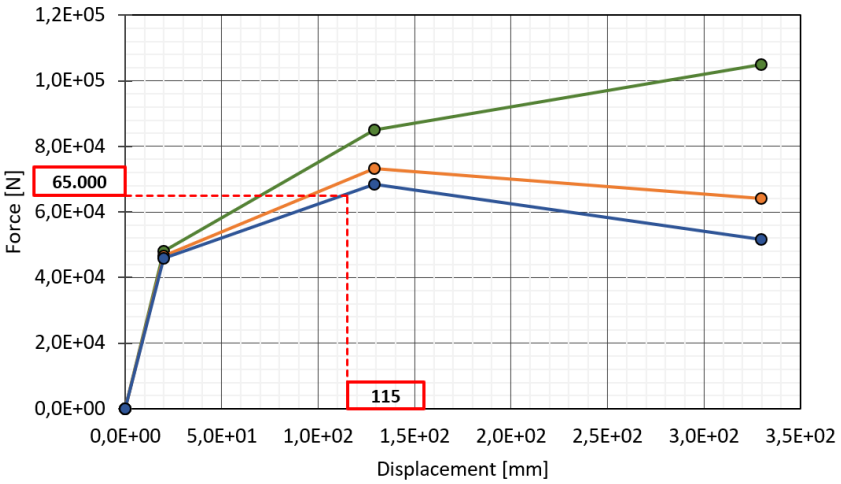

Figure 12.9: Performance Shear evaluation

In particular, in order to account for the presence of the panel, the total m has been defined as:

$$M = m_f + \alpha_B \cdot m_p \tag{12.20}$$

where m_f is the mass adopted for the evaluation of the Capacity Curve, which corresponds in this case to that of the single column, α_B is the participation mass coefficient defined as in (*5.15*) and m_p represents the mass of the panel.
The last step before entering the CQC rule is related to the evaluation of the correlation coefficient $\rho_i g$. Different theories have been proposed in the first part of the thesis. They must be now corrected due to the fact that the structure does not behave elastically anymore. To do so, the new formulations will make reference to the concept of equivalent period and equaivalent viscous damping. The results for each case are reported in Figure *12.10* as a function of the PGA. For a high structural periods, the different formulations provide quite close results, which turned out to be almost constant, regardless the value of the PGA.
Now, in order to obtain a lower bound limit solution, the formulation denoted as WX will be here adopted to compute the values of the correlation coefficient.
The next ection will be devoted to present the comparison comparison between the solutions obtained by implmenting the Performance Based response Spectrum Method (PBRSM) and the outputs provided by the Non Linear Time History Analysis from *Straus7*.

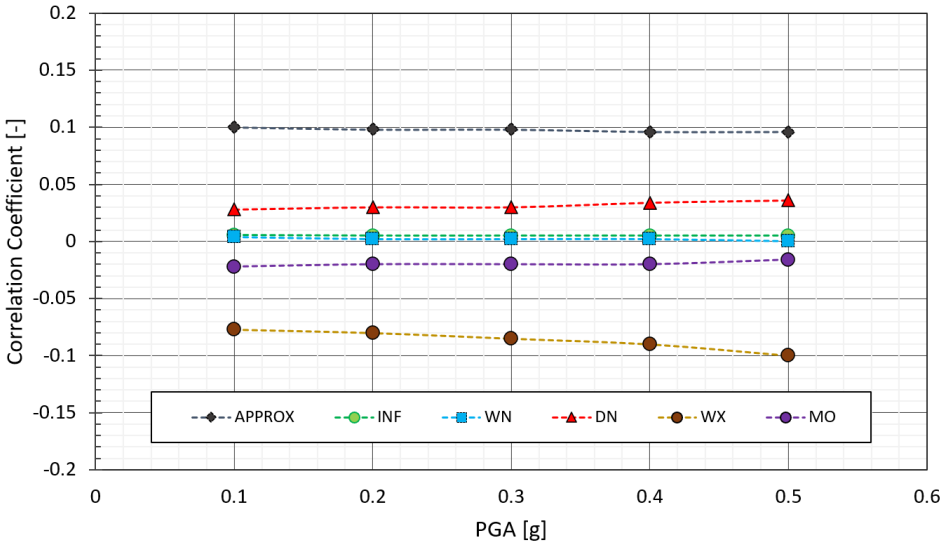

Figure 12.10: Correlation coefficients comparison

12.1.7 Presentation of the results

The aim of this section is to briefly recall the features of the models which have been used to implement the different proposed procedures. Between all the previously presented 16 structural schemes, the three models here analyzed have been chosen in such a way as to cover the widest range of periods possible. Together with the main structural characteristics, the Pushover curve and the results obtained via Capacity response Spectrum are shown. The comparison in terms of the reaction force at the top connection F_B between the reference results obtained from the Non Linear Time History Analyis from Straus and the proposed Response Spectrum Method are here presented.
The soultion obtained through the implementation of the RS has been obtained following three different procedures. A brief presentation of such procedures and the notation adopted in the different Plots is here reported:

1. PBRSM (d_{PERF}) are the outputs obtained by following the same steps presented in Section 12.1.7

2. PBRSM (T_{MAX}) are the outputs obtained by computing the acceleration in hypothesis of elastic-perfectly plastic law

3. PBRSM ($1^{ST}ORDER$) are the outputs obtained disregarding the second order associated both to the frame and the panels

4. PBRSM ($Straus$) are the outputs obtained by exploiting the perfoemnce points directly from provided by the software $Straus7$

5. $NLTHA$ are the outputs in terms of reaction forces directly provided by the Non Linear Time History Analysis implemented in $Straus7$

Together with the diagrams providing the trend of the curves for the two solutions as a function of the PGA, three tables have been created. This will give the reader the possibility to have an idea of the influence of the two components, static and dynamic, on the final value of F_B.
It is evident how, in general, the Response Spectrum formulation tends to underestimates the values of the reaction forces. In particular, by comparing the results between the three models, a general trend can be highlighted: the stiffer the model, and the better is the solution, with Model 11 able to follow almost perfectly the refernce solution from Straus7.

Model 1

Before analyzing the final solution in terms of reaction forces provided by the different methods, the outputs provided by the CSM are presented. Figure *12.12* refers to the capacity curve obtained via Pushover. On the other hand Figure *3.40* reports, together with equivalent damping ratio and the equivalent period, the performance points of the model. In Fig *12.13* (c) the value of the yielding displacement is reported as well

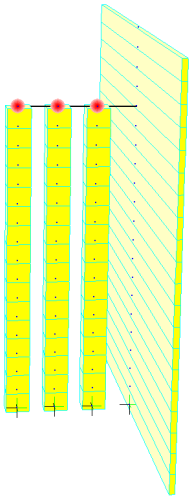

Section: $600 \times 600mm$
n° of columns: 3
Heigth of columns: 8m
$\eta : 0.25$
$T_s = 1.41sec$
$f_s = 0.71Hz$

Figure 12.11: Model 1 - Structural scheme

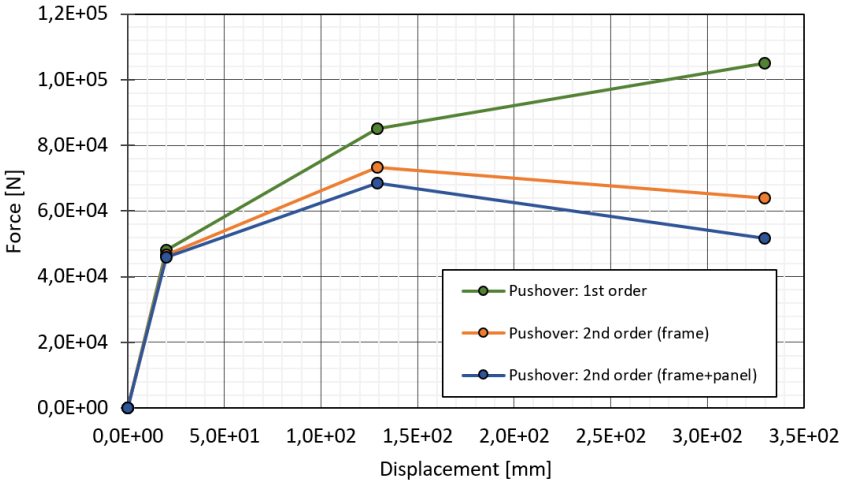

Figure 12.12: Load-Displacement curves comparison

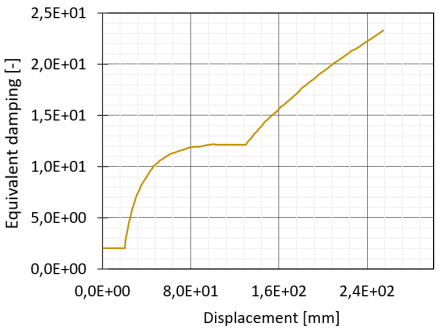

(a) ξ_{eq}

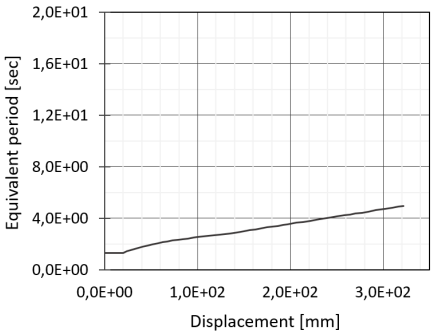

(b) T_{eq}

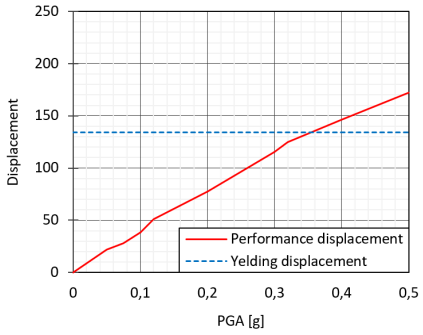

(c) d_{PERF}

Figure 12.13: CSM Results: Equivalent damping ratio (a), Equivalent Period (b) and Performance displacement (c)

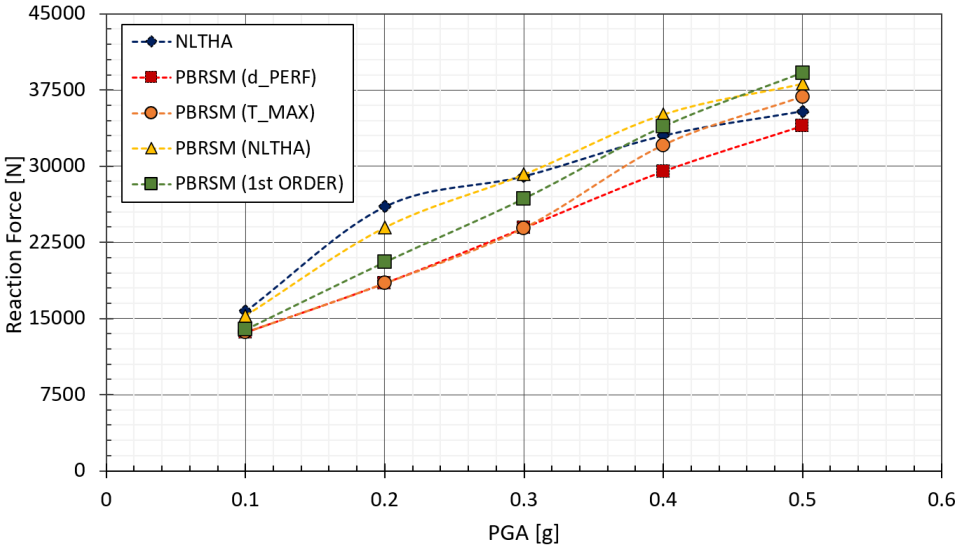

Figure 12.14: Results comparison (H=8m, η=0.25, α_B=0.502, β_B=0.104)

Model 6

Model 6 represents the most flexible between the structural schems analyzed, meaning that on one hand the absolute acceleration of the structure is expected to be lower than the other cases. On the other hand however, the static contribution to F_B due to the second order effects will be much more consistent. A peculiarity of this model is related to the fact that, as it could be observed from Figure *12.17* (c) the Capacity Spectrum Method was not able provide the values of performance displacements beyond the yielding threshold. This is due to the fact that, due to its high flexibility, the structure was not able to resists seismic actions with a PGA higher than 0.37g, leading to divergence of the soluton. This is why, all the formulations relying on the CSM outputs, will provide the solution in terms of F_B only for the first three values of PGA.

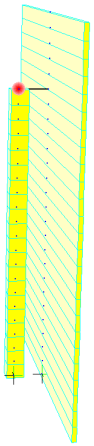

Section: $600 \times 600mm$
n° of columns: 3
Heigth of columns: 8m
η : 0.25
$T_s = 2.16sec$
$f_s = 0.46Hz$

Figure 12.15: Model 6: Structural scheme

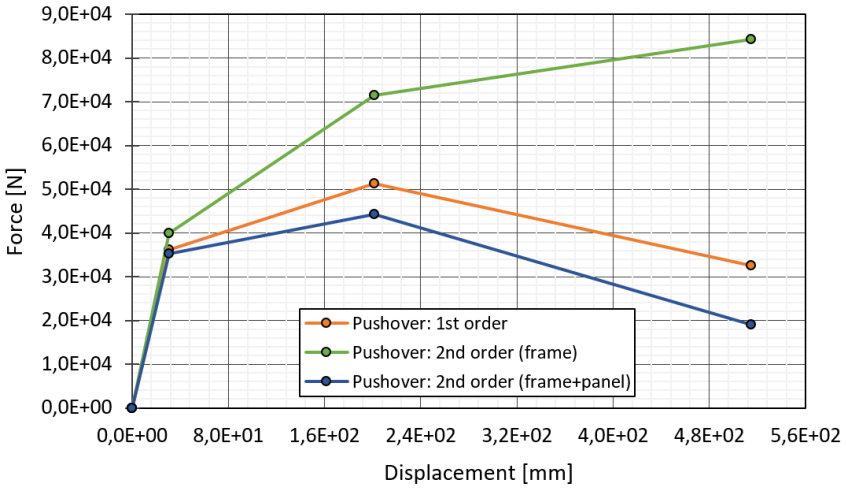

Figure 12.16: Model 6 Load-Displacement curves comparison

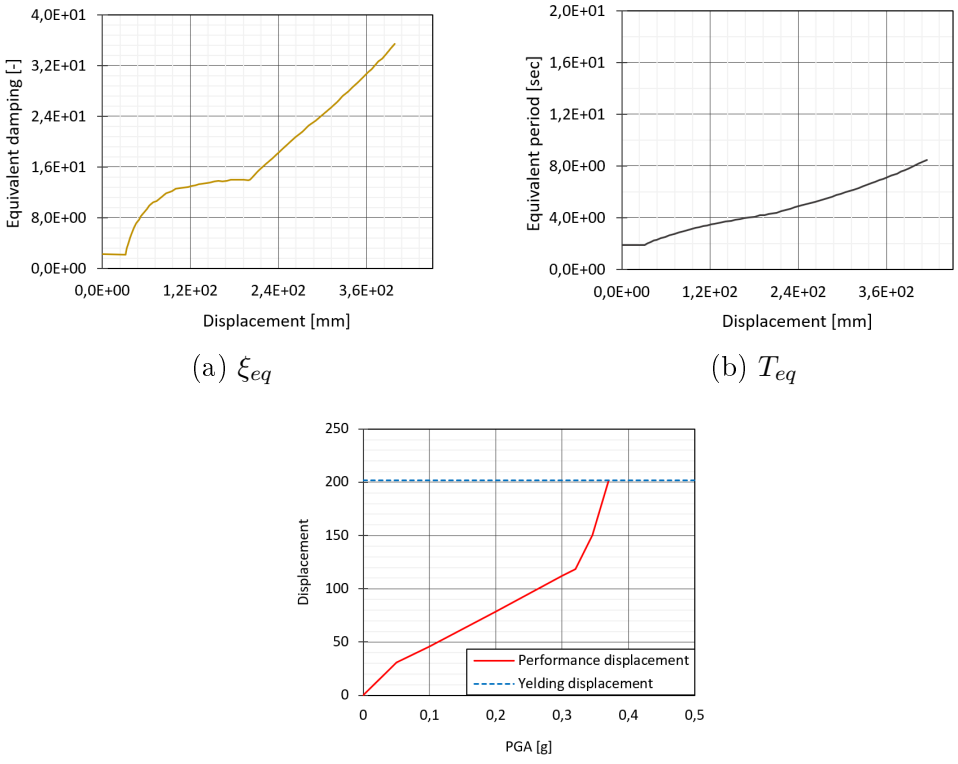

(a) ξ_{eq}

(b) T_{eq}

(c) d_{PERF}

Figure 12.17: CSM Results: Equivalent damping ratio (a), Equivalent Period (b) and Performance displacement (c)

By looking at Figure *12.18* it is evident how all the solutions provided by the proposed response Spectrum Method overestimate the reference results from Straus7. Moreover, between all the formulations based on the RS method, the one providing the best results is the procedure which directly

exploits the perfomance points given by Straus7, meaning that one of the reason

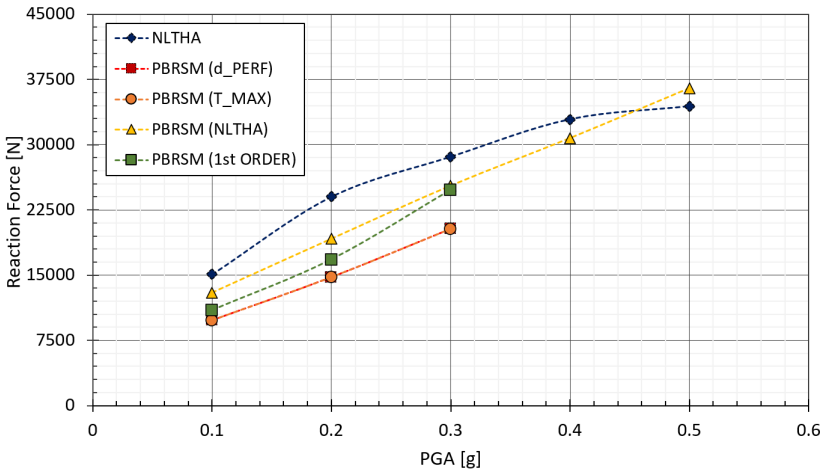

Figure 12.18: Results comparison (H=10m, η=0.25, α_B=0.502, β_B=0.104)

for this general trend is related to the difference between the performance solution provided respectively by the CSM and by Straus7.

Model 11

Finally, Model 11 is the structural scheme characterized by the highest value of the circular frequency. What can be said by looking at the final solutions reported in Figure *12.22* is that, between the analysed models, this one is for sure the one providing the better results. Except from the PBRSM d_{PERF}, all the other procedures provide conservative results for the whole PGA domain. Another time, the solution obtained by the implmentation of the RS method directly exploiting the performance behaviour computed by Straus, is the one assuring the highest values of the forces F_B.

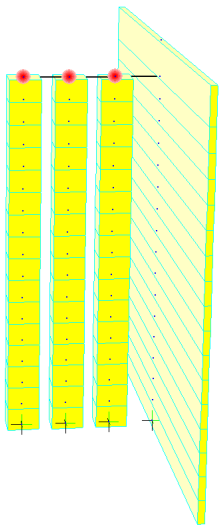

Section: $600 \times 600mm$
n° of columns: 3
Heigth of columns: 8m
η : 0.25
$T_s = 1.02sec$
$f_s = 0.98Hz$

Figure 12.19: Model 11: Structural scheme

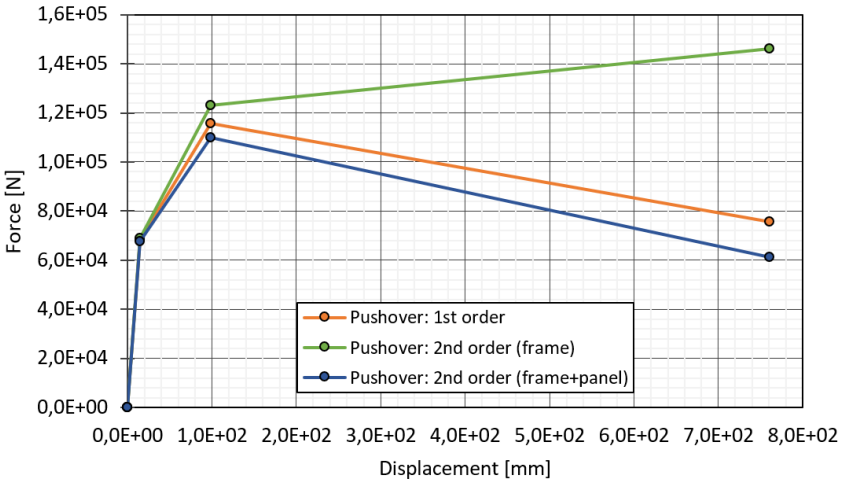

Figure 12.20: Model 11 Load-Displacement curves comparison

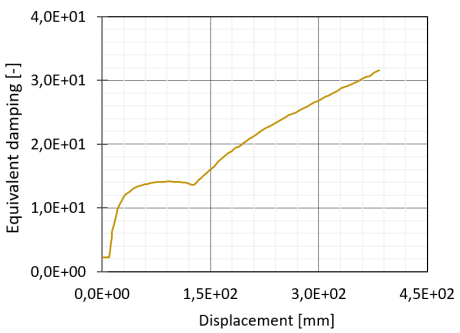

(a) ξ_{eq}

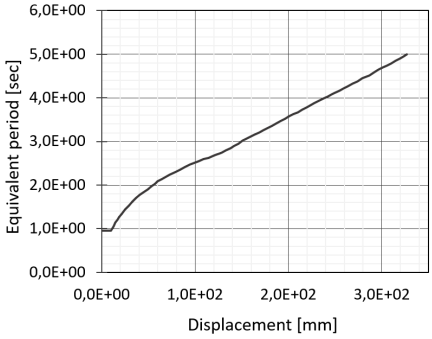

(b) T_{eq}

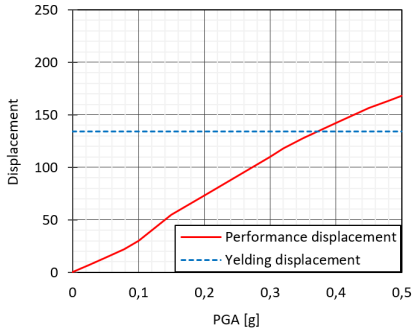

(c) d_{PERF}

Figure 12.21: CSM Results: Equivalent damping ratio (a), Equivalent Period (b) and Performance displacement (c)

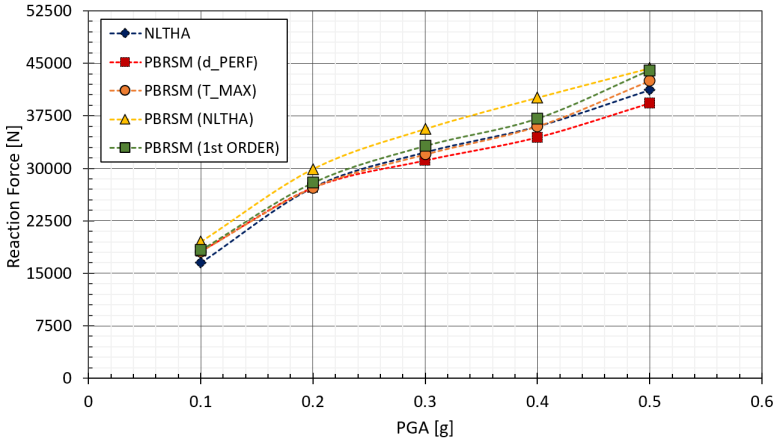

Figure 12.22: Results comparison (H=10m, η=0.1, α_B=0.403, β_B=0.146)

12.2 Code provision: Equivalent static force method

Seismic design practices for precast cladding panel are provided by the National codes of several countries all over the world.
All code requirements about cladding panels and related connections refer to a statically determined connection system and provide resistance requirements with respect to the out-of-plane seismic excitation on the base of the single panel mass. In all these cases, the equivalent static force method is used.
Moreover, the majoirity of such codes conceive the cladding panels as non-structural components, which is a strong hypothesis, still matter of debate.

12.2.1 European Standards

EC8 includes cladding panels in the list of non structural elements. The out of plane equivalent static forces actions are calculated as follows:

$$F_a = \frac{S_a W_a \gamma_a}{q_a} \tag{12.21}$$

where:

- F_a is the out of plane horizonthal force
- S_a is a seismic coefficient
- W_a is the weight of the element
- γ_a is the importance factor, equal to 1,0 for facade elements
- q_a is the behaviour factor, equal to 2,0 for facade elements

The seismic coefficient S_a is defined as:

$$S_a = \alpha S \left[\frac{3\left(1 + \frac{z}{H}\right)}{3 + \left(1 - \frac{T_a}{T_1}\right)^2} - 0,5 \right] \tag{12.22}$$

with α the ratio between the ground acceleration a_g on subsoil type A, an the acceleration of gravity g, S the soil factor, z the height of the non-structural element center of mass above the level of application of the seismic actions, H the building height measured from the foundation, T_a is the fundamental period of the panel and T_1 the fundamental vibration period of the structure.
Now, the panel is here modelled as a rigid element, therefore its natura period is zero, leading to the following a final equation which does not depend anymore on the natural period of the dual system either. This type of

analysis is derived from elastic structural analysis, which designers are very comfortable with, and have been adapted to inelastic structural behaviour through the definition of a behaviour factor that, taking into account the large dissipation of energy provided by hysteretic damping during ductile plastic behaviour, reduces the fictitious elastic force demand on the structure. The formulation is quite simple, and does not require any effort to be implmeneted. The weakness of the procedure however is related to the fact that the behaviour factor q_a is defined a priori, without taking into account the real capacity of the structure. In particular, the code allows to use a value of the reduction factor $q_a = 2$ when the points of connection between frame and panel yield. This is not so reasonable though, due to the fact that if the connections yield, the poise of the panel is compromised.
To have an idea of the results provided by the procedure proposed by EC8, a comparison in terms of F_B with the previously presented formulations is here reported for the three models.
The outputs for the three models are reported in Figure *12.23*, *12.23* and *12.23*. For what concerns the formulation proposed by EC8, the results have been computed considering two different values of the factor q_a (q_a=1 and q_a=2).
The trend for the three models is practically the same. The solution provided by the EC8 adopting a Q factor equal to one greatly overestimate the solution, with an error of over 200% for a 0.5g PGA. Things are more reasonable when adopting a a Q factor equal to 2. The problem is that now the outputs underestimate the solutions for low PGAs. The intrinsic problem of the formulation is related to the definition of the behavior factor q. The code in fact specifies that a value of q equal to 2 can be used after plasticization of the elements occurs. This is nonsense however, because it would involve the plasticization of the connections as well, which in reality cannot happen due to obvious reasons

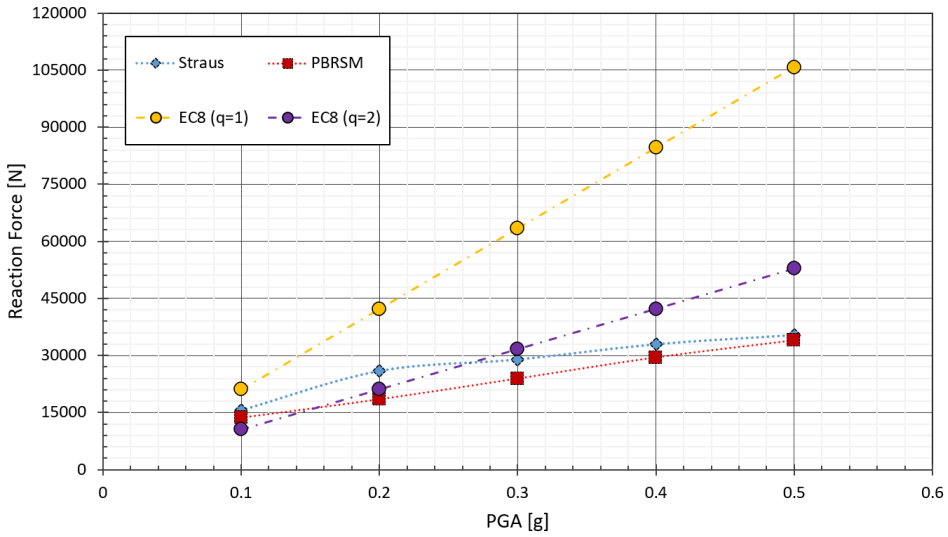

Figure 12.23: Model 1: Equivalent static vs RS method

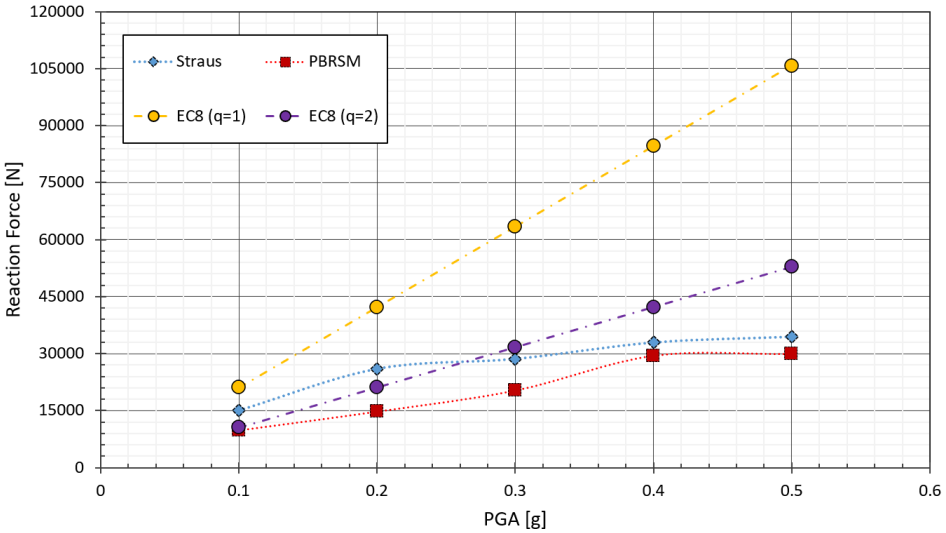

Figure 12.24: Model 7: Equivalent static vs RS method

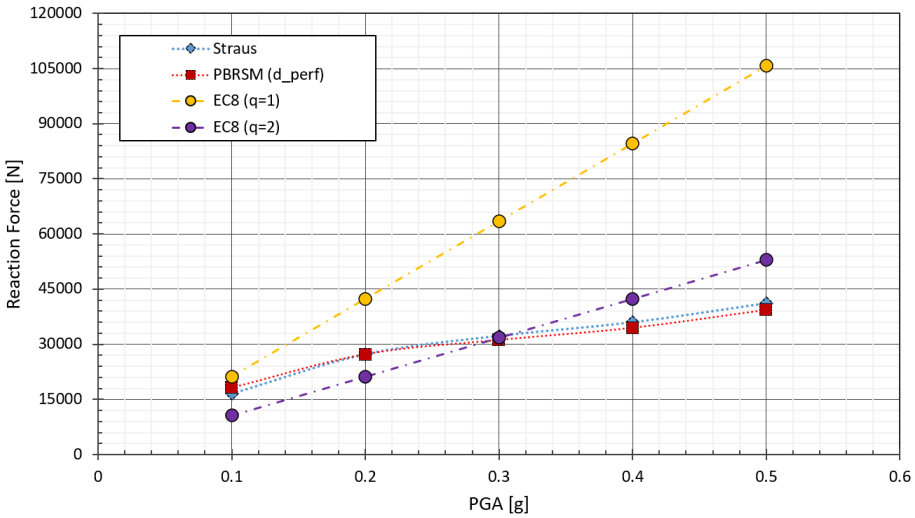

Figure 12.25: Model 11: Equivalent static vs RS method

Chapter 13

Conclusions

The inadequate seismic behaviour of the cladding panel connections of precast structures and the consequent failures occurred under recent earthquakes showed that a revision of the design philosophies currently adopted for this type of structural systems is necessary. This is why a general framework for the structural conception and seismic assessment of precast structures with cladding panels has been proposed. The work has been centered on the definition of a design method able to correctly model the influence of the claddings on the structural model, and consequantly the dynamics of the dual system frame-panel. By implementing the formulation proposed by Prof Luca Martinelli and Prof Farncesco Foti, the goal os to provide the designer an analytical formulation able to evaluate the values of the forces which generate at the connections.
Of reat importance has been the work of Der Kiureghian. Despite dealing with a conceptually different issue, i.e the evaluation of the peak floor acceleration, the proposed formulation provided quite helpful advices on how to treat the contribution of the highest frequency modes of a structure.
This has allowed to conceive the focal point around which the formulation here proposed is built, which sees the ground motion as a fictitious structural mode with infinite frequency, allowing to greatly reduce the computational costs involved. Doing so, due to the contributions of two modes, the mode of the dual system, and the fictitious mode of the ground acceleration, the maximum value of the reaction forces are obtained by applying a combination rule. The CQC rule has been implmented. To do so, it has been necessary to go through the computation of the correlation coefficients which account for the influence of one mode on the other. Different formulations have been proposed, and it will be up to the designer to choose the most proper one to be adopted, depending on the feature of the structure (natural period, damping model) The direct comparison with the solutions obtained through the direct integration of the equation of motion has cofirmed the goodness of the procedure in the elastic field.
For what concerns the validation of the formulation in the non-linear field, that is, once the yield has been reached, the use of finite element modeling has been made. And it is precisely through the comparison with the results obtained using the Straus7 software that it was possible to obtain a

more general overview of the behavior of the coupled system in a non-linear field. The constitutive model of the plastic hinges was modeled using the MathCad software thanks to the code provided by Prof Bruno Dal Lago. As for the geometric non-linearities, the presence of the panel generates a double second order contribution: 1) a dynamic contribution, which affects the Capacity of the model by reducing the stiffness of the structure, and therefore its acceleration, and 2) a static contribution, independent of the acceleration this time, which acts directly on the connections.
The comparison with the results obtained through finite element modeling shows how the proposed RS method is able to provide results that are as accurate as the model analyzed is rigid. On the contrary, for structures characterized by high periods, the procedure tends to underestimate the solution.
Finally, for what concerns the comparison with the EC8 design formulation, the results justify the doubts behind the EC8 procedure, whose oversimplified formulation lead to great inaccuracies in the reaction forces evaluation. This confirms even more the necessities to individuate a more accurate formulations, able to account in a more reasonable way for the ductility of the structure. This is why one of the objective of this work is to create the bases for future developments, aiming at individuating more accurate, but always simplified, design procedures.

Bibliography

[1] Matteo Pozzi and Armen Der Kiureghian. Response spectrum analysis for floor acceleration. *Earthq. Eng. Struct. Dyn.*, 44(12):2111–2127, 2015.

[2] Matteo Pozzi and Armen Der Kiureghian. Response Spectrum Compatible Psd for High-Frequency Range. *Conf. Struct. Mech. React. Technol.*, Division I(1):1–11, 2013.

[3] Luca Martinelli, Gianluca Barbella, and Anna Feriani. A numerical procedure for simulating the multi-support seismic response of submerged floating tunnels anchored by cables. *Eng. Struct.*, 33(10):2850–2860, 2011.

[4] G. Falsone and F Neri. Stochastic modelling of earthquake excitation following the EC8: power spectrum and filtering equations. *Eur Earthq. Eng*, 1(February):3–12, 2000.

[5] Giorgio Barone, Francesco Lo Iacono, Giacomo Navarra, and Alessandro Palmeri. A novel analytical model of power spectral density function coherent with earthquake response spectra. *UNCECOMP 2015 - 1st ECCOMAS Themat. Conf. Uncertain. Quantif. Comput. Sci. Eng.*, pages 394–406, 2015.

[6] V. Denoël. Multiple timescale spectral analysis. *Probabilistic Eng. Mech.*, 39:69–86, 2015.

[7] Lukas Moschen and Christoph Adam. Peak floor acceleration demand prediction based on response spectrum analysis of various sophistication. *Acta Mech.*, 228(4):1249–1268, 2017.

[8] Armen Der Kiureghian. On response of structures to stationary excitation. *Rep. No. UCB/EERC-79/32, Earthq. Eng. Res. Cent.*, (December):42, 1979.

[9] Bruno Dal Lago, Muhammad Naveed, and Marco Lamperti Tornaghi. Tension-only ideal dissipative bracing for the seismic retrofit of precast industrial buildings. *Bull. Earthq. Eng.*, 19(11):4503–4532, 2021.

[10] Vanmarcke E.H. Properties of spectral moments with applications to random vibration. *ASCE J Eng Mech Div*, 98(EM2):425–446, 1972.

[11] J. Penzien R.W. Clough. No Title. *Dyn. Struct. 2nd Ed.*, McGraw-Hil, 1993.

[12] Yoshimi Goda. *Random seas and design of maritime structures (3rd Edition).* 2010.

[13] L. A. Bergman, M. Shinozuka, and C. G. Bucher. A state-of-the-art report on computational stochastic mechanics. *Probabilistic Eng. Mech.*, 12(4):197–321, 1997.

[14] M. Di Paola and G. Navarra. Stochastic seismic analysis of MDOF structures with nonlinear viscous dampers. *Struct. Control Heal. Monit.*, 16(May 2011):303–318, 2011.

[15] Maharaj K. Kaul. Stochastic characterization of earthquakes through their response spectrum. *Earthq. Eng. Struct. Dyn.*, 6(5):497–509, 1978.

[16] Dieter D. Pfaffinger. Calculation of Power Spectra from Response Spectra. *J. Eng. Mech.*, 109(1):357–372, 1983.

[17] La Mendola L. Di Paola M. Dynamic of structures under seismic input motion (Eurocode 8). *Eur. Seism. Eng.*, 2:36–44, 1992.

[18] P. Cacciola, P. Colajanni, and G. Muscolinio. Combination of Modal Responses with Seismic Input Representation. *October*, 9445(April 2004):1562–1569, 2004.

[19] J Elorduy. Responses of linear systems to certain trascient disturbances. In *Fourth World Conf. Earthq. Eng.*, pages 185–196, 1969.

[20] A. Wilson, E. L., Der Kiureghian. A replaceent for the SRSS method in seismic analysis. *Earthq. Eng. Struct. Dyn.*, 9:187–192, 1981.

[21] Armen Der Kiureghian and Ansgar Neuenhofer. A response spectrum method for multiple-support seismic excitations. *Earthq. Eng. Res. Cent.*, UBC/EERC-9:1–59, 1991.

[22] A. Asfura. Floor response spectrum method for seismic analysis of multiply supported secondary systems. *Earthq. Eng. Struct. Dyn.*, 14:245–265, 1986.

[23] Nakamura Y. Der Kiureghian A. CQC modal combination rule for high-frequency modes. *Earthq. Eng. Struct. Dyn.*, (22:11):943–956, 1993.

[24] Gupta V.K. Kumari R. A modal combination rule for peak floor accelerations in multistoried buildings. *ISET J. Earthq. Technol.*, 44(1):213–231, 2007.

[25] Fahim Sadek, Bijan Mohraz, and Michael A. Riley. Linear Procedures for Structures with Velocity-Dependent Dampers. *J. Struct. Eng.*, 126(8):887–895, 2000.

[26] K. B. Singh, M. P., and Mehta. 'Seismic design response by an alternative SRSS rule. *Earthq. Eng. Struct. Dyn.*, 11:771–783, 1983.

[27] A.G. Davenport. The application of statistical concepts to the wind loading of structures. In *Proc. Inst. Civ. Eng. 1961*, pages 449–472, 19.

[28] A. Preumont. Random Vibration and Spectral Analysis. *Kluwer Acad. Publ. Lausanne*, 1994.

[29] Toshikazu Takeda, Mete A. Sozen, and N. Norby Nielsen. Reinforced Concrete Response to Simulated Earthquakes, 1970.